

Final Report

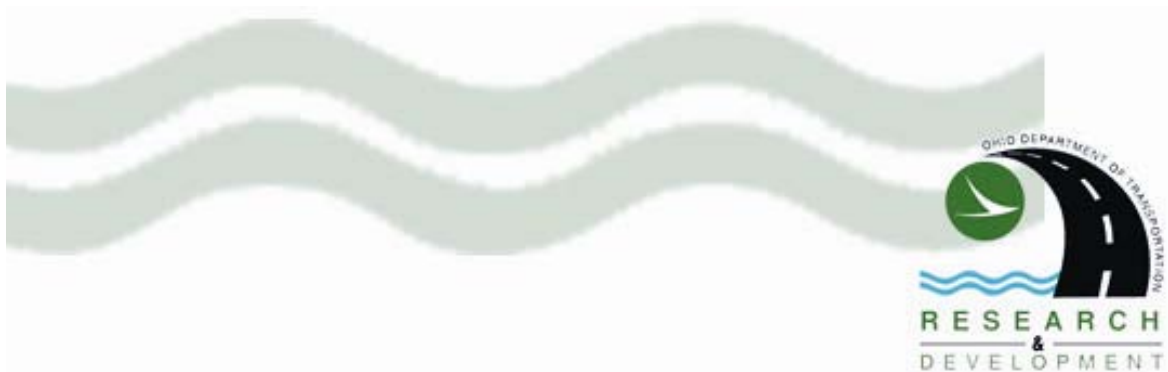
# Guidelines for Implementing NCHRP 1-37A M-E Design Procedures in Ohio: Volume 3—Sensitivity Analysis

Jagannath Mallela, Leslie Titus Glover, Michael I. Darter,  
Harold Von Quintus, Alex Gotlif, Mark Stanley

Applied Research Associates, Inc.  
100 Trade Centre Drive, Suite 200  
Champaign, IL 61820

Prepared in cooperation with  
the Ohio Department of Transportation, and  
the U.S. Department of Transportation,  
Federal Highway Administration  
State Job Number 134300

*November, 2009*





1. Report No. FHWA/OH-2009/9C	2. Government Accession No	3. Recipient's Catalog No	
3. Title and Subtitle Guidelines for Implementing NCHRP 1-37A M-E Design Procedures in Ohio: Volume 3 – Sensitivity Analysis		5. Report Date November, 2009	
		6. Performing Organization Code	
7. Authors Jagannath Mallela, Leslie Titus Glover, Michael I. Darter, Harold Von Quintus, Alex Gotlif, and Mark Stanley		8. Performing Organization Report No.	
9. Performing Organization Name and Address Applied Research Associates, Inc. 100 Trade Centre Dr., Suite 200 Champaign, IL 61820-7233		10. Work Unit No. (TRAIS) C6B	
		11. Contract or Grant No. 134300	
12. Sponsoring Agency Name and Address Ohio Department of Transportation 1980 West Broad Street Columbus, Ohio 43223		13. Type of Report and Period Covered	
		14. Sponsoring Agency Code	
15. Supplementary Notes			
16. Abstract The new Mechanistic-Empirical Pavement Design Guide (NCHRP 1-37A and 1-40D) is based on fundamental engineering principles and is far more comprehensive than the current empirical AASHTO Design Guide developed for conditions more than 40 years previous. The implementation process will require a number of years and additional resources for staffing, obtaining inputs (e.g., new equipment), and training. The benefits of implementation are very significant and range from achieving more cost effective and reliable designs, to lower initial and life cycle costs to the agency, to reduced highway user impact due to lane closures for maintenance and rehabilitation of pavements. This report addresses a key aspect of the implementation process that is identification of the most significant inputs based on current ODOT design and material specifications and Ohio site conditions (traffic, climate, subgrade). Identification of the most significant inputs was done by performing a comprehensive sensitivity analysis. Practical recommendations are made for each input studied. The results presented in this report (volume 3 of four volumes) are part of the first phase of a process to implement the new design guide in Ohio.			
17. Key Words NCHRP 1-37A, mechanistic empirical pavement design, distress, smoothness, performance prediction, reliability, implementation, flexible pavement, rigid pavement, overlays		18. Distribution Statement No restriction. This document is available to the public through the National Technical Information Service 5285 Port Royal Road Springfield VA 22161	
19. Security Classif.(of this report) Unclassified	19. Security Classif. (of this page) Unclassified	20. No. of Pages 173	21. Price

# SI\* (MODERN METRIC) CONVERSION FACTORS

## APPROXIMATE CONVERSIONS TO SI UNITS

Symbol	When You Know	Multiply By	To Find	Symbol
<b>LENGTH</b>				
in	inches	25.4	millimeters	mm
ft	feet	0.305	meters	m
yd	yards	0.914	meters	m
mi	miles	1.61	kilometers	km
<b>AREA</b>				
in <sup>2</sup>	square inches	645.2	square millimeters	mm <sup>2</sup>
ft <sup>2</sup>	square feet	0.093	square meters	m <sup>2</sup>
yd <sup>2</sup>	square yard	0.836	square meters	m <sup>2</sup>
ac	acres	0.405	hectares	ha
mi <sup>2</sup>	square miles	2.59	square kilometers	km <sup>2</sup>
<b>VOLUME</b>				
fl oz	fluid ounces	29.57	milliliters	mL
gal	gallons	3.785	liters	L
ft <sup>3</sup>	cubic feet	0.028	cubic meters	m <sup>3</sup>
yd <sup>3</sup>	cubic yards	0.765	cubic meters	m <sup>3</sup>
NOTE: volumes greater than 1000 L shall be shown in m <sup>3</sup>				
<b>MASS</b>				
oz	ounces	28.35	grams	g
lb	pounds	0.454	kilograms	kg
T	short tons (2000 lb)	0.907	megagrams (or "metric ton")	Mg (or "t")
<b>TEMPERATURE (exact degrees)</b>				
°F	Fahrenheit	5 (F-32)/9 or (F-32)/1.8	Celsius	°C
<b>ILLUMINATION</b>				
fc	foot-candles	10.76	lux	lx
fl	foot-Lamberts	3.426	candela/m <sup>2</sup>	cd/m <sup>2</sup>
<b>FORCE and PRESSURE or STRESS</b>				
lbf	poundforce	4.45	newtons	N
lbf/in <sup>2</sup>	poundforce per square inch	6.89	kilopascals	kPa

## APPROXIMATE CONVERSIONS FROM SI UNITS

Symbol	When You Know	Multiply By	To Find	Symbol
<b>LENGTH</b>				
mm	millimeters	0.039	inches	in
m	meters	3.28	feet	ft
m	meters	1.09	yards	yd
km	kilometers	0.621	miles	mi
<b>AREA</b>				
mm <sup>2</sup>	square millimeters	0.0016	square inches	in <sup>2</sup>
m <sup>2</sup>	square meters	10.764	square feet	ft <sup>2</sup>
m <sup>2</sup>	square meters	1.195	square yards	yd <sup>2</sup>
ha	hectares	2.47	acres	ac
km <sup>2</sup>	square kilometers	0.386	square miles	mi <sup>2</sup>
<b>VOLUME</b>				
mL	milliliters	0.034	fluid ounces	fl oz
L	liters	0.264	gallons	gal
m <sup>3</sup>	cubic meters	35.314	cubic feet	ft <sup>3</sup>
m <sup>3</sup>	cubic meters	1.307	cubic yards	yd <sup>3</sup>
<b>MASS</b>				
g	grams	0.035	ounces	oz
kg	kilograms	2.202	pounds	lb
Mg (or "t")	megagrams (or "metric ton")	1.103	short tons (2000 lb)	T
<b>TEMPERATURE (exact degrees)</b>				
°C	Celsius	1.8C+32	Fahrenheit	°F
<b>ILLUMINATION</b>				
lx	lux	0.0929	foot-candles	fc
cd/m <sup>2</sup>	candela/m <sup>2</sup>	0.2919	foot-Lamberts	fl
<b>FORCE and PRESSURE or STRESS</b>				
N	newtons	0.225	poundforce	lbf
kPa	kilopascals	0.145	poundforce per square inch	lbf/in <sup>2</sup>

\*SI is the symbol for the International System of Units. Appropriate rounding should be made to comply with Section 4 of ASTM E380. (Revised March 2003)

# **Guidelines for Implementing NCHRP 1-37A M-E Design Procedures in Ohio: Volume 3 – Sensitivity Analysis**

Final Report

Prepared by

Jagannath Mallela, Leslie Titus Glover, Michael I. Darter,  
Harold Von Quintus, Alex Gotlif, Mark Stanley

Applied Research Associates, Inc.  
100 Trade Centre Drive, Suite 200  
Champaign, IL 61820

Credit Reference: Prepared in cooperation with the Ohio Department of Transportation and the U.S. Department Transportation, Federal Highway Administration.

Disclaimer Statement: The contents of this report reflect the views of the authors who are responsible for the facts and the accuracy of the data presented herein. The contents do not necessarily reflect the official views or policies of the Ohio Department of Transportation or the Federal Highway Administration. This report does not constitute a standard, specification or regulation.

**November, 2009**

## **ACKNOWLEDGEMENTS**

The authors express their deep gratitude to the Ohio Department of Transportation (ODOT). We are particularly grateful to Mr. Roger Green, Mr. Aric Morse, Mr. David Powers, Ms. Vicki Fout, and Ms. Monique Evans for their useful, timely, and constructive comments throughout the planning and execution of this research project.

The authors also gratefully acknowledge the contributions of Dr. Suri Sadasivam of ARA Inc. for his assistance with preparing the project reports and Dr. Susanne Aref, the project's statistical consultant, for her guidance in model recalibration.

# TABLE OF CONTENTS

<b>CHAPTER 1. INTRODUCTION.....</b>	<b>1</b>
Background and Need for Sensitivity Analysis .....	1
Selected New and Rehabilitated Pavement Baseline Designs.....	1
Scope of the Report.....	1
<b>CHAPTER 2. SENSITIVITY ANALYSIS FOR NEW HMA PAVEMENT.....</b>	<b>3</b>
Overview .....	3
Baseline New HMA Pavement Construction Date and Analysis Period .....	3
Baseline New HMA Pavement Section Analysis Parameters (Initial IRI and Terminal Distress/IRI) .....	4
Baseline New HMA Pavement Section Location .....	4
Baseline New HMA Pavement Section Traffic .....	4
Climatic Data Input for Baseline New HMA Pavement Section .....	13
Pavement Surface Properties for Baseline New HMA Pavement Section.....	16
Layering of the HMA Pavement and Subgrade for Baseline New HMA Pavement.....	16
HMA Mix Properties for New HMA Baseline Design .....	17
New HMA Baseline Design Aggregate Base Properties.....	21
Subgrade Properties for New HMA Pavement Baseline Design.....	23
MEPDG Results for New HMA Baseline Design.....	25
Sensitivity Analysis Results for New HMA Pavements .....	33
<b>CHAPTER 3. NEW JPCP SENSITIVITY ANALYSIS .....</b>	<b>69</b>
New JPCP Baseline Design Construction Date and Analysis Period.....	69
New JPCP Baseline Design Analysis Parameters (Initial IRI) .....	70
New JPCP Baseline Design Location.....	70
New JPCP Baseline Design Traffic .....	70
Climatic Data Input for New JPCP Baseline Design.....	70
Surface Shortwave Absorptivity for New JPCP Baseline Design .....	71
Layering of the JPCP Pavement and Subgrade for New JPCP Baseline Design .....	71
PCC Layer Mix Properties for New JPCP Baseline Design .....	71
Base Properties for New JPCP Baseline Design.....	72
Subgrade for New JPCP Baseline Design.....	72
Design Features for Baseline ODOT JPCP .....	76
MEPDG Results for Baseline New JPCP Pavement.....	77
Sensitivity Analysis.....	77
Sensitivity Analysis Results for New JPCP Pavements.....	81

## TABLE OF CONTENTS, CONTINUED

<b>CHAPTER 4. SENSITIVITY ANALYSIS OF HMA OVERLAY DESIGN OF RUBBLIZED PCC PAVEMENTS.....</b>	<b>113</b>
Rehabilitation Design Types Considered .....	113
Description of the Existing JRCP Pavement to be used in the Baseline Designs for the Rubblization Example .....	113
HMA Over Rubblized PCC Baseline Design .....	114
Baseline HMA over Rubblized PCC Pavement Design Construction Date and Analysis Period.....	114
Analysis Parameters (Initial IRI) for the Baseline HMA over Rubblized PCC Design .....	114
Location of Baseline HMA over Rubblized PCC Pavement.....	114
20-yr Traffic Projections for the Baseline HMA over Rubblized PCC Pavement.....	115
Climate Data Input for Baseline HMA over Rubblized PCC Pavement Section.....	115
Pavement Surface Properties for Baseline HMA over Rubblized PCC Pavement Section .....	116
Structure and Materials of the HMA over Rubblized PCC Pavement Design.....	116
MEPDG Predicted Performance for Baseline HMA over Rubblized PCC Design.....	122
<b>CHAPTER 5. UNBONDED JPCP OVERLAY SENSITIVITY ANALYSIS.....</b>	<b>131</b>
Baseline Unbonded JPCP Overlay Design .....	131
Baseline Unbonded JPCP Overlay over Existing JRCP Design Construction Date and Analysis Period .....	131
Baseline Unbonded JPCP Overlay over Existing JRCP Design Analysis Parameters (Initial IRI).....	132
Baseline Unbonded JPCP Overlay over Existing JRCP Design Location .....	132
20-yr Traffic Projection for the Baseline Unbonded JPCP Overlay over Existing JRCP Design .....	132
Climate Data for Baseline Unbonded JPCP Overlay over Existing JRCP Design.....	133
Surface Shortwave Absorptivity for the Baseline Unbonded JPCP Overlay over Existing JRCP Design .....	133
Layering of the JPCP Pavement and Subgrade for Baseline Unbonded JPCP Overlay over Existing JRCP Design .....	133
Design Features for the Baseline Unbonded JPCP Overlay over Existing JRCP Design.....	137
MEPDG Results for the Baseline Unbonded JPCP Overlay over Existing JRCP Design.....	139

## TABLE OF CONTENTS, CONTINUED

<b>CHAPTER 6. CONCLUSIONS AND RECOMMENDATIONS.....</b>	<b>165</b>
Conclusions.....	165
Recommendations.....	165
<b>REFERENCES .....</b>	<b>173</b>

THIS PAGE INTENTIONALLY LEFT BLANK

## LIST OF FIGURES

Figure 1. General information for baseline new HMA pavement section.....	4
Figure 2. Map of Ohio highlighting LTPP sites from which traffic composition (vehicle class distribution and axle load distribution) data were obtained for sensitivity analysis. ....	6
Figure 3. Monthly truck volume adjustment factors (MEPDG default – no monthly adjustment) for baseline new HMA pavement section. ....	7
Figure 4. AADTT distribution by vehicle class for baseline new HMA pavement section (obtained from LTPP ID 39_9006). ....	8
Figure 5. Hourly truck distribution (MEPDG default) for baseline new HMA pavement section. ....	8
Figure 6. Truck traffic growth factor (8.44 percent linear growth assumed) for baseline new HMA pavement section. ....	9
Figure 7. Estimates of truck traffic applications for baseline new HMA pavement section over a 20 year period (initial 2-way AADTT = 12,893, directional distribution = 0.5, lane distribution = 0.825, and annual growth rate = 8.44 percent, linear) results in 70 million trucks. ....	9
Figure 8. Single axle distribution for each truck class (averaged over all months) for baseline new HMA pavement section (obtained from LTPP ID 39_9006). ....	10
Figure 9. Tandem axle distribution for each truck class (averaged over all months) for baseline new HMA pavement section (obtained from LTPP ID 39_9006). ....	10
Figure 10. Tridem axle distribution for each truck class (averaged over all months) for baseline new HMA pavement section (obtained from LTPP ID 39_9006).....	11
Figure 11. Quad axle distribution for each truck class (averaged over all months) for baseline new HMA pavement section (obtained from LTPP ID 39_9006).....	11
Figure 12. Lateral truck wander and mean number axles/truck for baseline new HMA pavement section (obtained from LTPP ID 39_9006).....	12
Figure 13. Truck axle configuration and tire pressure for baseline new HMA pavement section (MEPDG defaults).....	12
Figure 14. Truck tractor wheel base spacing and percentage for baseline new HMA pavement section (MEPDG defaults). ....	13
Figure 15. Map of Ohio highlighting the locations of cities/ weather stations used for simulating climatic conditions for sensitivity analysis Newark-Heath Airport used for baseline design).....	15
Figure 16. Climatic data input for baseline new HMA pavement section. ....	15
Figure 17. Baseline conventional new HMA pavement design to be used in sensitivity analysis.....	16
Figure 18. Layers used for baseline new HMA pavement section. ....	17
Figure 19. HMA layer thicknesses and gradations for baseline new HMA design.....	19
Figure 20. HMA layer binder properties for baseline new HMA pavement section.....	19
Figure 21. HMA layer mixture properties for baseline new HMA pavement section. ..	20

## LIST OF FIGURES, CONTINUED

Figure 22. HMA creep compliance properties for baseline new HMA pavement section (Superpave HMA Mix Surface Course, ODOT Item 442, Type A, 12.5mm (MEPDG Layer 1)).	20
Figure 23. Properties of unbound granular base layer for baseline new HMA pavement section.	22
Figure 24. Properties of unbound base layer for baseline new HMA pavement section.	22
Figure 25. Structural properties of subgrade for baseline new HMA pavement section.	23
Figure 26. Properties of subgrade soil for baseline new HMA pavement section.	24
Figure 27. Plot of mean predicted longitudinal cracking versus pavement age.	26
Figure 28. Plot of mean predicted alligator cracking versus pavement age.	26
Figure 29. Plot of mean predicted rutting versus pavement age.	27
Figure 30. Plot of mean predicted IRI versus pavement age.	27
Figure 31. Plot of mean predicted low temperature transverse cracking versus pavement age.	28
Figure 32. Plot of age versus top-down fatigue (longitudinal) cracking showing the effect of base type.	33
Figure 33. Plot of age versus bottom-up fatigue (alligator) cracking showing the effect of base type.	34
Figure 34. Plot of age versus temperature related (transverse) cracking showing the effect of base type.	34
Figure 35. Plot of age versus rutting showing the effect of base type.	35
Figure 36. Plot of age versus IRI showing the effect of base type.	35
Figure 37. Map of Ohio highlighting the locations of cities/ weather stations used for simulating climatic conditions for sensitivity analysis.	37
Figure 38. Plot of age versus top-down fatigue (longitudinal) cracking showing the effect of climate across Ohio.	37
Figure 39. Plot of age versus bottom-up fatigue (alligator) cracking showing the effect of climate across Ohio.	38
Figure 40. Plot of age versus low temperature related (transverse) cracking showing the effect of climate across Ohio.	38
Figure 41. Plot of age versus rutting showing the effect of climate across Ohio.	39
Figure 42. Plot of age versus rutting showing the effect of climate across Ohio.	39
Figure 43. Plot of age versus IRI showing the effect of climate across Ohio.	40
Figure 44. Plot of age versus top-down fatigue (longitudinal) cracking showing the effect of total HMA thickness.	41
Figure 45. Plot of age versus bottom-up fatigue (alligator) cracking showing the effect of total HMA thickness.	41
Figure 46. Plot of age versus temperature related (transverse) cracking showing the effect of total HMA thickness.	42

## LIST OF FIGURES, CONTINUED

Figure 47. Plot of age versus rutting showing the effect of total HMA thickness. ....	42
Figure 48. Plot of age versus IRI showing the effect of total HMA thickness. ....	43
Figure 49. Plot of age versus top-down fatigue (longitudinal) cracking showing the effect of subgrade type. ....	45
Figure 50. Plot of age versus bottom-up fatigue (alligator) cracking showing the effect of subgrade type. ....	45
Figure 51. Plot of age versus temperature related (transverse) cracking showing the effect of subgrade type. ....	46
Figure 52. Plot of age versus rutting showing the effect of subgrade type. ....	46
Figure 53. Plot of age versus IRI showing the effect of subgrade type. ....	47
Figure 54. Plot of age versus top-down fatigue (longitudinal) cracking showing the effect of stabilizing/treating the top 12-in of the subgrade soil. ....	48
Figure 55. Plot of age versus bottom-up fatigue (alligator) cracking showing the effect of stabilizing/treating the top 12-in of the subgrade soil. ....	48
Figure 56. Plot of age versus temperature related (transverse) cracking showing the effect of stabilizing/treating the top 12-in of the subgrade soil. ....	49
Figure 57. Plot of age versus rutting showing the effect of stabilizing/treating the top 12-in of the subgrade soil. ....	49
Figure 58. Plot of age versus IRI showing the effect of stabilizing/treating the top 12-in of the subgrade soil. ....	50
Figure 59. Plot of age versus bottom-up fatigue (alligator) cracking showing the effect of HMA in situ air void content in lower most HMA layer (MEPDG layer 3). ....	51
Figure 60b. Plot of age versus rutting showing the effect of HMA in situ air void content in the top layers (MEPDG layers 1 & 2). ....	52
Figure 61. Plot of age versus IRI showing the effect of HMA in situ air void content in the top layers (MEPDG layers 1 & 2). ....	53
Figure 62a. Plot of age versus alligator cracking showing the effect of HMA asphalt binder content (MEPDG layer 3). ....	54
Figure 63. Plot of age versus rutting showing the effect of HMA asphalt binder content (MEPDG layers 1 and 2). ....	55
Figure 64. Plot of age versus IRI showing the effect of HMA asphalt binder content (MEPDG layers 1 and 2). ....	56
Figure 65. Plot of age versus bottom-up fatigue (alligator) cracking showing the combined effect of varying HMA binder and air voids content in lower most HMA layer (MEPDG layer 3). ....	57
Figure 66. Plot of age versus rutting showing the effect of the combined effect of varying HMA binder and air voids content in the top layers (MEPDG layers 1 & 2). ....	57
Figure 67. Plot of age versus IRI showing the combined effect of varying HMA binder and air voids content in the top two HMA layers (MEPDG layers 1 & 2). ....	58

## LIST OF FIGURES, CONTINUED

Figure 68. Plot of age versus bottom-up fatigue (alligator) cracking showing the effect of traffic. ....	62
Figure 69. Plot of age versus rutting showing the effect of traffic. ....	62
Figure 70. Plot of age versus IRI showing the effect of traffic. ....	63
Figure 71. Plot of age versus top-down fatigue (longitudinal) cracking showing the effect of HMA mix type. ....	64
Figure 72. Plot of age versus bottom-up fatigue (alligator) cracking showing the effect of HMA mix type. ....	65
Figure 73. Plot of age versus temperature related (transverse) cracking showing the effect of HMA mix type. ....	65
Figure 74. Plot of age versus rutting showing the effect of HMA mix type. ....	66
Figure 75. Plot of age versus IRI showing the effect of HMA mix type. ....	66
Figure 76. General information for baseline new JPCP section. ....	69
Figure 77. Climatic data input for baseline new JPCP section. ....	70
Figure 78. Layers used for baseline new JPCP section. ....	71
Figure 79. PCC layer general and thermal properties used in baseline new JPCP section. ....	72
Figure 80. PCC mix properties used in baseline new JPCP section. ....	73
Figure 81. PCC strength properties used in baseline new JPCP section. ....	73
Figure 82. Properties of unbound granular base layer for baseline new JPCP section. ....	74
Figure 83. Properties of unbound base layer for baseline new JPCP section. ....	74
Figure 84. Structural properties of subgrade for baseline new JPCP section. ....	75
Figure 85. Properties of subgrade soil for baseline new JPCP section. ....	75
Figure 86. JPCP design features for baseline new JPCP section. ....	76
Figure 87. Plot showing predicted faulting versus age for baseline design. ....	77
Figure 88. Plot showing predicted percent slabs cracked versus age for baseline design. ....	78
Figure 89. Plot showing predicted IRI versus age for baseline design. ....	78
Figure 90. Plot of age versus transverse joint faulting showing the effect of base type. ....	81
Figure 91. Plot of age versus percent slabs cracked showing the effect of base type. ....	82
Figure 92. Plot of age versus IRI showing the effect of base type. ....	82
Figure 93. Map of Ohio highlighting the locations of cities/weather stations used for simulating climatic conditions for sensitivity analysis. ....	84
Figure 94. Plot of transverse joint faulting after a 20 year service life showing the effect of climate. ....	84
Figure 95. Plot of percent slabs cracked after a 20 year service life showing the effect of climate. ....	85
Figure 96. Plot of IRI after a 30 year service life showing the effect of climate. ....	85

## LIST OF FIGURES, CONTINUED

Figure 97. Plot of age versus transverse joint faulting showing the effect of PCC slab thickness and dowel diameter.....	86
Figure 98. Plot of age versus percent slabs cracked showing the effect of PCC slab thickness. ....	87
Figure 99. Plot of age versus IRI showing the effect of PCC slab thickness and dowel diameter.....	87
Figure 100. Plot of age versus transverse joint faulting showing the effect of subgrade type.....	90
Figure 101. Plot of age versus percent slabs cracked showing effect of subgrade type.....	90
Figure 102. Plot of age versus IRI showing the effect of subgrade type. ....	91
Figure 103. Plot of age versus transverse joint faulting showing the effect of stabilizing/treating the top 12-in of the subgrade soil. ....	92
Figure 104. Plot of age versus percent slabs cracked showing the effect of stabilizing/treating the top 12-in of the subgrade soil. ....	92
Figure 105. Plot of age versus IRI showing showing the effect of stabilizing/ treating the top 12-in of the subgrade soil. ....	93
Figure 106. Plot of age versus transverse joint faulting showing the effect of the JPCP slab length.....	94
Figure 107. Plot of age versus percent slabs cracked showing the effect of the JPCP slab length.....	94
Figure 108. Plot of age versus IRI showing the effect of the JPCP slab length.....	95
Figure 109. Plot of age versus transverse joint faulting showing the effect of CTE .....	96
Figure 110. Plot of age versus percent slabs cracked showing the effect of CTE. ....	96
Figure 111. Plot of age versus IRI showing the effect of CTE.....	97
Figure 112. Plot of age versus transverse joint faulting showing the effect using load transfer devices in the JPCP slab. ....	98
Figure 113. Plot of age versus percent slabs transversely cracked showing the effect using load transfer devices in the JPCP slab. ....	99
Figure 114. Plot of age versus IRI showing the effect of using load transfer devices in the JPCP slab.....	99
Figure 115. Plot of age versus transverse joint faulting showing the effect of PCC flexural strength and modulus of elasticity.....	101
Figure 116. Plot of age versus percent slabs cracked showing the effect of PCC flexural strength and modulus change. ....	101
Figure 117. Plot of age versus IRI showing the effect of PCC flexural strength and modulus change.....	102
Figure 118. Plot of age versus transverse joint faulting showing the effect of JPCP slab width. ....	103
Figure 119. Plot of age versus percent slabs cracked showing the effect of JPCP slab width. ....	103

## LIST OF FIGURES, CONTINUED

Figure 120. Plot of age versus IRI showing the effect of JPCP slab width.....	104
Figure 121. Plot of age versus transverse joint faulting showing the effect of changing aggregate type in baseline PCC.....	105
Figure 122. Plot of age versus percent slabs cracked showing the effect of changing aggregate type in baseline PCC.....	105
Figure 123. Plot of age versus IRI showing the effect of changing aggregate type in baseline PCC. ....	106
Figure 124. Plot of age versus transverse joint faulting showing the effect of type of PCC and aggregate.....	107
Figure 125. Plot of age versus percent slabs cracked showing the effect of type of PCC and aggregate.....	107
Figure 126. Plot of age versus IRI showing the effect of type of PCC and aggregate.....	108
Figure 127. Plot of age versus transverse joint faulting showing the effect of pavement edge support.....	109
Figure 128. Plot of age versus percent slabs cracked showing the effect of pavement edge support.....	109
Figure 129. Plot of age versus IRI showing the effect of pavement edge support. ....	110
Figure 130. Plot of age versus transverse joint faulting showing the effect of traffic composition. ....	111
Figure 131. Plot of age versus percent slabs cracked showing the effect of traffic composition. ....	111
Figure 132. Plot of age versus IRI showing the effect of traffic composition. ....	112
Figure 133. Existing JRCP structure prior to rehabilitation (i.e. rubblization and rolling, and placement of HMA overlay).....	114
Figure 134. General information for baseline HMA over rubblized PCC design. ....	115
Figure 135. Baseline HMA over Rubblized PCC pavement design to be used in sensitivity analysis. ....	116
Figure 136. Layers used for baseline HMA over Rubblized PCC pavement section....	117
Figure 137. Properties of rubblized PCC layer for baseline HMA over rubblized PCC pavement section.....	118
Figure 138. Plot of predicted longitudinal cracking versus pavement age. ....	119
Figure 139. Plot of predicted alligator cracking versus pavement age. ....	119
Figure 140. Plot of predicted total rutting versus pavement age.....	120
Figure 141. Plot of predicted IRI versus pavement age.....	120
Figure 142. Plot of predicted transverse cracking versus pavement age.....	121
Figure 143. Plot of age versus top-down fatigue (longitudinal) cracking showing the effect of total HMA overlay thickness. ....	123
Figure 144. Plot of age versus bottom-up fatigue (alligator) cracking showing the effect of total HMA overlay thickness.....	123

## LIST OF FIGURES, CONTINUED

Figure 145. Plot of age versus rutting showing the effect of total HMA overlay thickness. ....	124
Figure 146. Plot of age versus IRI showing the effect of total HMA overlay thickness. ....	124
Figure 147. Plot of age versus bottom-up fatigue (alligator) cracking showing the effect of rubblized PCC modulus. ....	126
Figure 148. Plot of age versus rutting cracking showing the effect of rubblized PCC modulus .....	126
Figure 149. Plot of age versus IRI showing the effect of rubblized PCC modulus .....	127
Figure 150. Plot of age versus bottom-up fatigue (alligator) cracking showing the effect of rubblized PCC thickness. ....	128
Figure 151. Plot of age versus rutting showing the effect of rubblized PCC thickness. ....	128
Figure 152. Plot of age versus IRI showing the effect of rubblized PCC thickness.....	129
Figure 153. General information for the baseline unbonded JPCP overlay over existing JRCP design.....	132
Figure 154. Baseline JPCP overlay over existing JRCP design (modeled as a JPCP). ...	133
Figure 155. Structure of baseline JPCP overlay over existing JRCP design.....	134
Figure 156. HMA separation layer properties for the baseline unbonded JPCP over existing JRCP design. ....	135
Figure 157. Existing JPCP slab mix and strength properties used in the baseline unbonded JPCP over existing JRCP design.....	138
Figure 158. Unbonded JPCP overlay design parameters used in the baseline design.	138
Figure 159. Plot showing predicted faulting versus age. ....	139
Figure 160. Plot showing predicted percent slabs cracked versus age. ....	140
Figure 161. Plot showing predicted IRI versus age.....	140
Figure 162. Plot of unbonded overlay age versus transverse joint faulting showing the effect of HMA separation layer thickness.....	143
Figure 163. Plot of unbonded overlay age versus percent slabs cracked showing the effect of HMA separation layer thickness.....	144
Figure 164. Plot of unbonded overlay age versus IRI showing the effect of HMA separation layer thickness. ....	144
Figure 165. Plot of age versus transverse joint faulting showing the effect using load transfer devices. ....	145
Figure 166. Plot of age versus percent slabs cracked showing the effect using load transfer devices. ....	146
Figure 167. Plot of age versus IRI showing the effect using load transfer devices. ....	146
Figure 168. Plot of age versus transverse joint faulting showing the effect of CTE.....	147
Figure 169. Plot of age versus percent slabs cracked showing the effect of CTE. ....	148
Figure 170. Plot of age versus IRI showing the effect of CTE.....	148

## LIST OF FIGURES, CONTINUED

Figure 171. Plot of age versus transverse joint faulting showing the effect of overlay flexural strength.....	149
Figure 172. Plot of age versus percent slabs cracked showing the effect of overlay flexural strength.....	150
Figure 173. Plot of age versus IRI showing the effect of overlay flexural strength.....	150
Figure 174. Plot of age versus transverse joint faulting showing the effect of overlay thickness. ....	151
Figure 175. Plot of age versus percent slabs cracked showing the effect of overlay thickness. ....	152
Figure 176. Plot of age versus IRI showing the effect of overlay thickness.....	152
Figure 177. Plot of age versus transverse joint faulting showing the effect of overlay joint spacing. ....	153
Figure 178. Plot of age versus percent slabs cracked showing the effect of overlay joint spacing. ....	154
Figure 179. Plot of age versus IRI showing the effect of overlay joint spacing.....	154
Figure 180. Plot of age versus transverse joint faulting showing the effect of overlay slab width. ....	155
Figure 181. Plot of age versus percent slabs cracked showing the effect of overlay slab width. ....	156
Figure 182. Plot of age versus IRI showing the effect of overlay slab width. ....	156
Figure 183. Plot of age versus transverse joint faulting showing the effect of changing aggregate type in baseline overlay concrete. ....	157
Figure 184. Plot of age versus percent slabs cracked showing the effect of changing aggregate type in baseline overlay concrete.....	158
Figure 185. Plot of age versus IRI showing the effect of changing aggregate type in baseline overlay concrete. ....	158
Figure 186. Plot of age versus transverse joint faulting showing the effect of existing JRCF elastic modulus.....	159
Figure 187. Plot of age versus percent slabs cracked showing the effect of existing slab elastic modulus.....	160
Figure 188. Plot of age versus IRI showing the effect of existing slab elastic modulus. ....	160
Figure 189. Plot of age versus transverse joint faulting showing the effect of pavement edge support. ....	161
Figure 190. Plot of age versus percent slabs cracked showing the effect of pavement edge support. ....	162
Figure 191. Plot of age versus IRI showing the effect of pavement edge support. ....	162

## LIST OF TABLES

Table 1. Detailed description of these LTPP sites location and highway characteristics.	5
Table 2. Description of default MEPDG weather stations in Ohio.....	14
Table 3. Summary of baseline design layer properties.....	18
Table 4. Summary of predicted distress and IRI obtained from the MEPDG (with national calibration coefficients). .....	28
Table 5. Input parameters of interest to be used for new HMA sensitivity analysis.....	30
Table 6. Summary of HMA Base layer material properties.....	31
Table 7. Summary of HMA SMA layer material properties (ODOT Item 443). .....	32
Table 8. Relative effect of base type on HMA pavement distress and IRI.....	36
Table 9. Relative effect of climate on HMA distress and IRI. ....	40
Table 10. Relative effect of HMA thickness on HMA distress and IRI. ....	43
Table 11. Recommended subgrade resilient modulus input (at optimum density and moisture) for flexible pavements and rehabilitation of flexible pavements....	44
Table 12. Relative effect of subgrade type on HMA distress and IRI.....	47
Table 13. Relative effect of subgrade treatment on HMA distress and IRI. ....	50
Table 14. Relative effect of HMA air voids on HMA distress and IRI. ....	53
Table 15. Relative effect of HMA volumetric binder content on HMA distress and IRI. ....	56
Table 16. Traffic description and corresponding vehicle (truck) class distribution values (percentages). ....	59
Table 17. Number of Single Axles/truck for the 12 LTPP Sites. ....	59
Table 18. Number of Tandem Axles/truck values for the vehicle (truck) class distribution.....	60
Table 19. Number of Tridem Axles/truck values for the vehicle (truck) class distribution.....	60
Table 20. Number of Quad Axles/truck values (percentages) for the vehicle (truck) class distribution. ....	61
Table 21. Relative effect of vehicle classification and axle load distribution on HMA distress and IRI.....	63
Table 22. Relative effect of HMA mix type on HMA distress and IRI. ....	67
Table 23. Summary of distress/IRI predicts for new JPCP baseline design. ....	79
Table 24. Input parameters of interest to be used for new JPCP sensitivity analysis. ....	80
Table 25. Relative effect of base type on JPCP distress and IRI. ....	83
Table 26. Relative effect of climate on JPCP distress and IRI. ....	86
Table 27. Relative effect of slab thickness on JPCP distress and IRI.....	88
Table 28. Recommended Subgrade/Embankment Resilient Modulus Input (at optimum density and moisture) for Rigid Pavements and Rehabilitation of Rigid Pavements. . ....	89
Table 29. Relative effect of subgrade type on JPCP distress and IRI.....	91
Table 30. Relative effect of subgrade treatment on JPCP distress and IRI. ....	93
Table 31. Relative effect of transverse joint spacing on JPCP distress and IRI. ....	95

## LIST OF TABLES, CONTINUED

Table 32. Relative effect of concrete coefficient of thermal expansion (CTE) on JPCP distress and IRI.....	97
Table 33. Relative effect of transverse joint load transfer devices on JPCP distress and IRI. ....	100
Table 34. Relative effect of concrete flexural strength and modulus of elasticity on JPCP distress and IRI.....	102
Table 35. Relative effect of slab width (12, 13, and 14-ft) on JPCP distress and IRI. ....	104
Table 36. Relative effect of coarse aggregate type on JPCP distress and IRI.....	106
Table 37. Relative effect of concrete class and coarse aggregate type on JPCP distress and IRI.....	108
Table 38. Relative effect of edge support on JPCP distress and IRI.....	110
Table 39. Relative effect of traffic composition on JPCP distress and IRI.....	112
Table 40. Summary of predicted distress and IRI obtained from the MEPDG for HMA overlay of rubblized JRCP. ....	121
Table 41. Input parameters of interest to be used for HMA over Rubblized PCC sensitivity analysis. ....	122
Table 42. Relative effect of HMA overlay thickness on HMA/rubblized PCC distress and IRI. ....	125
Table 43. Relative effect of rubblized PCC modulus on HMA overlay distress and IRI. ....	127
Table 44. Relative effect of rubblized PCC thickness on HMA distress and IRI. ....	129
Table 45. Summary of baseline design HMA separation layer properties. ....	135
Table 46. Summary of distress/IRI predicts for baseline unbonded JPCP over existing JRCP design.....	141
Table 47. Input parameters to be used in JPCP overlay over existing JRCP sensitivity analysis. ....	142
Table 48. Relative effect of HMA separation layer thickness on overlay distress and IRI. ....	145
Table 49. Relative effect of transverse joint load transfer devices on overlay distress and IRI. ....	147
Table 50. Relative effect of concrete coefficient of thermal expansion (CTE) on JPCP overlay distress and IRI.....	149
Table 51. Relative effect of concrete overlay flexural strength and modulus on overlay distress and IRI.....	151
Table 52. Relative effect of concrete overlay thickness on overlay distress and IRI. ....	153
Table 53. Relative effect of concrete overlay joint spacing on overlay distress and IRI. ....	155
Table 54. Relative effect of concrete overlay slab width (12, 13 and 14-ft) on overlay distress and IRI.....	157
Table 55. Relative effect of coarse concrete overlay aggregate type on overlay distress and IRI.....	159

## LIST OF TABLES, CONTINUED

Table 56. Relative effect of existing slab elastic modulus on overlay distress and IRI.	161
Table 57. Relative effect of edge support on overlay distress and IRI. ....	163
Table 58. New HMA pavement summary of sensitivity results and input recommendations.....	166
Table 59. New JPCP pavement summary of sensitivity results and input recommendations.....	168
Table 60. HMA overlay over rubblized PCC pavement summary of sensitivity results and input recommendations.. ....	171
Table 61. Unbonded JPCP Overlay Summary of Sensitivity Results and Input Recommendations.....	172

THIS PAGE INTENTIONALLY LEFT BLANK

# CHAPTER 1. INTRODUCTION

## Background and Need for Sensitivity Analysis

A sensitivity analysis is the process of varying model input parameters (subgrade type, asphalt grade, base type, PCC strength, etc.) over a practical range and observing the relative change in model response (e.g., HMA rutting, JPCP transverse joint faulting, HMA fatigue [bottom-up] cracking, and IRI). By doing this for typical Ohio conditions, the mechanistic-empirical pavement design guide (MEPDG) inputs can be rated according to their overall effect on pavement performance in Ohio. The information gathered through the sensitivity analysis is beneficial in determining (1) level of importance of each data item needed for pavement design/analysis using the MEPDG and (2) strategies for data collection activities. Both of these items are important for the successful implementation of the MEPDG in Ohio. In general, more accurate estimates are required for the inputs for which the MEPDG models are very sensitive as opposed to inputs for which the MEPDG models are relatively insensitive.

## Selected New and Rehabilitated Pavement Baseline Designs

The major new or reconstruct pavement design types considered by ODOT are (1) deep-strength hot-mix asphalt (HMA) pavement and (2) jointed plain concrete pavement (JPCP). The two major existing rigid pavement rehabilitation design types considered are (1) HMA over a rubblized portland cement concrete (PCC) pavement and (2) unbonded JPCP over an existing PCC pavement. Baseline designs were developed for each of these four new and rehabilitation types using a central Ohio location site conditions and other inputs that would typically be used. The baseline designs were then used for a comprehensive sensitivity analysis by varying the values of key inputs over a practical range and determining their impact on predictions of the Mechanistic Empirical Pavement Design Guide (MEPDG) performance models. Recommendations as to the importance of each input were developed for use in further MEPDG implementation activities.

The baseline designs were reviewed by ODOT for accuracy and reasonableness. After ODOT's review and comment, a detailed sensitivity analysis using the nationally calibrated MEPDG models was performed for various input factors around the input values established for the baseline designs.

## Scope of the Report

This report presents the results of a sensitivity analysis performed for major Ohio DOT (ODOT) new pavement and rehabilitation of existing rigid pavement designs. Chapter 2

describes the new HMA baseline design and presents the results of the sensitivity analysis. Chapter 3 describes the new JPCP baseline design and presents the results of the sensitivity analysis. Chapter 4 describes the HMA overlay of rubblized JPCP baseline design and presents the results of the sensitivity analysis. Chapter 5 describes the JPCP unbonded overlay baseline design and presents the results of the sensitivity analysis. Chapter 6 provides a summary and conclusions for all of the baseline designs and inputs.

## CHAPTER 2. SENSITIVITY ANALYSIS FOR NEW HMA PAVEMENT

### Overview

The baseline ODOT new/reconstruct HMA pavement design used for sensitivity analysis was developed using information gathered from various sources including (1) ODOT pavement design and construction specifications and manuals, (2) ODOT research reports, and (3) the Long-Term Pavement Program (LTPP) database. A description of the “baseline” ODOT HMA pavement design is presented in this chapter.

Sensitivity analysis was conducted by varying the design features, material properties, climate, etc. of the baseline design to determine how changes to these MEPDG input parameters influences the prediction of the following key HMA pavement distresses:

- Longitudinal “top down” fatigue cracking.
- Alligator “bottom-up” fatigue cracking.
- Rutting (HMA rutting and total measured rutting at the pavement surface).
- Transverse “low temperature” cracking.
- Smoothness expressed in terms of the International Roughness Index (IRI).

The results of the sensitivity analysis are presented at the end of this chapter.

### Baseline New HMA Pavement Construction Date and Analysis Period

The baseline ODOT HMA pavement was assumed to be constructed in September/October and opened to traffic in November of the same year. An analysis period of 20 years was selected which covers the service life of the typical ODOT new HMA pavement. Figure 1 shows the dates of construction and opening to traffic for the baseline ODOT HMA design.

Figure 1. General information for baseline new HMA pavement section.

### **Baseline New HMA Pavement Section Analysis Parameters (Initial IRI and Terminal Distress/IRI)**

The initial IRI at construction for the baseline HMA pavement was assumed to be 63 in/mile.

### **Baseline New HMA Pavement Section Location**

The baseline new HMA pavement section was located in the city of Newark in central Ohio.

### **Baseline New HMA Pavement Section Traffic**

Several inputs are required by the MEPDG to characterize traffic volume and composition. For the baseline design, detailed traffic information (AADT, percent trucks, vehicle and axle load distributions, axles per truck for each vehicle class, etc.) for the 13 LTPP sites in Ohio was examined. The LTPP sites were located on both urban and rural highway corridors with different functional classes. The traffic data for these

LTPP sites were obtained from weigh-in-motion (WIM) stations located throughout Ohio. A detailed description of these LTPP sites location and highway characteristics is presented in table 1. Figure 2 presents the geographic locations of these LTPP sites.

Table 1. Detailed description of these LTPP sites location and highway characteristics.

SHRP ID	Const. Date	Total Lanes (2-way)	Pavement Type	County	Functional Class	Direction of Travel	MP	Route No.	Designation
0100	01-Nov-95	4	AC	Delaware	RPA (non-Interstate)	S	17.48	US-23	R1
0200	01-Oct-96	4	PCC	Delaware	RPA (non-Interstate)	N	17.48	US-23	R2
3013	01-Jul-70	2	PCC	Brown	Rural Minor Arterial	S	19.12	US-68	R3
5003	22-Sep-88	4	PCC	Lorain	RPA (non-Interstate)	E	11.11	US-20	R4
5010	01-Jul-75	4	PCC	Mahoning	RPA (Interstate)	N	14.76	I-680	R5
9006	01-Sep-85	4	PCC	Clinton	RPA (Interstate)	S	5.93	I-71	R6
0900	01-Jan-95	2	AC	Delaware	RPA (non-Interstate)	S	18.5	US-23	R7
3801	23-Dec-83	4	PCC	Belmont	UPA (Freeways or Expressways)	S	12.33	US-7	U1
4018	05-Jul-75	4	PCC	Greene	UPA (Interstate)	N	15.4	I-675	U2
4031	23-May-69	6	PCC	Franklin	UPA (Interstate)	N	9.82	I-270	U3
5569	01-Jun-85	4	PCC	Athens	UPA (Freeways or Expressways)	S	13.41	US-33	U4
7021	29-Jun-85	6	AC/PCC	Wood	UPA (Interstate)	S	31.32	I-75	U5
9022	01-Jun-88	6	PCC	Franklin	UPA (Interstate)	N	32.96	I-270	U6

RPA = Rural Principal Arterial.

UPA = Urban Principal Arterial.

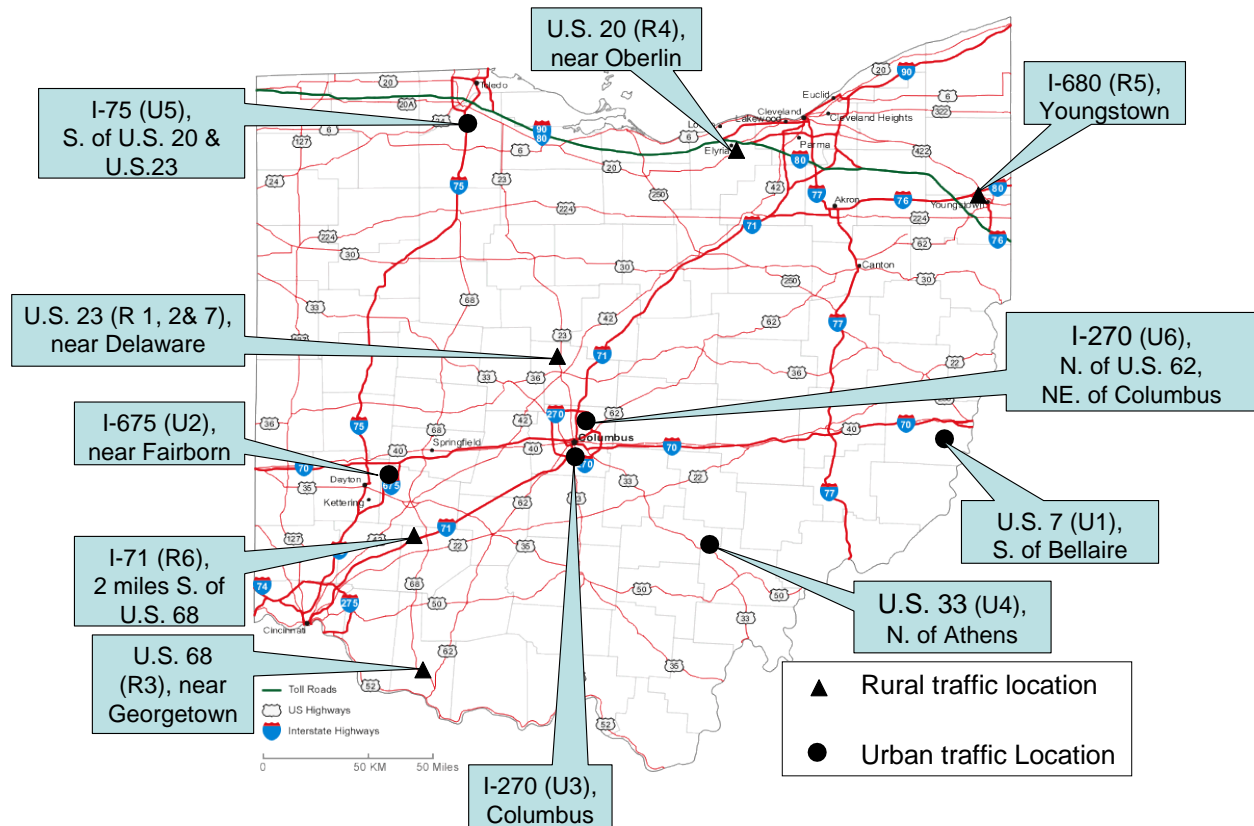


Figure 2. Map of Ohio highlighting LTPP sites from which traffic composition (vehicle class distribution and axle load distribution) data were obtained for sensitivity analysis.

The unique combination of vehicle class and axle load distributions for these LTPP sections were designated R1 through R7 and U1 through U6 for rural and urban highways, respectively (see table 1). For the baseline HMA design, traffic inputs (vehicle class distribution, axle load distribution, etc.) from a typical Ohio 4-lane access controlled rural principal arterial roadway – LTPP Section 39\_9006 – were adopted. LTPP Section 39\_9006 is located on Interstate 71 (south bound outer lane), 2 miles south of US-68 and 3 miles north of ST-73. It is also 1.2 miles south of Gurneyville Road. The pavement section lies South East of Dayton and North East of Cincinnati, ODOT district 8, Clinton County (see figure 1). Approximately 8 years of historic traffic data were available for this site.

LTPP Section 39\_9006 was originally constructed in 1964 and overlaid with a JRCP in 1985. Traffic data are available after 1985. Actual measured traffic for 39\_9006 is presented below. For the baseline design, current ODOT design traffic – 20 year cumulative ESALs = 86 million (flexible) – for high type pavement facilities (i.e. Interstate) was adopted. This translated into approximately 70 million cumulative trucks applied over a 20 year period. This represents a very heavily trafficked highway.

Actual Measured Traffic for LTPP Project 39_9006	Traffic Estimated For Baseline Pavements Based on Current ODOT Design Procedures
<ul style="list-style-type: none"> <li>• 2-way AADT (in 1985) = 22,182.</li> <li>• Percent trucks = 27.1.</li> <li>• 2-way AADTT (in 1985) = 6,011.</li> <li>• Directional distribution = 50 percent.</li> <li>• Lane distribution: <ul style="list-style-type: none"> <li>○ Inner lane (southbound direction) = 17.5 percent.</li> <li>○ Outer lane (southbound direction) = 82.5 percent.</li> </ul> </li> <li>• Growth rate 8.44 percent (linear).</li> </ul>	<ul style="list-style-type: none"> <li>• Cumulative trucks over 20 years = 70 million in heaviest lane (approximately 86 million flexible and 129 million rigid ESALs).</li> <li>• 2-way AADT = 47,576.</li> <li>• Percent trucks = 27.1.</li> <li>• 2-way AADTT = 12,893.</li> <li>• Directional distribution = 50 percent.</li> <li>• Lane distribution: <ul style="list-style-type: none"> <li>○ Inner lane (southbound direction) = 17.5 percent.</li> <li>○ Outer lane (southbound direction) = 82.5 percent.</li> </ul> </li> <li>• Growth rate 8.44 percent (linear).</li> </ul>

Thus, an initial AADTT of 12,893 was used (in design lane, i.e., outer lane in the southbound direction) that corresponds to 70 million trucks over 20 years. Additional traffic inputs adopted for the baseline design (from LTPP Project 39\_9006) are presented in figures 3 through 14. As noted in the figures, MEPDG defaults were assumed for some of the data items where site specific information was not readily available.

Month	Class 4	Class 5	Class 6	Class 7	Class 8	Class 9	Class 10	Class 11	Class 12	Class 13
January	1.00	1.00	1.00	1.00	1.00	1.00	1.00	1.00	1.00	1.00
February	1.00	1.00	1.00	1.00	1.00	1.00	1.00	1.00	1.00	1.00
March	1.00	1.00	1.00	1.00	1.00	1.00	1.00	1.00	1.00	1.00
April	1.00	1.00	1.00	1.00	1.00	1.00	1.00	1.00	1.00	1.00
May	1.00	1.00	1.00	1.00	1.00	1.00	1.00	1.00	1.00	1.00
June	1.00	1.00	1.00	1.00	1.00	1.00	1.00	1.00	1.00	1.00
July	1.00	1.00	1.00	1.00	1.00	1.00	1.00	1.00	1.00	1.00
August	1.00	1.00	1.00	1.00	1.00	1.00	1.00	1.00	1.00	1.00
September	1.00	1.00	1.00	1.00	1.00	1.00	1.00	1.00	1.00	1.00
October	1.00	1.00	1.00	1.00	1.00	1.00	1.00	1.00	1.00	1.00
November	1.00	1.00	1.00	1.00	1.00	1.00	1.00	1.00	1.00	1.00
December	1.00	1.00	1.00	1.00	1.00	1.00	1.00	1.00	1.00	1.00

Figure 3. Monthly truck volume adjustment factors (MEPDG default—no monthly adjustment) for baseline new HMA pavement section.

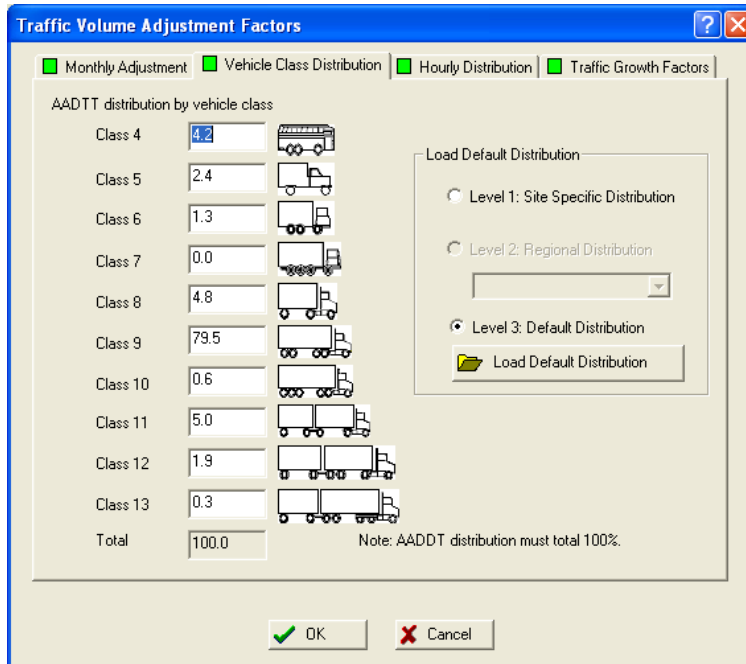


Figure 4. AADTT distribution by vehicle class for baseline new HMA pavement section (obtained from LTPP ID 39\_9006).

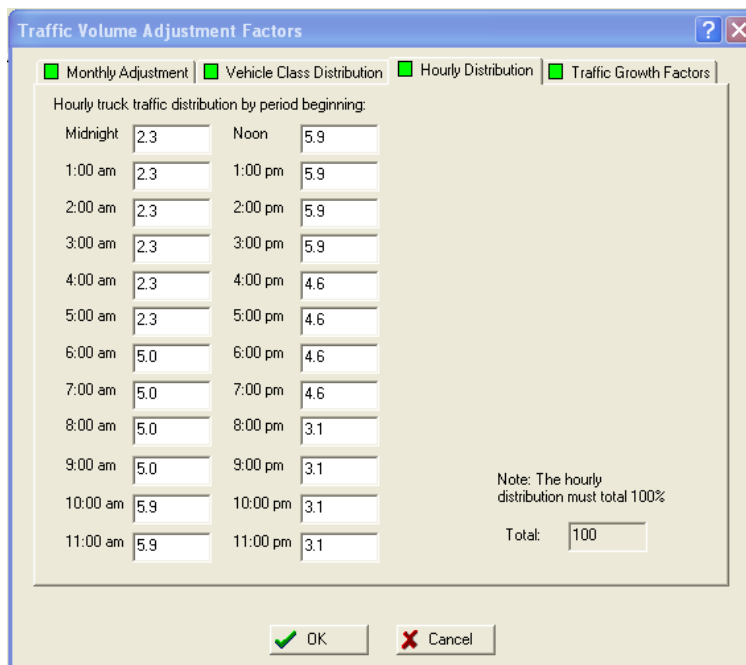


Figure 5. Hourly truck distribution (MEPDG default) for baseline new HMA pavement section.

**Traffic Volume Adjustment Factors**

Monthly Adjustment  
 Vehicle Class Distribution  
 Hourly Distribution  
 Traffic Growth Factors

Opening Date:      
AADTT:  ...

Design Life (years):  ...     
% Traffic Design Direction:

Vehicle-class specific traffic growth     
% Traffic Design Lane:

Default Growth Function:

- No Growth
- Linear Growth
- Compound Growth

Default growth rate (%):

Note: Vehicle-class distribution factors are needed to view the effects of traffic growth.

Figure 6. Truck traffic growth factor (8.44 percent linear growth assumed) for baseline new HMA pavement section.

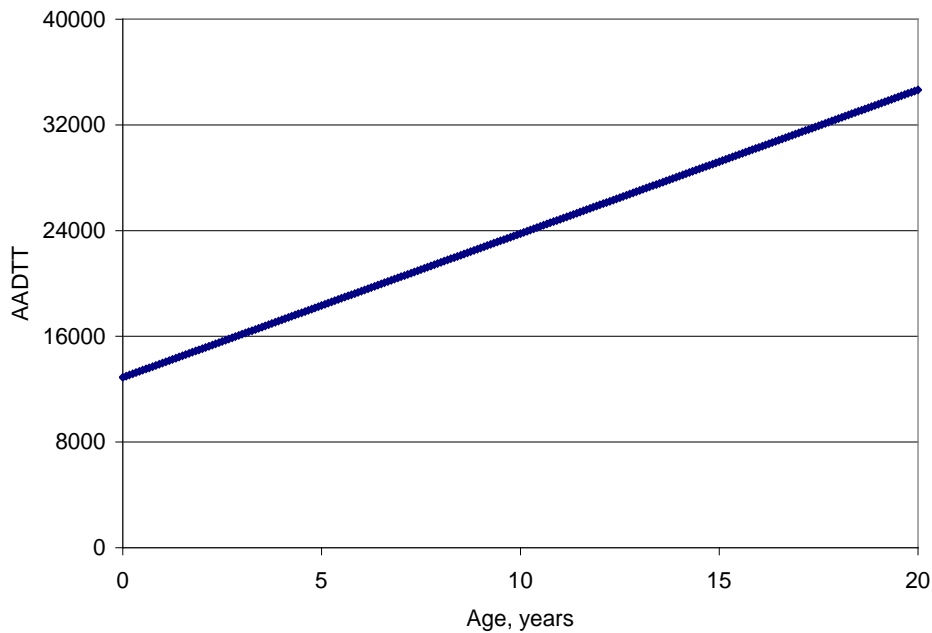


Figure 7. Estimates of truck traffic applications for baseline new HMA pavement section over a 20 year period (initial 2-way AADTT = 12,893, directional distribution = 0.5, lane distribution = 0.825, and annual growth rate = 8.44 percent, linear) results in 70 million trucks.

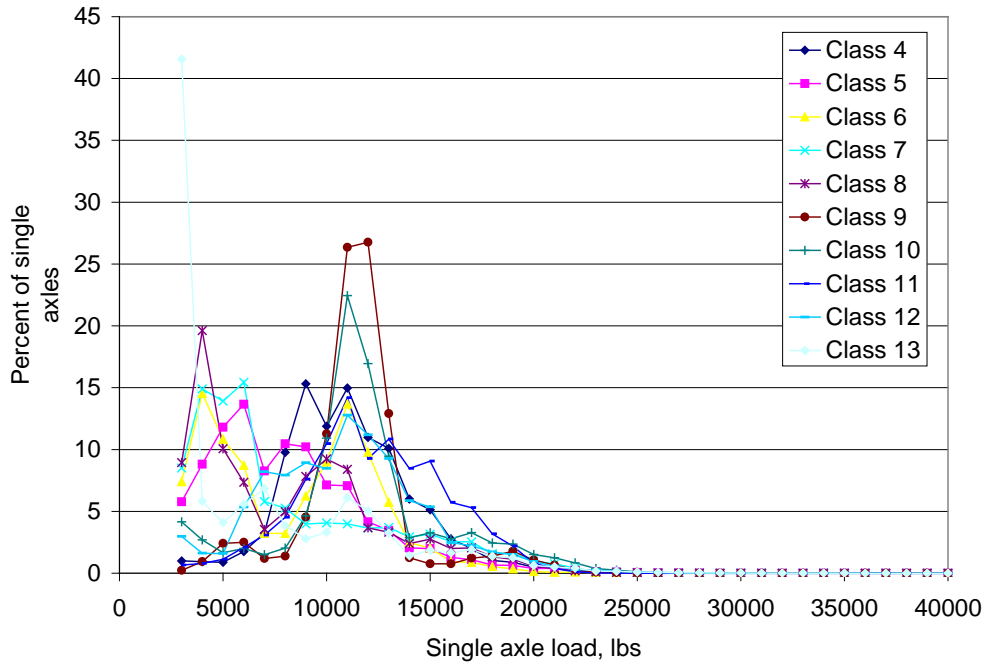


Figure 8. Single axle distribution for each truck class (averaged over all months) for baseline new HMA pavement section (obtained from LTPP ID 39\_9006).

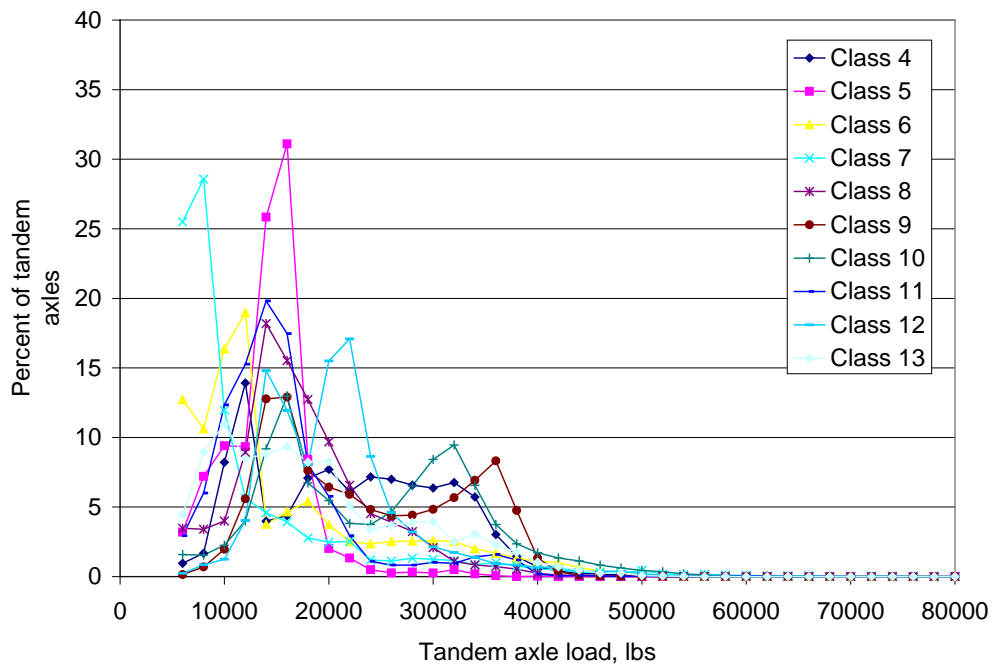


Figure 9. Tandem axle distribution for each truck class (averaged over all months) for baseline new HMA pavement section (obtained from LTPP ID 39\_9006).

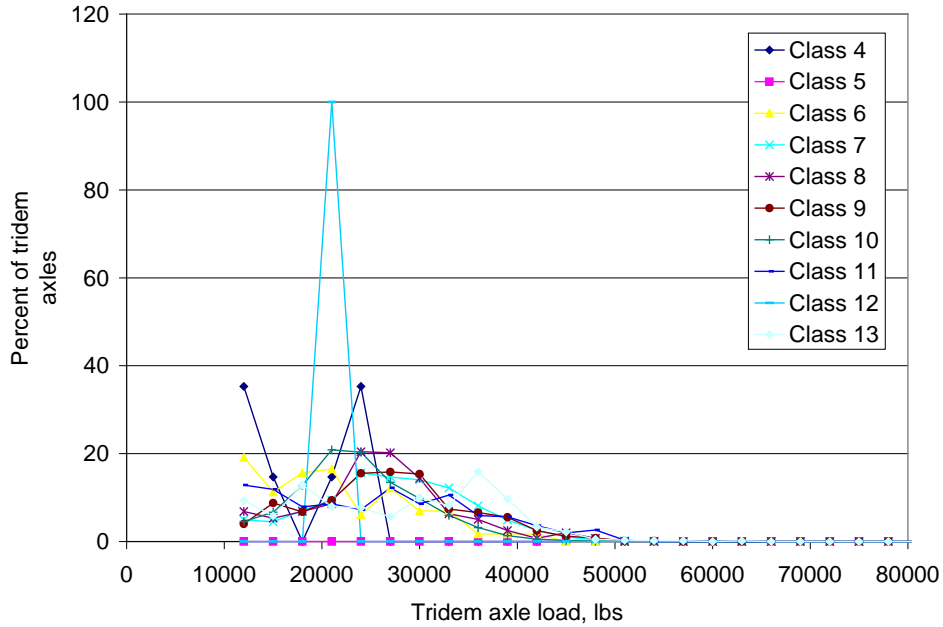


Figure 10. Tridem axle distribution for each truck class (averaged over all months) for baseline new HMA pavement section (obtained from LTPP ID 39\_9006).

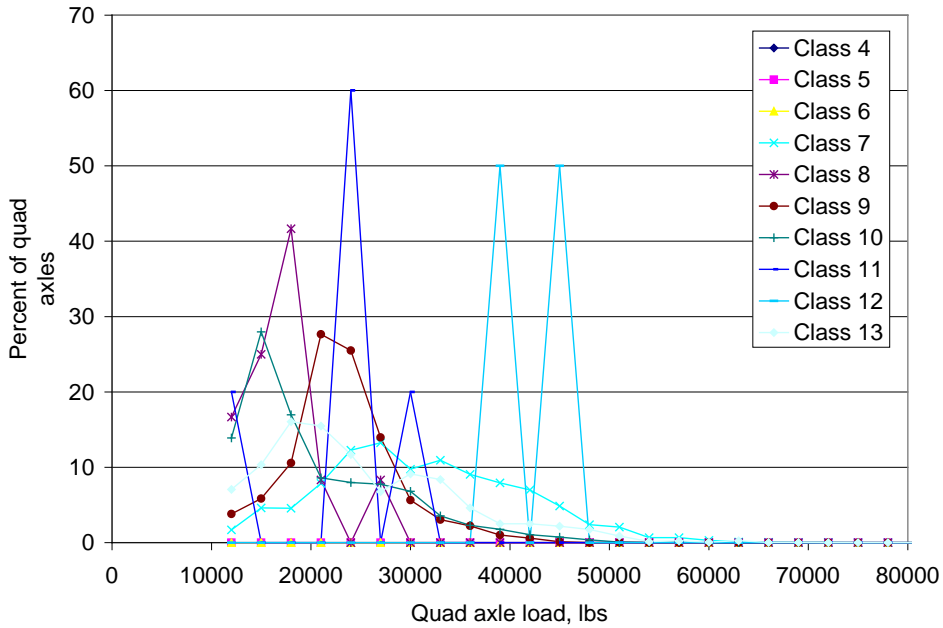


Figure 11. Quad axle distribution for each truck class (averaged over all months) for baseline new HMA pavement section (obtained from LTPP ID 39\_9006).

**General Traffic Inputs** [?] [X]

Lateral Traffic Wander

Mean wheel location (inches from the lane marking):

Traffic wander standard deviation (in):

Design lane width (ft): (Note: This is not slab width)

Number Axles/Truck  Axle Configuration  Wheelbase

	Single	Tandem	Tridem	Quad
Class 4	1.34	0.21	0.00	0.00
Class 5	2.47	0.02	0.00	0.00
Class 6	1.14	0.95	0.01	0.00
Class 7	2.59	0.86	1.07	0.48
Class 8	2.43	0.58	0.00	0.00
Class 9	1.23	1.81	0.00	0.00
Class 10	1.16	1.12	0.66	0.13
Class 11	4.81	0.01	0.01	0.00
Class 12	3.87	0.97	0.00	0.00
Class 13	1.01	0.82	0.33	0.34

[OK] [Cancel]

Figure 12. Lateral truck wander and mean number axles/truck for baseline new HMA pavement section (obtained from LTPP ID 39\_9006).

**General Traffic Inputs** [?] [X]

Lateral Traffic Wander

Mean wheel location (inches from the lane marking):

Traffic wander standard deviation (in):

Design lane width (ft): (Note: This is not slab width)

Number Axles/Truck  Axle Configuration  Wheelbase

Average axle width (edge-to-edge) outside dimensions(ft):

Dual tire spacing (in):

Tire Pressure (psi):

Axle Spacing (in)

Tandem axle:

Tridem axle:

Quad axle:

[OK] [Cancel]

Figure 13. Truck axle configuration and tire pressure for baseline new HMA pavement section (MEPDG defaults).

**General Traffic Inputs**

Lateral Traffic Wander

Mean wheel location (inches from the lane marking): 18

Traffic wander standard deviation (in): 10

Design lane width (ft): (Note: This is not slab width) 12

Number Axles/Truck  Axle Configuration  Wheelbase

Wheelbase distribution information for JPCP top-down cracking. The wheelbase refers to the spacing between the steering and the first device axle of the truck-tractors or heavy single units.

	Short	Medium	Long
Average Axle Spacing (ft)	12	15	18
Percent of trucks (%)	33.0	33.0	34.0

OK Cancel

Figure 14. Truck tractor wheel base spacing and percentage for baseline new HMA pavement section (MEPDG defaults).

### Climatic Data Input for Baseline New HMA Pavement Section

The MEPDG software includes climate data from 27 weather stations located in Ohio. However, since the southeastern part of the State is not well represented by the weather stations in the MEPDG, three additional stations from neighboring West Virginia were included. The data represents hourly temperature, rainfall, percent sunshine, wind speed, and relative humidity at these sites for several years. The weather stations are mostly located at airports as shown in table 2. However, only those weather stations which had no missing weather data during the collection period were selected for the sensitivity analysis. The geographic locations of the selected weather stations with complete data are shown in figure 15.

For the baseline HMA design, a weather station located in central Ohio was selected (Newark-Heath Airport) was adopted (see figure 15). The exact location in terms of longitude and latitude and elevation is as follows:

- Latitude: 40.024.
- Longitude: -82.461.
- Elevation: 884-ft.

Climate data from this weather station was used for the baseline project specific climatic data as shown in figure 16. An annual average ground water table depth of 10-ft was used for this site.

Table 2. Description of default MEPDG weather stations in Ohio.

City	Weather Station Location	Months with Weather Data Available
Akron (1)	Fulton International Airport	82
Akron (2)	Akron-Canton Regional Airport	116
Ashtabula	Ashtabula County Airport	87
Cincinnati	Cincinnati Municipal Airport	101
Cleveland (1)	Brake Lakefront Airport	97
Cleveland (2)	Cleveland-Hopkins International-airport	116
Columbus (1)	Ohio State University airport	100
Columbus (2)	Port Columbus International airport	116
Covington/Cincinnati	Cincinnati/NRN KY International airport	116
Dayton (1)	Dayton-Wright Bros airport	100
Dayton (2)	J M Cox Dayton airport	116
Defiance	Defiance Memorial airport	98
Findlay	Findlay airport	67
Hamilton	Butler County Regional airport	105
Lancaster	Fairfield County airport	116
Lima	Lima-Allen County airport	97
Lorain/Elyria	Lorain County Regional airport	97
Mansfield	Mansfield Lahm Regional airport	116
Marion	Marion Municipal airport	94
New Philadelphia	Harry Clever Field airport	97
Newark*	Newark-Heath airport*	84
Toledo (1)	Metcalf Field airport	98
Toledo (2)	Toledo Express airport	116
Wilmington	Airbourne Airpark airport	95
Wooster	Wayne county airport	110
Youngtown/Warren	Youngtown/Warren Regional airport	116
Zanesville	Zanesville Municipal airport	66
Huntington, WV	M.J. Ferguson airport	114
Parkersburg, WV	Wood County airport	64
Wheeling, WV	Wheeling-Ohio County airport	95

\*Weather station used for baseline designs.

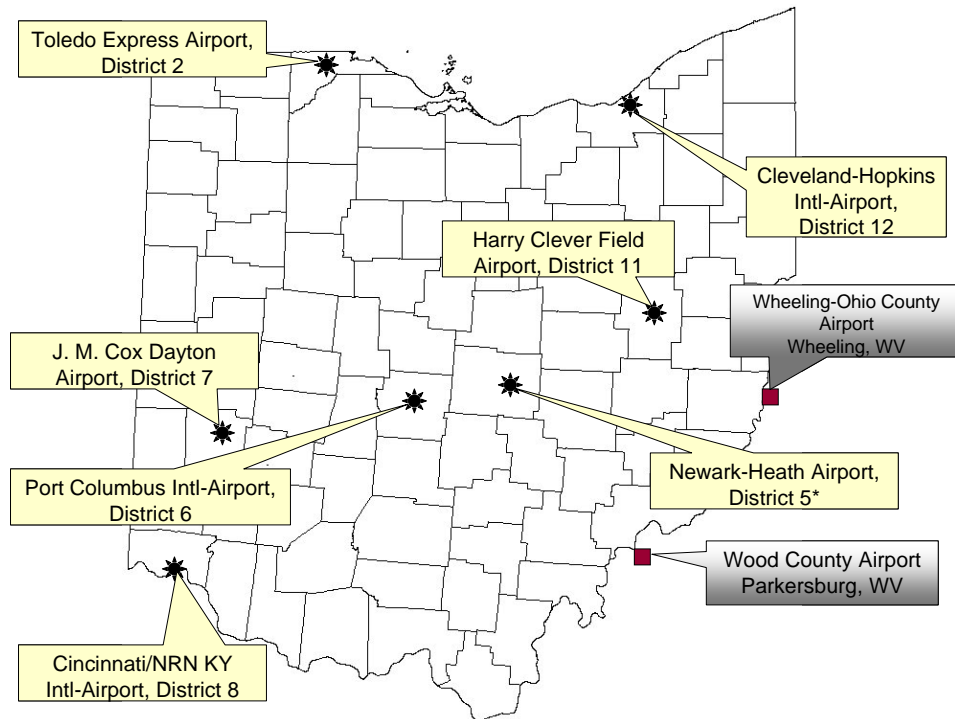


Figure 15. Map of Ohio highlighting the locations of cities/weather stations used for simulating climatic conditions for sensitivity analysis Newark-Heath Airport used for baseline design).

Environment/Climatic

Latitude (degrees.minutes): 40.01  
 Longitude (degrees.minutes): -82.28  
 Elevation (ft): 882

Climatic data for a specific weather station.  
 Interpolate climatic data for given location.

Seasonal

Depth of water table (ft)	
Annual average	10

Note: Ground water table depth is a positive number measured from the pavement surface.

0.0 miles NEWARK, OH - NEWARK-HEATH AIRPORT Lat. 40.01 Lon. -82.28 Ele. 882 Months: 84 (C)  
 20.3 miles LANCASTER, OH - FAIRFIELD COUNTY AIRPORT Lat. 39.46 Lon. -82.4 Ele. 855 Months: 116 (M1)  
 22.2 miles COLUMBUS, OH - PORT COLUMBUS INTL AIRPORT Lat. 39.59 Lon. -82.53 Ele. 849 Months: 116 (C)  
 31.4 miles ZANESVILLE, OH - ZANESVILLE MUNICIPAL ARPT Lat. 39.56 Lon. -81.53 Ele. 881 Months: 66 (C)  
 32.9 miles COLUMBUS, OH - OHIO STATE UNIVERSITY ARPT Lat. 40.05 Lon. -83.05 Ele. 923 Months: 100 (C)  
 52.1 miles MARION, OH - MARION MUNICIPAL AIRPORT Lat. 40.37 Lon. -83.04 Ele. 991 Months: 94 (C)

Generate  
 Cancel

Select stations for generating interpolated climatic files. The best interpolation occurs by selecting stations that are geographically close in differing directions. A station without missing any data is denoted (C)complete. (M#) denotes missing month.  
 Press the Generate button after selecting desired weather stations and inputting Elevation and Depth of Water Table. Missing data for a given station will be interpolated from complete stations.

Figure 16. Climatic data input for baseline new HMA pavement section.

## Pavement Surface Properties for Baseline New HMA Pavement Section

A surface shortwave absorptivity (required by the enhanced integrated climate model embedded in the MEPDG software to predict daily changes in temperature and moisture profiles through the pavement system) of 0.85 was assumed (used in all global calibration work during the development of the MEPDG).

## Layering of the HMA Pavement and Subgrade for Baseline New HMA Pavement

The ODOT baseline new HMA pavement structure (Superpave HMA mix) included a 12.25-in HMA layer over a 6.0-in dense granular aggregate base (A-1-a), over a prepared (A-6) subgrade with the top 12.0-in compacted. The 12.25-in HMA layer consisted of a 1.5-in Superpave HMA mix surface course (ODOT Item 442, type A, 12.5 mm), a 1.75-in Superpave HMA mix intermediate course (ODOT Item 442, type A, 19.0 mm), and a 9.0-in Marshall mix bituminous base course (ODOT Item 302).

The pavement structure used as the baseline design is shown in figure 17. Figure 18 shows the baseline new HMA pavement structure as coded in the MEPDG. The properties of the Superpave HMA and the Marshall Mix layers are presented in the following sections.

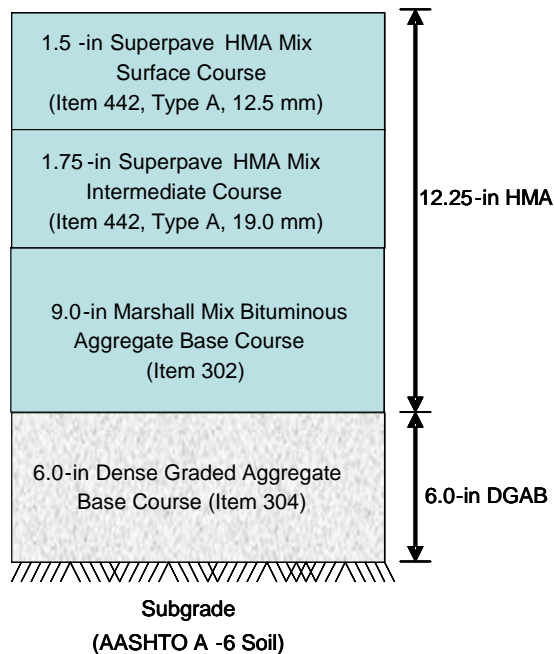


Figure 17. Baseline conventional new HMA pavement design to be used in sensitivity analysis.

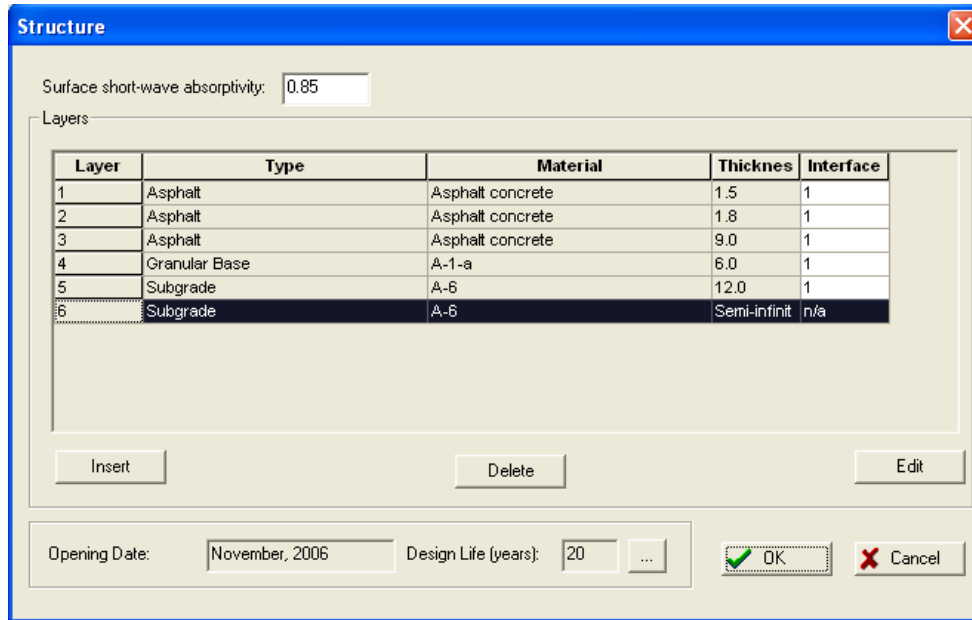


Figure 18. Layers used for baseline new HMA pavement section.

### HMA Mix Properties for New HMA Baseline Design

Typical HMA mix properties were obtained from the ODOT 2005 Construction and Material Specifications (sections 300, 400, and 700), the ODOT 2006 Construction Inspection Manual (sections 300 and 400), and the ODOT Pavement Design & Rehabilitation Manual (section 400). Additional information was obtained from ODOT staff. The information gathered from all of these documents/sources was used to develop baseline Superpave and conventional Marshall HMA layer properties. The HMA properties of interest included unit weight, Poisson's ratio, gradation, asphalt content, and AC binder type. A summary of HMA layer material properties used in sensitivity analysis is presented in table 3. The HMA materials presented in table 3 are recommended by ODOT for use in high-type pavement construction (e.g., Interstates, freeways, etc.).

The MEPDG input screens for the baseline conventional new HMA design are presented in figures 19 to 22. Additional mixture properties are provided below.

- Tensile strength—350 psi (estimated from mix volumetrics using MEPDG Level 3 correlations).
- Total unit weight as-built—145 pcf (assumed)
- Creep compliance for HMA surface course (Item 442, Type A, 12.5 mm) (estimated from mix volumetrics using MEPDG level 3 correlations) (see figure 22).

Table 3. Summary of baseline design layer properties.

Layer No.	Material Type	Binder PG Grade	Gradation (Percent Passing Sieve Size)*													Vol. Binder Content, percent**	In-place HMA Mix Air Voids***
			2-in	1.5-in	1.0-in	3/4-in	1/2-in	3/8-in	No. 4	No. 8	No. 16	No. 30	No. 50	No. 100	No. 200		
1	Superpave HMA Mix Surface Course (Item 442, Type A, 12.5mm)	PG 70-22M	100	100	100	100	98	95	76	41	28	17	10	6	4.1	11.1	5.5
2	Superpave HMA Mix Intermediate Course (Item 442, Type A, 19mm)	PG 64-28	100	100	100	99	86	76	57	35	22	14	10	6	4.0	9.6	5.5
3	Marshall Mix Bituminous Aggregate Base Course (Item 302)	PG 64-22	100	100	83	69	46	39	26	21	17	13	9	6	3.9	8.7	9.5

\* Typical mix design gradations obtained from ODOT. Note that the MEPDG requires only the percent retained on the following sieve sizes 3/4-in, 3/8-in, and No. 4 along with percent passing the No. 200 sieve size for estimating the dynamic modulus.

\*\*Estimated based on VMA and estimated in-place air voids etc.

\*\*\* Typical air voids based on field compaction specifications and typical field densities obtained from ODOT.

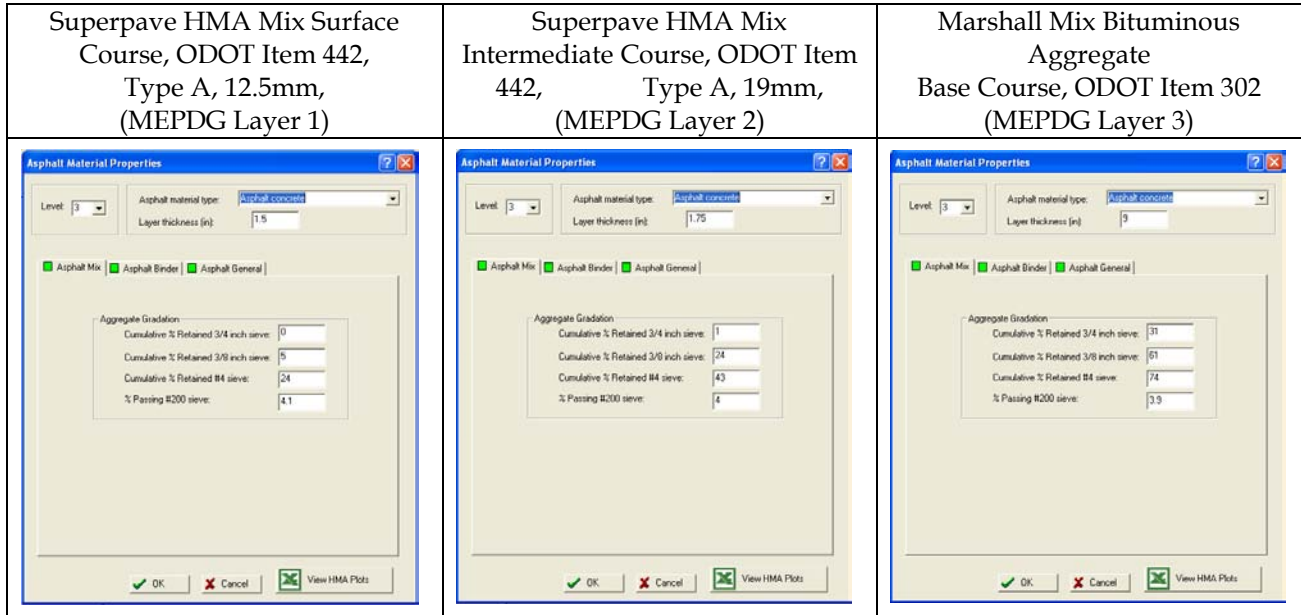


Figure 19. HMA layer thicknesses and gradations for baseline new HMA design.

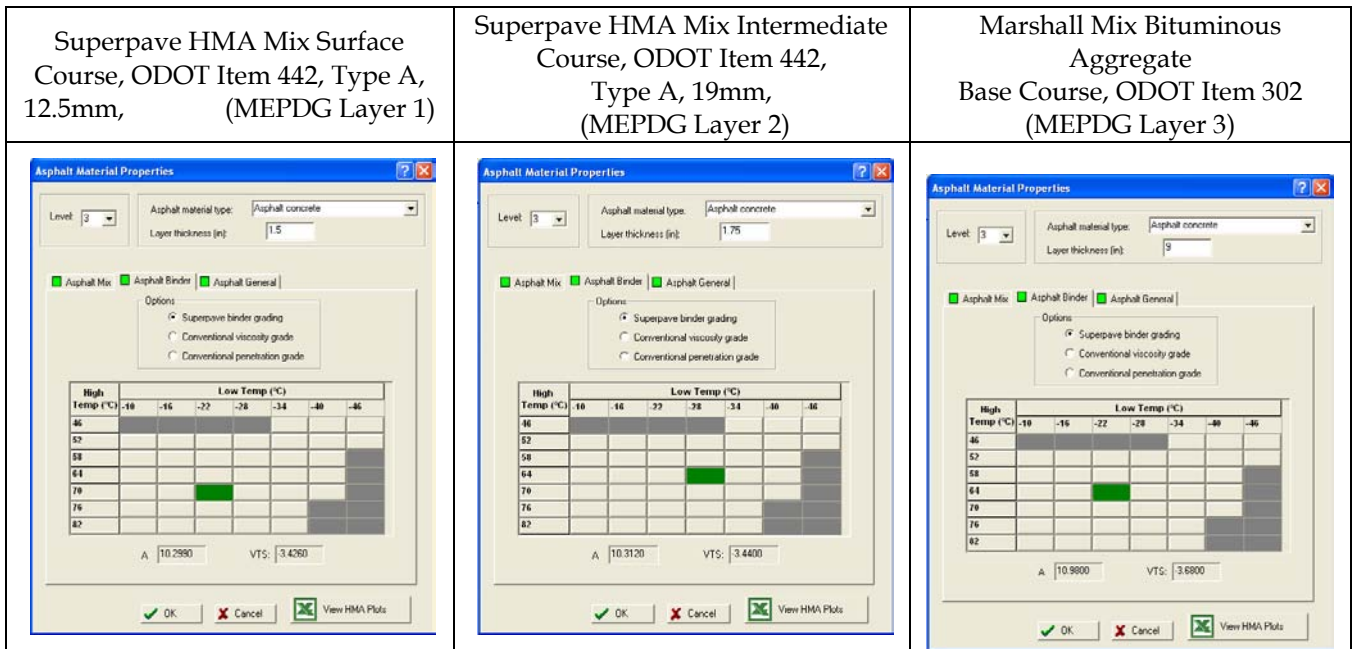


Figure 20. HMA layer binder properties for baseline new HMA pavement section.

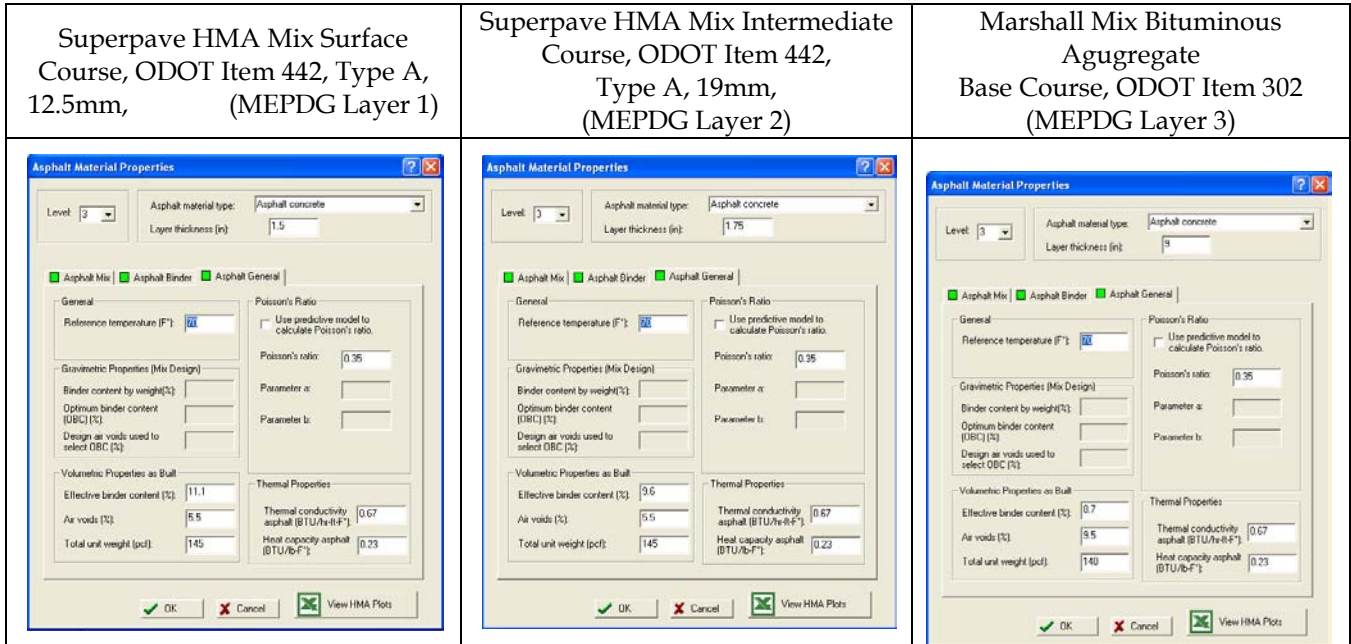


Figure 21. HMA layer mixture properties for baseline new HMA pavement section.

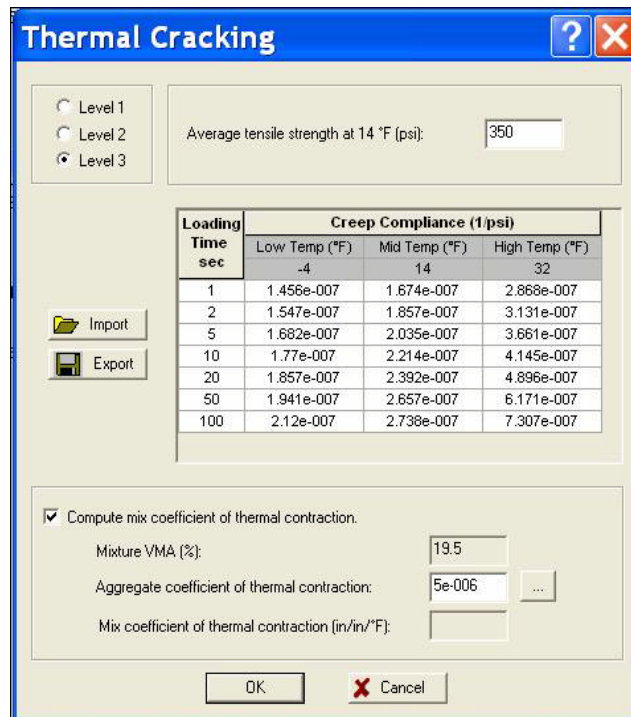


Figure 22. HMA creep compliance properties for baseline new HMA pavement section (Superpave HMA Mix Surface Course, ODOT Item 442, Type A, 12.5mm (MEPDG Layer 1)).

## New HMA Baseline Design Aggregate Base Properties

The representative base type was a 6.0-in dense graded aggregate base (DGAB) course (Item 304). Input properties for representative DGAB for the baseline design along with other ODOT base types used for new HMA construction were developed using information from the ODOT 2005 Construction and Material Specifications (sections 300), the ODOT 2006 Construction Inspection Manual (sections 300), and the ODOT Pavement Design & Rehabilitation Manual (section 400).

For the baseline DGAB the following MEPDG required inputs were adopted:

- Resilient modulus at optimum moisture: 20,000 psi (after Masada et al.).
- Plasticity index (PI): 1 (default MEPDG input for A-1-a).
- Liquid limit (LL): 6 (default MEPDG input for A-1-a).
- Gradation (see below):

Sieve Size	Percent Passing			
	Obtained from ODOT 2005 Construction and Material Specifications, Item 304 (typical mid range values)	Obtained from MEPDG (default values for A-1-a)	Obtained from Sargand et al. (2000)*	Obtained from Sargand & Hazen (1996)
3.5-in	—	97.6	—	—
3-in	—	—	—	—
2-in	100	—	100	100
2.5-in	—	91.6	—	—
1.5-in	—	85.8	100	100
1-in	85	78.8	92	88
¾-in	70	72.7	86	75
½-in	—	63.1	73	59
3/8-in	—	57.2	65	—
No. 4	45	44.7	44	49
No. 8	—	—	22	32
No. 10	—	33.8	—	—
No. 16	—	—	22	24
No. 20	—	—	—	—
No. 30	24	—	10	18
No.40	—	20	10	—
No. 50	—	—	10	10
No. 60	—	—	—	—
No. 80	—	12.9	—	—
No. 100	—	—	10	—
No. 200	—	8.7	6.6	6.4

\* Sargand et al. (2000) was adopted for baseline design.

The adopted DGAB materials properties for the baseline (Item 304) are provided in figures 23 and 24. Note that the value of maximum dry unit weight, specific gravity of soils, saturated hydraulic conductivity, optimum gravimetric water content, and degree of saturation presented in figure 24 were computed internally by the MEPDG software using regression equations and the adopted inputs.

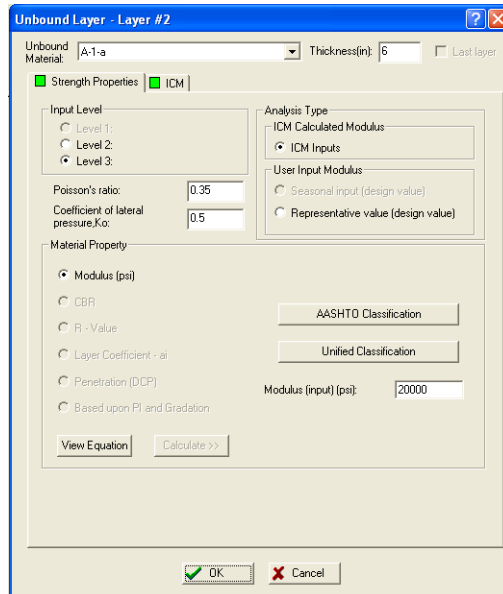


Figure 23. Properties of unbound granular base layer for baseline new HMA pavement section.

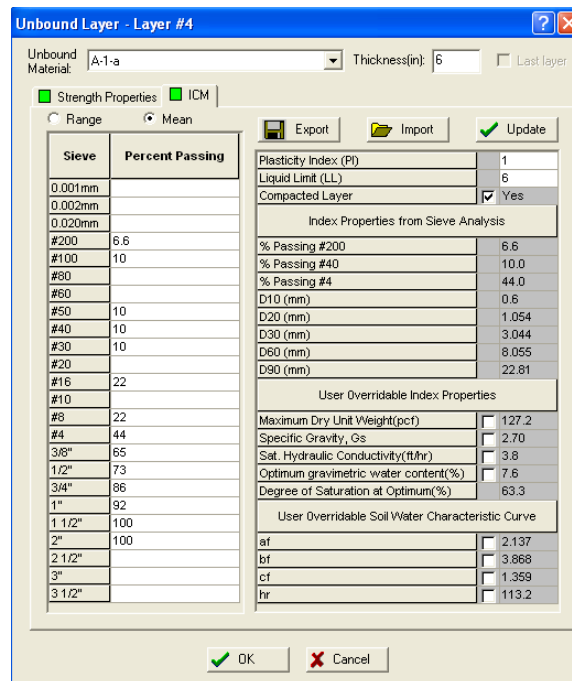


Figure 24. Properties of unbound base layer for baseline new HMA pavement section.

## Subgrade Properties for New HMA Pavement Baseline Design

A typical subgrade material (AASHTO soil class A-6) was adopted for the baseline new HMA pavement design. The top 12.0-in of the subgrade was assumed to be compacted. The A-6 subgrade resilient modulus and other relevant properties were obtained from default MEPDG libraries and ODOT reports such as Masada et al. (2004). Resilient modulus at optimum moisture for A-6 bases was estimated to be 10,000 psi (by Masada et al.). Subgrade resilient modulus used in the analysis is shown in figure 25. Note that this value drops significantly with in situ moisture content. Soil properties (plasticity index, gradation, etc.) values are provided in figure 26.

The screenshot shows a software dialog box titled "Unbound Layer - Layer #3". At the top, "Unbound Material" is set to "A-6" and "Last layer" is checked. The "Strength Properties" section is active, with "ICM" selected. Under "Input Level", "Level 3" is selected. "Poisson's ratio" is 0.35 and "Coefficient of lateral pressure, K<sub>o</sub>" is 0.5. The "Material Property" section has "Modulus (psi)" selected, with a value of 10000 entered in the "Modulus (input) (psi)" field. There are buttons for "View Equation", "Calculate >>", "AASHTO Classification", and "Unified Classification". At the bottom are "OK" and "Cancel" buttons.

Figure 25. Structural properties of subgrade for baseline new HMA pavement section.

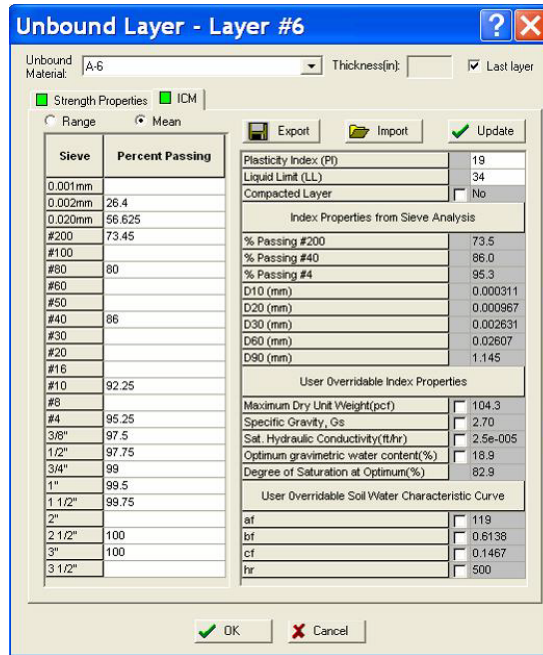


Figure 26. Properties of subgrade soil for baseline new HMA pavement section.

The default soil properties was used for computing other subgrade soil properties such as maximum dry unit weight, specific gravity of soils, saturated hydraulic conductivity, optimum gravimetric water content, and degree of saturation. For the baseline subgrade the following MEPDG required inputs were adopted:

- Resilient modulus of subgrade at optimum moisture: 10,000 psi (after Masada et al.).
- Atterberg Limits of subgrade (shown below):

Material Type	Atterberg Limit		
	Plastic Limit (PL)	Liquid Limit (LL)	Plasticity Index (PI)
ODOT A-6a*	12.7	30.6	17.9
ODOT A-6b*	17.0	37.0	20.0
ODOT A-6†	15.0	34.0	19.0
MEPDG A-6**	17.0	33.0	16.0

\* after Masada et al. (2002).

† average values of Atterberg limits for ODOT A-6 (after Masada et al. [2002]). These values were selected for use in the baseline design

\*\* MEPDG default values developed using test data from hundreds of LTPP pavements in the U.S.

- Subgrade Gradation (shown below):

Sieve Size	Percent Passing					
	Obtained from MEPDG (default values for A-6)	Obtained from LTPP Project 39_0202	Obtained from LTPP Project 39_0205	Obtained from LTPP Project 39_0207	Obtained from LTPP Project 39_0211	Mean values from LTPP Projects*
3.5-in	100	—	—	—	—	—
3-in	—	100	100	100	100	100
2-in	—	100	100	100	100	100
2.5-in	99.8	—	—	—	—	—
1.5-in	99.5	99	100	100	100	99.75
1-in	99	99	100	99	100	99.5
¾-in	98.4	98	100	99	99	99
½-in	97.4	97	99	98	97	97.75
3/8-in	96.4	96	99	98	97	97.5
No. 4	93.5	94	97	95	95	95.25
No. 8	—	—	—	—	—	—
No. 10	90.2	91	95	92	91	92.25
No. 16	—	—	—	—	—	—
No. 20	—	—	—	—	—	—
No. 30	—	—	—	—	—	—
No.40	82.4	84	90	85	85	86
No. 50	—	—	—	—	—	—
No. 60	—	—	—	—	—	—
No. 80	73.5	78	85	79	78	80
No. 100	—	—	—	—	—	—
No. 200	63.2	71.1	79.4	71.8	71.5	73.45
0.001mm	—	54.6	64.2	56.8	58.9	58.625
0.002mm	—	27.4	27.1	28.6	30.5	28.4
0.020mm	—	—	—	—	—	—

\*Mean value of gradations obtained from the LTPP sections were adopted for the baseline design.

### MEPDG Results for New HMA Baseline Design

Figures 27 through 31 and table 4 show predicted distress and IRI for the base line design presented. Information presented shows reasonable as expected predictions of distress/IRI.

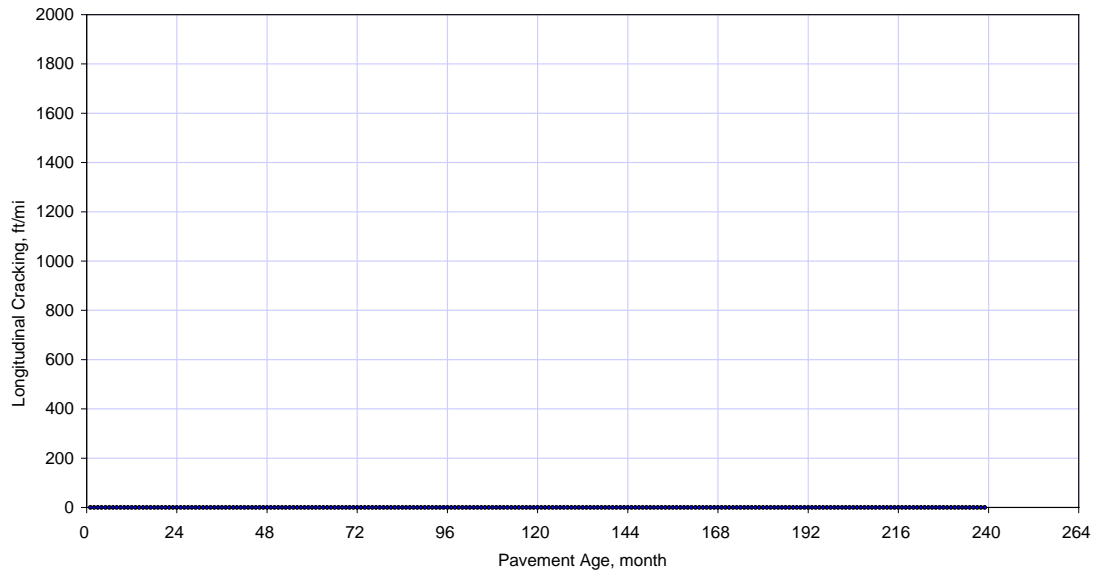


Figure 27. Plot of mean predicted longitudinal cracking versus pavement age.

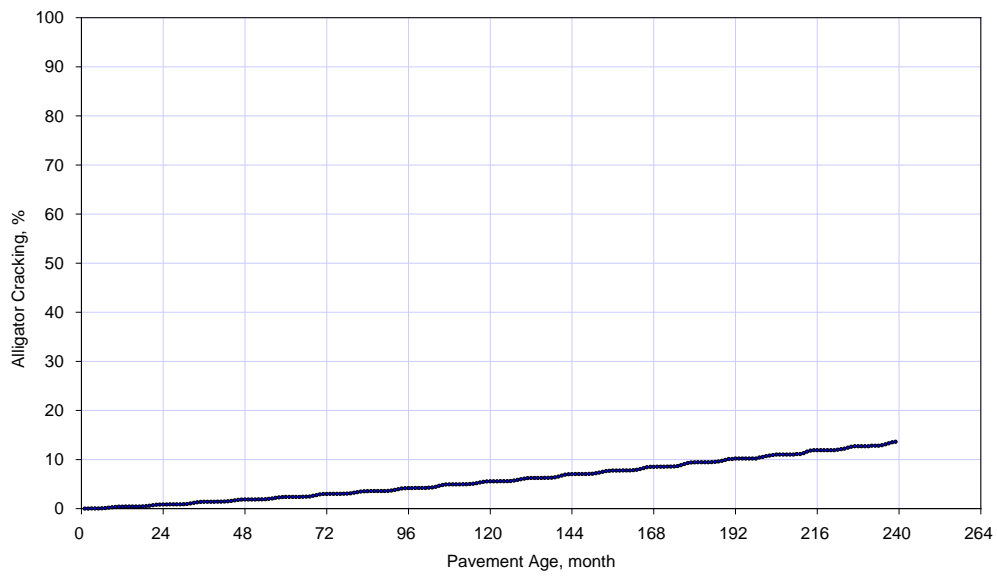


Figure 28. Plot of mean predicted alligator cracking versus pavement age.

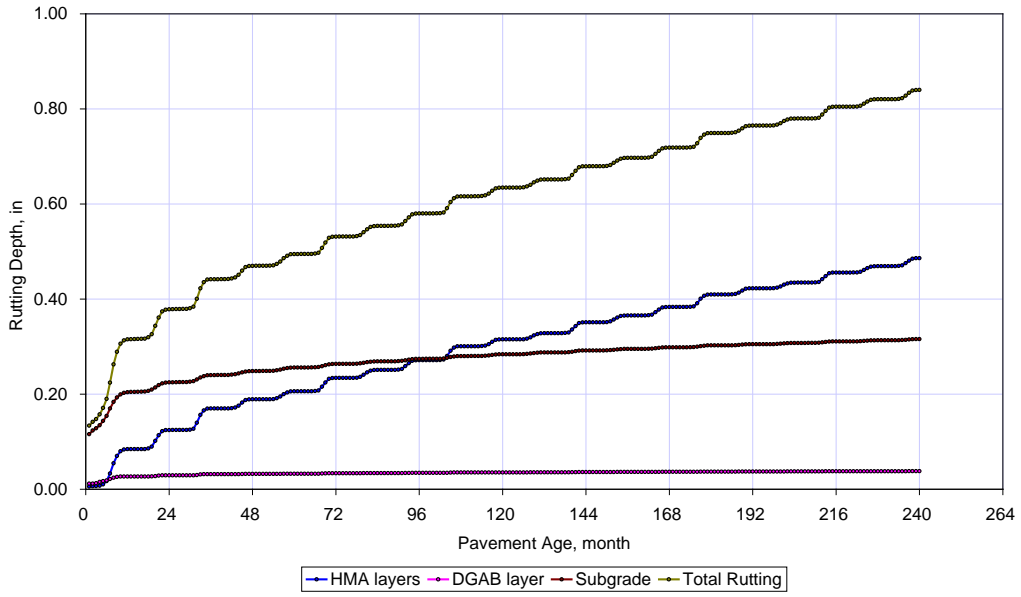


Figure 29. Plot of mean predicted rutting versus pavement age.

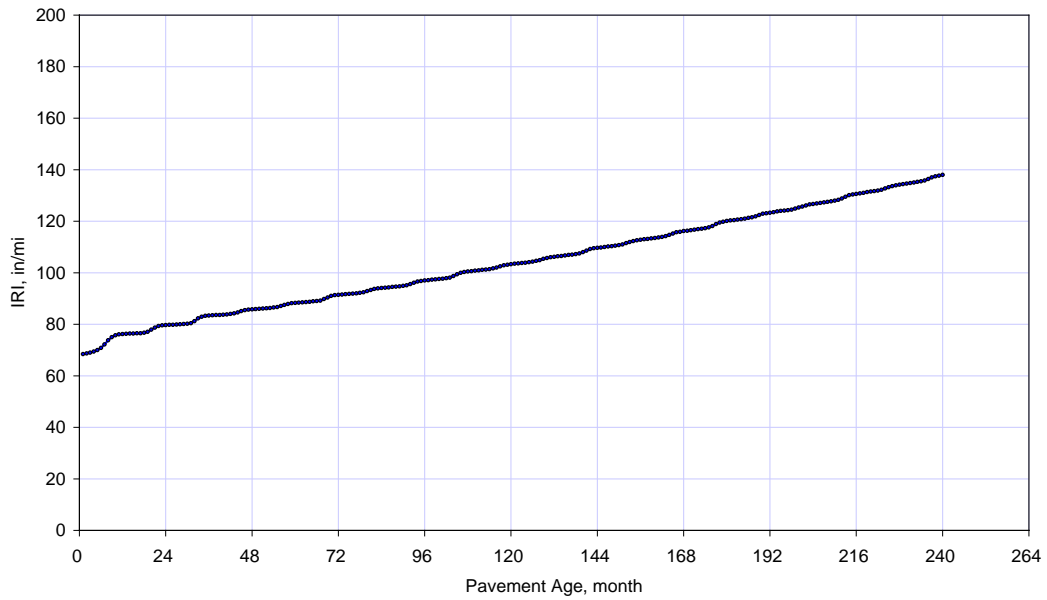


Figure 30. Plot of mean predicted IRI versus pavement age.

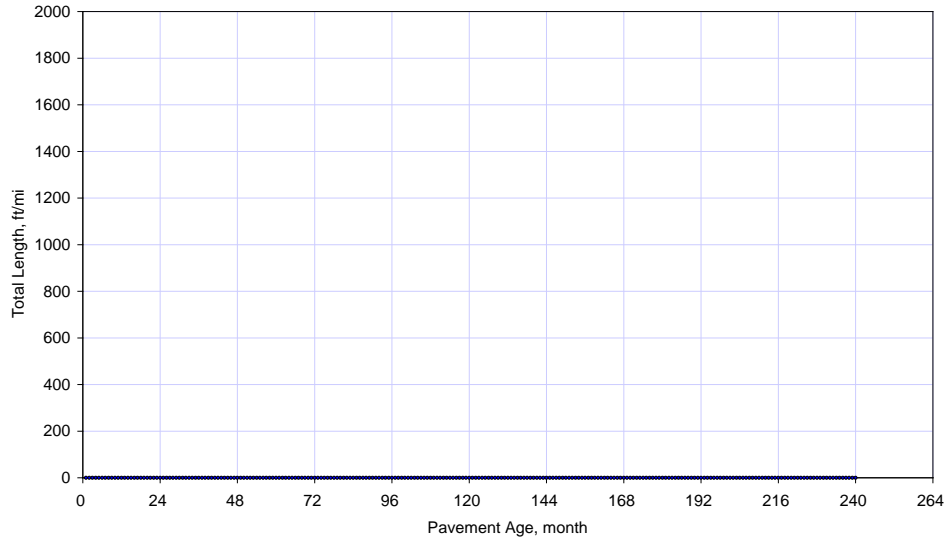


Figure 31. Plot of mean predicted low temperature transverse cracking versus pavement age.

Table 4. Summary of predicted distress and IRI obtained from the MEPDG (with national calibration coefficients).

Pavement Age, years	Longitudinal Cracking (ft/mi)	Alligator Cracking (Percent Area)	Transverse Cracking (ft/mi)	Total Rutting (in)	IRI (in/mi)	Heavy Trucks (cumulative)
0.08	0	0.009	0	<b>0.134</b>	<b>68.4</b>	161,878
1	0	0.4	0	<b>0.315</b>	<b>76.2</b>	1,942,530
2	0	0.835	0	<b>0.379</b>	<b>79.7</b>	4,049,010
3	0	1.38	0	<b>0.442</b>	<b>83.4</b>	6,319,440
4	0	1.84	0	<b>0.47</b>	<b>85.8</b>	8,753,830
5	0	2.36	0	<b>0.495</b>	<b>88.3</b>	11,352,200
6	0.01	2.98	0	<b>0.531</b>	<b>91.4</b>	14,114,400
7	0.01	3.55	0	<b>0.554</b>	<b>94</b>	17,040,700
8	0.01	4.17	0	<b>0.58</b>	<b>97</b>	20,130,800
9	0.02	4.93	0	<b>0.616</b>	<b>100.4</b>	23,385,000
10	0.02	5.55	0	<b>0.634</b>	<b>103.3</b>	26,803,100
11	0.02	6.22	0	<b>0.651</b>	<b>106.1</b>	30,385,100
12	0.03	7.02	0	<b>0.679</b>	<b>109.6</b>	34,131,100
13	0.03	7.74	0	<b>0.697</b>	<b>112.7</b>	38,041,000
14	0.04	8.51	0	<b>0.719</b>	<b>116.1</b>	42,114,900
15	0.04	9.42	0	<b>0.749</b>	<b>120</b>	46,352,700
16	0.05	10.2	0	<b>0.765</b>	<b>123.3</b>	50,754,500
17	0.05	11	0	<b>0.78</b>	<b>126.6</b>	55,320,200
18	0.06	11.9	0	<b>0.804</b>	<b>130.5</b>	60,049,900
19	0.07	12.7	0	<b>0.82</b>	<b>134.1</b>	64,943,500
20	0.08	13.6	0	<b>0.84</b>	<b>137.9</b>	70,001,100

A review of the MEPDG predictions for the HMA baseline design indicates the following:

- The baseline HMA design is representative of current ODOT new HMA pavement design and construction practices.
- The traffic level of 70 million heavy trucks in the design lane is a very heavy level of traffic over the 20 year period.
- Models appear to predict reasonable levels of distress and IRI making the design suitable as the basis for sensitivity analysis. Note that the only prediction of concern is large total rutting. This distress model has required adjustment in some other states and thus it is recommended that it be validated using Ohio data during this implementation effort. However, this will not affect the sensitivity analysis because the conclusions are drawn on changes in distress, not absolute predicted value.

Table 5 shows a summary of several input parameters that are of interest to the new HMA pavement sensitivity analysis. Table 6 shows HMA base layer material properties. Table 7 shows input parameters used to define the SMA surfacing material.

Table 5. Input parameters of interest to be used for new HMA sensitivity analysis.

MEPDG Input Parameter	Levels of Input (*indicates the baseline representative design)
Base type	<ul style="list-style-type: none"> <li>• Dense graded aggregate base course (Item 304)*                             <ul style="list-style-type: none"> <li>○ Resilient modulus = 20,000 psi.</li> <li>○ Plasticity Index = 1.</li> <li>○ Liquid Index = 6</li> <li>○ See Table 3 for more details</li> </ul> </li> <li>• Bituminous or asphalt concrete base (Items 301 and 302)                             <ul style="list-style-type: none"> <li>○ Unit weight = 140 pcf.</li> <li>○ See Table 6 for more details.</li> </ul> </li> </ul>
Climate (weather stations)	<ul style="list-style-type: none"> <li>• Cleveland (Cleveland-Hopkins International-airport)</li> <li>• Columbus (Port Columbus International airport)</li> <li>• Covington/Cincinnati (Cincinnati/NRN KY International airport)</li> <li>• Dayton (J M Cox Dayton airport)</li> <li>• New Philadelphia (Harry Clever Field airport)</li> <li>• Newark (Newark-Heath airport)*</li> <li>• Toledo (Toledo Express airport)</li> <li>• Parkersburg, WV (Wood County airport)</li> <li>• Wheeling, WV (Wheeling-Ohio County airport)</li> </ul>
HMA thickness	8-, 10-, 12.25-*, 14-, 16-in (varying the bituminous base thickness only)
Subgrade type/modulus**	<ul style="list-style-type: none"> <li>• Coarse (A-1-a, A-1-b, A-2-4, A-2-5, A-2-6, A-2-7 and A-3)</li> <li>• Fine (A-4, A-5, A-6*, A-7-5 and A-7-6)</li> </ul>
HMA air voids content	Surface/Intermediate: 5.5*, 6.5, 7.5, 8.5, 9.5, 10.5 percent Base: 5.5, 6.5, 7.5, 8.5, 9.5*, 10.5 percent
HMA volumetric binder content	Baseline binder content (surface course = 11.1 percent, intermediate course = 9.6 percent and base course = 8.7 percent) +4.0, +2.0-, -2.0-, and -4.0 percent of the baseline binder content across all three HMA layers.
HMA type (surface course)***	<ul style="list-style-type: none"> <li>• Superpave HMA Mix Surface Course, ODOT Item 442, Type A, 12.5mm, (MEPDG Layer 1)</li> <li>• SMA surface course (Item 443)</li> </ul>
Traffic composition	13 LTPP pavement sites representing urban and rural traffic in Ohio (refer figure 2 for WIM site locations)
Subgrade type	<ul style="list-style-type: none"> <li>• Natural A-6 material with top 12-in compacted</li> <li>• Natural A-6 material with top 12-in lime stabilized and compacted</li> <li>• Natural A-6 material with top 12-in cement stabilized and compacted</li> <li>• Natural A-2-4 material with top 12-in compacted</li> <li>• Natural A-2-4 material with top 12-in cement stabilized and compacted</li> </ul>

\*New HMA baseline project.

\*\*Default MEPDG gradations will be used, where applicable.

\*\*\*For the sensitivity analysis, two other HMA materials types—SuperPave (Item 442, Type A, 12.5-mm) and stone matrix asphalt (SMA) (Item 443) were considered. For SuperPave, the equivalent ODOT SuperPave surface and intermediate course mixes were used to replace the 1.75-in surface course and 1.75-in intermediate course of the baseline design. For SMA, only the 1.75-in surface course was replaced with the SMA surface course.

Table 6. Summary of HMA Base layer material properties.

HMA Material Types	Perf. PG Grade	Gradation (Percent Passing Sieve Size)												Vol. Binder Content, percent*	In-place HMA Mix Air Voids	
		2-in	1.5-in	1.0-in	¾-in	½-in	3/8-in	No. 4	No. 8	No. 16	No. 30	No. 50	No. 100			No. 200
Bituminous Aggregate Base Course (Item 301) Marshall Mix***	PG 64-22	100.0	—	87.5	—	67.5	—	42.5	30.0	22.5	—	10.5	—	4.0	7.0*	9.5
Bituminous Aggregate Base Course (Item 302) Marshall Mix****	PG 64-22	100.0	100.0	83.0	69.0	46.0	39.0	26.0	21.0	17.0	13.0	9.0	6.0	3.9	8.7**	9.5

\* Estimated based on nominal maximum aggregate size (FHWA, 2002).

\*\*Estimated based on VMA and estimated in-place air voids etc.

\*\*\* Mid band values and typical as-constructed gradations obtained from ODOT Construction and Specification Manual (Item 301). Note that the MEPDG requires only the percent retained on the following sieve sizes ¾-in, 3/8-in, and No. 4 along with percent passing the No. 200 sieve size.

\*\*\*\*Typical mix design gradations obtained from ODOT.

† Estimated based on a 2.5 percent by weight AC content.

Table 7. Summary of HMA SMA layer material properties (ODOT Item 443).

MEPDG Layer number	HMA Material Types	Perf. PG Grade	Gradation (Percent Passing Sieve Size)*													Vol. Binder Content, percent**	In-place HMA Mix Air Voids***
			2-in	1.5-in	1.0-in	¾-in	½-in	3/8-in	No. 4	No. 8	No. 16	No. 30	No. 50	No. 100	No. 200		
1	SMA Surface Course (Item 443)****	PG 70-22M	—	—	—	100	92.5	62.5	24	19.5	—	—	15	—	10	10.2	3.5
2	Superpave HMA Mix Intermediate Course (Item 442, Type A, 19mm)	PG 64-28	100	100	100	99	86	76	57.0	35	22	14	10	6	4	9.6	5.5
3	Marshall Mix Bituminous Aggregate Base Course (Item 302)	PG 64-22	100	100	83	69	46	39	26	21	17	13	9	6	3.9	8.7	9.5

\* Mid band values and typical as-constructed gradations obtained from ODOT Construction and Specification Manual (Item 443). Note that the MEPDG requires only the percent retained on the following sieve sizes ¾-in, 3/8-in, and No. 4 along with percent passing the No. 200 sieve size.

\*\*Estimated based on mix gradations, gravimetric binder content, and other volumetric properties such as air voids, VMA, VFA, etc.

\*\*\* Typical lab. measured mix air voids obtained from ODOT.

\*\*\*\* Based on ODOT specifications for Item 443.

## Sensitivity Analysis Results for New HMA Pavements

The results of the sensitivity analysis are presented in the following sections.

### Effect of Base Type on MEPDG Predicted HMA Pavement Performance

The base types considered were the DGAB, ATB\_301, and ATB\_302. All three base types were 6-in thick.

Figures 32 through 36 show the effect of base type on new HMA distress and IRI. A summary of the relative effect of base type on all distress /IRI is presented in table 8 which shows that base type highly influenced predicted fatigue alligator cracking, low temperature transverse cracking, and rutting. The unbound aggregate base causes the highest levels of the distress. These results indicate that the use of DGAB shows increased fatigue cracking, low temperature transverse cracking, and rutting when compared to ATB material. Longitudinal fatigue cracking was not affected by base type. The impact on alligator fatigue cracking is logical due to the much higher bending strain at the bottom of the HMA with an unbound aggregate base than an HMA base. For rutting, there was lower permanent deformation in the asphalt treated base compared to the unbound aggregate base. Published literature have indicated that HMA and base interface friction, base stiffness (for all base types) and the cohesion and friction angle on unbound bases do influence the tensile stresses generated with an HMA surface layer and thus transverse thermal cracking. As shown in figure 34, the pavement with a weaker base exhibited a higher level of transverse cracking.

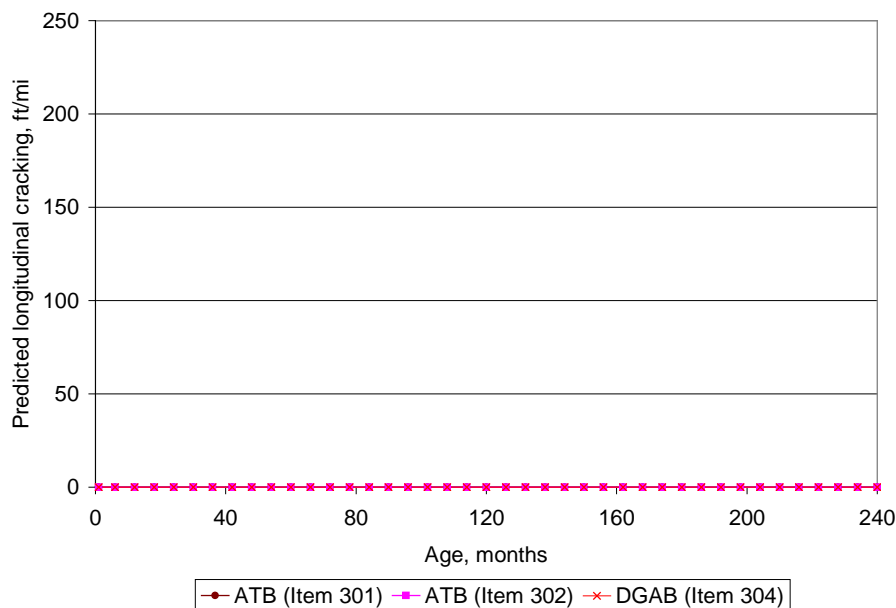


Figure 32. Plot of age versus top-down fatigue (longitudinal) cracking showing the effect of base type.

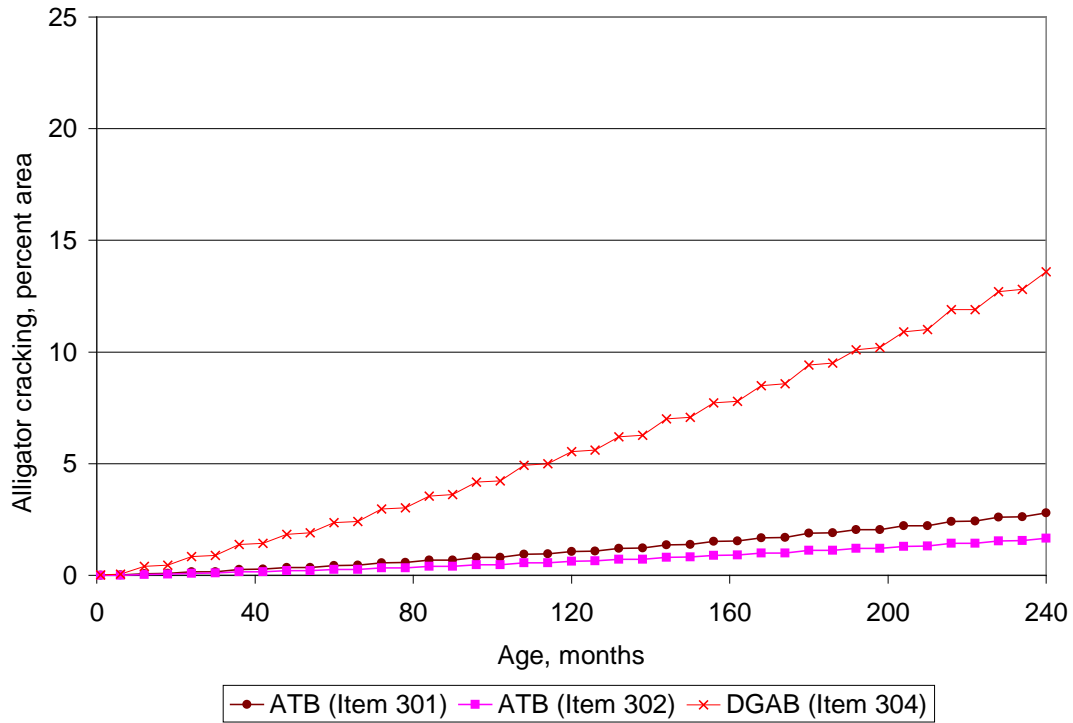


Figure 33. Plot of age versus bottom-up fatigue (alligator) cracking showing the effect of base type.

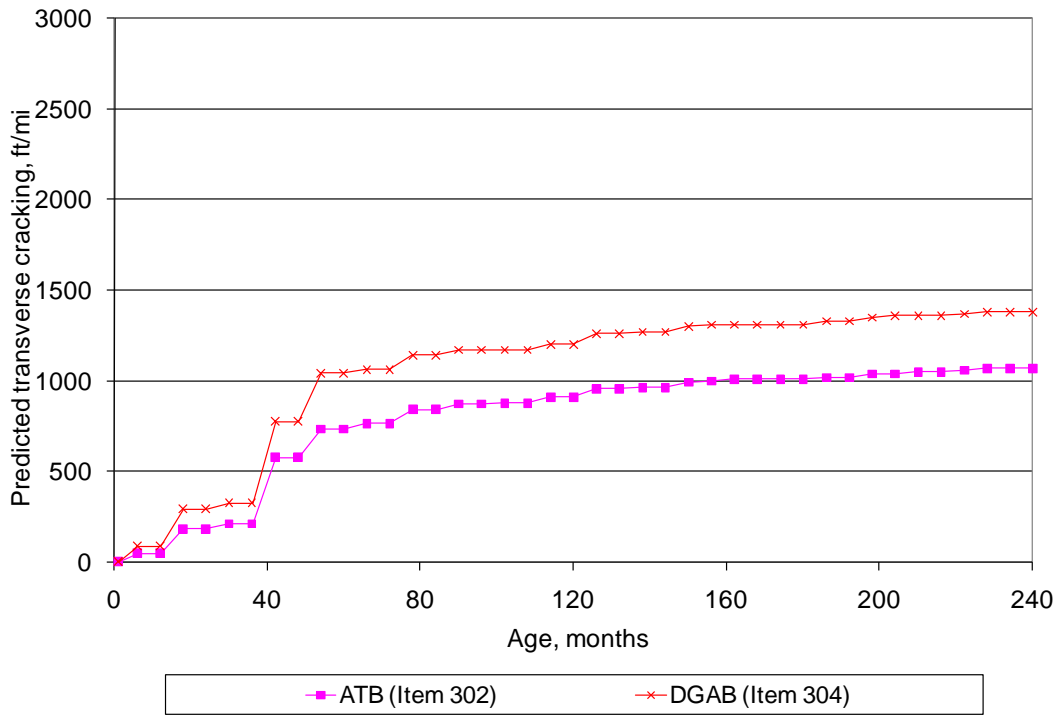


Figure 34. Plot of age versus temperature related (transverse) cracking showing the effect of base type.

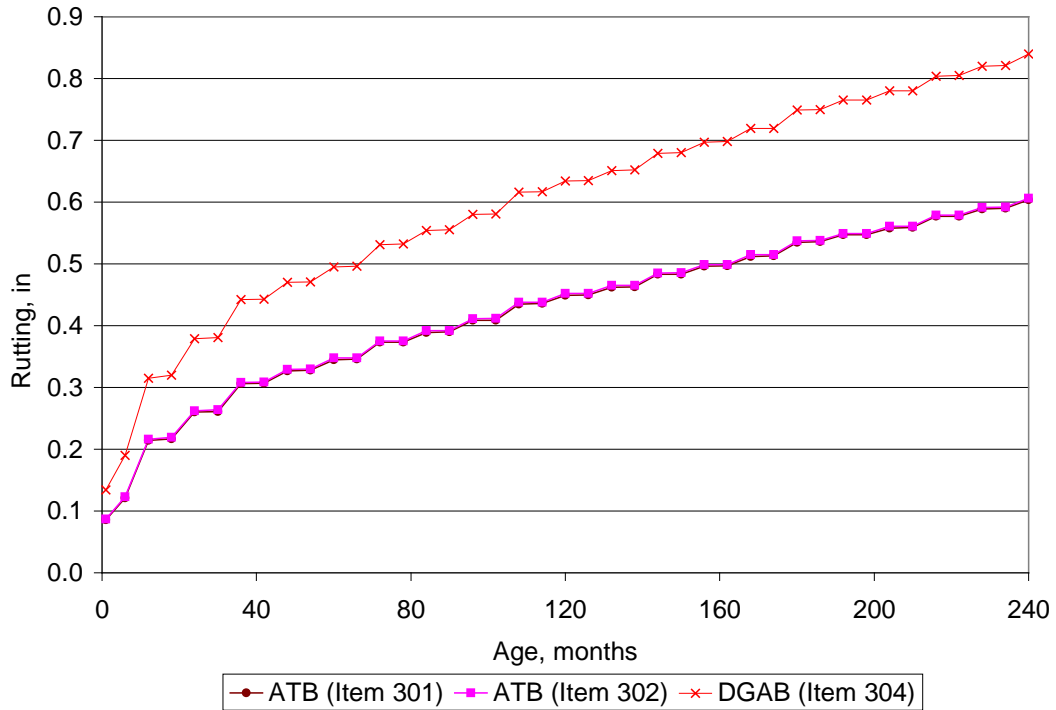


Figure 35. Plot of age versus rutting showing the effect of base type.

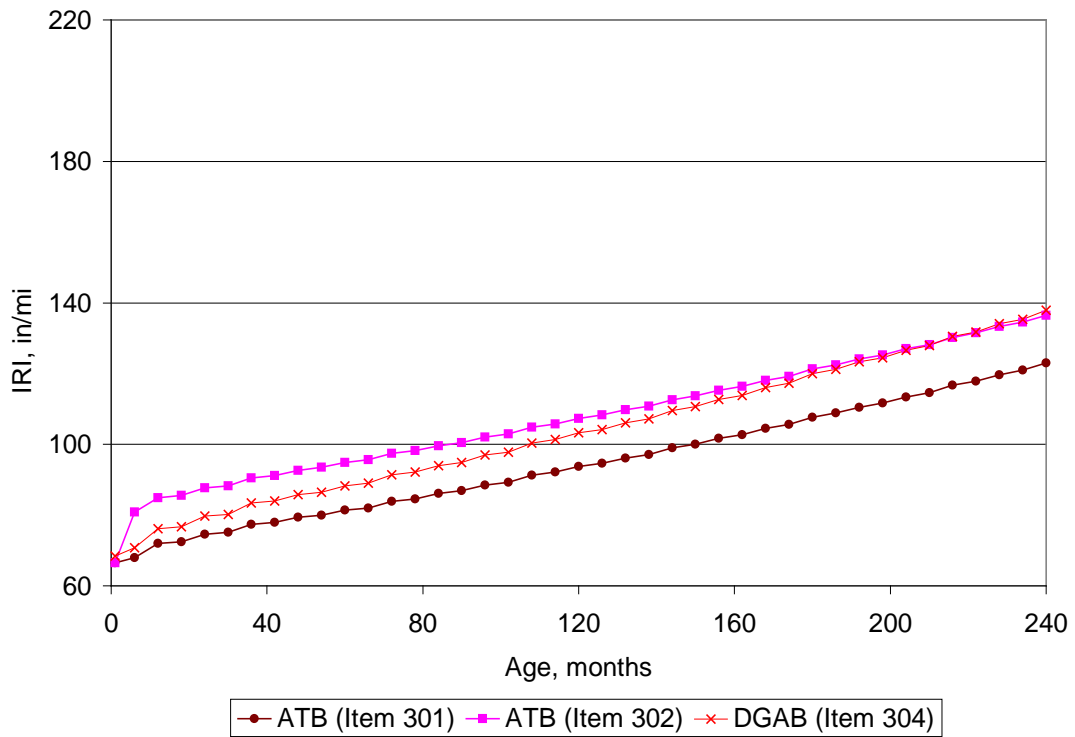


Figure 36. Plot of age versus IRI showing the effect of base type.

Table 8. Relative effect of base type on HMA pavement distress and IRI.

<b>Distress/IRI</b>	<b>Effect of Base Type on Distress/IRI</b>
Longitudinal fatigue cracking	None
Low temperature transverse cracking	High
Bottom-up fatigue (alligator) cracking	High
Rutting	High
IRI	Moderate

### Effect of Climate

The effect of climate on predicted distress and IRI was determined by selecting representative weather stations for each ODOT district and using the representative the selected weather stations to simulate climate condition across the state. The objective was to determine whether the effect of climate on performance across the state was significantly different. Climatic conditions were simulated using approximately 9 years of climate data (i.e., temperature, precipitation, cloud cover, sunshine, and so on) collected from available weather stations. The exact locations of these cities across Ohio are shown in figure 37. As shown in figure 37 the weather stations selected cover the entire geographical area of Ohio. The results of the sensitivity analysis are presented in figures 38 through 43 for alligator cracking, rutting, and IRI, respectively.

Table 9 shows the relative effect of climate on all distress types and IRI. Information presented shows that longitudinal fatigue cracking was not affected by climate across Ohio. The effect of climate on alligator cracking, and rutting was moderate while the effect of climate on transverse “thermal” cracking was high. The Parkersburg area had the most fatigue cracking and rutting and Cleveland area has the least for the same level of traffic. This may be due to generally warmer temperatures in the southern Parkersburg area. For transverse cracking, Newark, Toledo, and Dayton all in colder central and northern regions exhibited the highest levels of the distress. The low levels of predicted transverse cracking in Cleveland were contrary to expectations. A critical evaluation of the quality of climate related data for this city in the NCDC database is warranted.

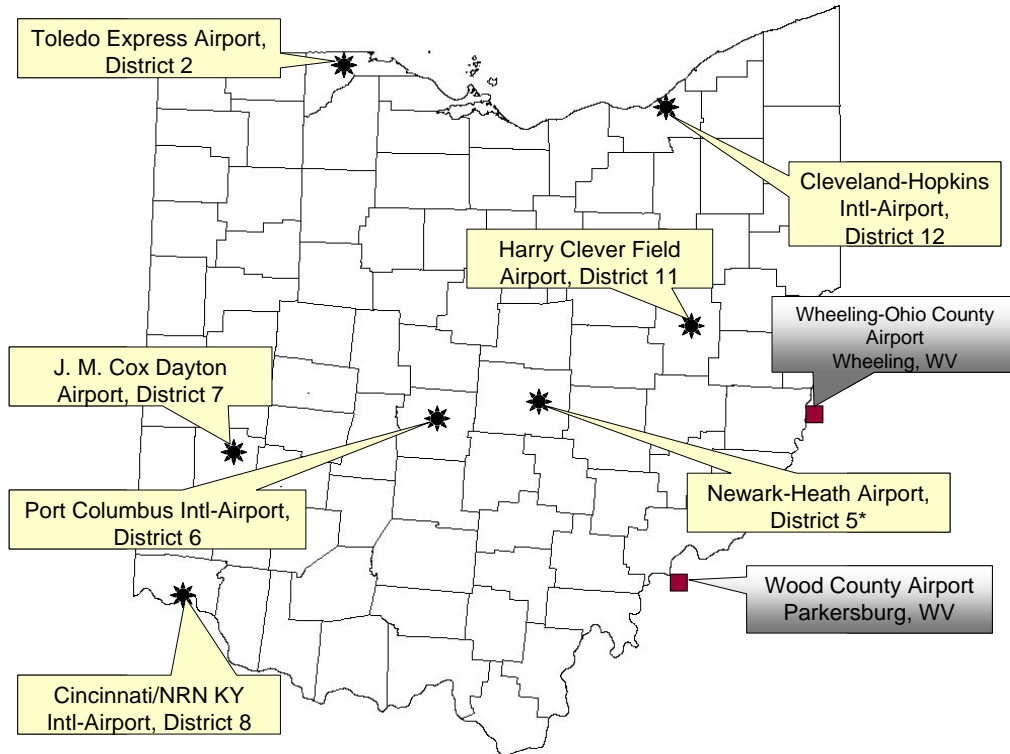


Figure 37. Map of Ohio highlighting the locations of cities/ weather stations used for simulating climatic conditions for sensitivity analysis.

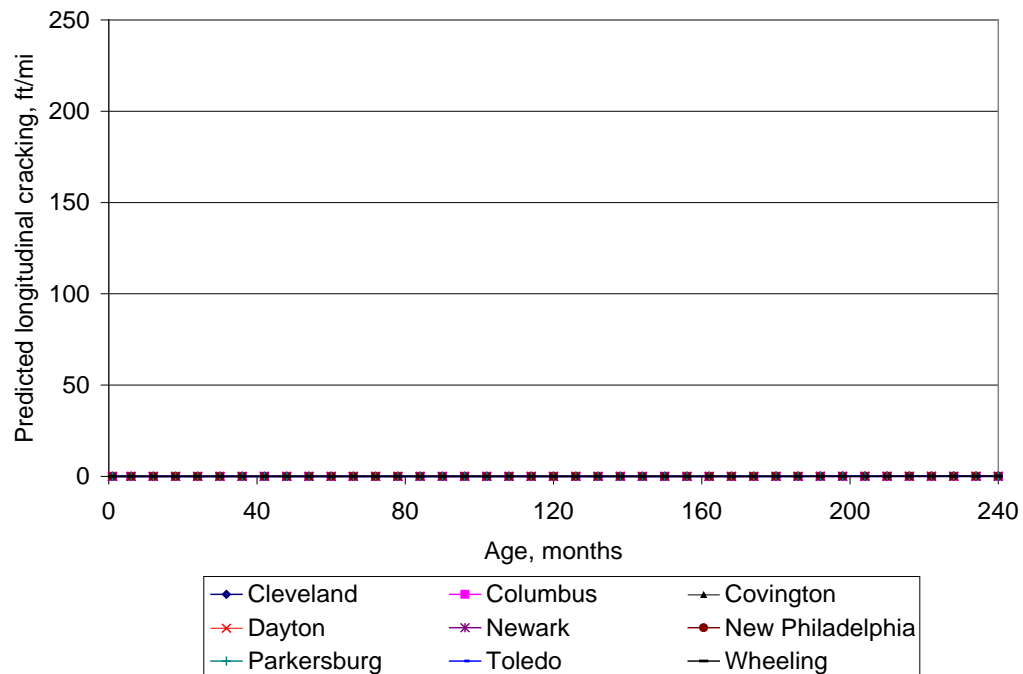


Figure 38. Plot of age versus top-down fatigue (longitudinal) cracking showing the effect of climate across Ohio.

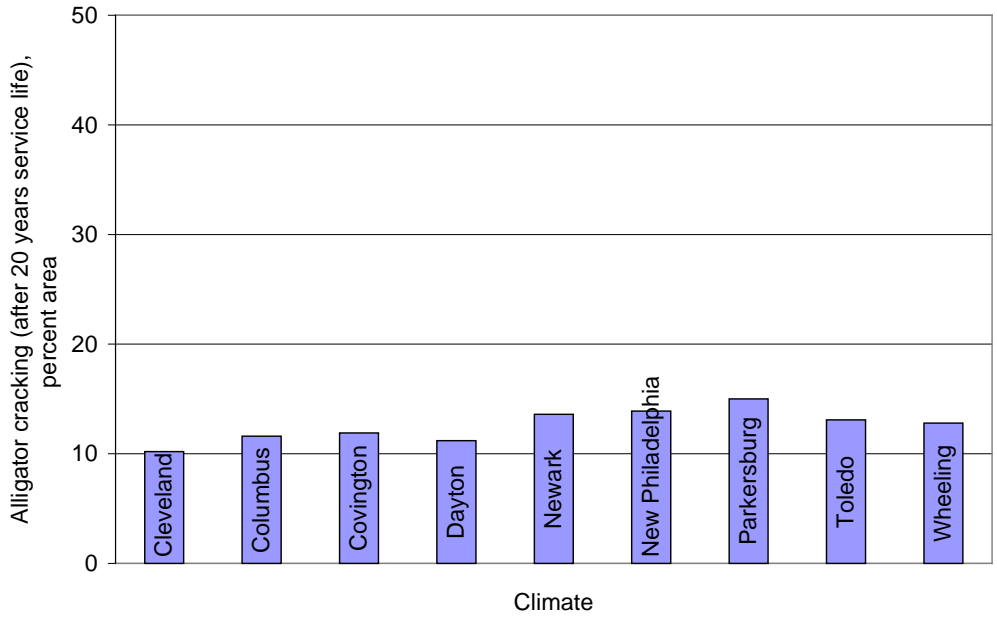


Figure 39. Plot of age versus bottom-up fatigue (alligator) cracking showing the effect of climate across Ohio.

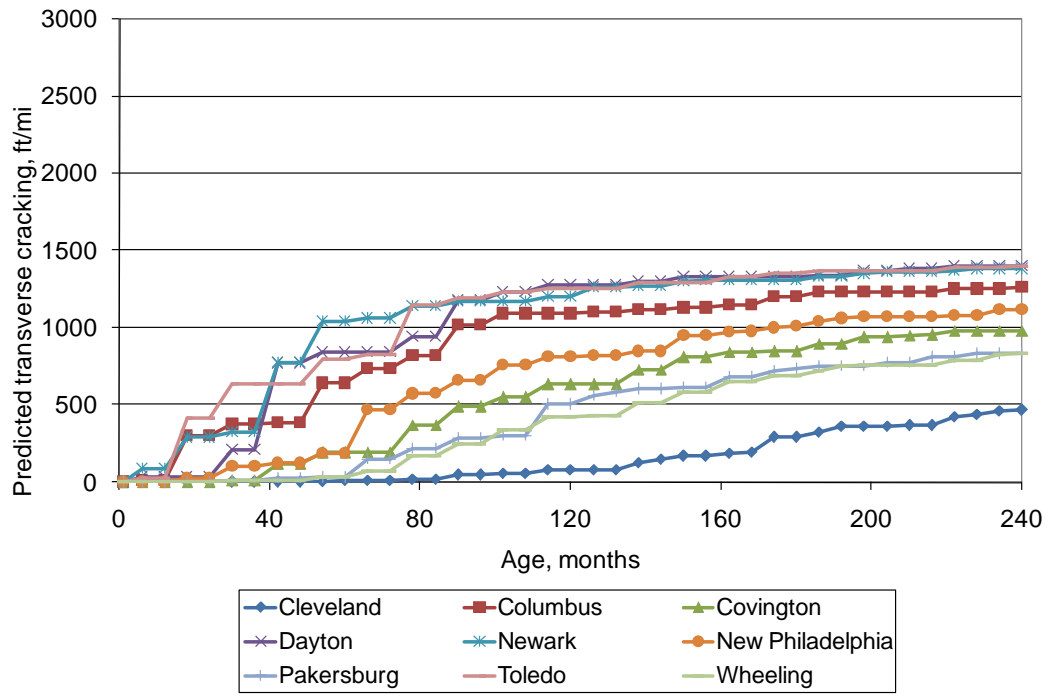


Figure 40. Plot of age versus low temperature related (transverse) cracking showing the effect of climate across Ohio.

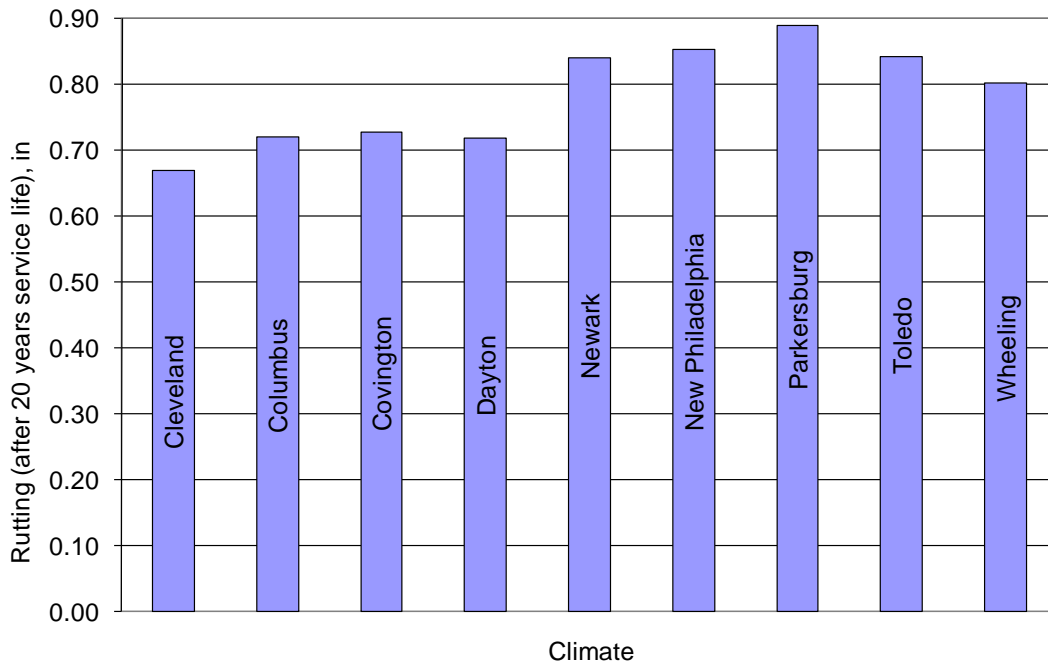


Figure 41. Plot of age versus rutting showing the effect of climate across Ohio.

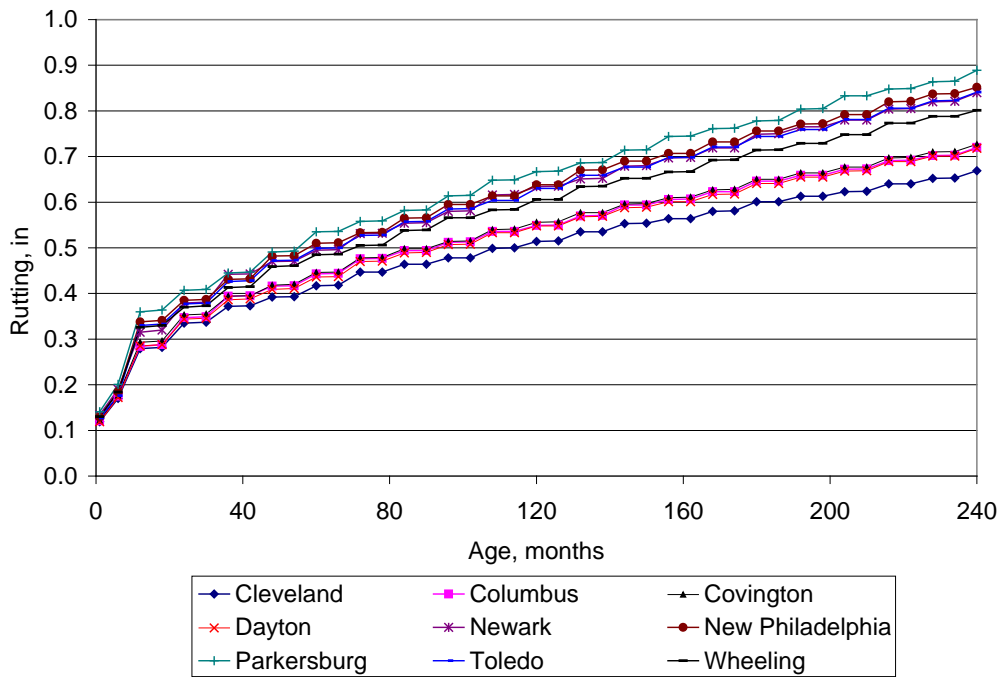


Figure 42. Plot of age versus rutting showing the effect of climate across Ohio.

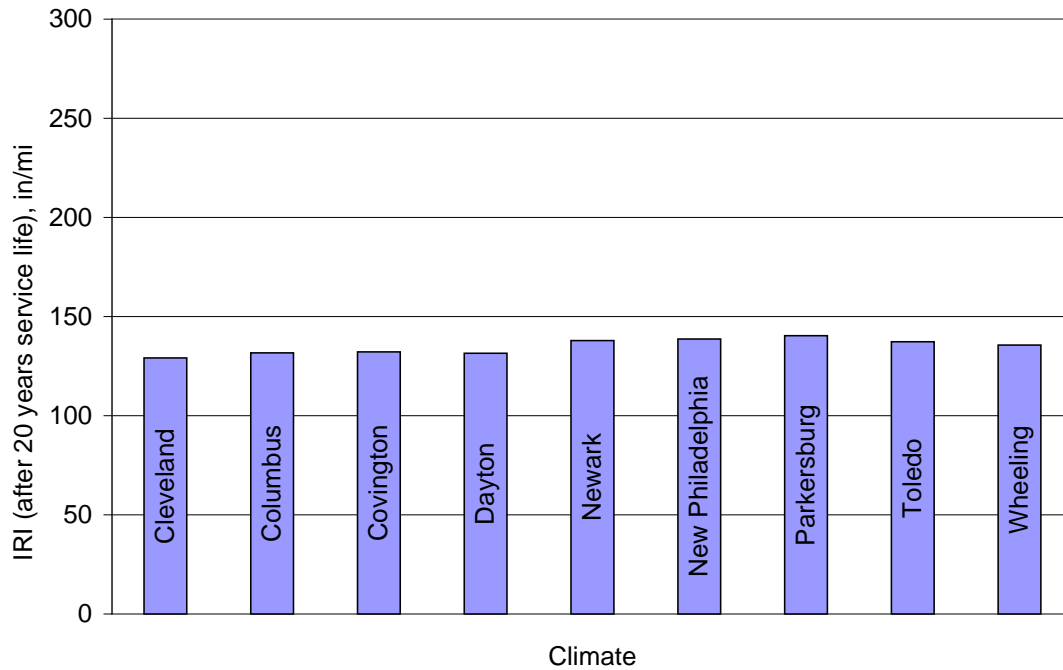


Figure 43. Plot of age versus IRI showing the effect of climate across Ohio.

Table 9. Relative effect of climate on HMA distress and IRI.

<b>Distress/IRI</b>	<b>Effect of Climate on Distress/IRI</b>
Top-down fatigue (longitudinal) cracking	None
Bottom-up fatigue (alligator) cracking	Low
Thermal (transverse) cracking	High
Rutting	Moderate
IRI	Low

#### Effect of HMA Thickness

Longitudinal fatigue (top down) cracking was affected only when HMA thickness was reduced to 8-in which caused it to increase greatly. HMA thickness had a large effect on both alligator cracking and rutting and thus IRI as one would expect. These effects are shown in figures 44 through 48 for a thickness range of 8 to 16 in. Information presented in figures 44 through 48 summarizes all of these effects. The trends observed were reasonable with the highest distress/IRI observed for the thinner HMA. Alligator cracking, transverse cracking, rutting, and IRI all decreased with increased HMA thickness.

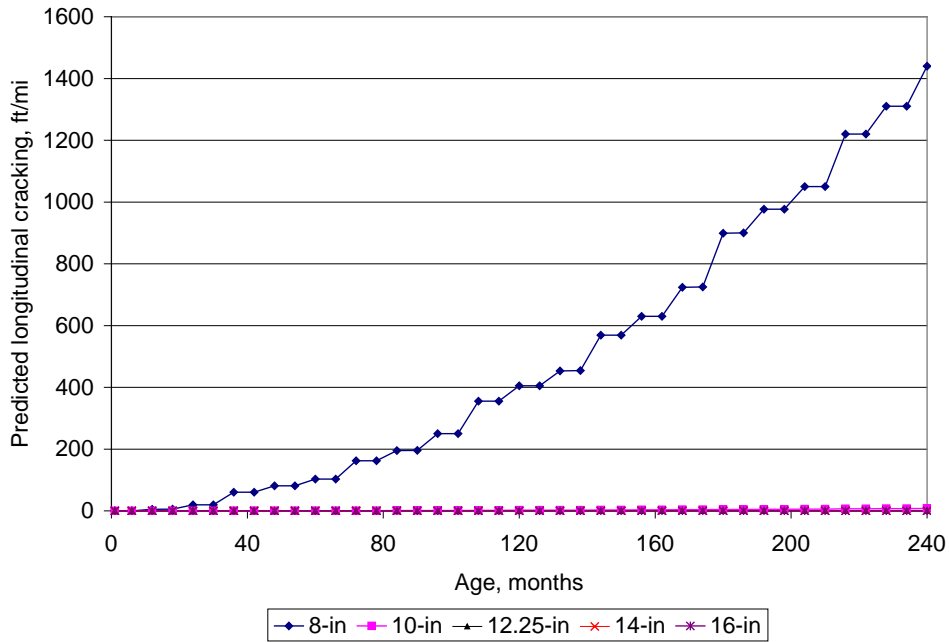


Figure 44. Plot of age versus top-down fatigue (longitudinal) cracking showing the effect of total HMA thickness.

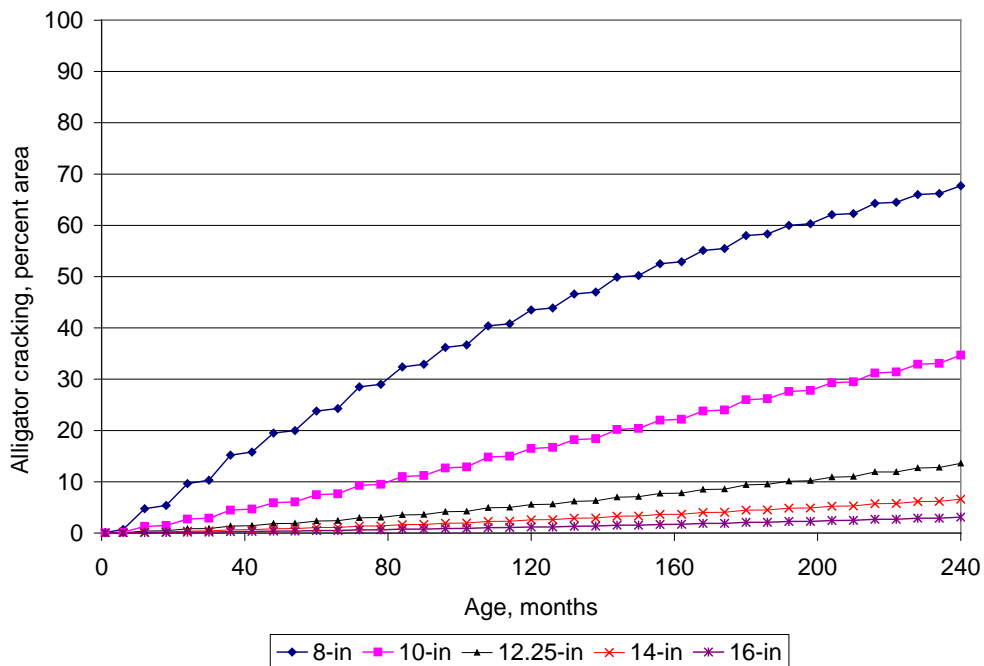


Figure 45. Plot of age versus bottom-up fatigue (alligator) cracking showing the effect of total HMA thickness.

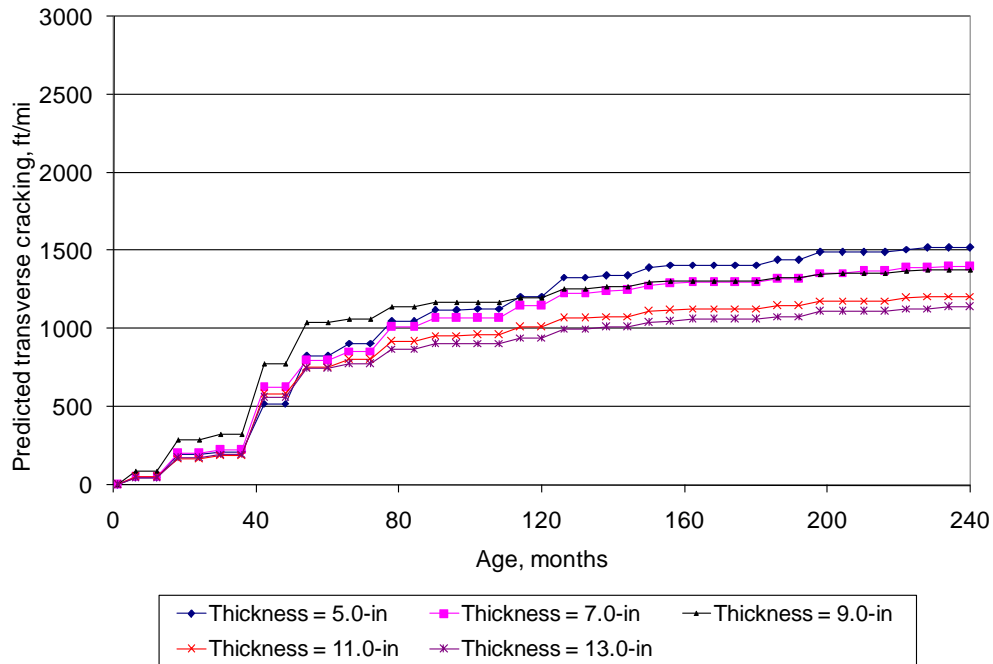


Figure 46. Plot of age versus temperature related (transverse) cracking showing the effect of total HMA thickness.

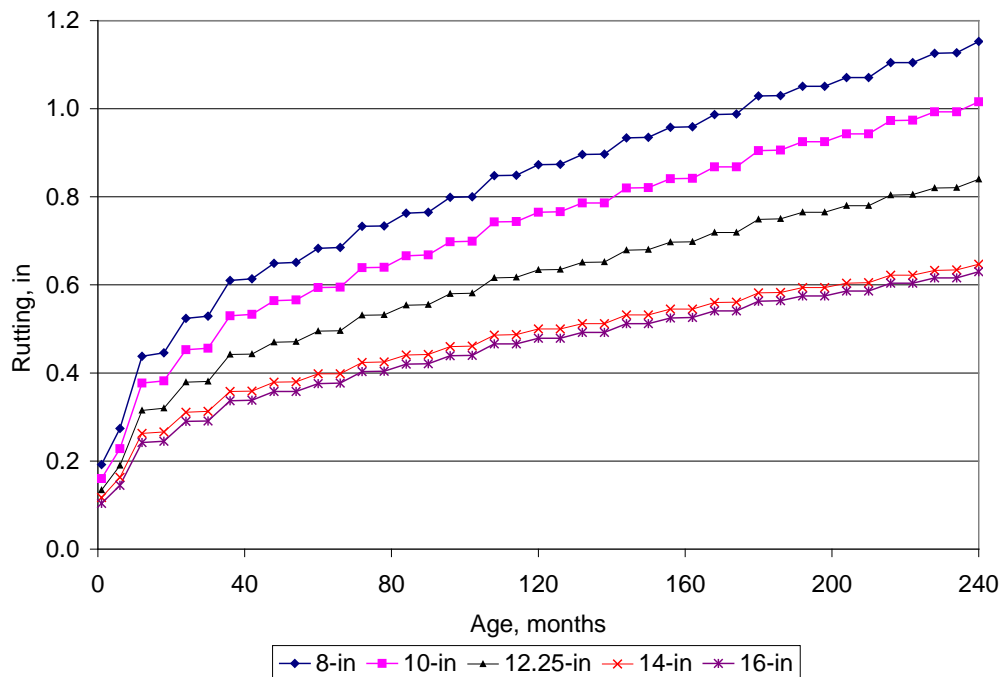


Figure 47. Plot of age versus rutting showing the effect of total HMA thickness.

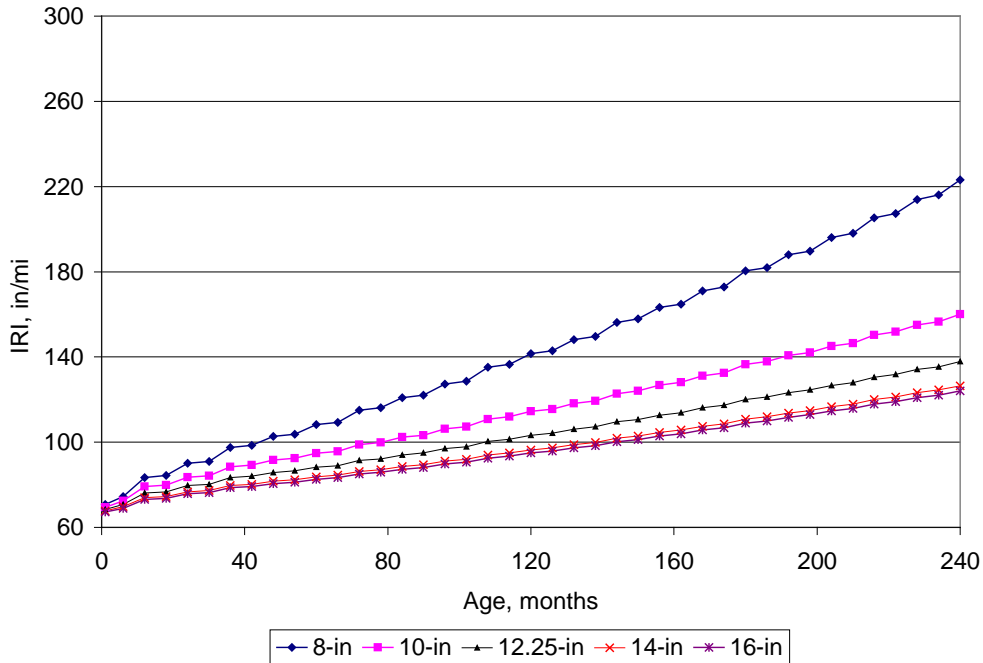


Figure 48. Plot of age versus IRI showing the effect of total HMA thickness.

Table 10 summarizes the relative effect of HMA thickness on all distress and IRI. Information presented in table 10 shows that alligator cracking, rutting, and IRI were all highly influenced by HMA thickness. As HMA increases in thickness the alligator cracking, rutting, and IRI all decrease as would be expected.

Table 10. Relative effect of HMA thickness on HMA distress and IRI.

Distress/IRI	Effect of HMA Thickness on Distress/IRI
Low temperature transverse cracking	Moderate
Longitudinal fatigue cracking	Large effect < 8-in HMA
Bottom-up fatigue (alligator) cracking	High
Rutting	High
IRI	High

### Effect of Subgrade Type

The effect of subgrade type (AASHTO Classification) on performance was determined by comparing distress and IRI over time with subgrade types. The subgrade properties included in the MEPDG that change with the various subgrade soil types are resilient

modulus, gradation, and Atterberg limits. The most significant property affecting distress development is the resilient modulus which affects stress, strains, and deformations in the pavement and subgrade. Four soil types were chosen along with typical default inputs recommended for use in the MEPDG and shown in table 11.

As the subgrade modulus decreases, tensile strain in the bottom of the HMA layer as well as vertical strain at the top of the subgrade increase. Figures 49 through 53 present the effect of subgrade soil type (A-1-b, A-3, A-6, and A-7-6) on predicted distress and smoothness. In general, the lower the subgrade type/modulus the higher alligator fatigue cracking, rutting, and IRI.

Table 11. Recommended subgrade resilient modulus input (at optimum density and moisture) for flexible pavements and rehabilitation of flexible pavements.

<b>AASHTO Soil Class</b>	<b>Mean LTPP NDT Moduli (Std. dev.) (psi)*</b>	<b>Mean LTPP NDT Moduli for Subgrades (Std. dev.) (psi)*</b>	<b>Recommended Input Optimum Resilient Modulus (psi)**</b>
A-1-a	35,397 (20,115)	46,764 (15,950)	36,000 (25,203)
A-3	35,413 (19,652)	32,047 (14,251)	28,500 (12,849)
A-6	25,969 (5,937)	24,665 (5,518)	40,500 (8,429)
A-7-6	11,360 (8,106)	12,638 (8,758)	17,500 (12,898)

\*Information provided in this table was obtained from the LTPP database.

\*\*Information obtained after correcting the NDT values by environmental conditions, using the environmental factors given by the Design Guide. This is resilient modulus at optimum moisture content.

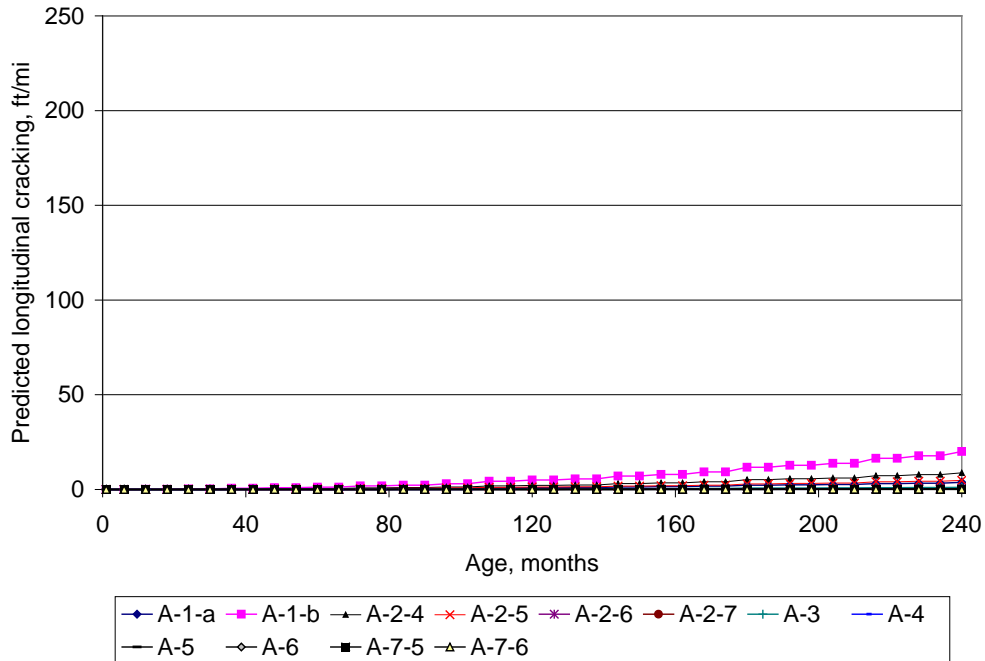


Figure 49. Plot of age versus top-down fatigue (longitudinal) cracking showing the effect of subgrade type.

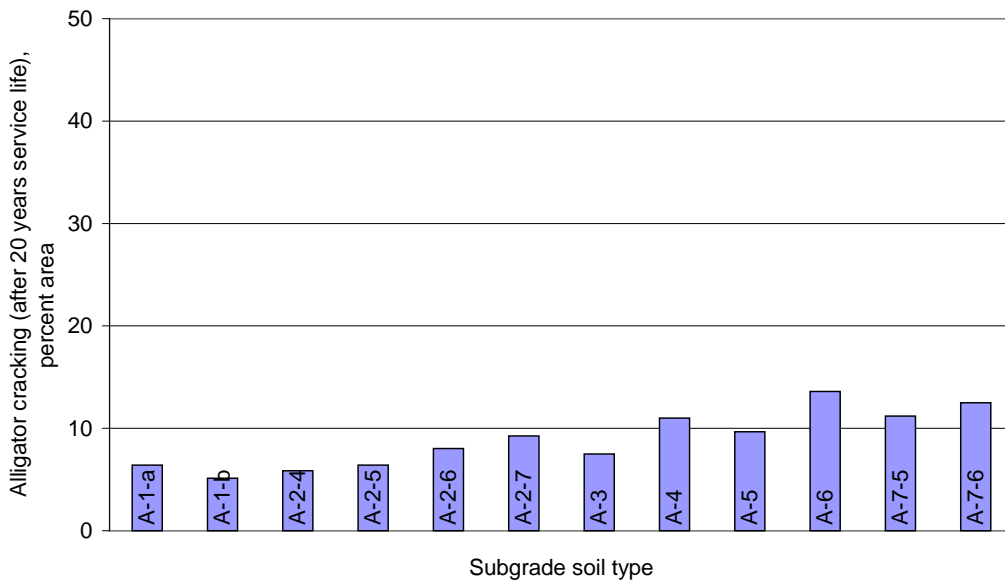


Figure 50. Plot of age versus bottom-up fatigue (alligator) cracking showing the effect of subgrade type.

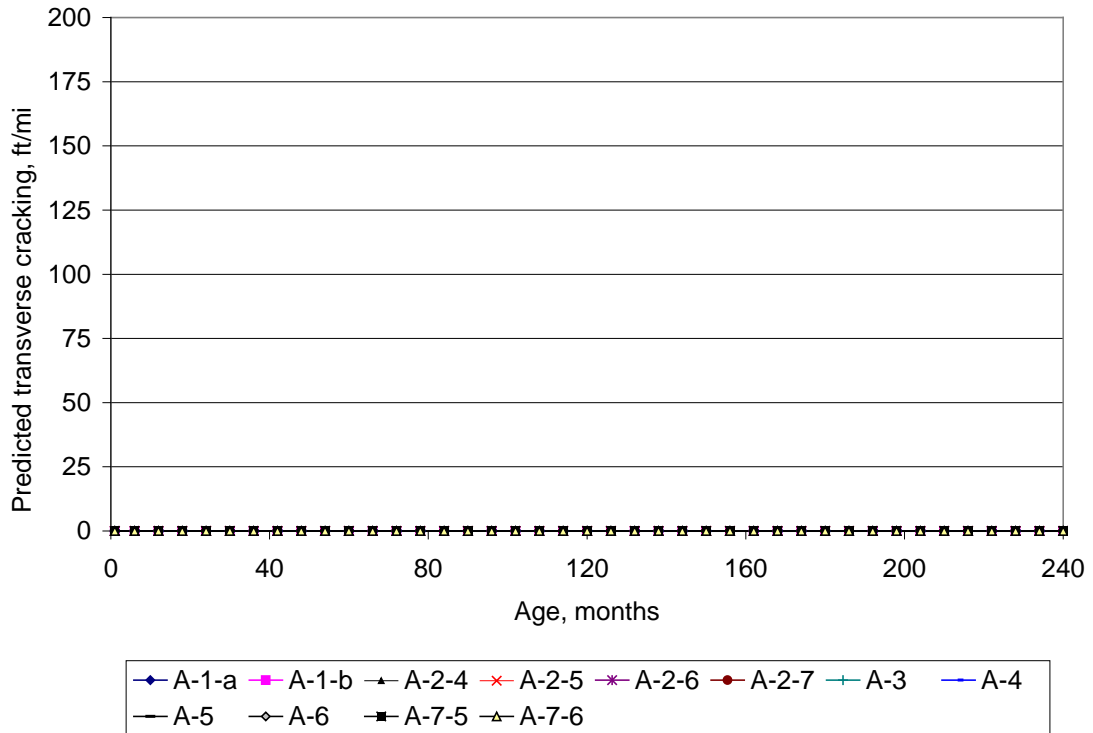


Figure 51. Plot of age versus temperature related (transverse) cracking showing the effect of subgrade type.

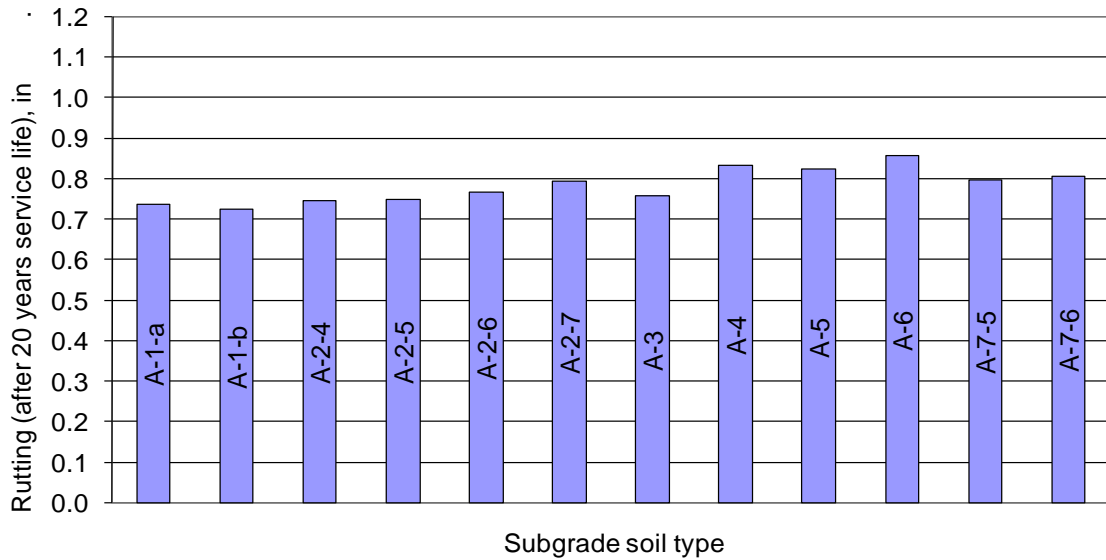


Figure 52. Plot of age versus rutting showing the effect of subgrade type.

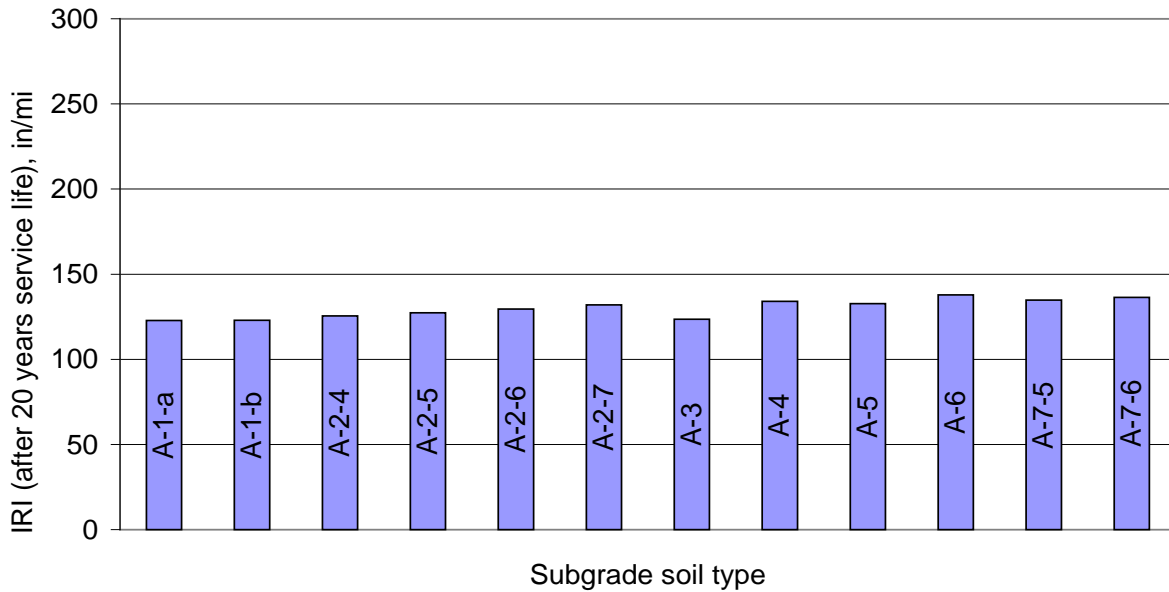


Figure 53. Plot of age versus IRI showing the effect of subgrade type.

Table 12 show the relative effect of subgrade type on all distress types and IRI. Information presented in table 12 shows that some distresses and IRI were influenced by subgrade type. The impact was greatest on bottom-up alligator (fatigue) cracking were the softer subgrade showed the most fatigue cracking and the most rutting.

Table 12. Relative effect of subgrade type on HMA distress and IRI.

Distress/IRI	Effect of Subgrade Type on Distress/IRI
Longitudinal (fatigue) cracking	None
Low temperature transverse cracking	None
Bottom-up fatigue (alligator) cracking	Moderate
Rutting	Moderate
IRI	Low

Effect of Treated Subgrade

Two prominent subgrade soil types were identified in Ohio including A-2-4 and A-6. The effects of treating the top 12 inches of the A-6 subgrade soil with cement and lime were compared with having just a 12-in compacted A-6 subgrade soil layer. For A-2-4 subgrade soil type only cement stabilization option was used and compared with simply compacting the top 12-in of the A-2-4 subgrade soil.

Subgrade treatment had a significant effect on alligator (fatigue) cracking and on rutting for each soil type (see figures 54 to 58 and table 13). This effect also carried over to IRI. In all cases, lime and cement treatment reduced these distresses and IRI. Longitudinal cracking and low temperature cracking showed no response to subgrade treatment. These results indicate the potential benefits of treating the top 12 in of the subgrade.

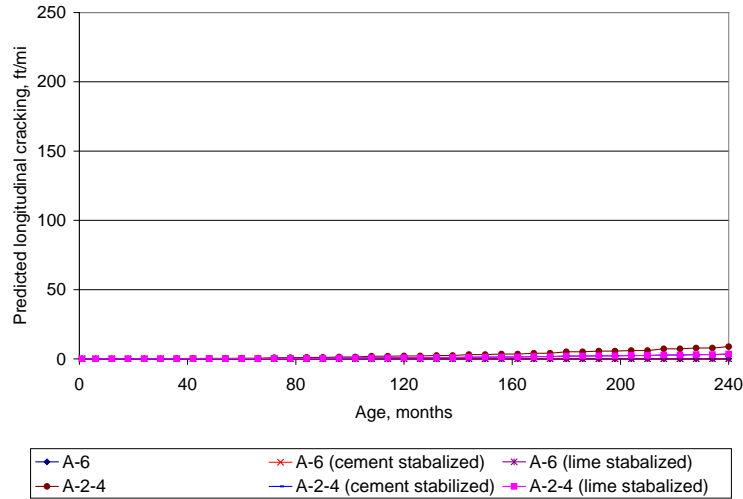


Figure 54. Plot of age versus top-down fatigue (longitudinal) cracking showing the effect of stabilizing/treating the top 12-in of the subgrade soil.

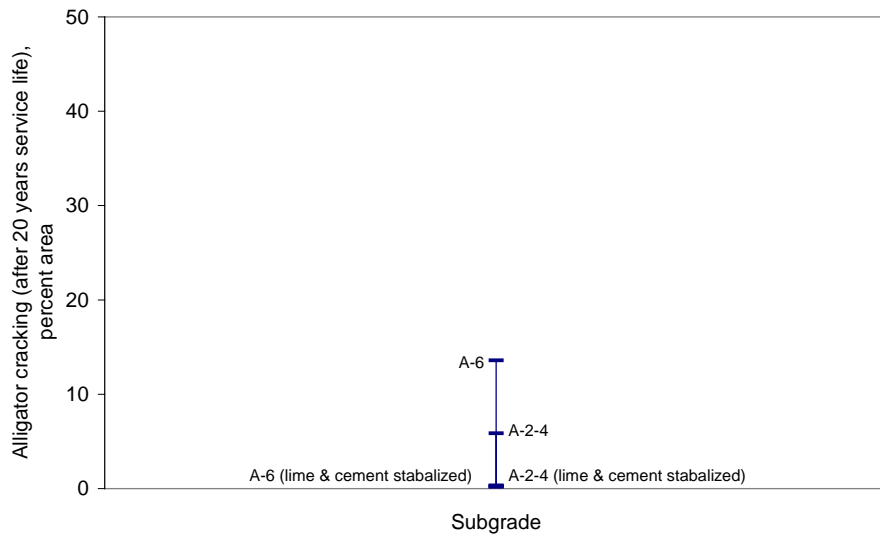


Figure 55. Plot of age versus bottom-up fatigue (alligator) cracking showing the effect of stabilizing/treating the top 12-in of the subgrade soil.

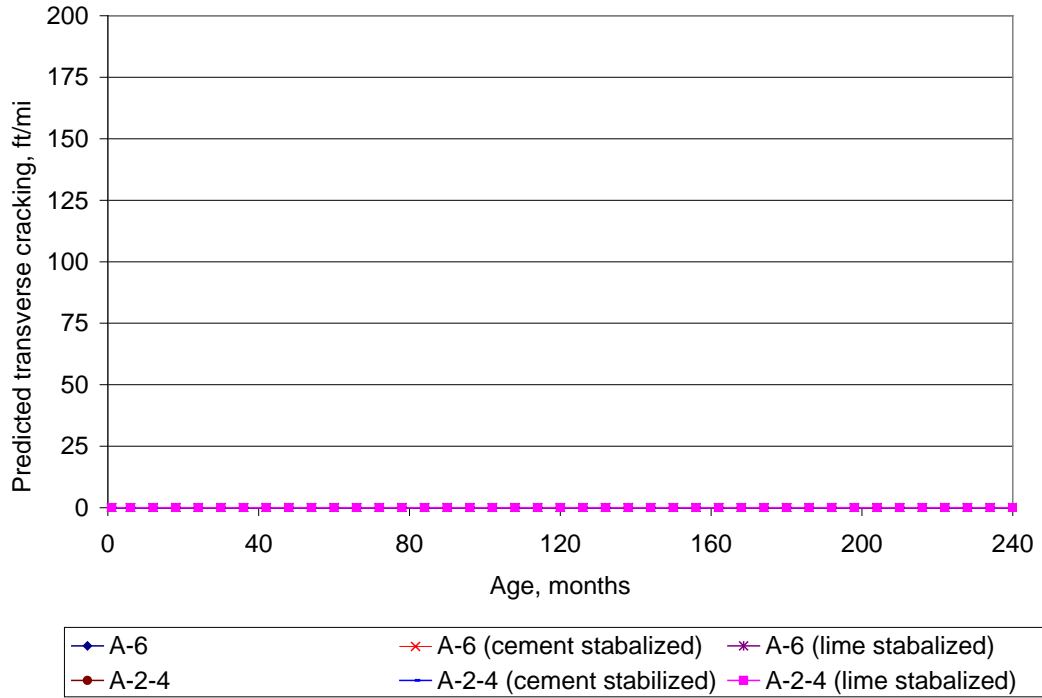


Figure 56. Plot of age versus temperature related (transverse) cracking showing the effect of stabilizing/treating the top 12-in of the subgrade soil.

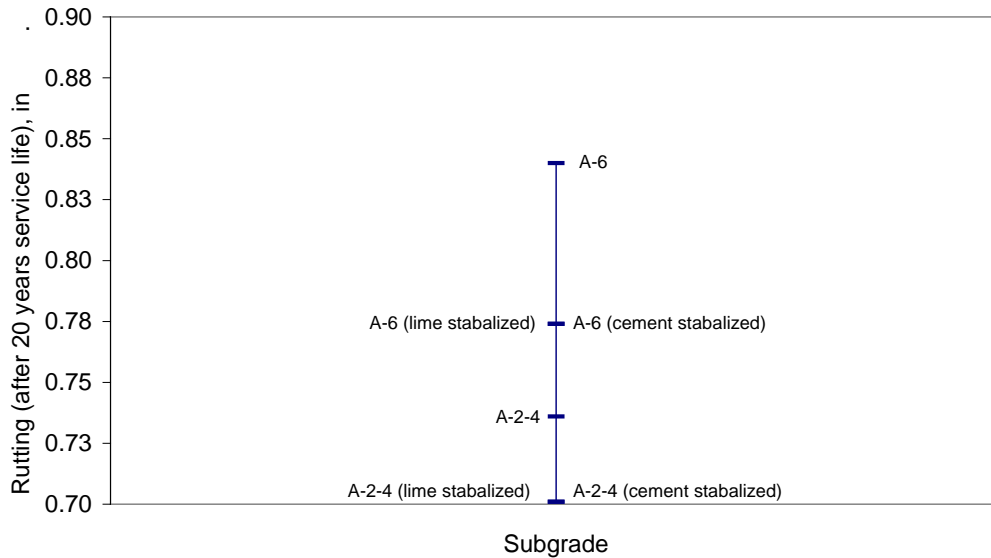


Figure 57. Plot of age versus rutting showing the effect of stabilizing/treating the top 12-in of the subgrade soil.

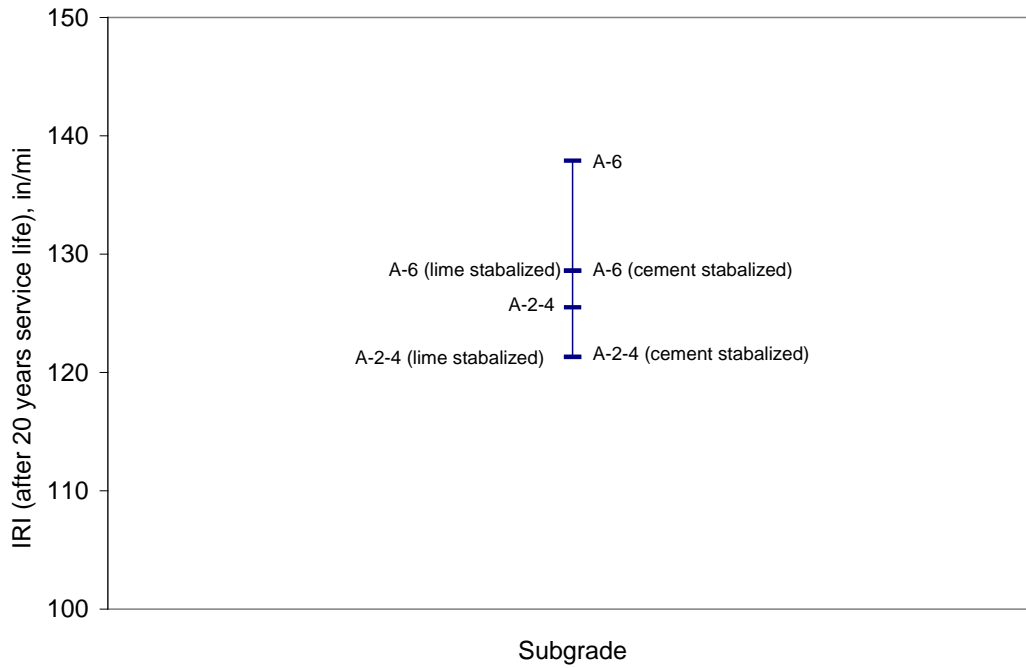


Figure 58. Plot of age versus IRI showing the effect of stabilizing/treating the top 12-in of the subgrade soil.

Table 13. Relative effect of subgrade treatment on HMA distress and IRI.

<b>Distress/IRI</b>	<b>Effect of Subgrade Treatment on Distress/IRI</b>
Longitudinal (fatigue) cracking	None
Low temperature transverse cracking	None
Bottom-up fatigue (alligator) cracking	Moderate
Rutting	Moderate
IRI	Moderate

## Effect of HMA In-Situ Air Voids

Changes in HMA parameters such as air voids are expected to have an effect on distresses since they may affect the dynamic modulus and other properties. Figure 59 shows the effect of the air voids in the base layer (lowermost HMA layer) on predicted alligator fatigue cracking. As can be noted, an increase of in situ air void content in the lowermost HMA layer results in a large increase in alligator cracking. Figure 60a shows that an increase of in situ air void content (in the upper most two layers) impacts the rate of progression of transverse cracking in the first five years post construction. Figure 60b shows that an increase of in situ air void content (in the upper most two layers) also results in an increase in rutting. IRI shows the same but is not affected much by a change of in situ air void content over this range (figure 61). Other distresses showed no effect of in situ air voids. Table 14 summarizes the relative effect of HMA in situ air void content on all distress types and IRI. HMA air voids had the most significant effect on alligator cracking.

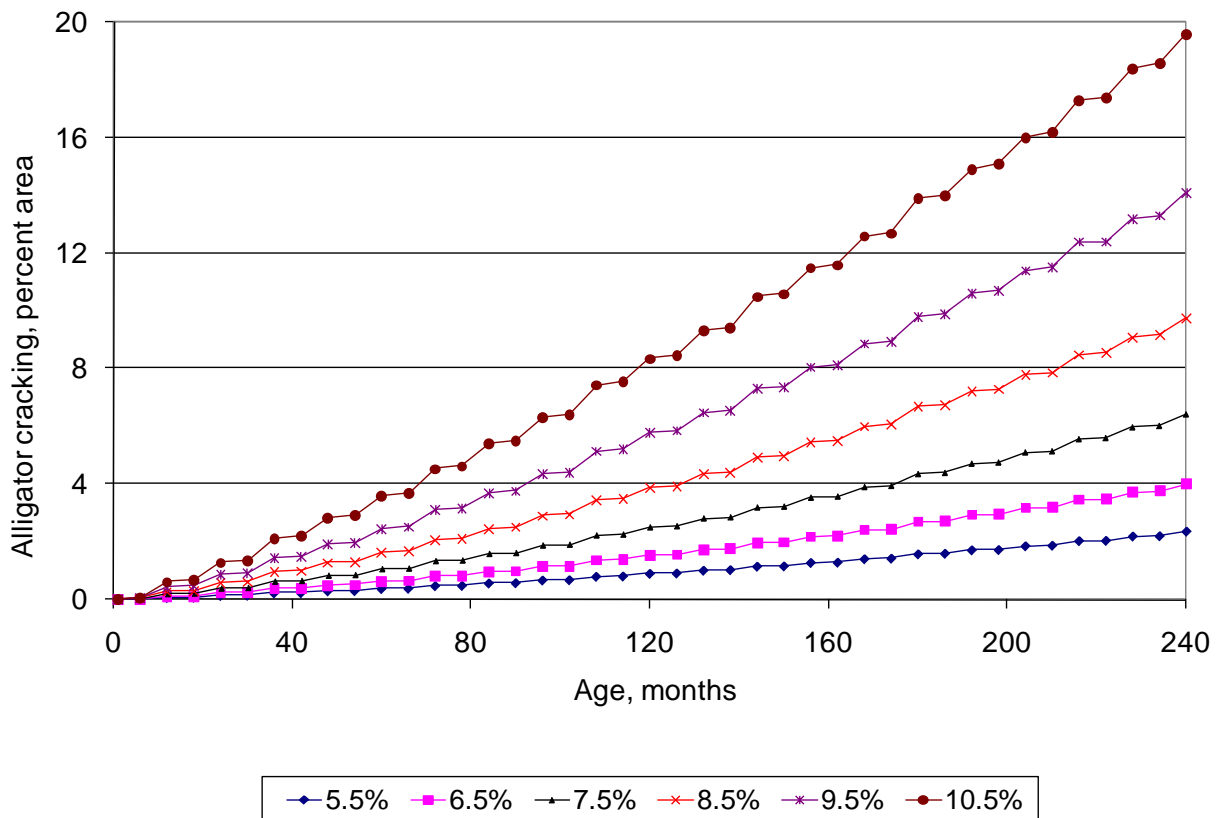


Figure 59. Plot of age versus bottom-up fatigue (alligator) cracking showing the effect of HMA in situ air void content in lower most HMA layer (MEPDG layer 3).

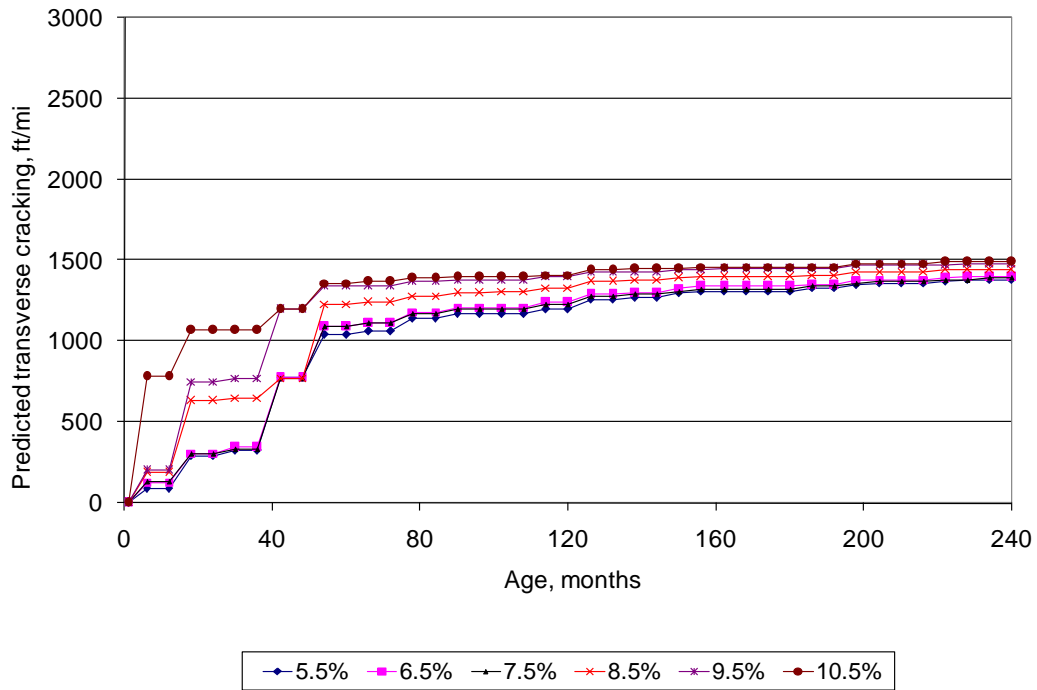


Figure 60a. Plot of age versus thermal (transverse cracking) showing the effect of HMA in situ air void content in upper most HMA layer. (MEPDG layer 1)

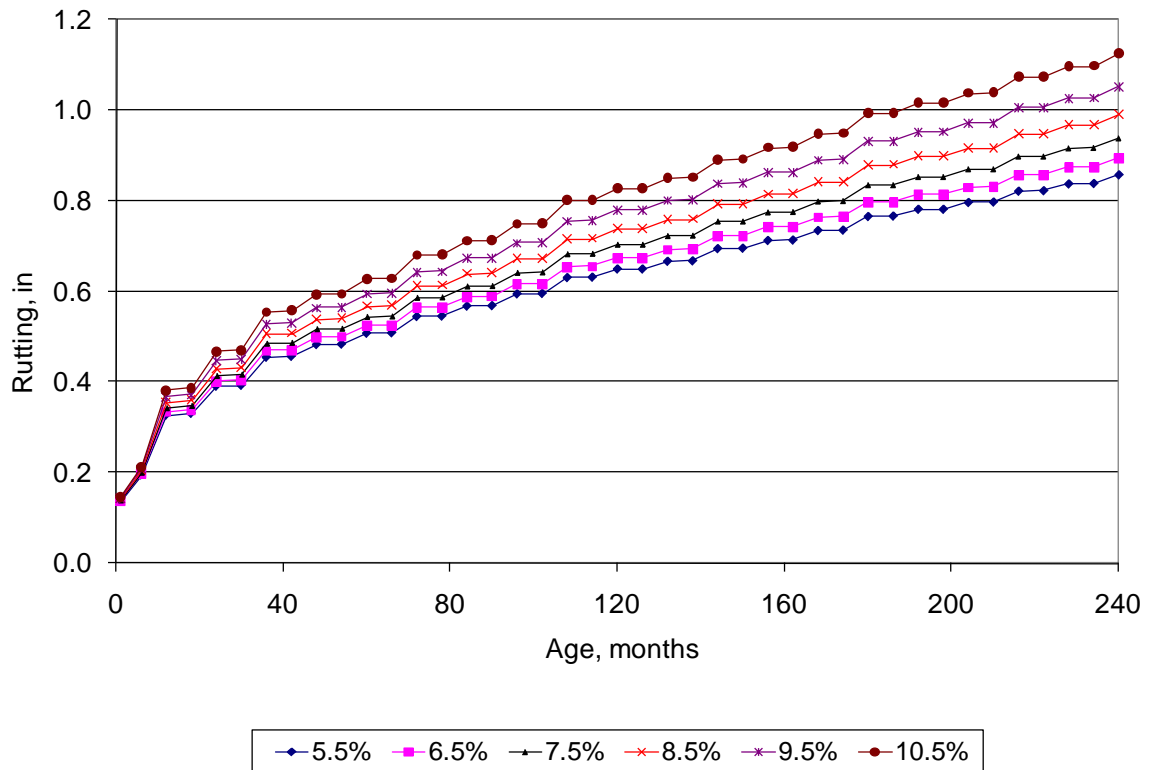


Figure 60b. Plot of age versus rutting showing the effect of HMA in situ air void content in the top layers (MEPDG layers 1 & 2).

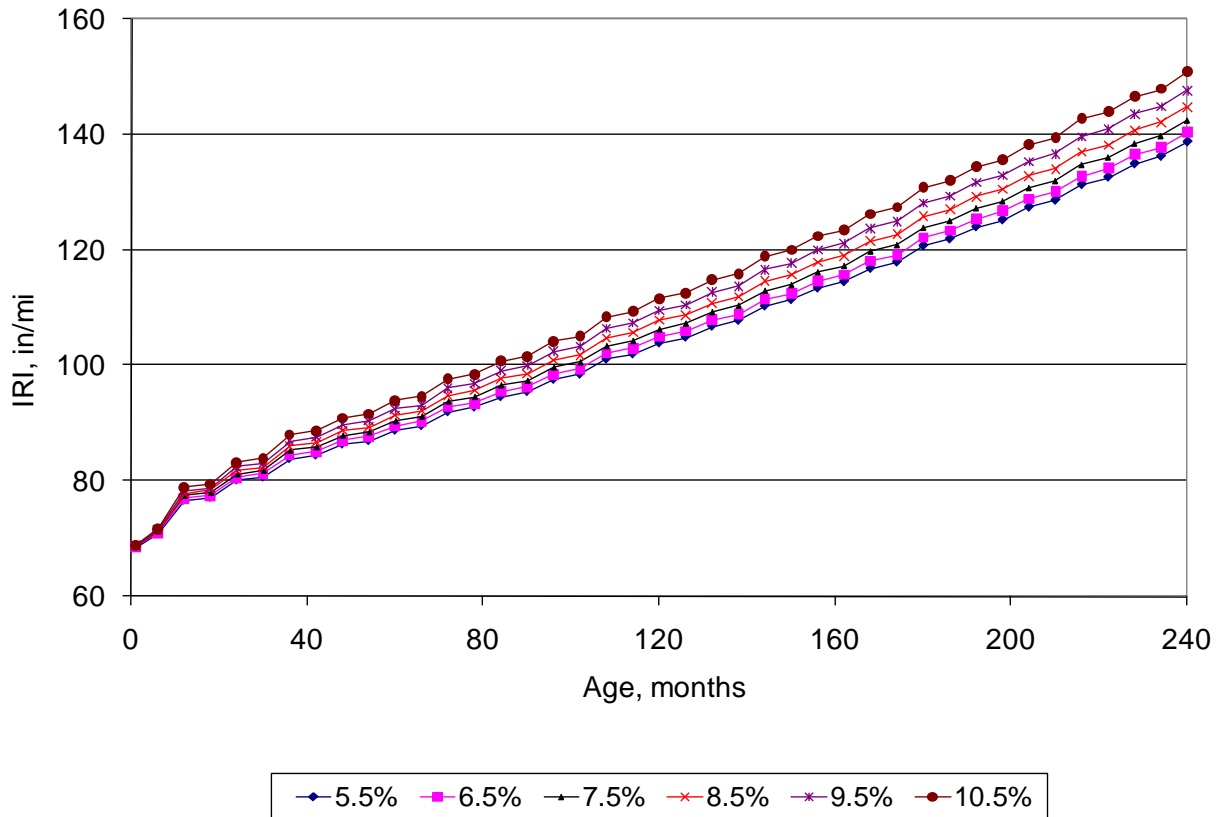


Figure 61. Plot of age versus IRI showing the effect of HMA in situ air void content in the top layers (MEPDG layers 1 & 2).

Table 14. Relative effect of HMA air voids on HMA distress and IRI.

<b>Distress/IRI</b>	<b>Effect of HMA Air Voids on Distress/IRI</b>
Low temperature transverse cracking	Low to moderate (in the first five years). None afterwards
Longitudinal fatigue cracking	None (voids change in the upper most HMA layer)
Bottom-up fatigue (alligator) cracking	Moderate (voids change in the lower most HMA layer)
Rutting	Moderate (voids change in the upper two HMA layers)
IRI	Low (voids change in the upper two HMA layers)

## Effect of HMA Binder Content

HMA binder content also affects the dynamic modulus ( $E^*$ ) and other mixture parameters. Note that in situ air voids were held constant for this sensitivity at 8.5 percent. Figures 62 through 64 show the effect of HMA binder content on distress and IRI. The figures show that while increasing binder content reduces alligator cracking it significantly increases rutting. Table 15 shows the relative effect of HMA volumetric binder content on all distress types and IRI.

## Effect of HMA Air Voids And Binder Content

Recognizing that air voids and binder content are interrelated to some degree and analysis was performed where both the HMA air voids and binder content are varied at the same time. Figures 65, 66, and 67 show the combined effect of air voids and binder content changes on the MEPDG alligator cracking, rutting and IRI predictions. The results show the following:

- Alligator fatigue cracking is the highest when air voids are increased (alone this would increase alligator cracking) and at the same time asphalt binder content is decreased (alone this would also increase alligator cracking). See figure 65 for this result.
- Alligator fatigue cracking is the lowest when air voids are reduced and asphalt binder content is increased (in the lower HMA layer). See figure 65 for this result.
- When air void content and asphalt binder content are varied as above, they seem to offset the effects of each other and combined have little effect on rutting as shown in figure 66.

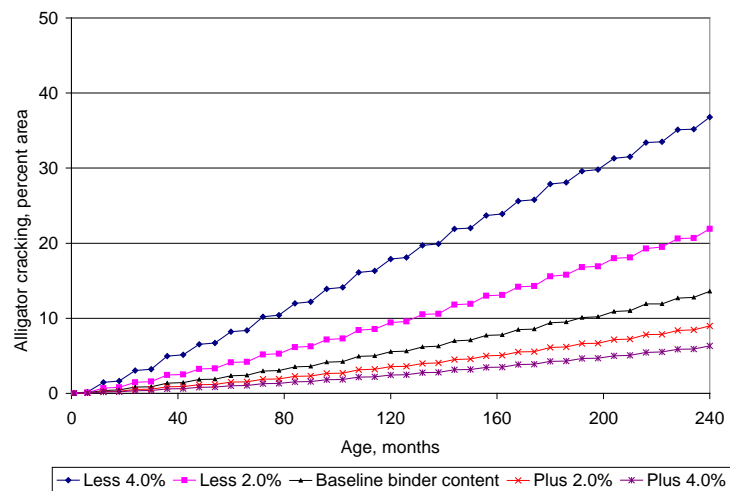


Figure 62a. Plot of age versus alligator cracking showing the effect of HMA asphalt binder content (MEPDG layer 3).

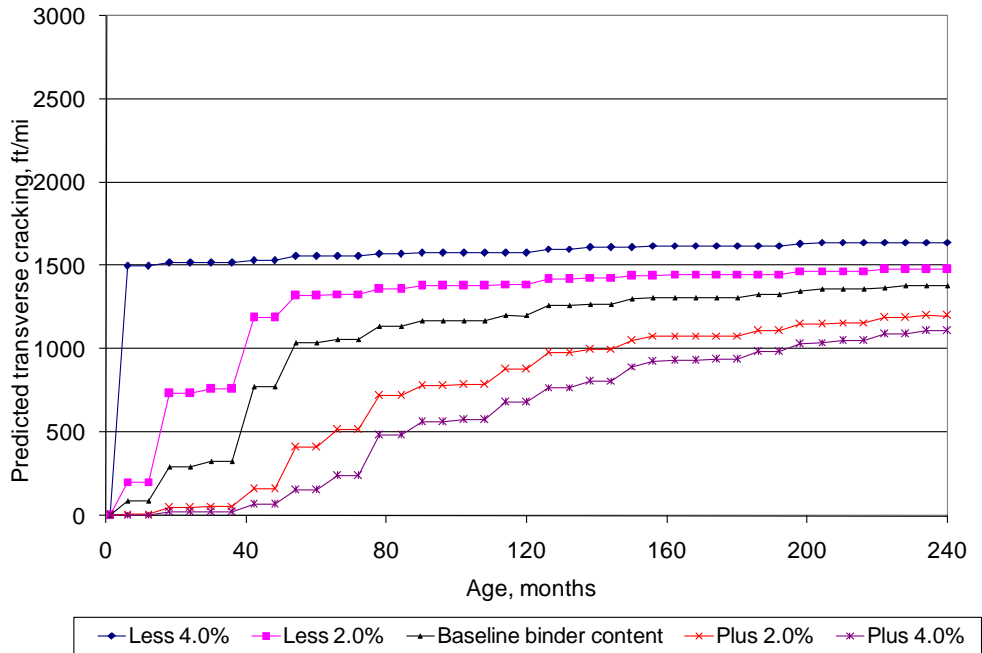


Figure 62a. Plot of age versus thermal (transverse) cracking showing the effect of HMA asphalt binder content (MEPDG layer 1).

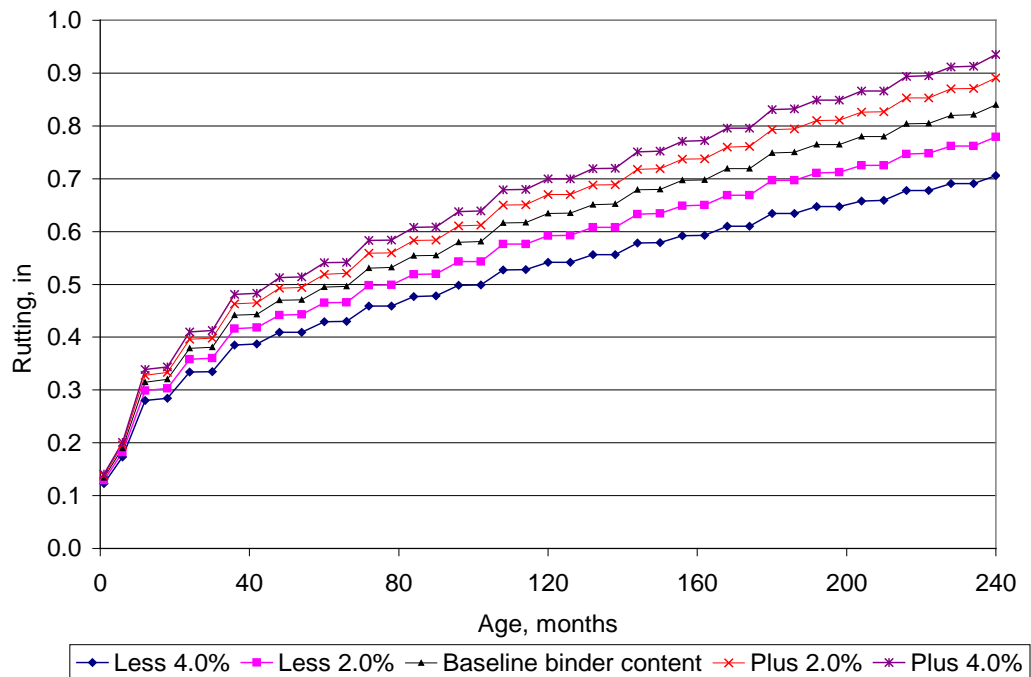


Figure 63. Plot of age versus rutting showing the effect of HMA asphalt binder content (MEPDG layers 1 and 2).

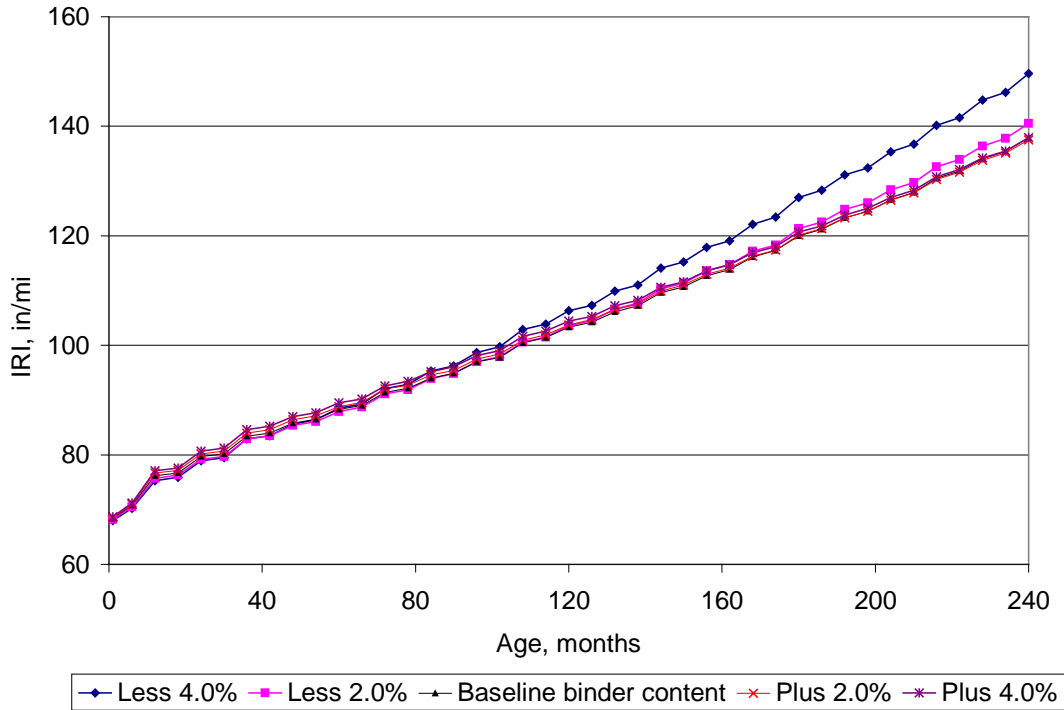


Figure 64. Plot of age versus IRI showing the effect of HMA asphalt binder content (MEPDG layers 1 and 2).

Table 15. Relative effect of HMA volumetric binder content on HMA distress and IRI.

Distress/IRI	Effect of HMA Volumetric Binder Content on Distress/IRI
Longitudinal (fatigue) cracking	None
Low Temperature thermal cracking	Moderate to high
Bottom-up fatigue (alligator) cracking	High (change in binder content in lower layer)
Rutting	High (change in binder content in upper two layers)
IRI	Low

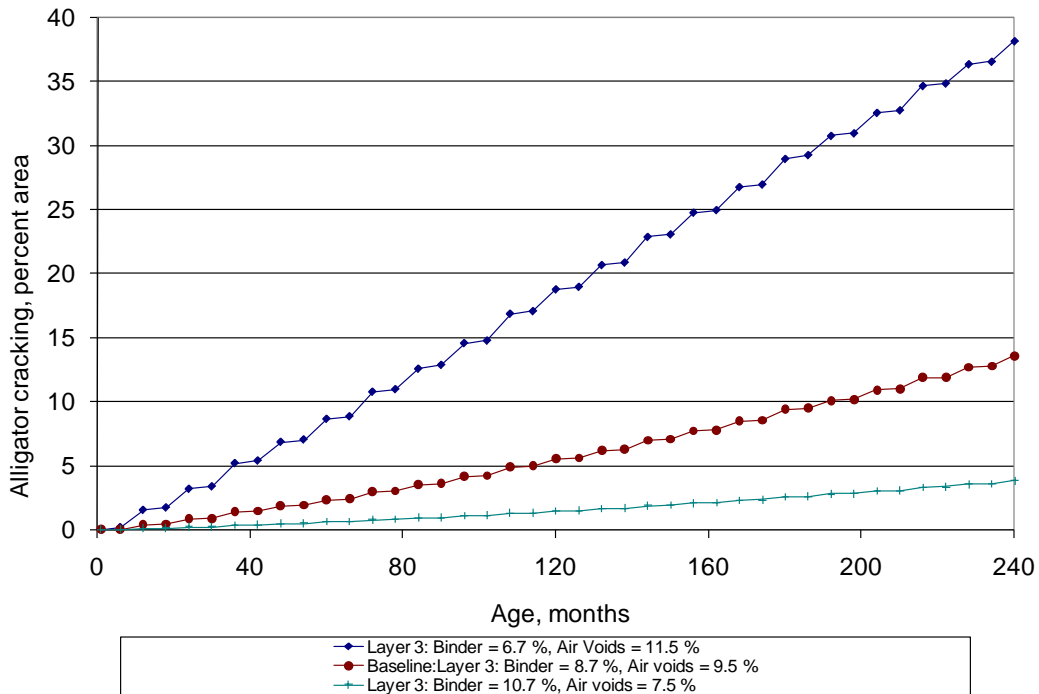
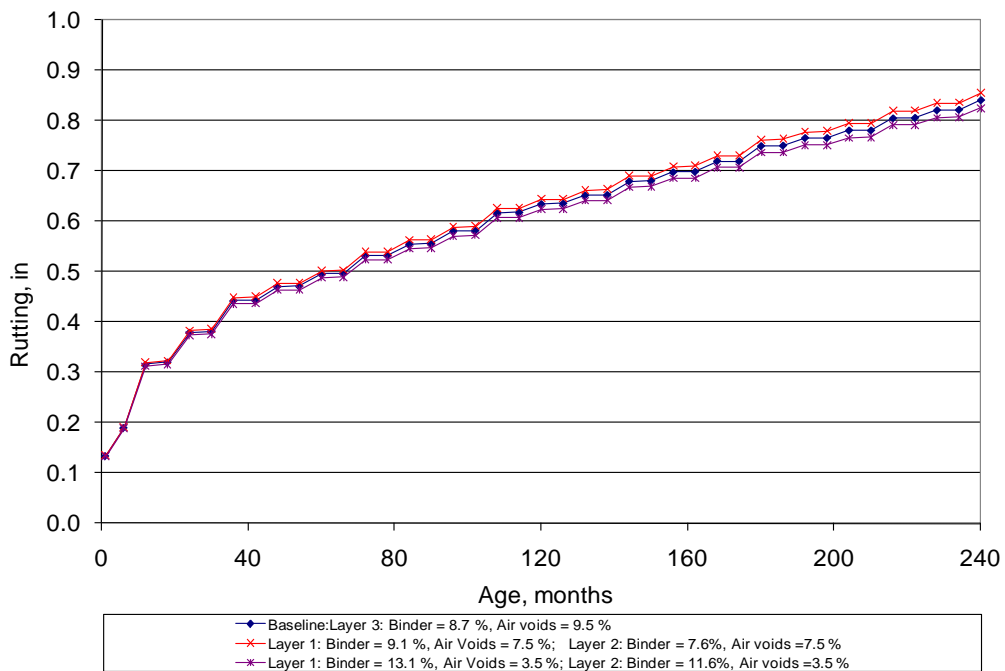


Figure 65. Plot of age versus bottom-up fatigue (alligator) cracking showing the combined effect of varying HMA binder and air voids content in lower most HMA layer (MEPDG layer)



3).

Figure 66. Plot of age versus rutting showing the effect of the combined effect of varying HMA binder and air voids content in the top layers (MEPDG layers 1 & 2).

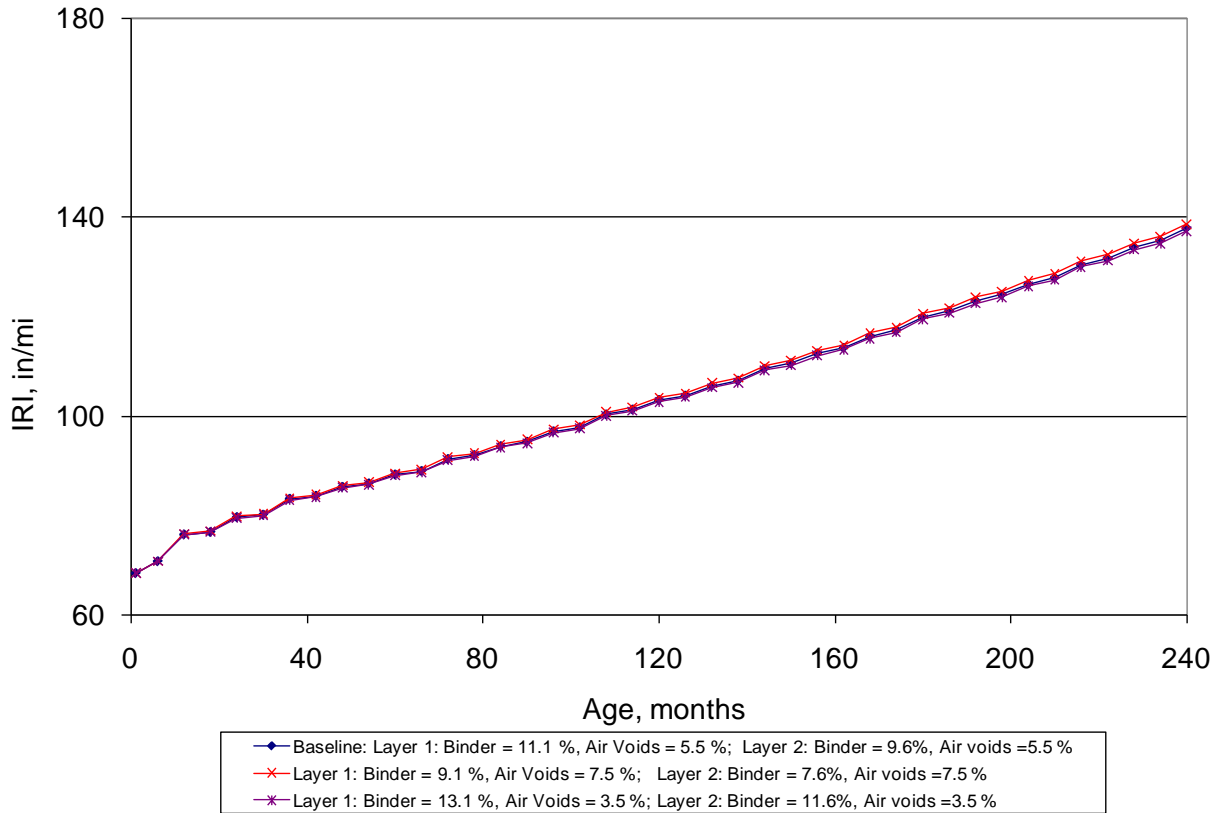


Figure 67. Plot of age versus IRI showing the combined effect of varying HMA binder and air voids content in the top two HMA layers (MEPDG layers 1 & 2).

### Effect of HMA Traffic Composition

Traffic composition (i.e., vehicle class distribution and axle load distribution) are expected to influence the extent of pavement condition deterioration. Typically, pavement deterioration is significantly increased as the traffic composition is dominated by heavier trucks and axle loads.

For this sensitivity study, various combinations of traffic composition representing ODOT rural and urban highways (varying truck class distribution and axle load distribution) were applied. A total of 12 (6 urban and 6 rural) combined vehicle class/axle load distributions were applied (see table 16). The traffic composition data was obtained from WIM sites located throughout Ohio. The data was collected by ODOT and processed by both ODOT and LTPP. The vehicle class distribution of the 12 LTPP sites along with single, tandem, tridem, and quad axle load distributions for the 12 LTPP sites have been presented in table 16. Tables 17 through 20 present estimates of single, tandem, tridem, and quad axles per truck ratios computed for each of the 12 LTPP sites.

Table 16. Traffic description and corresponding vehicle (truck) class distribution values (percentages).

Designation	LTPP Section ID	Location	Vehicle/Truck Class Distribution (percent)									
			4	5	6	7	8	9	10	11	12	13
R1	39_0100*	Rural	5.66	5.66	3.44	0.55	6.79	73.14	1.53	2.20	0.38	0.67
R2	39_0200*	Rural	5.89	6.36	3.07	0.78	7.21	70.43	1.68	2.27	0.45	1.86
R3	39_3013	Rural	15.43	16.81	15.37	0.71	19.45	28.88	1.99	0.56	0.09	0.72
R4	39_5003	Rural	0.64	16.18	18.21	2.10	8.70	48.59	3.79	0.14	0.46	1.19
R5	39_5010	Rural	8.31	6.81	2.61	0.33	9.84	66.56	2.61	0.59	0.75	1.59
R6	39_9006	Rural	4.24	2.43	1.28	0.04	4.75	79.54	0.64	5.04	1.85	0.19
U1	39_3801	Urban	9.11	8.62	9.59	2.33	6.48	61.27	1.92	0.37	0.05	0.26
U2	39_4018	Urban	8.08	13.95	4.85	0.44	7.76	61.28	1.19	1.71	0.46	0.29
U3	39_4031	Urban	10.71	10.16	8.69	0.52	8.68	52.99	1.83	4.93	0.40	1.10
U4	39_5569	Urban	14.36	13.81	12.34	1.06	10.44	42.44	3.58	1.48	0.07	0.42
U5	39_7021	Urban	6.59	4.09	3.68	0.19	4.77	74.60	1.79	2.37	0.35	1.57
U6	39_9022	Urban	1.03	28.94	9.95	0.64	8.84	48.05	1.06	0.94	0.13	0.42

\* Since these experiments are built in the median of the DEL 23 highway, lane closures for maintenance or detailed pavement investigations are common. Therefore, the traffic data needs to be more carefully analyzed for validation/calibration to ensure that the lane closures are accounted for. The data in this table represents what is contained in the LTPP traffic tables (which computes average traffic based on total volumes). This level of data resolution is considered adequate for a sensitivity study. The traffic data from these sites were analyzed in more detail for validation/calibration.

Table 17. Number of Single Axles/truck for the 12 LTPP Sites.

Designation	LTPP Section ID	Location	No. of Single Axles/truck by Vehicle/Truck Class Distribution									
			4	5	6	7	8	9	10	11	12	13
R1	39_0100	Rural	1.67	3.62	1.56	1.14	2.53	1.23	1.47	4.66	4.02	1.99
R2	39_0200	Rural	1.79	3.67	1.28	1.87	2.46	1.19	1.12	4.22	3.79	5.29
R3	39_3013	Rural	1.59	2.79	1.88	1.83	2.73	1.16	0.97	4.89	13.55	4.07
R4	39_5003	Rural	1.74	1.74	1.01	1.00	1.82	1.24	1.07	6.01	4.02	3.59
R5	39_5010	Rural	1.67	1.98	1.02	1.58	2.11	1.29	1.11	4.88	4.68	0.56
R6	39_9006	Rural	1.73	3.76	1.06	1.83	2.62	1.25	1.03	4.86	3.93	0.89
U1	39_3801	Urban	1.58	1.99	1.05	1.08	2.53	1.33	0.76	5.34	8.46	2.93
U2	39_4018	Urban	1.60	1.95	1.43	1.65	2.40	1.36	1.13	4.44	3.71	1.74
U3	39_4031	Urban	1.67	3.05	0.97	1.20	2.27	1.10	1.19	21.95	3.76	1.68
U4	39_5569	Urban	1.68	2.05	1.07	1.25	2.60	1.22	1.10	4.56	9.44	1.44
U5	39_7021	Urban	1.58	3.65	1.46	1.14	2.40	1.21	1.33	4.90	3.60	0.99
U6	39_9022	Urban	0.83	1.67	0.97	1.53	1.82	0.59	1.10	5.03	5.19	1.36

Table 18. Number of Tandem Axles/truck values for the vehicle (truck) class distribution.

Designation	LTPP Section ID	Location	No. of Tandem Axles/truck by Vehicle/Truck Class Distribution									
			4	5	6	7	8	9	10	11	12	13
R1	39_0100	Rural	0.34	0.00	1.56	0.06	0.49	1.90	1.17	0.06	1.08	0.90
R2	39_0200	Rural	0.27	0.01	1.27	0.53	0.44	1.88	0.86	0.21	0.95	0.84
R3	39_3013	Rural	0.33	0.00	1.85	0.43	0.28	1.87	0.65	0.36	1.17	2.20
R4	39_5003	Rural	0.33	0.00	1.01	0.21	0.53	1.86	0.77	0.01	1.03	1.14
R5	39_5010	Rural	0.31	0.07	0.98	0.81	0.80	1.83	1.14	0.41	1.17	0.85
R6	39_9006	Rural	0.24	0.02	0.85	0.78	0.60	1.87	1.19	0.01	0.99	0.62
U1	39_3801	Urban	0.44	0.03	0.98	0.16	0.44	1.81	0.61	0.49	2.15	1.09
U2	39_4018	Urban	0.38	0.02	1.43	0.65	0.58	1.82	0.93	0.04	1.00	1.55
U3	39_4031	Urban	0.32	0.01	0.89	0.32	0.61	1.94	1.27	0.15	0.94	0.94
U4	39_5569	Urban	0.28	0.01	0.94	0.57	0.43	1.88	1.33	0.25	2.80	1.47
U5	39_7021	Urban	0.29	0.01	1.46	0.17	0.62	1.89	1.20	0.03	0.93	1.17
U6	39_9022	Urban	0.17	0.00	0.97	0.58	0.51	0.96	1.29	0.00	1.30	0.97

Table 19. Number of Tridem Axles/truck values for the vehicle (truck) class distribution.

Designation	LTPP Section ID	Location	No. of Tridem Axles/truck by Vehicle/Truck Class Distribution									
			4	5	6	7	8	9	10	11	12	13
R1	39_0100	Rural	0.00	0.00	0.01	1.07	0.00	0.00	0.82	0.02	0.00	0.16
R2	39_0200	Rural	0.01	0.00	0.00	0.83	0.00	0.00	0.74	0.02	0.01	0.06
R3	39_3013	Rural	0.00	0.00	0.00	1.25	0.01	0.02	0.44	0.13	0.29	1.17
R4	39_5003	Rural	0.01	0.00	0.00	1.00	0.01	0.02	0.21	0.00	0.82	0.20
R5	39_5010	Rural	0.10	0.00	0.01	0.87	0.01	0.00	0.90	0.14	0.00	0.09
R6	39_9006	Rural	0.00	0.00	0.00	0.81	0.00	0.00	0.65	0.01	0.00	0.20
U1	39_3801	Urban	0.00	0.00	0.01	0.95	0.03	0.00	0.46	0.21	0.00	1.13
U2	39_4018	Urban	0.00	0.00	0.01	0.42	0.01	0.00	0.83	0.02	0.06	0.43
U3	39_4031	Urban	0.00	0.00	0.01	0.57	0.01	0.00	0.44	0.11	0.01	0.06
U4	39_5569	Urban	0.01	0.00	0.01	0.89	0.01	0.01	0.56	0.11	0.00	0.06
U5	39_7021	Urban	0.00	0.00	0.00	0.91	0.01	0.00	0.50	0.01	0.00	0.20
U6	39_9022	Urban	0.00	0.00	0.00	0.50	0.00	0.00	0.68	0.00	0.00	0.31

Table 20. Number of Quad Axles/truck values (percentages) for the vehicle (truck) class distribution.

Designation	LTPP Section ID	Location	No. of Quad Axles/truck by Vehicle/Truck Class Distribution									
			4	5	6	7	8	9	10	11	12	13
R1	39_0100	Rural	0.00	0.00	0.00	0.89	0.00	0.00	0.18	0.00	0.01	0.60
R2	39_0200	Rural	0.00	0.00	0.00	0.00	0.00	0.00	0.08	0.00	0.01	0.09
R3	39_3013	Rural	0.00	0.00	0.00	1.11	0.00	0.01	0.28	0.01	0.33	1.58
R4	39_5003	Rural	0.00	0.00	0.00	0.02	0.00	0.00	0.00	0.00	1.21	0.33
R5	39_5010	Rural	0.00	0.00	0.00	0.01	0.00	0.00	0.01	0.00	0.00	0.10
R6	39_9006	Rural	0.00	0.00	0.00	0.42	0.00	0.00	0.04	0.00	0.01	0.35
U1	39_3801	Urban	0.00	0.00	0.00	0.44	0.01	0.00	0.00	0.01	0.00	0.66
U2	39_4018	Urban	0.00	0.00	0.00	0.40	0.00	0.00	0.11	0.00	0.06	0.23
U3	39_4031	Urban	0.00	0.00	0.00	0.04	0.00	0.00	0.50	0.01	0.06	0.82
U4	39_5569	Urban	0.00	0.00	0.00	0.01	0.00	0.00	0.19	0.00	0.05	1.24
U5	39_7021	Urban	0.00	0.00	0.00	0.00	0.00	0.00	0.09	0.00	0.06	0.35
U6	39_9022	Urban	0.00	0.00	0.00	0.00	0.00	0.00	0.00	0.00	0.00	0.81

Figures 68 through 70 show the effect of traffic composition on HMA pavement distress and IRI after the application of 70 million cumulative trucks in 20-year period. Information presented in the plots show that truck composition obtained from the selected LTPP sites in Ohio had a moderate effect on alligator cracking and a more significant effect on rutting. R1 and R7 showed the highest amount of alligator cracking (e.g., 16 percent) and U6 showed the lowest (5 percent). Reasons for this could be attributed to differences in the heavy truck (class 9 and above) at each site as well as axles per truck and load distributions on each axle. The main conclusion is that vehicle class and axle load distribution causes differences in fatigue cracking and rutting and should thus be measured and used in design for a given project. Table 21 presents relative effect of vehicle classification and axle load distribution on HMA distress and IRI.

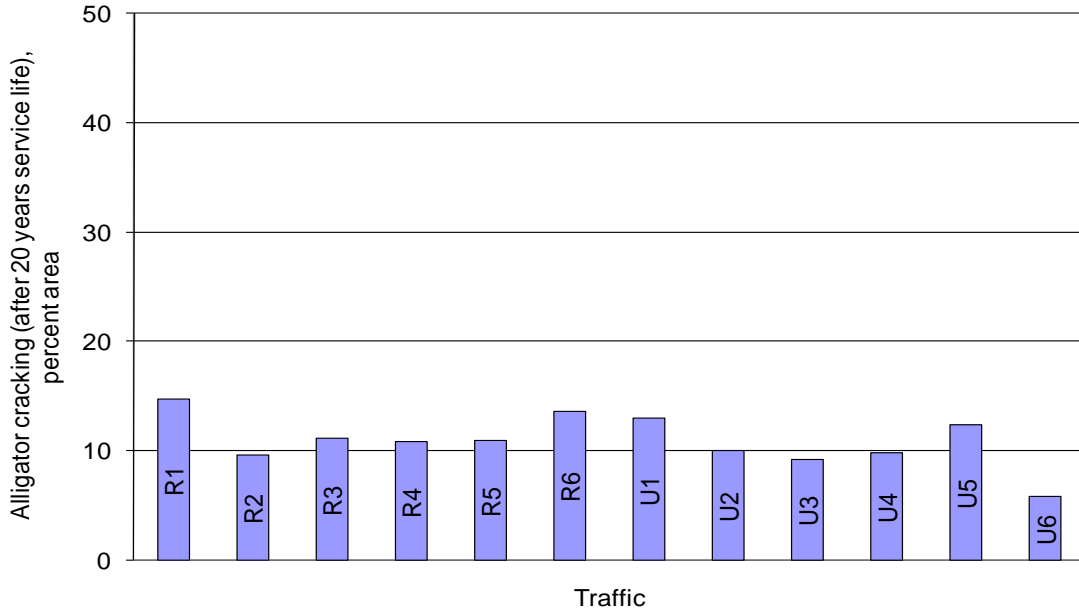


Figure 68. Plot of age versus bottom-up fatigue (alligator) cracking showing the effect of traffic.

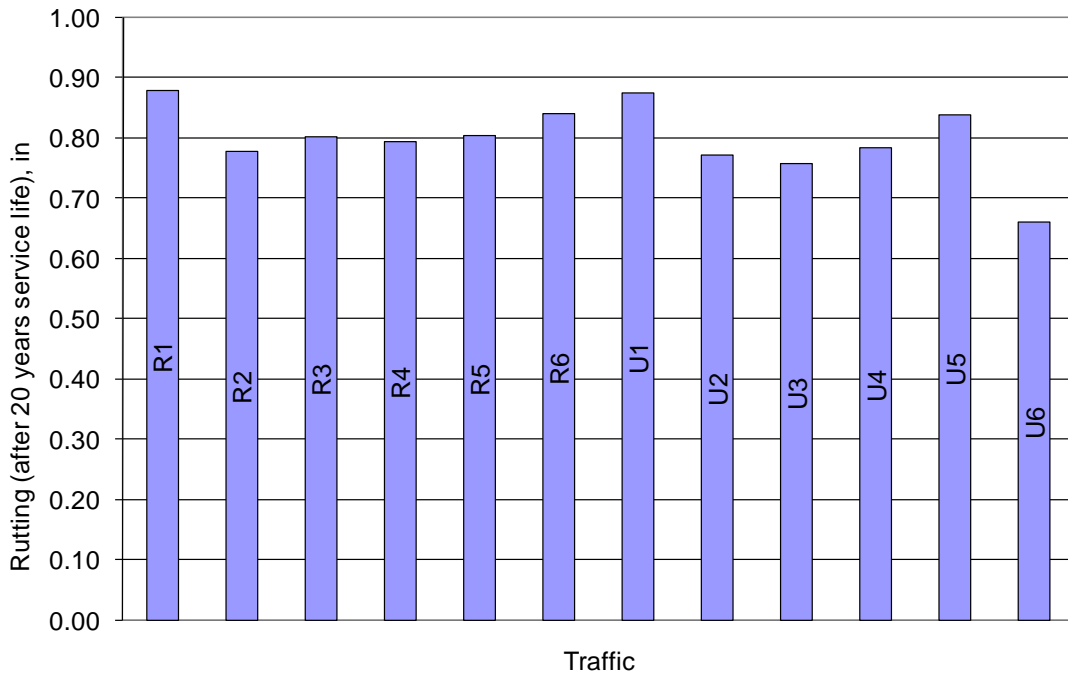


Figure 69. Plot of age versus rutting showing the effect of traffic.

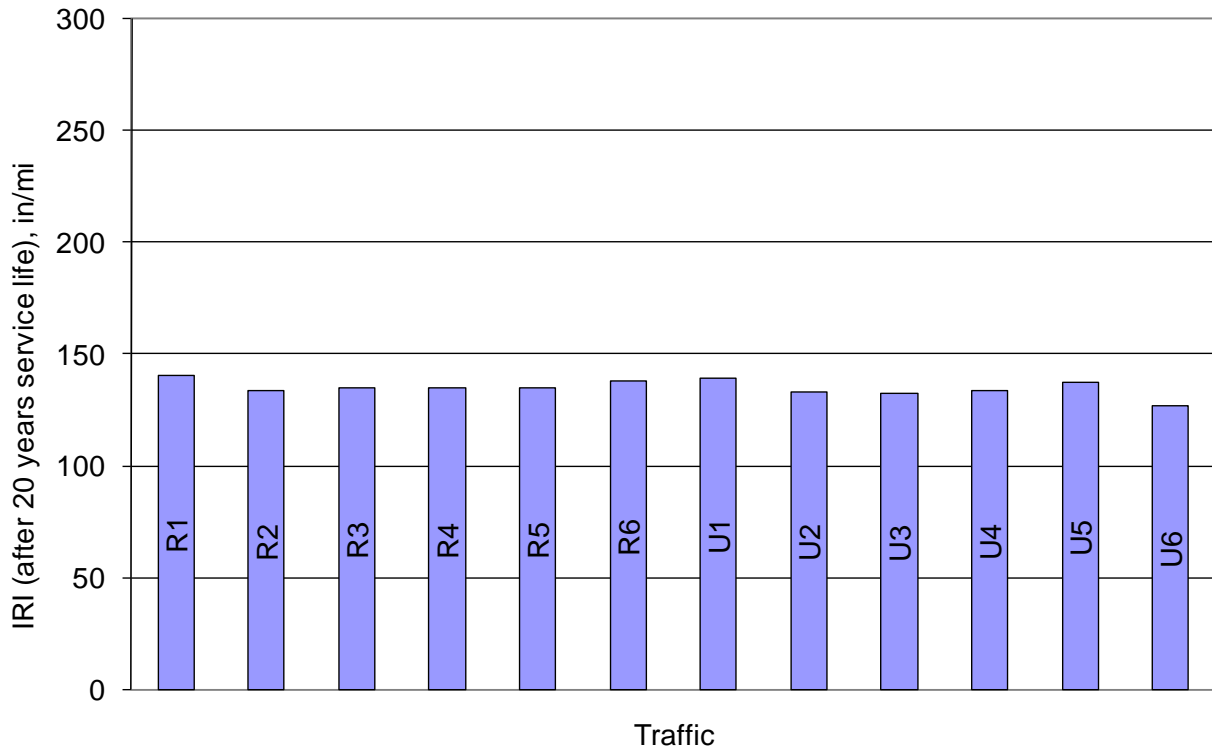


Figure 70. Plot of age versus IRI showing the effect of traffic.

Table 21. Relative effect of vehicle classification and axle load distribution on HMA distress and IRI.

Distress/IRI	Effect of vehicle classification and axle load distribution on HMA Distress/IRI
Longitudinal fatigue cracking	None
Low temperature transverse cracking	None
Bottom-up fatigue (alligator) cracking	Moderate
Rutting	High
IRI	Low

## Effect of ODOT Surface HMA Mix Type

ODOT uses several different types of HMA mixes for high-type pavement surfacing. The three commonly used mix types are Item 446 (conventional HMA), Item 442 (SuperPave) and SMA. For most pavements, a 1.5-in surface course is applied.

Figures 71 through 75 show the effect of HMA surfacing type (Superpave and SMA) on distress and IRI. The figures show that the surfacing type has very little effect on predicted distress/IRI for site conditions represented by the baseline location (City of Newark in central Ohio). Table 22 summarizes the relative effect of surfacing material type on all distress types and IRI. Information presented in table 22 shows that mix type had very little effect on all the distresses and IRI.

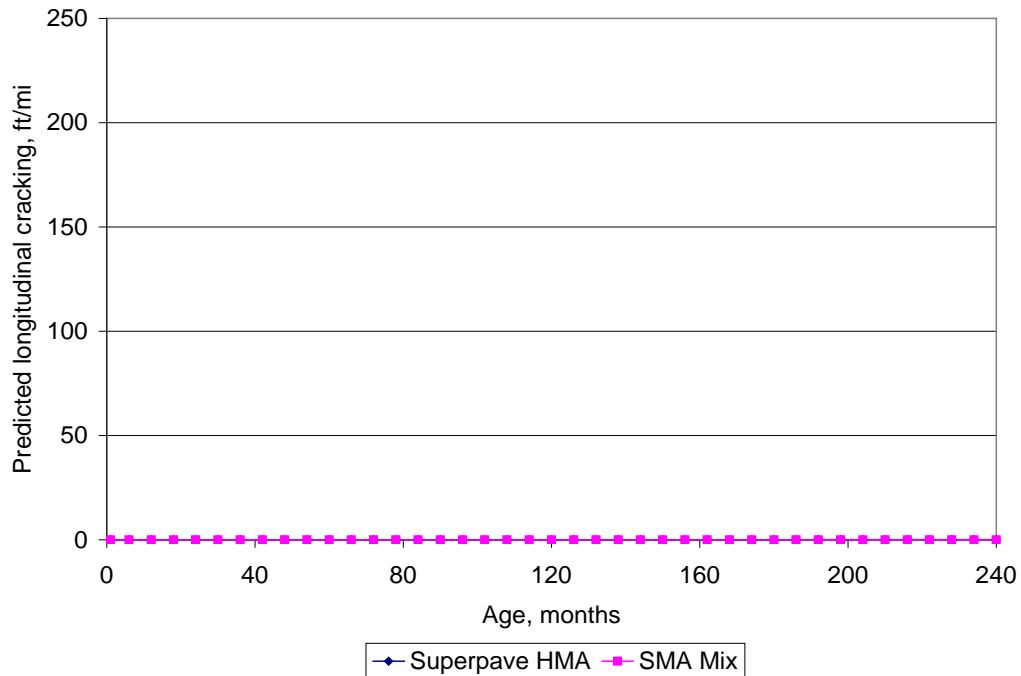


Figure 71. Plot of age versus top-down fatigue (longitudinal) cracking showing the effect of HMA mix type.

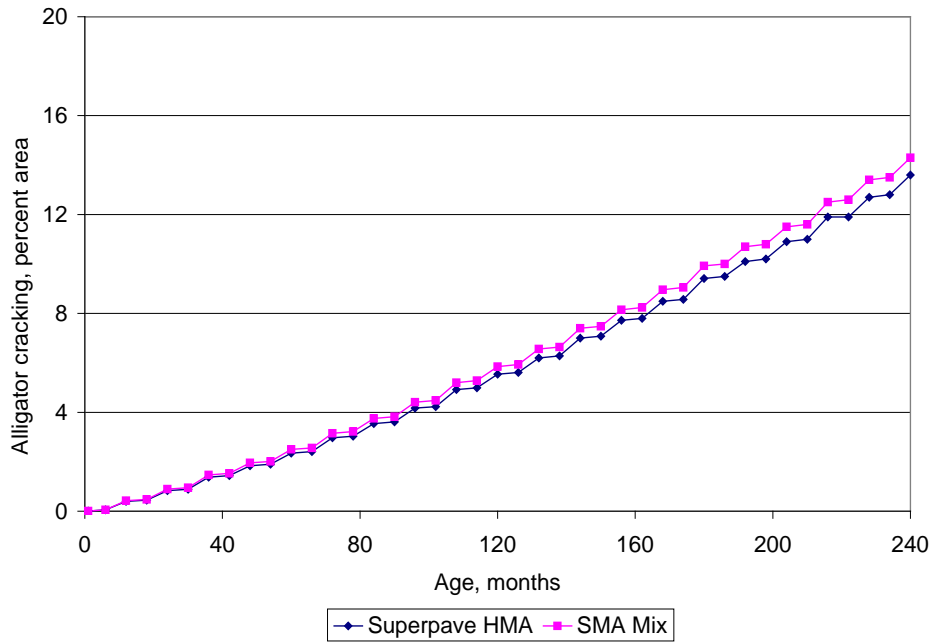


Figure 72. Plot of age versus bottom-up fatigue (alligator) cracking showing the effect of HMA mix type.

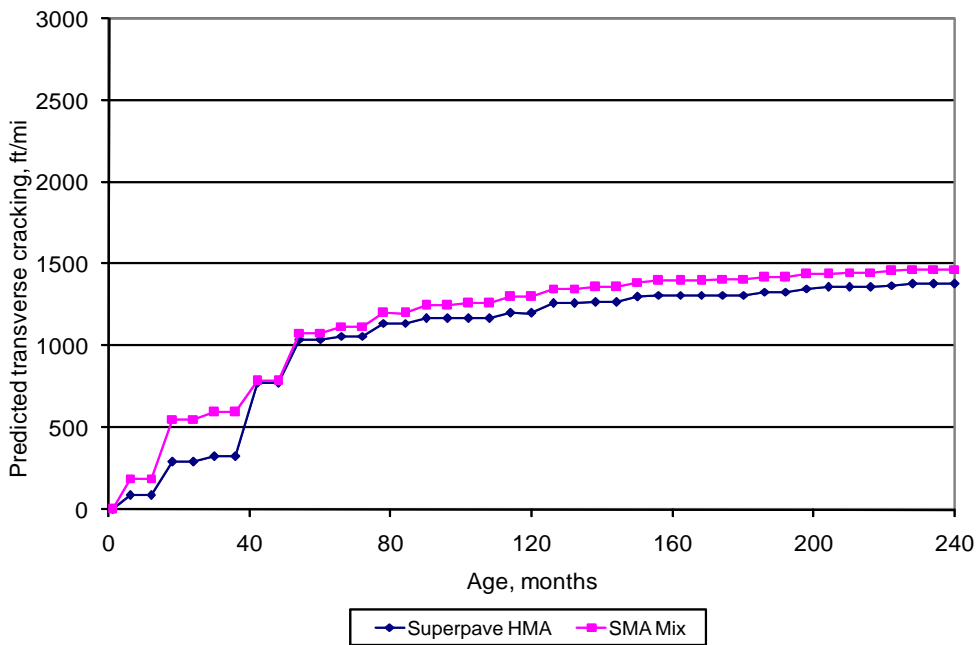


Figure 73. Plot of age versus temperature related (transverse) cracking showing the effect of HMA mix type.

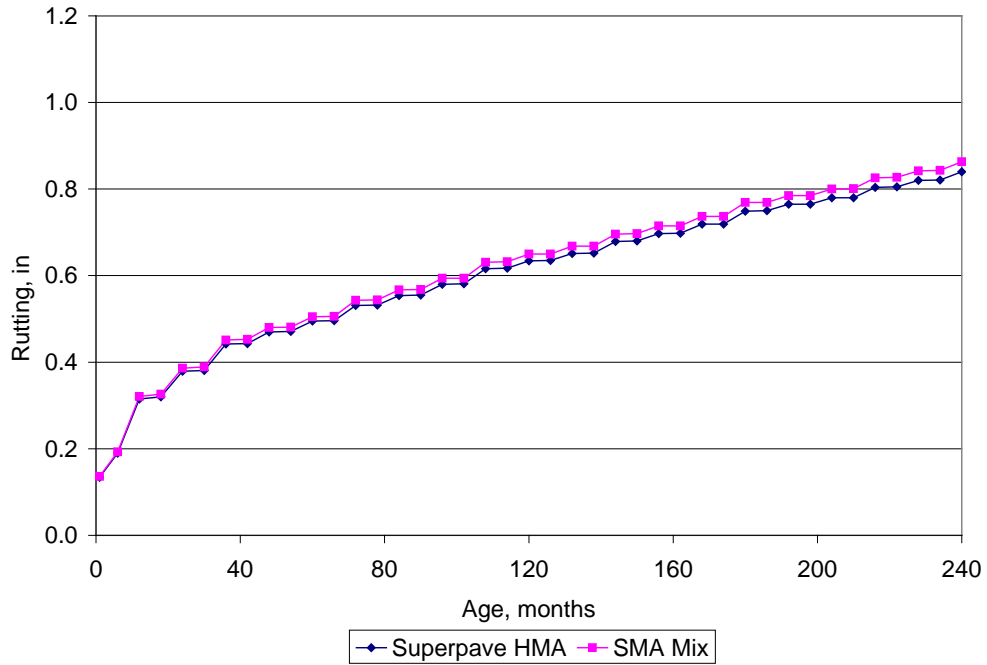


Figure 74. Plot of age versus rutting showing the effect of HMA mix type.

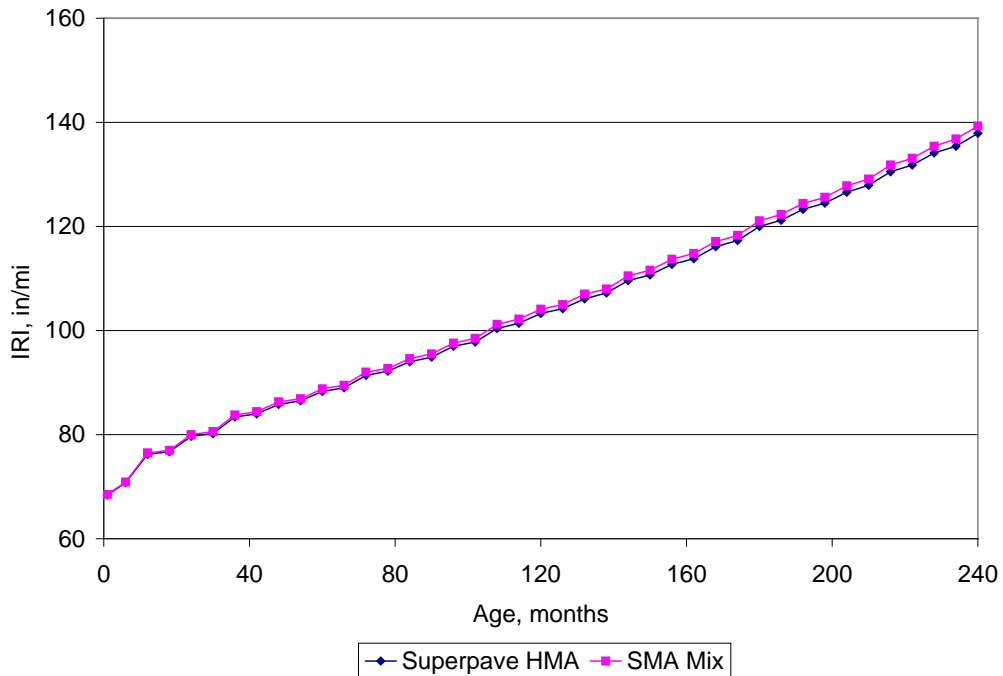


Figure 75. Plot of age versus IRI showing the effect of HMA mix type.

Table 22. Relative effect of HMA mix type on HMA distress and IRI.

Distress/IRI	Effect of HMA Mix Type on Distress/IRI
Longitudinal fatigue cracking	None
Low temperature transverse cracking	Low
Bottom-up fatigue (alligator) cracking	Low
Rutting	Low
IRI	Low



## CHAPTER 3. NEW JPCP SENSITIVITY ANALYSIS

Sensitivity analysis is performed based on typical representative ODOT JPCP designs. The representative ODOT JPCP design also called the baseline design was developed using information gathered from various sources including (1) ODOT pavement design and construction manuals, (2) ODOT research reports, and (3) LTPP database. The sensitivity analysis was conducted to determine how MEPDG input parameters were sensitive to the following:

- Slab “transverse” fatigue cracking.
- Transverse joint faulting.
- IRI.

A description of the baseline ODOT JPCP pavement design used in sensitivity analysis is presented in the following sections.

### New JPCP Baseline Design Construction Date and Analysis Period

The baseline ODOT JPCP was assumed to be constructed in October and opened to traffic in November. An analysis period of 20 years was selected which is ODOT practice. Figure 76 shows the dates of construction and opening to traffic for the baseline ODOT JPCP design.

The screenshot shows a software dialog box titled "General Information". It contains the following fields and options:

- Project Name: 1\_baseline
- Description: (empty text area)
- Design Life (years): 20
- Base/Subgrade Construction Month: (empty dropdown) Year: (empty dropdown)
- Pavement Construction Month: October Year: 2006
- Traffic open month: November Year: 2006
- Type of Design:
  - New Pavement:
    - Flexible Pavement
    - Jointed Plain Concrete Pavement (JPCP)
    - Continuously Reinforced Concrete Pavement (CRCP)
  - Restoration:
    - Jointed Plain Concrete Pavement (JPCP)
  - Overlay:
    - Asphalt Concrete Overlay
    - PCC Overlay

Buttons for OK and Cancel are at the bottom.

Figure 76. General information for baseline new JPCP section.

## New JPCP Baseline Design Analysis Parameters (Initial IRI)

The initial IRI at construction for the baseline JPCP was assumed to be approximately 63 in/mile.

## New JPCP Baseline Design Location

The baseline new JPCP section is located in the city of Newark in central Ohio.

## New JPCP Baseline Design Traffic

The traffic inputs used for developing new JPCP baseline design were the same as those used for new HMA baseline design and described earlier (refer Chapter 2, figure 6). Initial 2-way AADTT was assumed to be 12,893 with a 0.5 directional distribution factor, and a lane distribution factor of 0.825. This results in a total of 70 million trucks over the 20 year period.

## Climatic Data Input for New JPCP Baseline Design

The location of the baseline new JPCP pavement section was the same as the new HMA pavement and is described in chapter 2 of this report. Climate input for the MEPDG is presented in figure 77.

Environment/Climatic

Climatic data for a specific weather station.  
 Interpolate climatic data for given location.

Latitude (degrees.minutes): 40.01  
Longitude (degrees.minutes): -82.28  
Elevation (ft): 882

Seasonal

Depth of water table (ft)	
Annual average	10

Note: Ground water table depth is a positive number measured from the pavement surface.

0.0 miles NEWARK, OH - NEWARK-HEATH AIRPORT Lat. 40.01 Lon. -82.28 Ele. 882 Months: 84 (C)  
 20.3 miles LANCASTER, OH - FAIRFIELD COUNTY AIRPORT Lat. 39.46 Lon. -82.4 Ele. 855 Months: 116 (M1)  
 22.2 miles COLUMBUS, OH - PORT COLUMBUS INTL AIRPORT Lat. 39.59 Lon. -82.53 Ele. 849 Months: 116 (C)  
 31.4 miles ZANESVILLE, OH - ZANESVILLE MUNICIPAL ARPT Lat. 39.56 Lon. -81.53 Ele. 881 Months: 66 (C)  
 32.9 miles COLUMBUS, OH - OHIO STATE UNIVERSITY ARPT Lat. 40.05 Lon. -83.05 Ele. 923 Months: 100 (C)  
 52.1 miles MARION, OH - MARION MUNICIPAL AIRPORT Lat. 40.37 Lon. -83.04 Ele. 991 Months: 94 (C)

Select stations for generating interpolated climatic files. The best interpolation occurs by selecting stations that are geographically close in differing directions. A station without missing any data is denoted (C)complete. (M) denotes missing month.  
Press the Generate button after selecting desired weather stations and inputting Elevation and Depth of Water Table. Missing data for a given station will be interpolated from complete stations.

Figure 77. Climatic data input for baseline new JPCP section.

## Surface Shortwave Absorptivity for New JPCP Baseline Design

A surface shortwave absorptivity of 0.85 was assumed (used in all calibration).

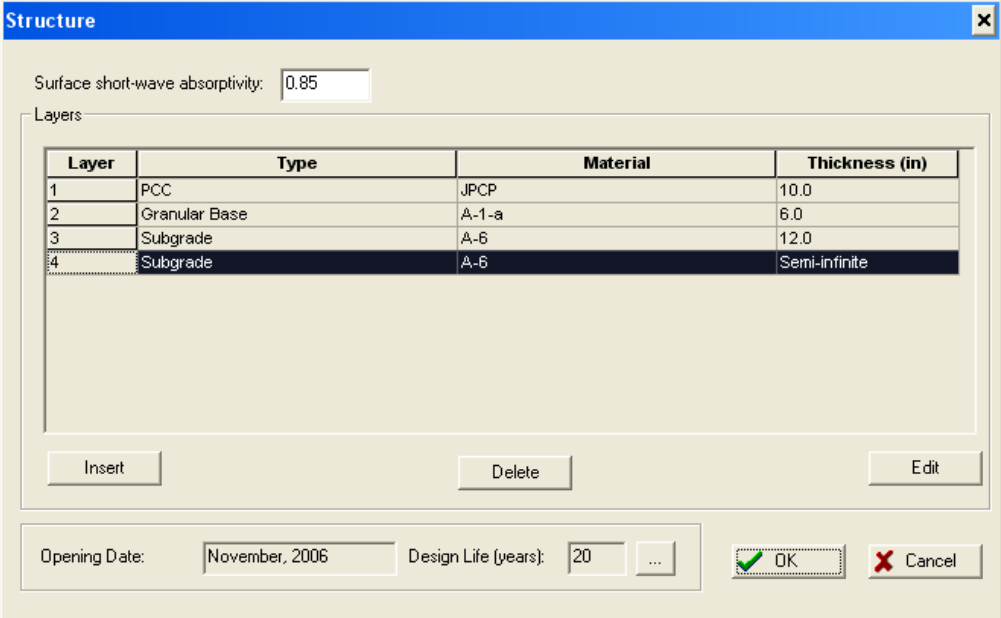
## Layering of the JPCP Pavement and Subgrade for New JPCP Baseline Design

The baseline JPCP pavement structure included a 10-in JPCP layer over a 6.0-in granular base (A-1-a), over a prepared (A-6) subgrade with the top 12.0-in compacted. The pavement structure used as the baseline for sensitivity analysis is shown in figure 78.

## PCC Layer Mix Properties for New JPCP Baseline Design

Typical ODOT JPCP design consists of a 10-in PCC slab placed over a 6-in DGAB over a prepared subgrade. For the baseline design, the PCC slab properties were assumed based on information provided in ODOT pavement design and construction manuals, ODOT research reports, and the LTPP database.

The PCC properties of interest included unit weight, Poisson's ratio, cement content, water to cement ratio, coefficient of thermal expansion, flexural strength, and elastic modulus. The baseline PCC properties were derived from ODOT class C concrete. ODOT class C concrete had the following properties:



The screenshot shows a software dialog box titled "Structure". At the top, there is a text field for "Surface short-wave absorptivity" with the value "0.85". Below this is a section labeled "Layers" containing a table with four columns: "Layer", "Type", "Material", and "Thickness (in)". The table lists four layers: Layer 1 (PCC, JPCP, 10.0), Layer 2 (Granular Base, A-1-a, 6.0), Layer 3 (Subgrade, A-6, 12.0), and Layer 4 (Subgrade, A-6, Semi-infinite). Below the table are "Insert", "Delete", and "Edit" buttons. At the bottom of the dialog, there are fields for "Opening Date" (November, 2006) and "Design Life (years)" (20), along with "OK" and "Cancel" buttons.

Layer	Type	Material	Thickness (in)
1	PCC	JPCP	10.0
2	Granular Base	A-1-a	6.0
3	Subgrade	A-6	12.0
4	Subgrade	A-6	Semi-infinite

Figure 78. Layers used for baseline new JPCP section.

- Cement type: Type I.
- Cement content: 600 lbs/yd<sup>3</sup>.
- Aggregate type: Limestone, Gravel, or Slag (limestone was selected for the baseline design).
- PCC CTE:  $5.4 \times 10^{-6}/^{\circ}\text{F}$  (based on the selected aggregate type; limestone. The CTE value was obtained from testing conducted on PCC cores extracted from LTPP rigid pavements in Ohio).
- 28-day flexural strength MR of 650 psi (Masada et al. 2004).
- Water-to-cement ratio: 0.5.

Default MEPDG input values were assumed for other concrete properties such as unit weight, Poisson’s ratio, etc. Input values assumed are shown in figures 79 through 81.

### Base Properties for New JPCP Baseline Design

The ODOT DGAB was used as the baseline design (see chapter 2 and figures 82 and 83).

### Subgrade for New JPCP Baseline Design

The subgrade soil material type selected for the base line design was AASHTO Class A-6. Detailed description of the material selection is provided in chapter 2. Figures 84 and 85 show the subgrade material properties as coded in the MEPDG.

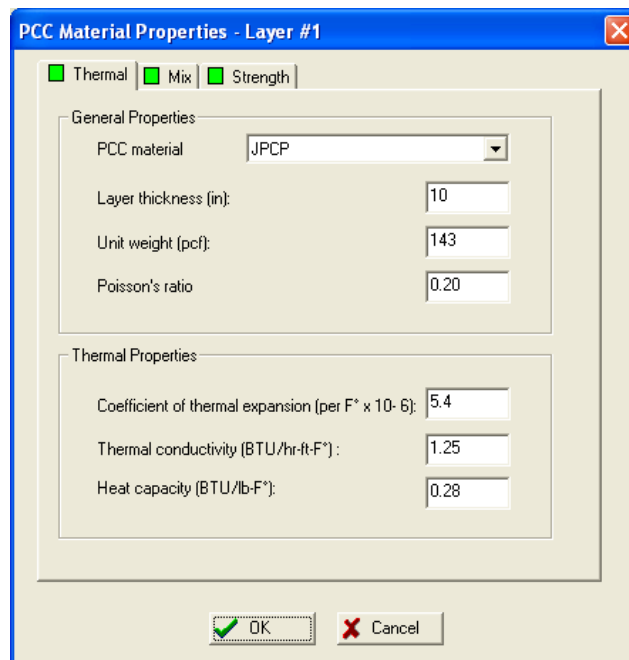


Figure 79. PCC layer general and thermal properties used in baseline new JPCP section.

**PCC Material Properties - Layer #1**

Thermal
  Mix
  Strength

Cement type:

Cementitious material content (lb/yd<sup>3</sup>):

Water/cement ratio:

Aggregate type:

PCC zero-stress temperature (F°)  ...

Ultimate shrinkage at 40% R.H (microstrain)  ...

Reversible shrinkage (% of ultimate shrinkage):

Time to develop 50% of ultimate shrinkage (days):

Curing method:

OK
  Cancel

Figure 80. PCC mix properties used in baseline new JPCP section.

**PCC Material Properties - Layer #1**

Thermal
  Mix
  Strength

Input Level:
   
 Level 1
   
 Level 2
   
 Level 3

Time	E (psi)	MR (psi)
7 Day	3680000	598
14 Day	3840000	624
28 Day	4000000	650
90 Day	4240000	689
20 Year/28 Day	1.2	1.2

OK
  Cancel

Figure 81. PCC strength properties used in baseline new JPCP section.

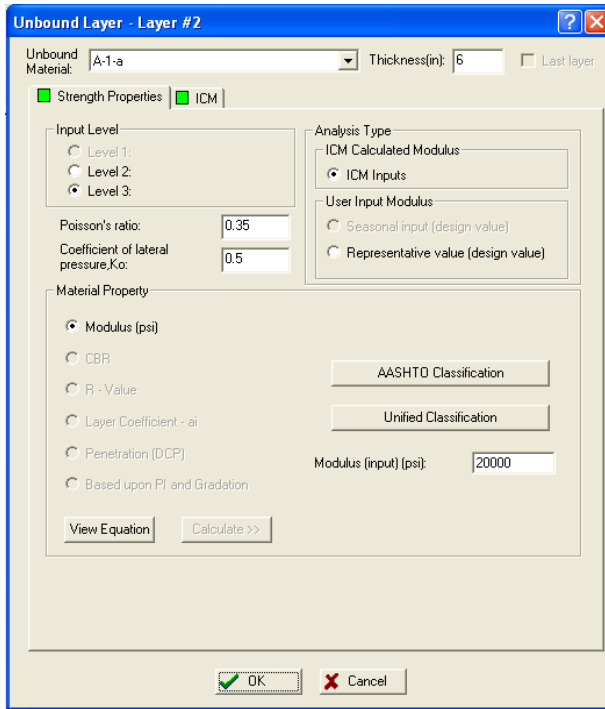


Figure 82. Properties of unbound granular base layer for baseline new JPCP section.

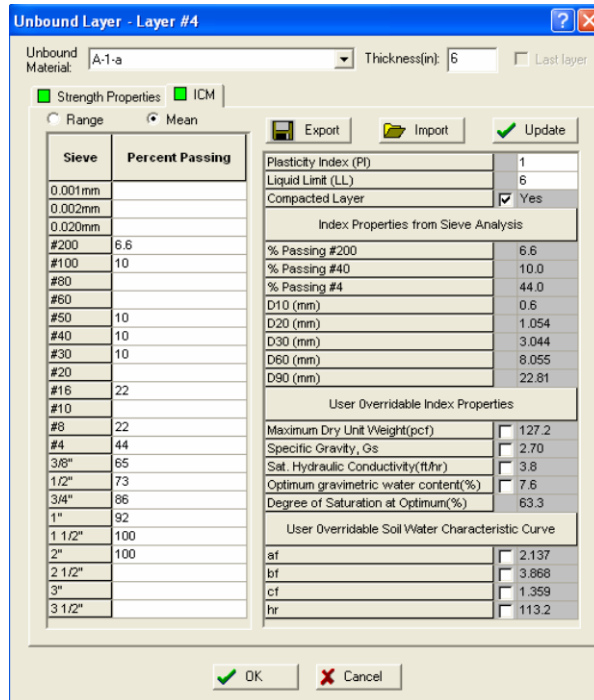


Figure 83. Properties of unbound base layer for baseline new JPCP section.

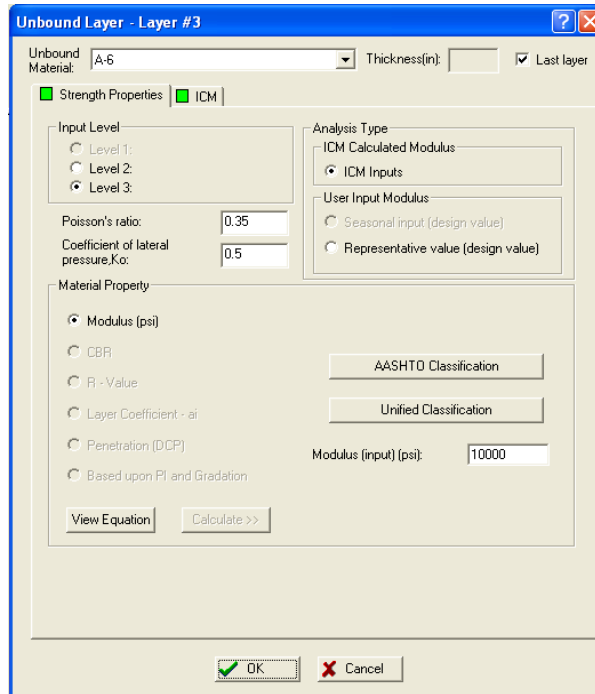


Figure 84. Structural properties of subgrade for baseline new JPCP section.

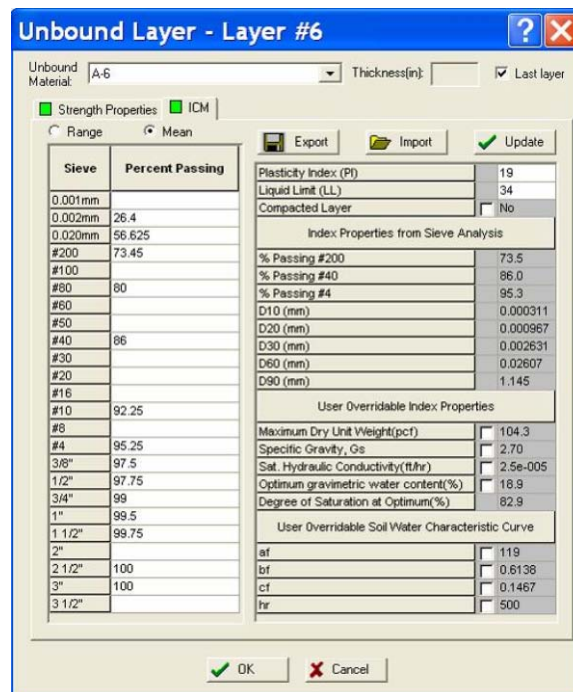


Figure 85. Properties of subgrade soil for baseline new JPCP section.

## Design Features for Baseline ODOT JPCP

Typical ODOT design features were obtained mostly from the ODOT pavement design and construction manuals and some ODOT research reports. The baseline design inputs are as follows (see figure 86):

- The joint spacing was uniform. Joint spacing was 15-ft.
- For the 10-in PCC slab, ODOT specified the use of a 1.25-in dowel bar. For the other slab thicknesses applied as part of sensitivity analysis the following dowel sizes are used as specified by ODOT:
  - Slab thickness < 8.5-in: Dowel diameter = 1.0-in.
  - Slab thickness between 8.5- and 10.0-in: Dowel diameter =1.25-in.
  - Slab thickness > 10.0-in: Dowel diameter =1.5-in.
- Edge support condition:
  - Shoulder type: asphalt shoulders.
  - Slab width: 12-ft.
- The granular base was assumed to be fairly erodible. An erosion factor of 4 (fairly erodible) was assumed for DGAB. The granular base has full friction with the PCC slab over the 20 year period.

The temperature gradient during construction and curing conditions over time will typically induce a built-in permanent curl/warp equivalent to -10 deg F as used in national calibration. Thus, for this baseline design, a -10 deg F was selected. It is assumed that a curing compound was used during the curing process.

The screenshot shows the 'JPCP Design Features' dialog box with the following settings:

- Slab thickness (in): 10
- Permanent curl/warp effective temperature difference (°F): -10
- Joint Design:
  - Joint spacing (ft): 15
  - Sealant type: Preformed
  - Random joint spacing(ft):
  - Doweled transverse joints:
  - Dowel diameter (in): 1.25
  - Dowel bar spacing (in): 12
- Edge Support:
  - Tied PCC shoulder:
  - Long-term LTE(%): 40
  - Widened slab:
  - Slab width(ft):
- Base Properties:
  - Base type: Granular
  - PCC-Base Interface:
    - Full friction contact:
    - Zero friction contact:
  - Erodiability index: Fairly Erodiable (4)
  - Loss of full friction (age in months): 360

Buttons: OK, Cancel

Figure 86. JPCP design features for baseline new JPCP section.

## MEPDG Results for Baseline New JPCP Pavement

Figures 87 through 89 and table 23 show predicted distress and IRI for the base line design presented. Information presented shows reasonable predictions of distress/IRI.

A review of the MEPDG predictions indicates the following:

- The baseline JPCP design is representative of current ODOT new JPCP pavement design and construction practices.
- Predicts reasonable levels of distress and IRI making the design suitable as the basis for sensitivity analysis.

### Sensitivity Analysis

Sensitivity analysis was completed to determine the sensitivity of predicted distress/IRI using the MEPDG to changes in input parameters. In general, it is accepted that if a practical change in a parameter results in relatively large changes in predicted distress/IRI, then predicted distress/IRI are said to be sensitive to that parameter. This indicates that the input is important and should be estimated adequately when designing a project. A shortlist of key input parameters known to influence JPCP distress/IRI was developed and used as the basis for sensitivity analysis based on the familiarity of the project team with the MEPDG prediction models. The short listed input parameters along with the levels of variations are presented in table 24.

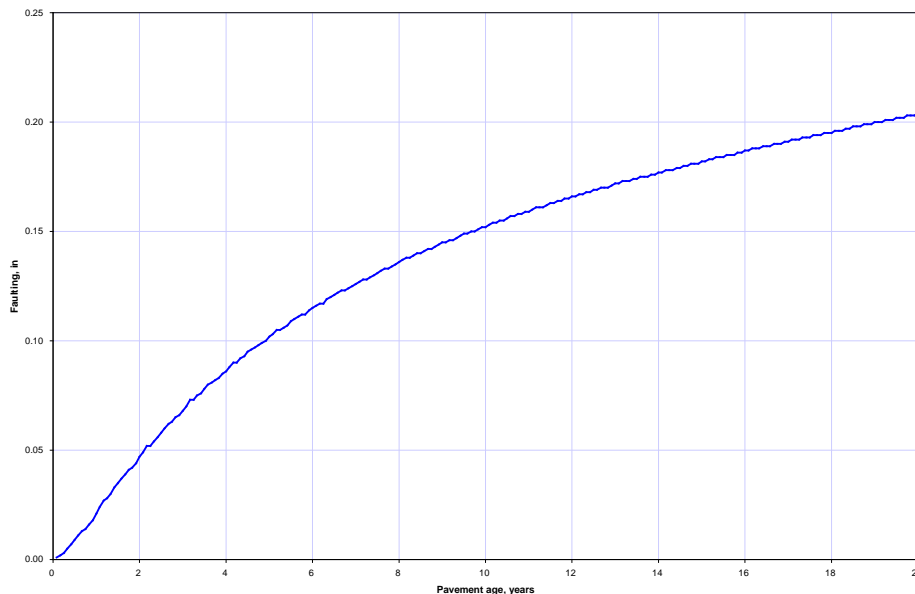


Figure 87. Plot showing predicted faulting versus age for baseline design.

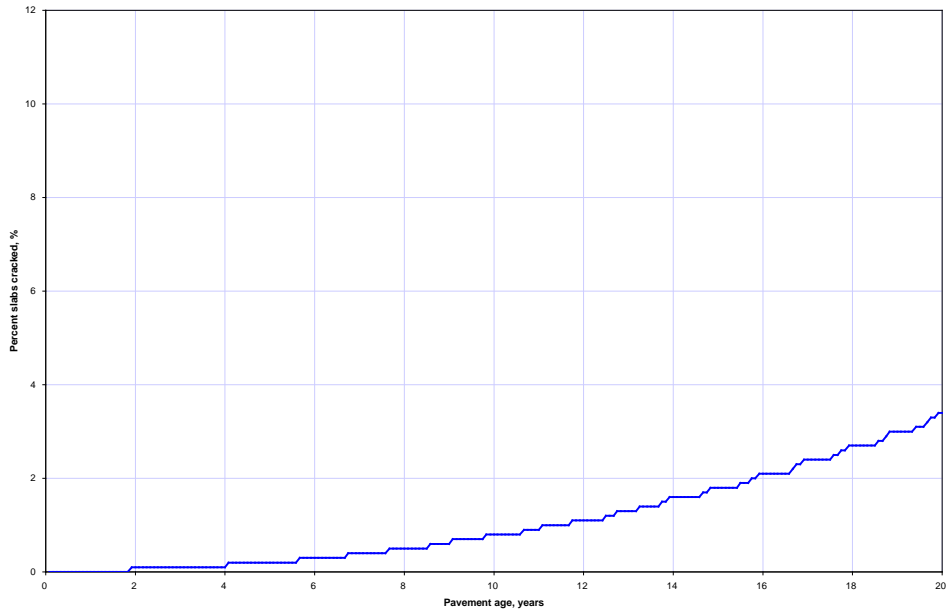


Figure 88. Plot showing predicted percent slabs cracked versus age for baseline design.

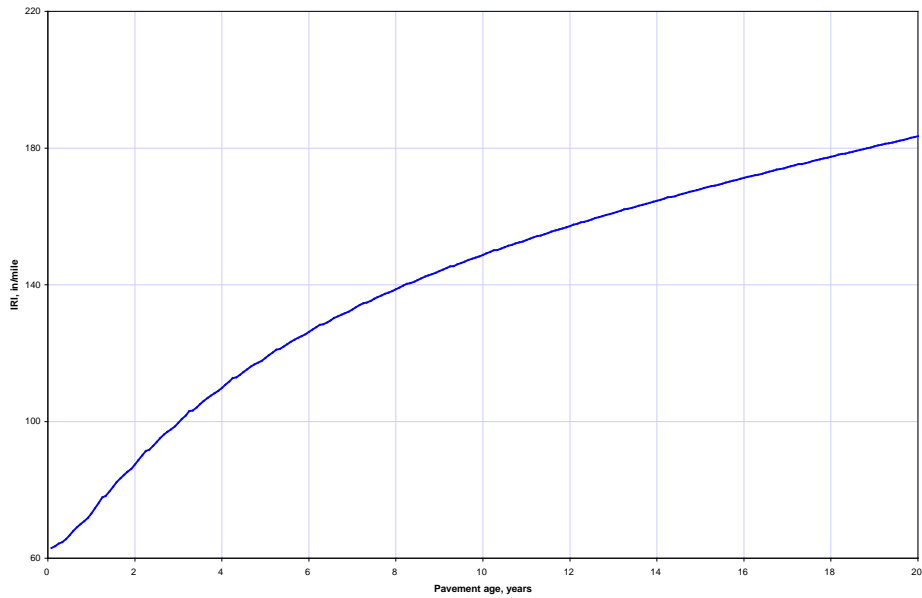


Figure 89. Plot showing predicted IRI versus age for baseline design.

Table 23. Summary of distress/IRI predicts for new JPCP baseline design.

Pavement Age, Years	PCC Elastic Modulus, Mpsi	Base Modulus, ksi	Dynamic Modulus of Subgrade Reaction (k-value), psi/in	Mean Transverse Joint Faulting, In*	Mean Percent slabs cracked*	Mean IRI in/mile*	Cumulative Heavy Trucks
0.08	4.09	16.58	138	0.001	0	63	161,878
1	4.48	16.52	138	0.021	0	73.1	1,942,530
2	4.57	16.52	138	0.047	0.1	87.4	4,049,010
3	4.62	16.52	138	0.068	0.1	99.6	6,319,440
4	4.65	16.52	138	0.086	0.1	109.8	8,753,830
5	4.68	16.52	138	0.102	0.2	118.6	11,352,200
6	4.7	16.52	138	0.115	0.3	126.1	14,114,400
7	4.71	16.52	138	0.126	0.4	132.7	17,040,700
8	4.73	16.52	138	0.136	0.5	138.6	20,130,800
9	4.74	16.52	138	0.145	0.6	143.9	23,385,000
10	4.75	16.52	138	0.152	0.8	148.7	26,803,100
11	4.75	16.52	138	0.159	0.9	153.1	30,385,100
12	4.76	16.52	138	0.166	1.1	157.2	34,131,100
13	4.77	16.52	138	0.172	1.3	161	38,041,000
14	4.77	16.52	138	0.177	1.6	164.5	42,114,900
15	4.78	16.52	138	0.182	1.8	168	46,352,700
16	4.78	16.52	138	0.187	2.1	171.3	50,754,500
17	4.79	16.52	138	0.191	2.4	174.4	55,320,200
18	4.79	16.52	138	0.195	2.7	177.5	60,049,900
19	4.8	16.52	138	0.2	3	180.5	64,943,500
20	4.8	16.52	138	0.203	3.4	183.4	70,001,100

\*Mean prediction at 50 percent reliability.

Table 24. Input parameters of interest to be used for new JPCP sensitivity analysis.

MEPDG Input Parameter	Levels of Input (*Indicates the Baseline ODOT Representative Design)
Base type (See table 5 and 6 for more details)	<ul style="list-style-type: none"> <li>Dense graded aggregate base course (Item 304)*</li> <li>Bituminous or asphalt concrete base (items 301 and 302)</li> </ul>
Climate (weather stations)	<ul style="list-style-type: none"> <li>Cleveland (Cleveland-Hopkins International airport)</li> <li>Columbus (Port Columbus International airport)</li> <li>Covington/Cincinnati (Cincinnati/NRN KY International airport)</li> <li>Dayton (J M Cox Dayton airport)</li> <li>New Philadelphia (Harry Clever Field airport)</li> <li>Newark (Newark-Heath airport)*</li> <li>Toledo (Toledo Express airport)</li> <li>Parkersburg, WV (Wood County airport)</li> <li>Wheeling, WV (Wheeling-Ohio County airport)</li> </ul>
Transverse joint load transfer efficiency (LTE)	No dowel (0-in), 1.0-, 1.25-*, and 1.5-in
PCC CTE	5.2-, 5.4-*, and $6.7 \times 10^{-6}/^{\circ}\text{F}$
PCC flexural strength and elastic modulus	601-, 650-*, 736-, and 850-psi
PCC thickness	8-, 9-, 10-*, 11-, 12-, 13-, and 14-in
PCC slab joint spacing	12.5-, 15.0-*, 17.5-, 20.0-, 22.5-ft
PCC slab width	12-*, 13-, and 14.0-ft
PCC concrete type	<p>Class C*, and high early strength concrete                      For the sensitivity analysis, other commonly used ODOT PCC material types were used. Specifically the following were considered:</p> <ul style="list-style-type: none"> <li>ODOT class C concrete with limestone (PCC CTE = <math>5.4 \times 10^{-6}/^{\circ}\text{F}</math>).</li> <li>ODOT class C concrete with gravel (PCC CTE = <math>6.4 \times 10^{-6}/^{\circ}\text{F}</math>).</li> <li>ODOT class C concrete with slag (PCC CTE = <math>6.3 \times 10^{-6}/^{\circ}\text{F}</math>).</li> <li>ODOT class S concrete with limestone (PCC CTE = <math>5.4 \times 10^{-6}/^{\circ}\text{F}</math>).</li> <li>ODOT class S concrete with gravel (PCC CTE = <math>6.4 \times 10^{-6}/^{\circ}\text{F}</math>).</li> <li>ODOT class S concrete with slag (PCC CTE = <math>6.3 \times 10^{-6}/^{\circ}\text{F}</math>).</li> </ul> <p>Additional properties for the class S concretes are as follows:</p> <ul style="list-style-type: none"> <li>Cement type: Type I.</li> <li>Cementitious content: 715 lbs/yd<sup>3</sup>.</li> <li>Aggregate type: Limestone, Gravel, or Slag (limestone selected for baseline design).</li> <li>28-day flexural strength: 800 psi (Masada et al. 2004).</li> <li>Water-to-cementitious material ratio: 0.44.</li> </ul> <p>Default MEPDG input values were assumed for other PCC properties such as unit weight, Poisson's ratio, etc.</p>
PCC aggregate type	Gravel, Limestone*, and Slag
Shoulder type	Tied PCC* and no tied PCC
Traffic composition	TTC group R1 through 7 (for Rural traffic; R6*) and U1 through 6 (for Urban traffic), refer figure 2 for WIM site locations
Subgrade type	<ul style="list-style-type: none"> <li>Natural A-6 material with top 12-in compacted*</li> <li>Natural A-6 material with top 12-in lime treated and compacted</li> <li>Natural A-6 material with top 12-in cement treated and compacted</li> <li>Natural A-2-4 material with top 12-in compacted</li> <li>Natural A-2-4 material with top 12-in lime stabilized and compacted</li> <li>Natural A-2-4 material with top 12-in cement stabilized and compacted</li> </ul>

\*New JPCP baseline design.

\*\*Default MEPDG gradations used, where needed.

## Sensitivity Analysis Results for New JPCP Pavements

The results of the sensitivity analysis are presented in the following sections.

### Effect of Base Type on MEPDG Predicted JPCP Pavement Performance

The base types considered were the DGAB, ATB\_301, and ATB\_302. All three base types were 6-in thick. Other base material properties were described previously.

Figures 90 through 92 show the effect of base type on new JPCP joint faulting, slab transverse cracking, and IRI. A summary of the relative effect of base type on all distress /IRI is presented in table 25. Information presented in table 25 shows that base type highly influenced predicted joint faulting with the DGAB being significantly higher than the ATB. The higher erosion potential with DGAB is the reason for the difference. The impact of base type on transverse (fatigue) cracking was similar with DGAB showing the highest amount of fatigue cracking. The lower modulus of the DGAB versus the ATB is responsible for the higher cracking (overall thinner equivalent slab). Both of these effects carried over into the IRI where the DGAB results in a higher IRI over the design life.

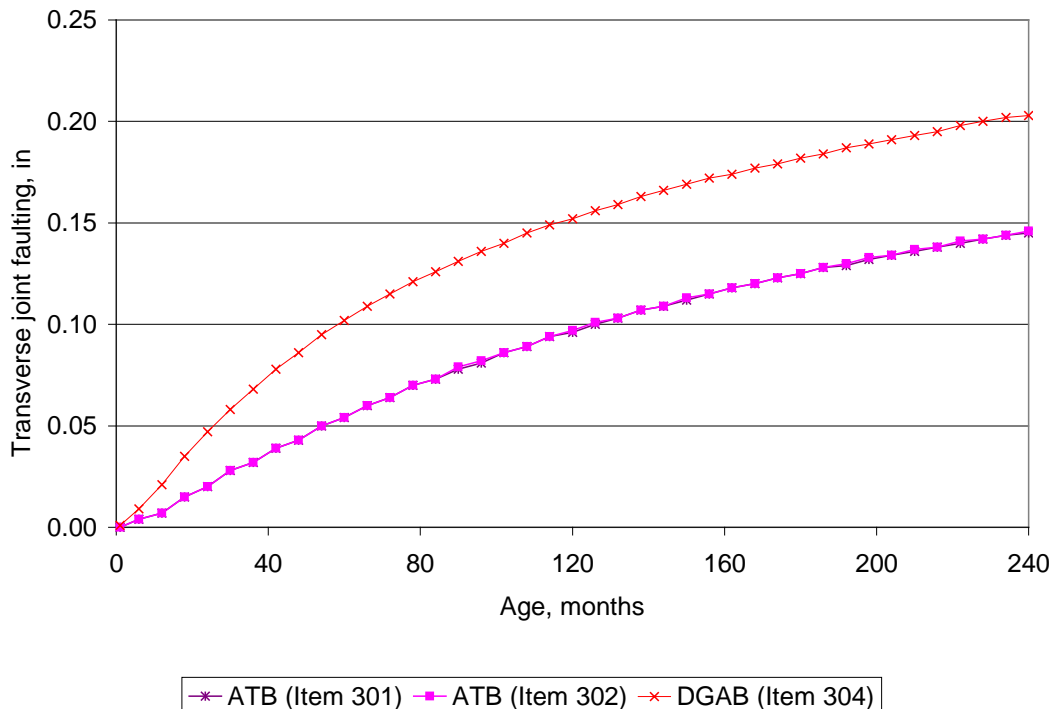


Figure 90. Plot of age versus transverse joint faulting showing the effect of base type.

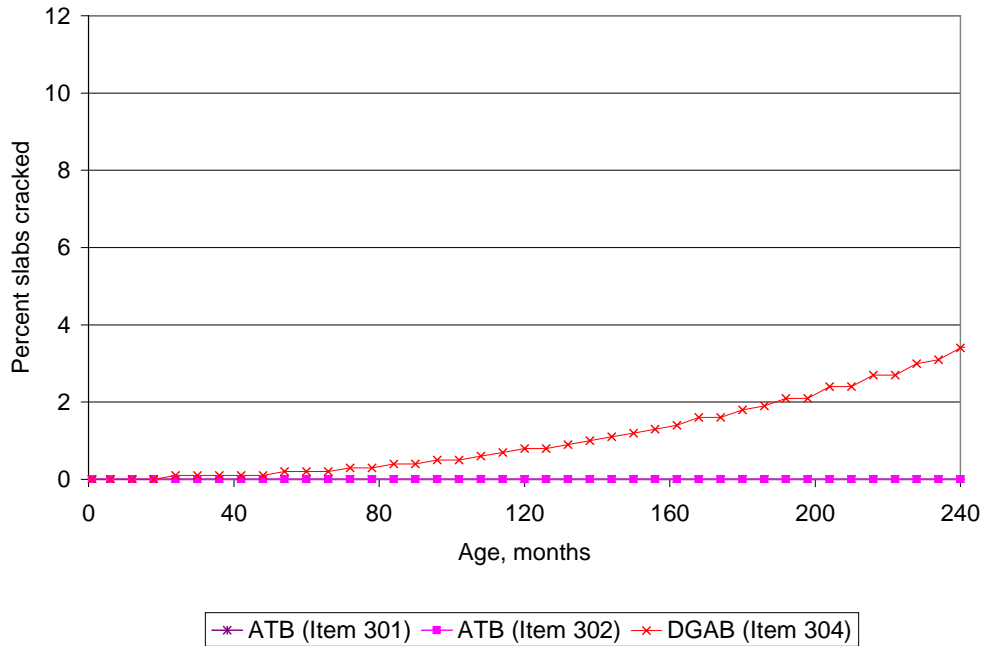


Figure 91. Plot of age versus percent slabs cracked showing the effect of base type.

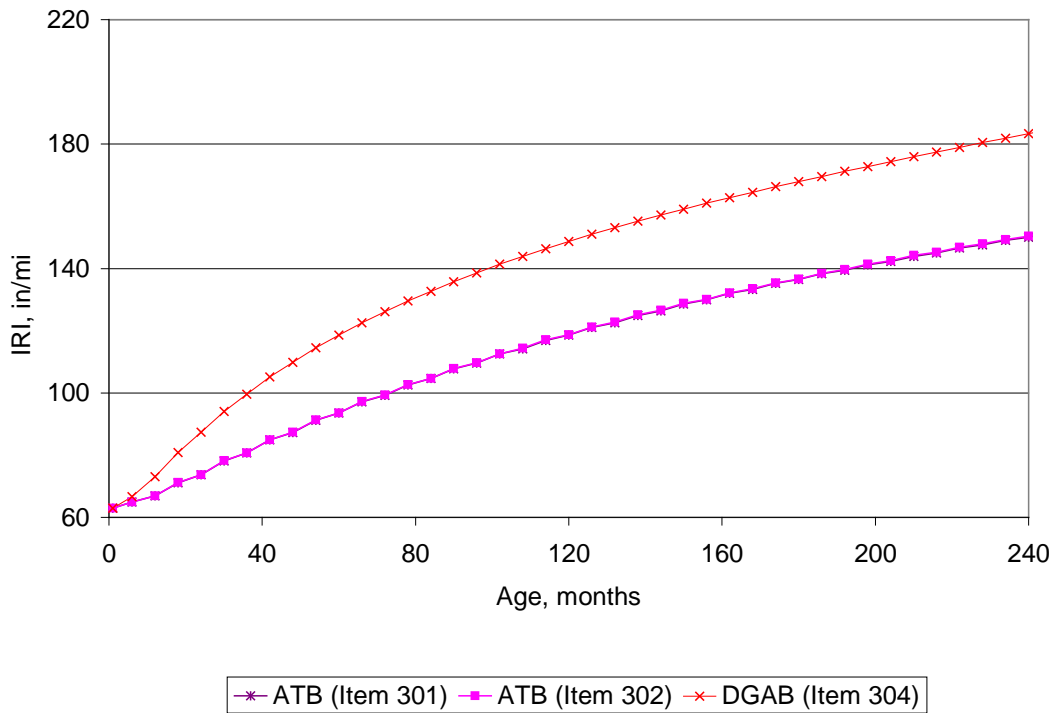


Figure 92. Plot of age versus IRI showing the effect of base type.

Table 25. Relative effect of base type on JPCP distress and IRI.

Distress/IRI	Effect of Base Type on Distress/IRI
Joint faulting	Moderate
Transverse (fatigue) cracking	Moderate
IRI	High

### Effect of Climate

The effect of climate on predicted distress and IRI was determined by selecting representative weather stations for each ODOT district and using them to simulate climate condition across the state. The objective was to determine whether the effect of climate within the state was significantly different. Climatic conditions were simulated using approximately 9 years of climate data (i.e., temperature, precipitation, cloud cover, sunshine, and so on) collected from weather stations located in the 9 cities.

The exact locations of these cities across Ohio are shown in figure 93. As shown in figure 89 the weather stations selected cover the entire geographical area of Ohio. The results of the sensitivity analysis are presented in figures 94 through 96 for faulting, transverse cracking, and IRI, respectively.

Table 26 shows the relative effect of climate on all distress types and IRI. Results show that slab transverse cracking was highly affected with the highest in Toledo. However, joint faulting and IRI were only moderately influenced by climate across Ohio.

### Effect of PCC Thickness

PCC thickness theoretically has an effect on both transverse joint faulting and cracking and thus IRI. The effects from the sensitivity analysis are shown in figures 97 through 99 for a thickness range of 8 to 14 in. Slab thickness coupled with dowel diameter have a very large effect on slab cracking, joint faulting (where both slab thickness and dowel diameter are changing), and IRI. Faulting, cracking, and IRI all decreased with increasing slab thickness. Information presented in table 27 summarizes these effects. The trends observed are reasonable with the highest distress/IRI observed for the 8-in JPCP.

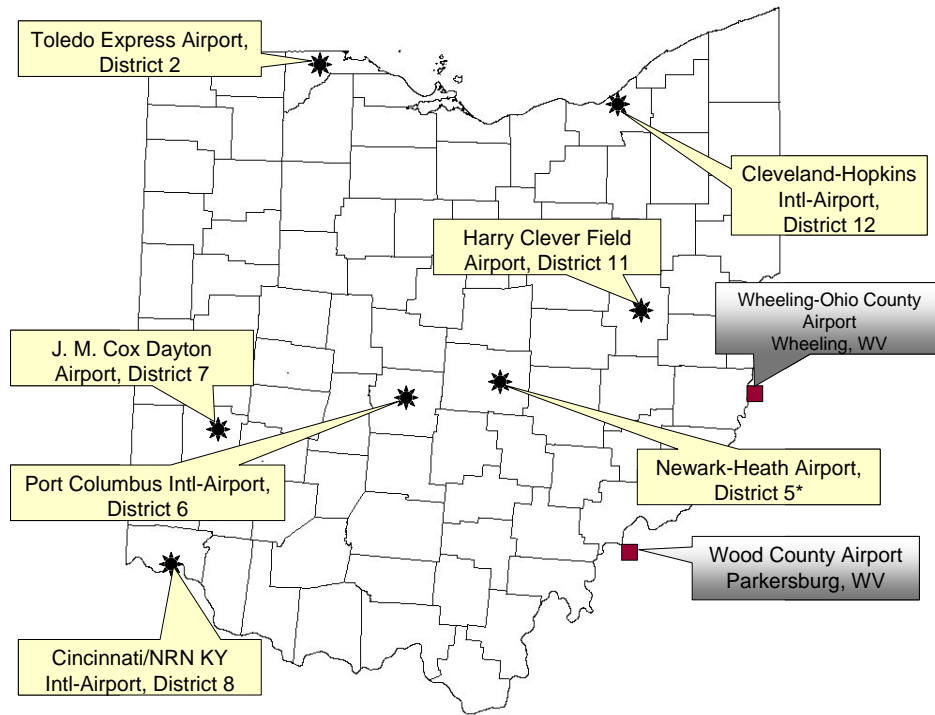


Figure 93. Map of Ohio highlighting the locations of cities/weather stations used for simulating climatic conditions for sensitivity analysis.

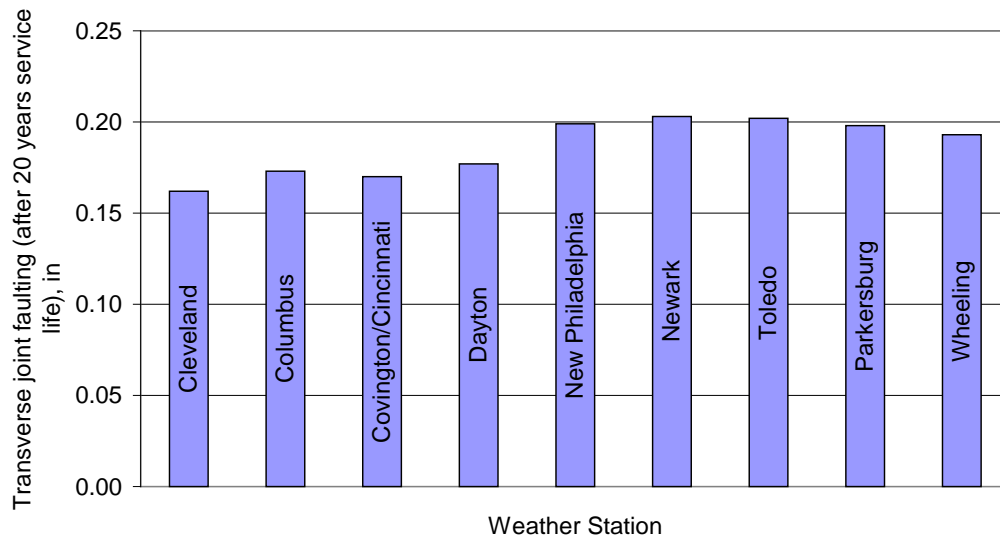


Figure 94. Plot of transverse joint faulting after a 20 year service life showing the effect of climate.

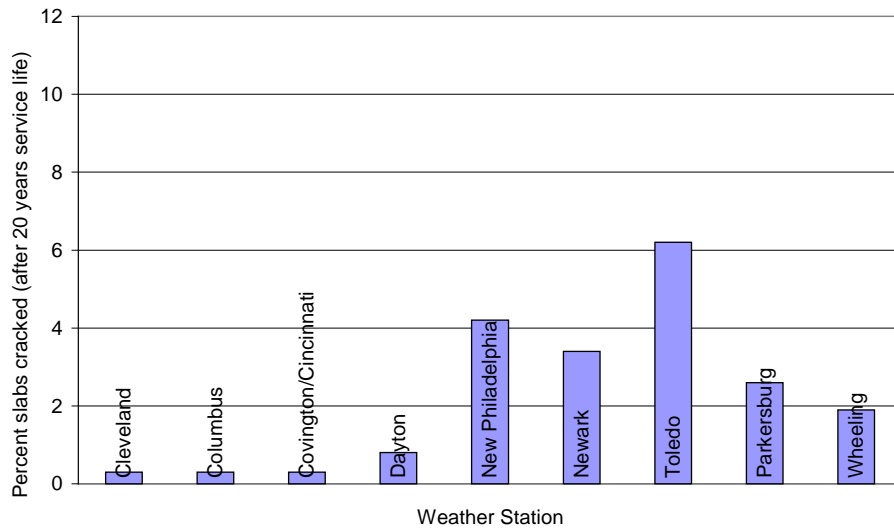


Figure 95. Plot of percent slabs cracked after a 20 year service life showing the effect of climate.

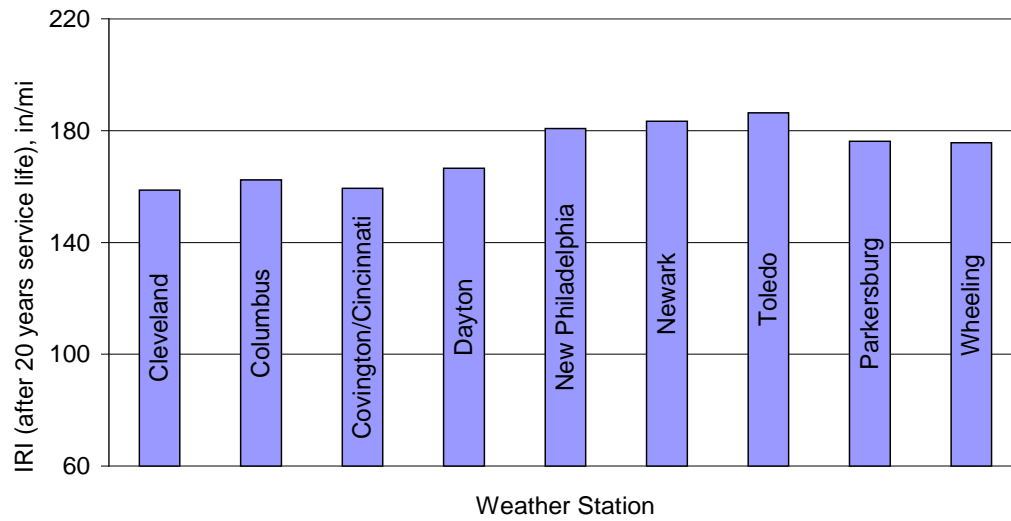


Figure 96. Plot of IRI after a 30 year service life showing the effect of climate.

Table 26. Relative effect of climate on JPCP distress and IRI.

Distress/IRI	Effect of Base Type on Distress/IRI
Joint faulting	Low
Transverse slab cracking	High
IRI	Moderate

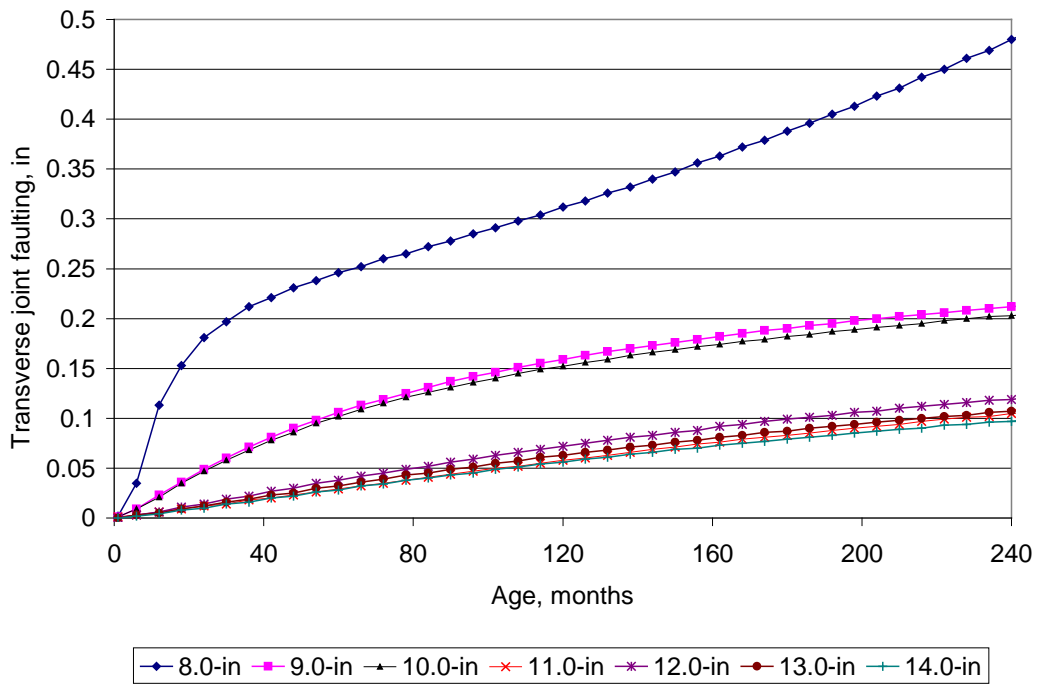


Figure 97. Plot of age versus transverse joint faulting showing the effect of PCC slab thickness and dowel diameter.

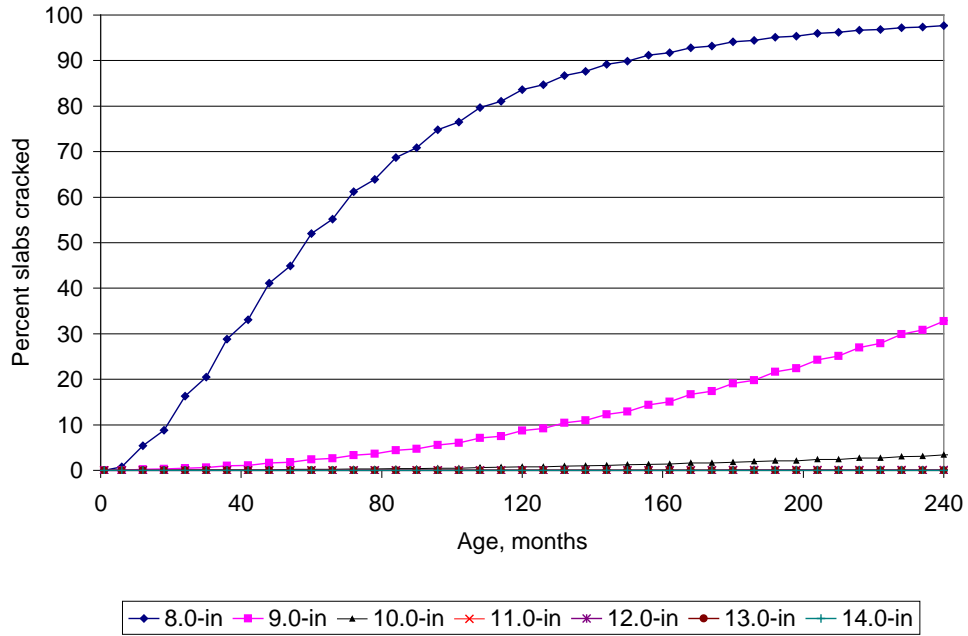


Figure 98. Plot of age versus percent slabs cracked showing the effect of PCC slab thickness.

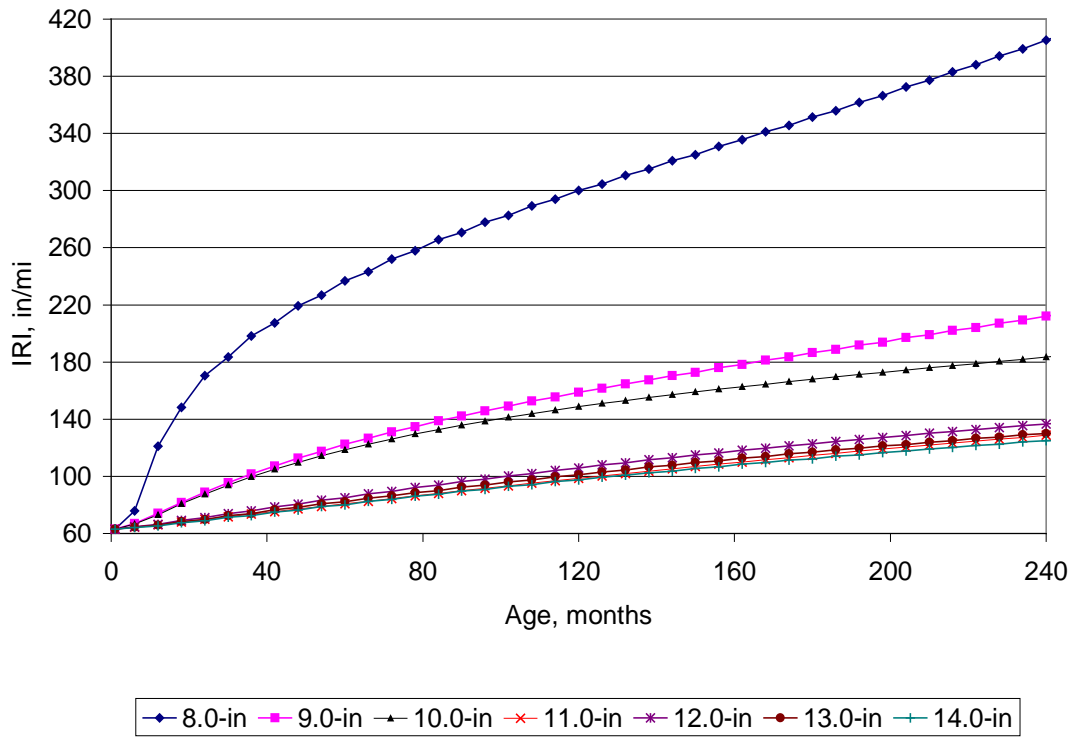


Figure 99. Plot of age versus IRI showing the effect of PCC slab thickness and dowel diameter.

Table 27. Relative effect of slab thickness (and dowel diameter) on JPCP distress and IRI.

<b>Distress/IRI</b>	<b>Effect of JPCP Thickness on Distress/IRI</b>
Joint faulting	High
Transverse slab cracking	High
IRI	High

Effect of Subgrade Type

The subgrade properties included in the MEPDG that change with the various subgrade soil types are resilient modulus, gradation, and Atterberg limits. The most significant property affecting distress development is the resilient modulus which was selected based on AASHTO soil classification as shown in table 28. The other subgrade properties were the same as those used for the flexible pavement sensitivity analysis. Figures 100 through 102 present the effect of subgrade soil type (A-1-b, A-3, A-6, and A-7-6) on predicted distress and smoothness.

Joint faulting shows that the lower the subgrade type/modulus (e.g., fine grained soils vs coarse grained soils) the higher the faulting development over time and traffic. This is a logical result based on lack of subdrainage and erosion of subgrade materials. Slab cracking shows a more complex relationship to subgrade type. The lower the subgrade type/modulus the lower the slab cracking development over time and traffic. While this may seem different than conventional wisdom, the MEPDG takes into account the slab temperature gradient and moisture gradient curling/warping effects. Thus, a stiffer subgrade causes increased slab stresses over a practical range which results in increased fatigue damage and transverse cracking.

Table 29 show the relative effect of subgrade type on all distress types and IRI. Information presented in table 29 shows that all distresses and IRI were influenced by subgrade type.

Table 28. Recommended Subgrade/Embankment Resilient Modulus Input (at optimum density and moisture) for Rigid Pavements and Rehabilitation of Rigid Pavements. [Do not use these resilient modulus values for compacted base or subbase course. Use appropriate table for base/subbase course resilient modulus].

Subgrade AASHTO Soil Class	Optimum Dry Density (mean, std. dev.)*	Optimum Moisture Content (mean)*	Design Guide Input Resilient Modulus at Optimum Density/Moist. (mean, std. dev.)**	Design Guide Backcalculated Output Dynamic k-value (mean, std. dev.)**	Recommended Input Subgrade Resilient Modulus (Opt. Density/Moisture Content)
A-1-a	128 pcf, 17 pcf	11 %	13,228 psi, 3,083 psi	322 psi/in, 68 psi/in	18,000 psi
A-1-b	122, 9	11%	14,760, 8,817	335, 92	18,000
A-3	NA	NA	NA	NA	16,500
A-2-4	119, 7	11%	14,002, 5,730	256, 79	16,000
A-2-5	NA	NA	NA	NA	16,000
A-2-6	120, 6	12	16,610, 6,620	289, 51	16,000
A-2-7	NA	NA	NA	NA	16,000
A-4	119, 7	12	17,763, 8,889	270, 88	15,000
A-5	NA	NA	NA	NA	8,000
A-6	114, 5	14	14,109, 5,935	211, 54	14,000
A-7-5	103, 19	19	7,984, 3,132	148, 32	10,000
A-7-6	102, 8	20	13,218, 322	203, 53	13,000

\*Information provided in this table were obtained from the LTPP database (optimum density and moisture).

\*\*Information obtained from Design Guide backcalculation and from use of the Design Guide (input subgrade resilient modulus, Mr, at optimum density and moisture).

\*\*\*These results are based on about 250 JPCP and CRCP pavements located across the U.S. and used in the calibration of the Design Guide rigid pavements.

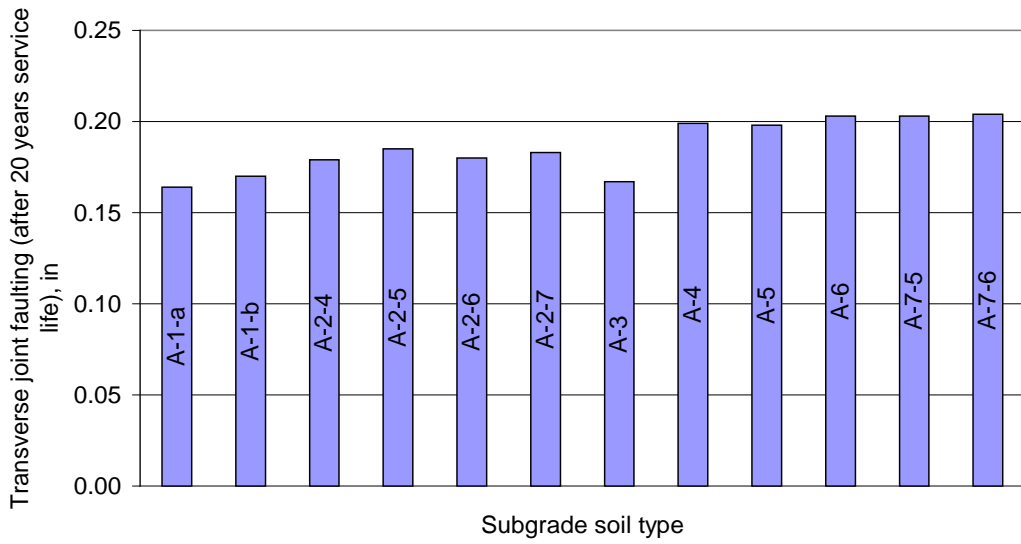


Figure 100. Plot of age versus transverse joint faulting showing the effect of subgrade type.

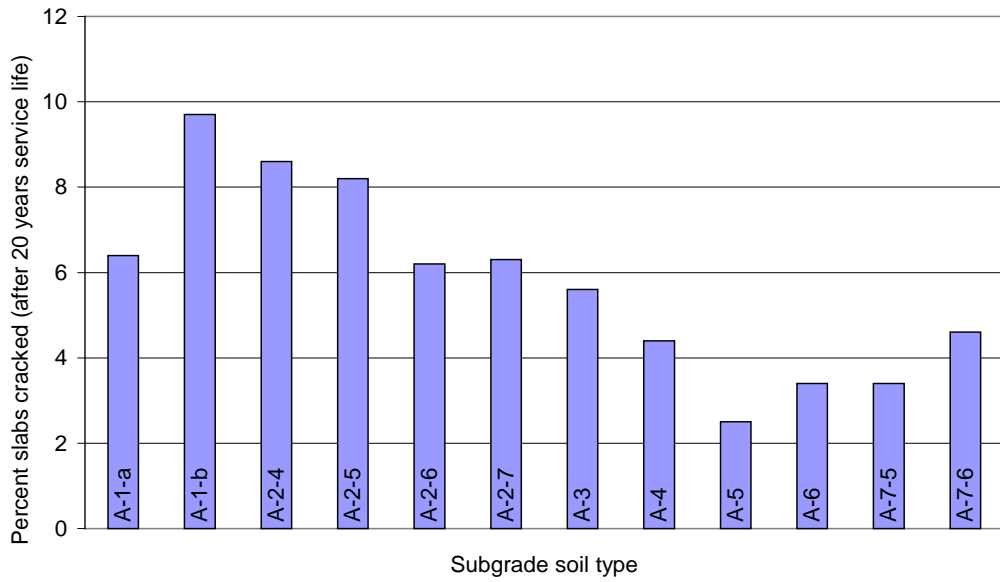


Figure 101. Plot of age versus percent slabs cracked showing effect of subgrade type.

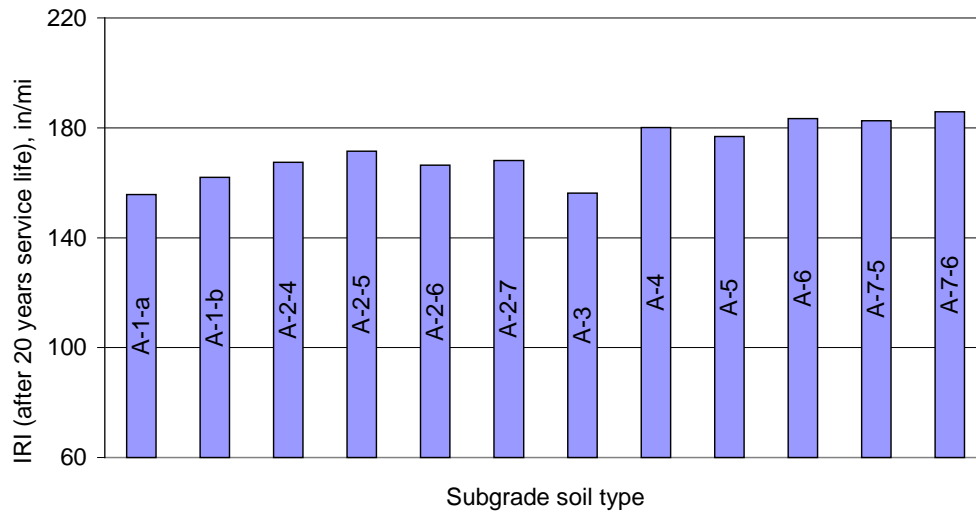


Figure 102. Plot of age versus IRI showing the effect of subgrade type.

Table 29. Relative effect of subgrade type on JPCP distress and IRI.

Distress/IRI	Effect of Subgrade Type on Distress/IRI
Joint faulting	Low
Slab transverse cracking	Moderate
IRI	Moderate

### Effect of Treated Subgrade

Two prominent subgrade soil types were identified in Ohio including A-2-4 and A-6. The effects of treating the top 12 inches of the A-6 subgrade soil with cement and lime were compared with having just a 12-in compacted A-6 subgrade soil layer. For A-2-4 subgrade soil type only cement stabilization option was used and compared with simply compacting the top 12-in of the A-2-4 subgrade soil. Results are shown in figures 103 through 105. Faulting shows little effect but cracking shows a very significant effect. The stiffer the sublayers the more cracking that occurs. Again, this is due to the effect of stiffening the subgrade has on temperature curling and moisture warping stresses. When these increase, slab cracking will also increase. Table 30 shows the relative effect of treated subgrade on distress and IRI.

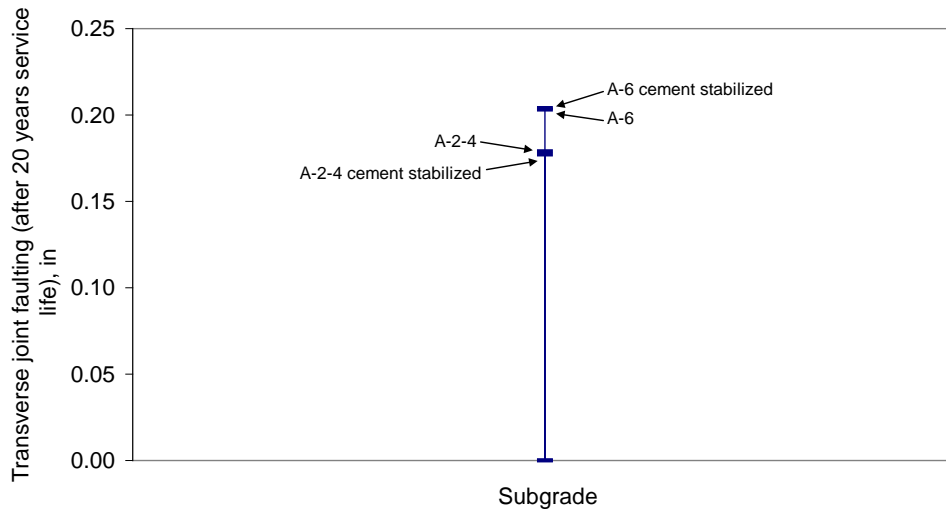


Figure 103. Plot of age versus transverse joint faulting showing the effect of stabilizing/treating the top 12-in of the subgrade soil.

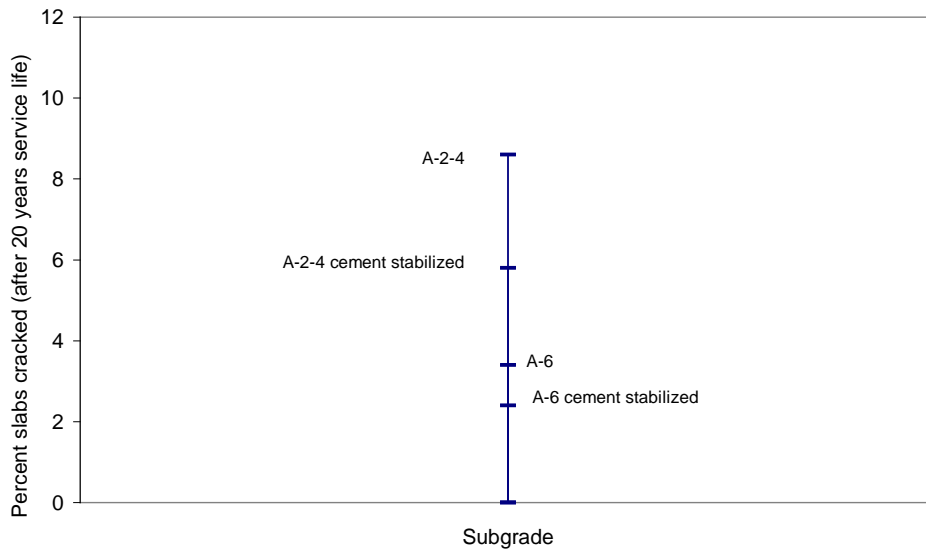


Figure 104. Plot of age versus percent slabs cracked showing the effect of stabilizing/treating the top 12-in of the subgrade soil.

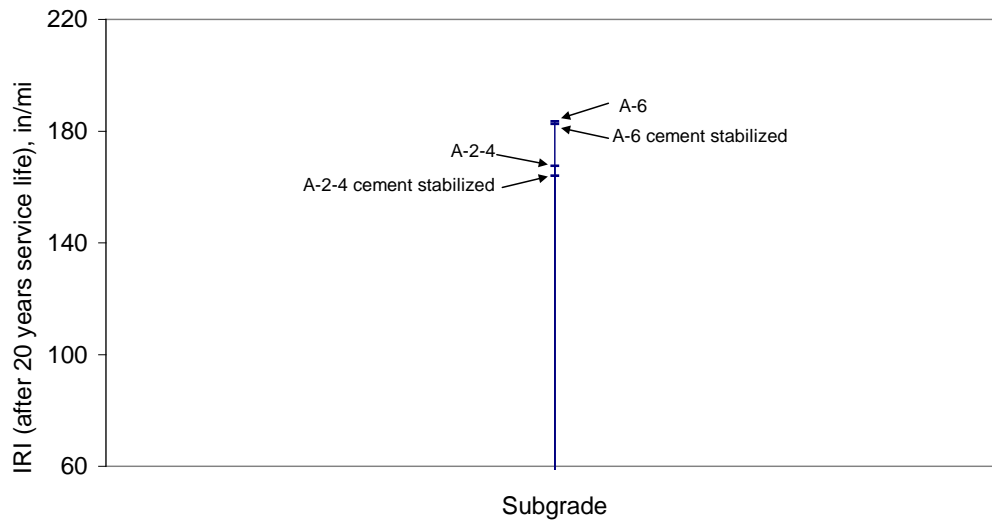


Figure 105. Plot of age versus IRI showing showing the effect of stabilizing/treating the top 12-in of the subgrade soil.

Table 30. Relative effect of subgrade treatment on JPCP distress and IRI.

<b>Distress/IRI</b>	<b>Effect of Subgrade Type on Distress/IRI</b>
Joint faulting	None
Slab transverse cracking	Moderate
IRI	None

#### Effect of PCC slab length/Joint spacing

The standard joint spacing in Ohio is 15 ft and this was used as the baseline. Spacing was varied from 12 to 22 ft to show its impact. As joint spacing is increased, additional joint opening as well as curling stresses occur leading to an expectation of increased joint faulting and slab cracking. Figure 106 to 108 show the sensitivity plots for faulting, cracking, and IRI. As joint spacing increases, all distresses and smoothness increase greatly as expected. A summary of these results is given in Table 31.

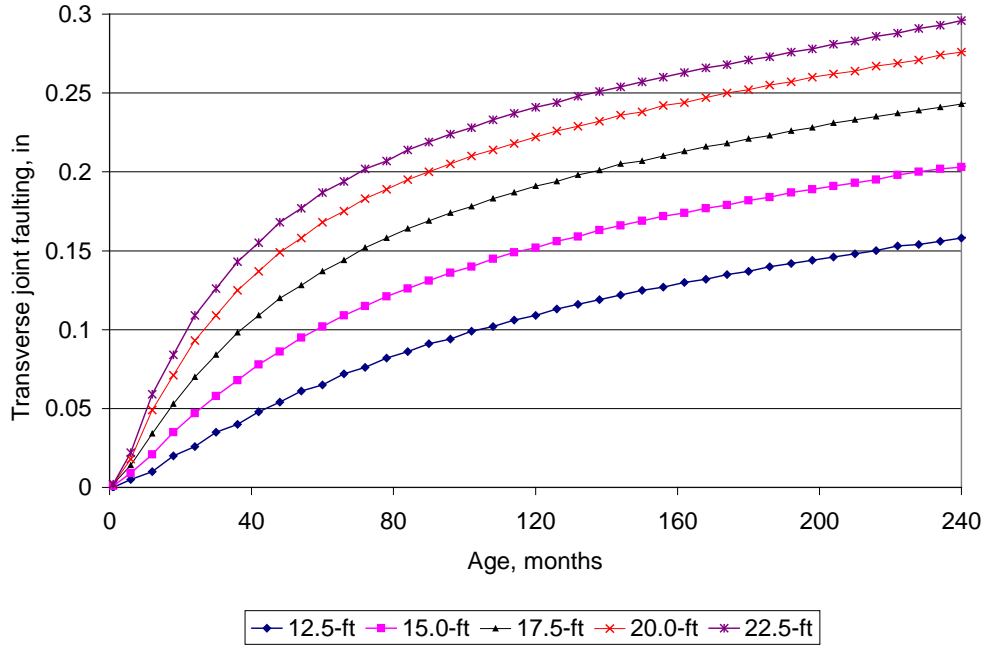


Figure 106. Plot of age versus transverse joint faulting showing the effect of the JPCP slab length.

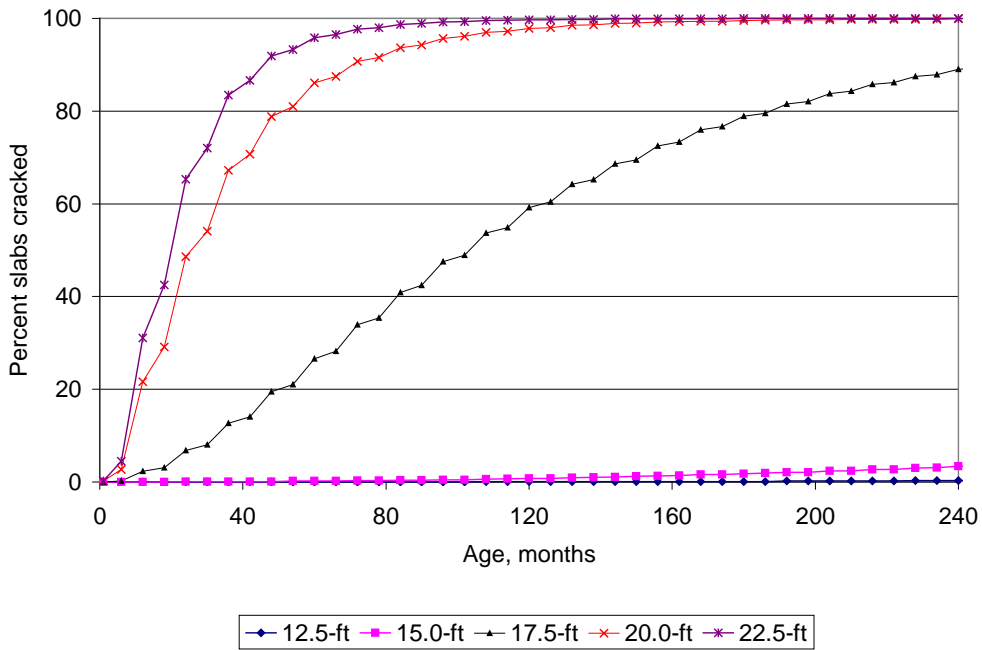


Figure 107. Plot of age versus percent slabs cracked showing the effect of the JPCP slab length.

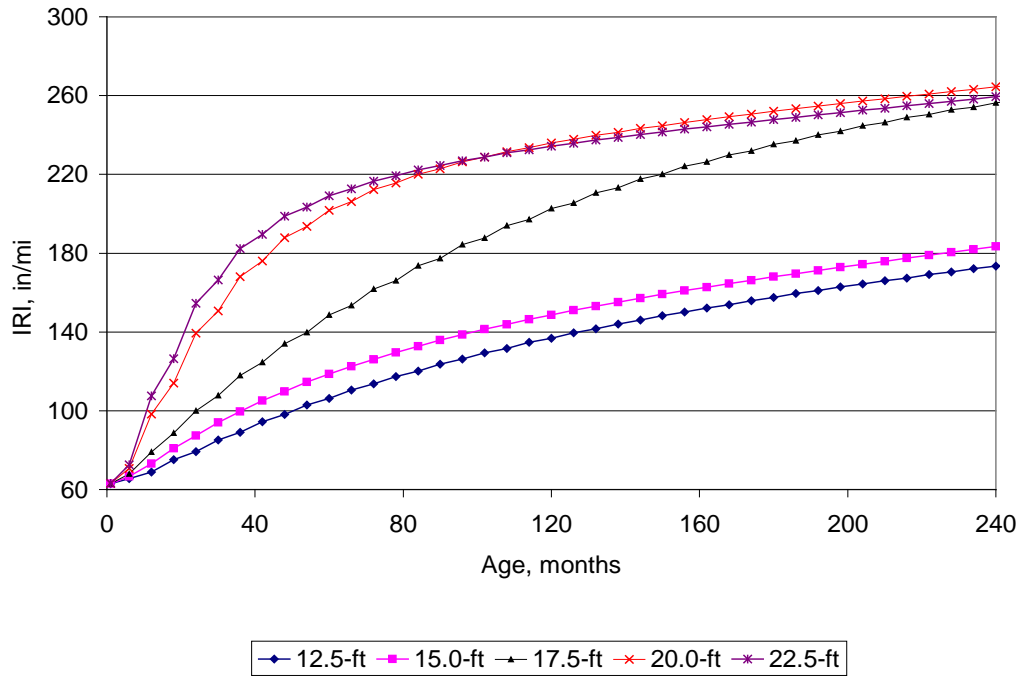


Figure 108. Plot of age versus IRI showing the effect of the JPCP slab length.

Table 31. Relative effect of transverse joint spacing on JPCP distress and IRI.

Distress/IRI	Effect of Transverse Joint Spacing on Distress/IRI
Joint faulting	High
Slab transverse cracking	High
IRI	High

### Effect of Coefficient of Thermal Expansion

The CTE of the concrete was varied from  $5.2$  to  $6.7 \times 10^{-6}/^{\circ}\text{F}$  which represents a wide range in large aggregate type. As CTE increases, joint opening increases as well as thermal curling of the slabs increases resulting in an increase in joint faulting and slab cracking. The sensitivity analysis confirmed these theoretical results as shown in figures 109 to 111. The joint faulting, slab cracking, and IRI all increase greatly over this range of CTE; particularly for aggregates with CTE over  $6.7 \times 10^{-6}/^{\circ}\text{F}$  such as Ohio gravels and slag aggregates. A summary is provided in table 32. CTE is thus a very critical input and must be recognized in the design process. When high CTE aggregate are used, other design features such as joint spacing, slab thickness, or edge support should be so chosen to ensure that high distresses are not developed over the design life of the pavement.

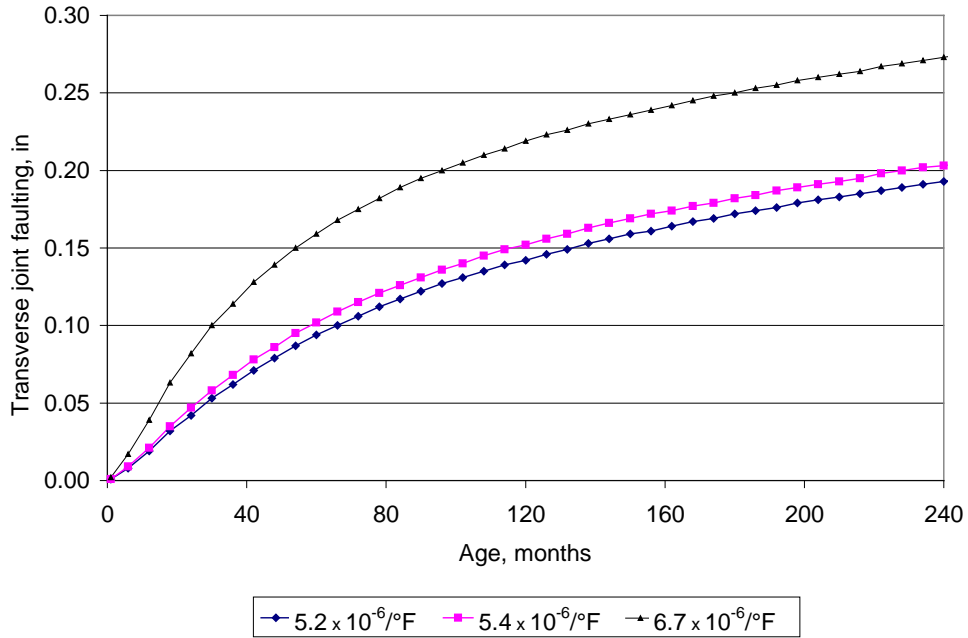


Figure 109. Plot of age versus transverse joint faulting showing the effect of CTE

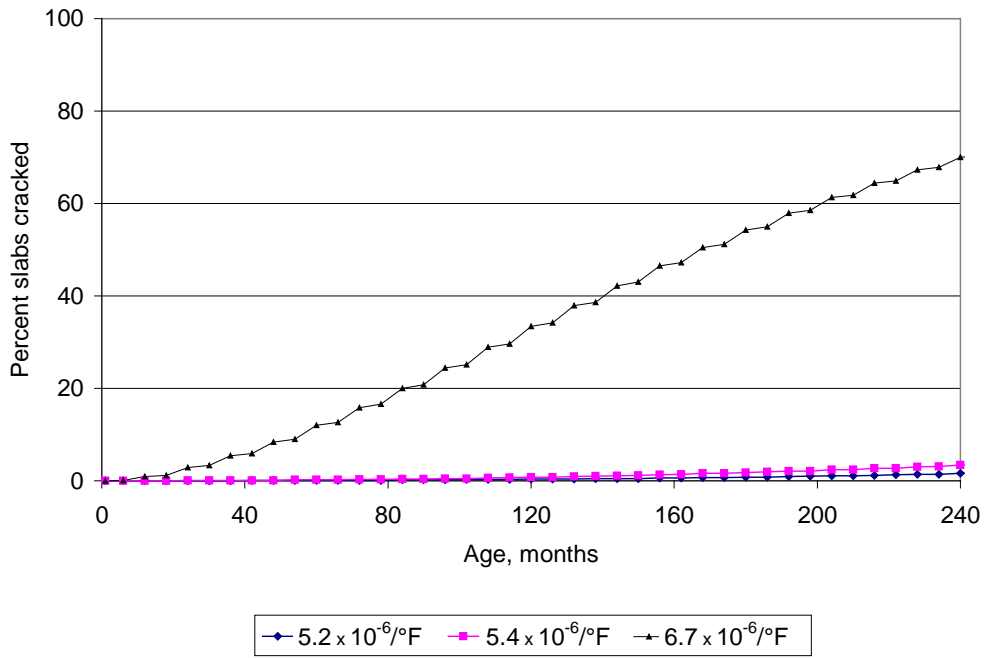


Figure 110. Plot of age versus percent slabs cracked showing the effect of CTE.

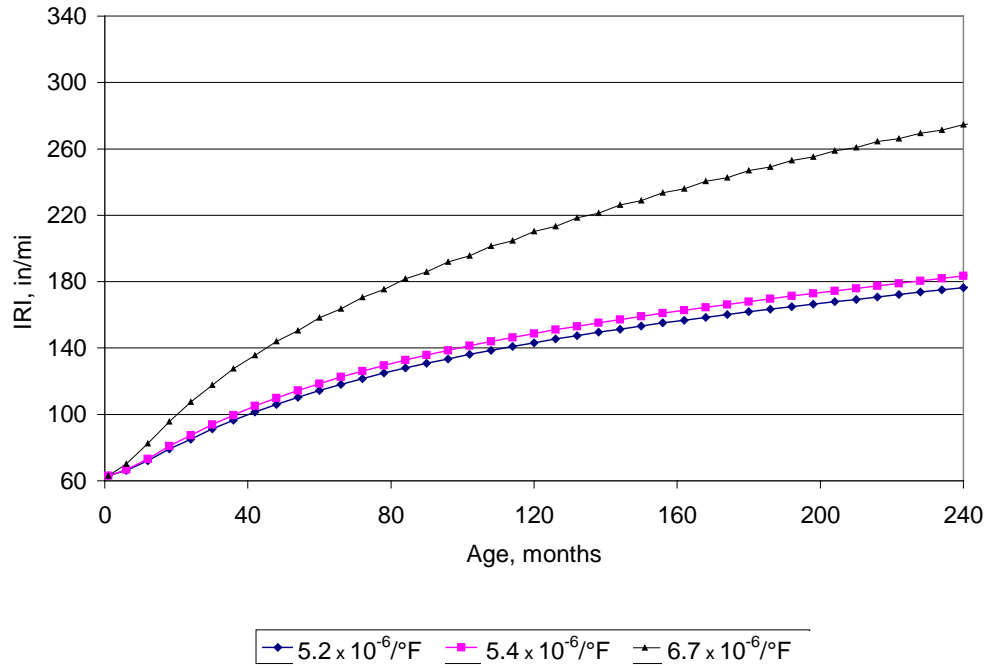


Figure 111. Plot of age versus IRI showing the effect of CTE.

Table 32. Relative effect of concrete coefficient of thermal expansion (CTE) on JPCP distress and IRI.

Distress/IRI	Effect of Coefficient of Thermal Expansion (CTE) on Distress/IRI
Joint faulting	High
Slab transverse cracking	High
IRI	High

## Effect of using load transfer devices on transverse joint load transfer efficiency (LTE)

The impact of load transfer devices on transverse joint load transfer efficiency was determined through varying the presence and diameter of steel dowel bars. As the bar increases in diameter the steel/concrete bearing stress reduces greatly which results in lower wearing away at the interface. Thus the bar is more effective in transferring load across the transverse joint reducing any differential deflection between the loaded and unloaded side of the joint. This reduces erosion and ultimately joint faulting. Figures 112 to 114 show the effects of joint LTE on faulting, transverse cracking, and IRI. There is no effect on transverse cracking (there would be an effect on corner cracking however) but there is a large effect on joint faulting and thus on IRI. The use of dowels and larger dowels reduces joint faulting and roughness greatly. Table 33 shows a summary of the effect of transverse joint LTE.

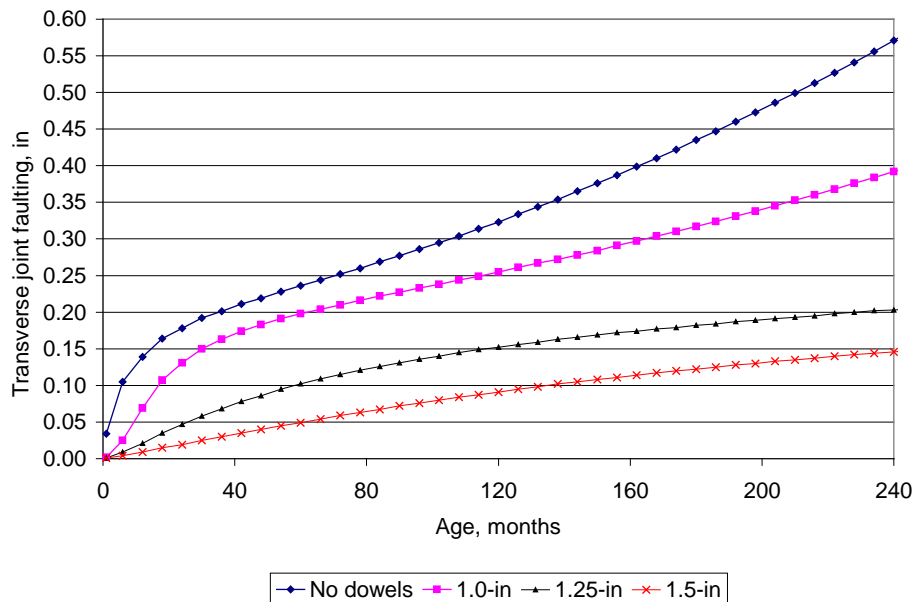


Figure 112. Plot of age versus transverse joint faulting showing the effect using load transfer devices in the JPCP slab.

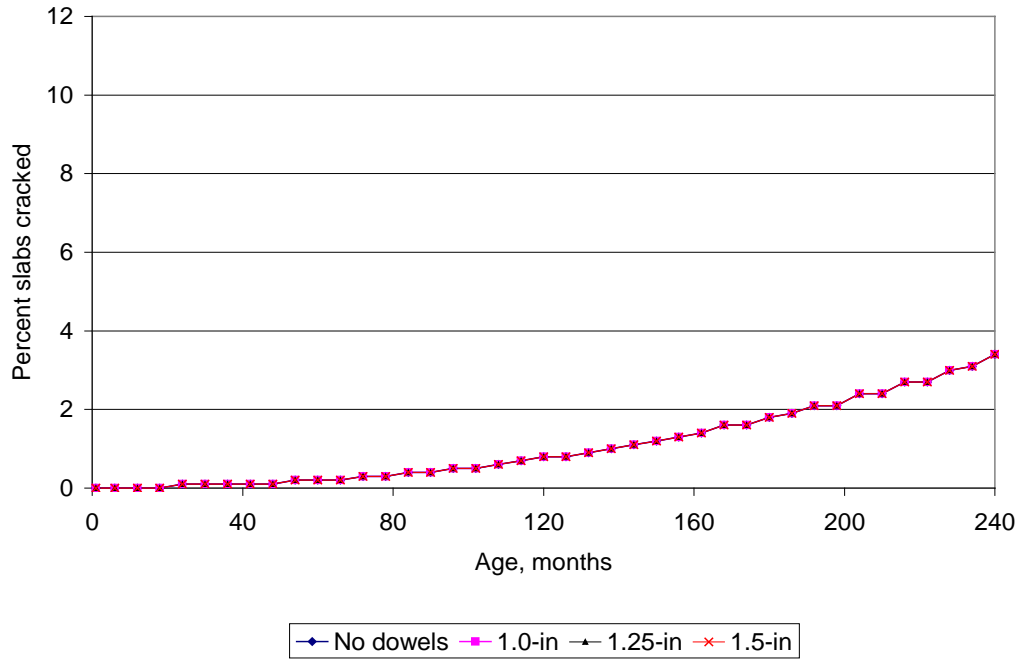


Figure 113. Plot of age versus percent slabs transversely cracked showing the effect using load transfer devices in the JPCP slab.

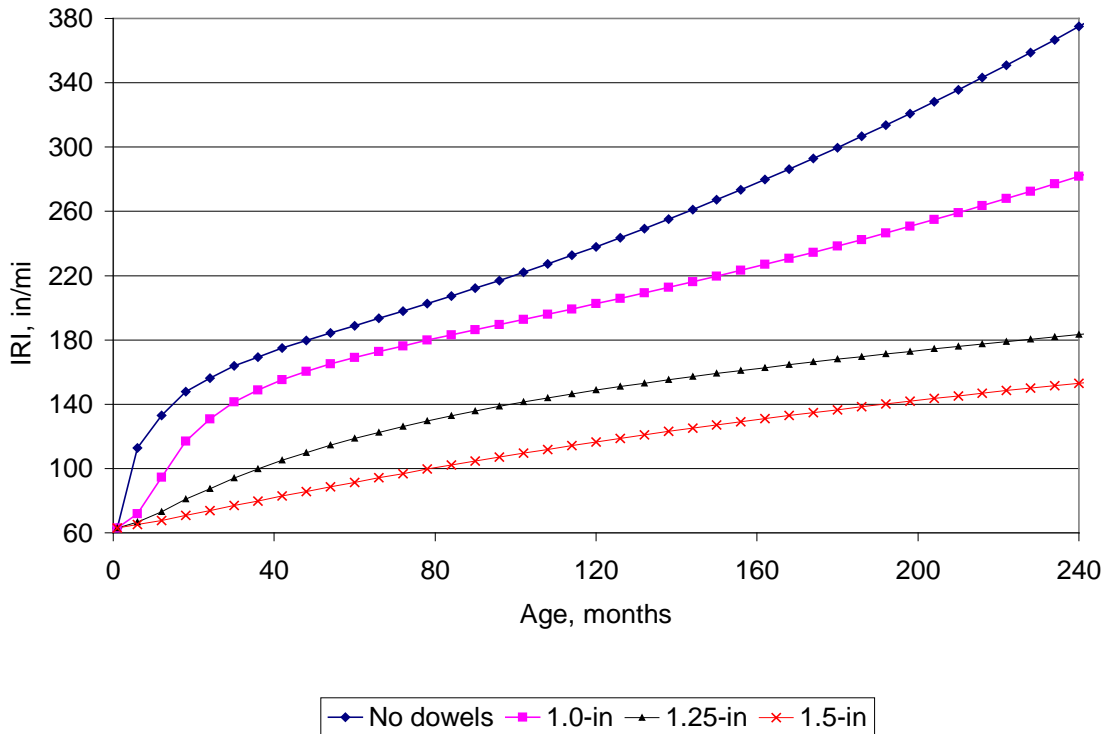


Figure 114. Plot of age versus IRI showing the effect of using load transfer devices in the JPCP slab.

Table 33. Relative effect of transverse joint load transfer devices on JPCP distress and IRI.

<b>Distress/IRI</b>	<b>Effect of Transverse Joint Load Transfer Devices on Distress/IRI</b>
Joint faulting	High
Slab transverse cracking	None
IRI	High

Effect of PCC flexural strength and modulus of elasticity

Concrete strength is expected to have a significant effect on slab cracking because of its reduction in fatigue damage. However, when strength increases for the same mix, the modulus of elasticity also changes. This sensitivity analysis included the natural change in the modulus of elasticity along with strength. (Note that other PCC properties such as shrinkage, CTE, etc. could also change with change in strength depending on how the strength change was accomplished in the mix design. However, for simplicity, only elastic modulus – which has the strongest and well established correlation with strength by far – has been chosen to co-vary with strength). These two effects tend to negate each other to some extent in that as the modulus increases the stress also increases. Figures 115 to 117 show the effects for joint faulting, slab cracking, and IRI. Joint faulting shows little effect while slab cracking shows a large reduction with an increase in concrete strength/modulus. The IRI has only a moderate effect. A summary of the results is given in Table 34.

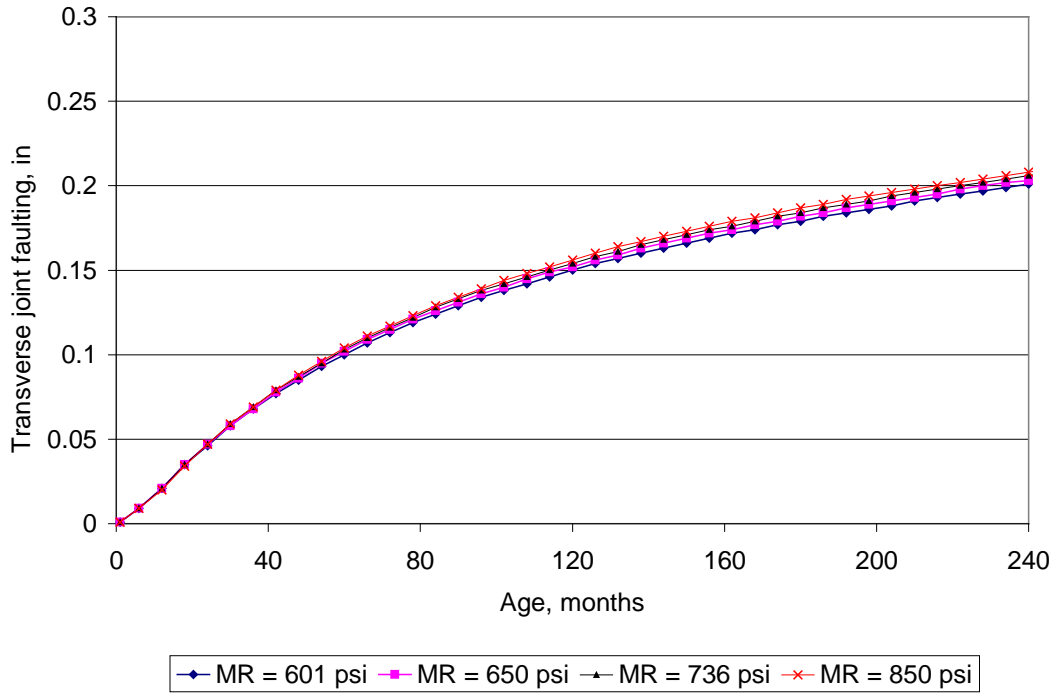


Figure 115. Plot of age versus transverse joint faulting showing the effect of PCC flexural strength and modulus of elasticity.

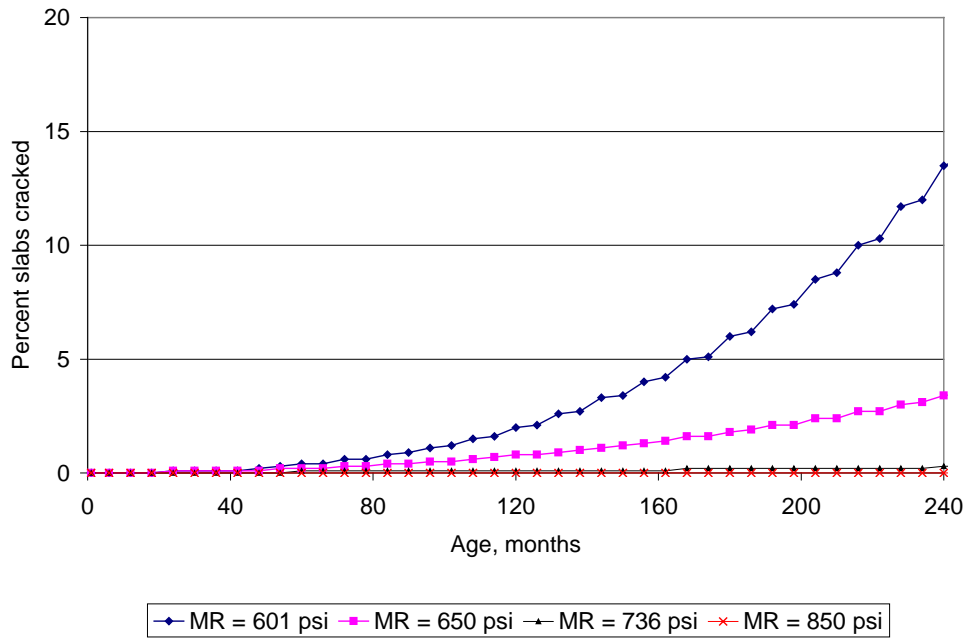


Figure 116. Plot of age versus percent slabs cracked showing the effect of PCC flexural strength and modulus change.

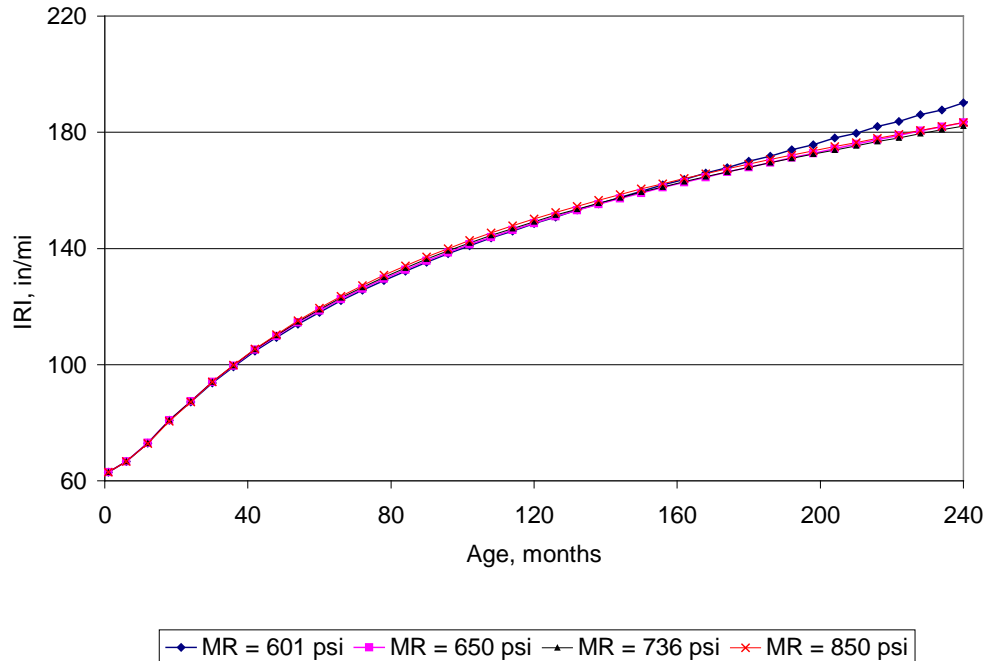


Figure 117. Plot of age versus IRI showing the effect of PCC flexural strength and modulus change.

Table 34. Relative effect of concrete flexural strength and modulus of elasticity on JPCP distress and IRI.

Distress/IRI	Effect of Concrete Flexural Strength/Modulus of Elasticity on Distress/IRI
Joint faulting	Low
Slab transverse cracking	High
IRI	Low

### Effect of JPCP slab width

Slab width determines the number of edge loadings that will apply high deflections and stresses to the slab. The higher the number of edge loadings the more fatigue and erosion damage that may occur over time and traffic. Sensitivity was conducted for 12, 13 and 14-ft wide slabs. Figures 118 to 120 show the results over a 20 year period. The results show that joint faulting, slab cracking, and IRI are all significantly affected by slab width. The wider the slab the lower the distress and IRI. However, the greatest benefit is going from 12-ft to 13-ft and there is little additional benefit by going to a 14-ft slab. Table 35 shows a summary of these results.

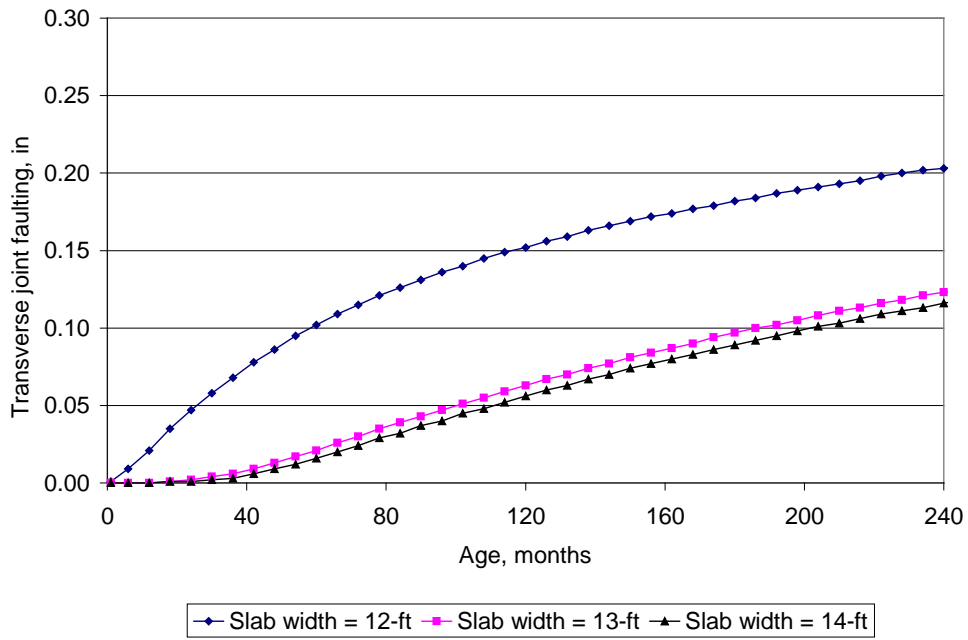


Figure 118. Plot of age versus transverse joint faulting showing the effect of JPCP slab width.

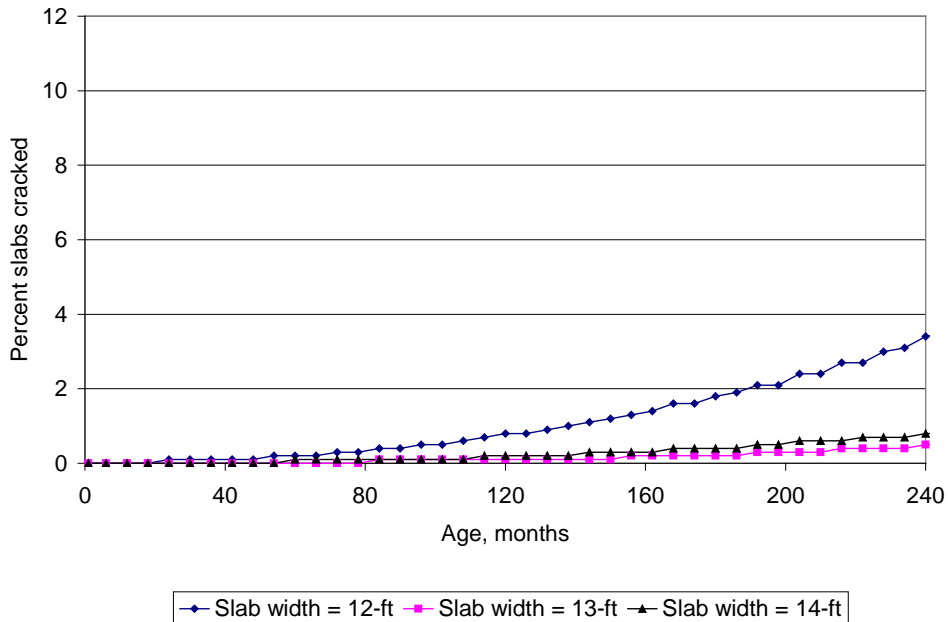


Figure 119. Plot of age versus percent slabs cracked showing the effect of JPCP slab width.

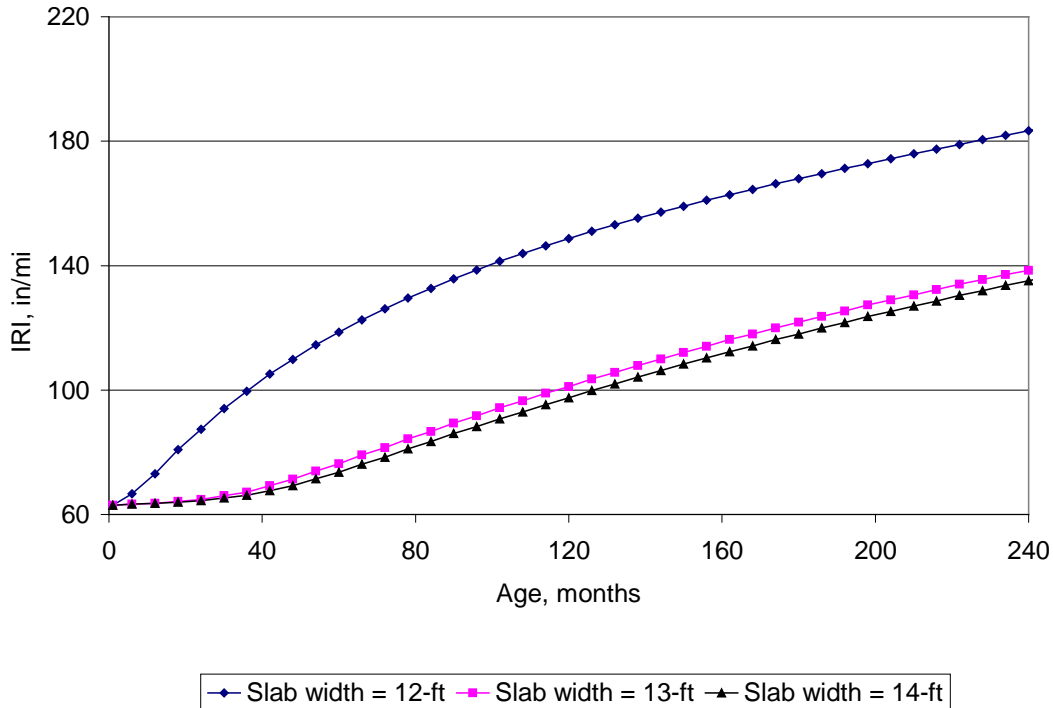


Figure 120. Plot of age versus IRI showing the effect of JPCP slab width.

Table 35. Relative effect of slab width (12, 13, and 14-ft) on JPCP distress and IRI.

Distress/IRI	Effect of Slab Width on Distress/IRI
Joint faulting	High
Slab transverse cracking	High
IRI	High

### Effect of changing aggregate type on baseline PCC

Three different aggregate types were Class C gravel, slag, and limestone. These were each run with the baseline design and distress and IRI predicted as shown in figures 121 to 123. The main difference was the CTE of the coarse aggregate with values of  $6.4 \times 10^{-6}/^{\circ}\text{F}$  for gravel,  $6.2 \times 10^{-6}/^{\circ}\text{F}$  for slag, and  $5.4 \times 10^{-6}/^{\circ}\text{F}$  for limestone. The results show a large difference in faulting, cracking, and IRI between limestone (with the low CTE) and the other two aggregates. Table 36 shows the summary of the effect. This is obviously an input that must be carefully considered in design, possibly through specifications.

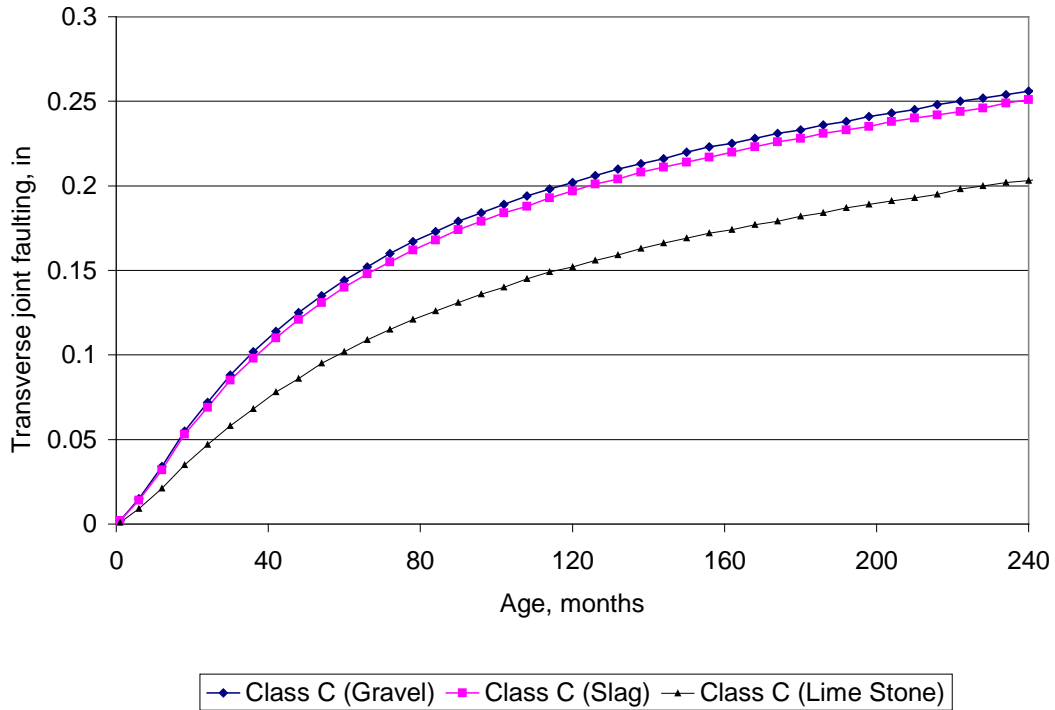


Figure 121. Plot of age versus transverse joint faulting showing the effect of changing aggregate type in baseline PCC.

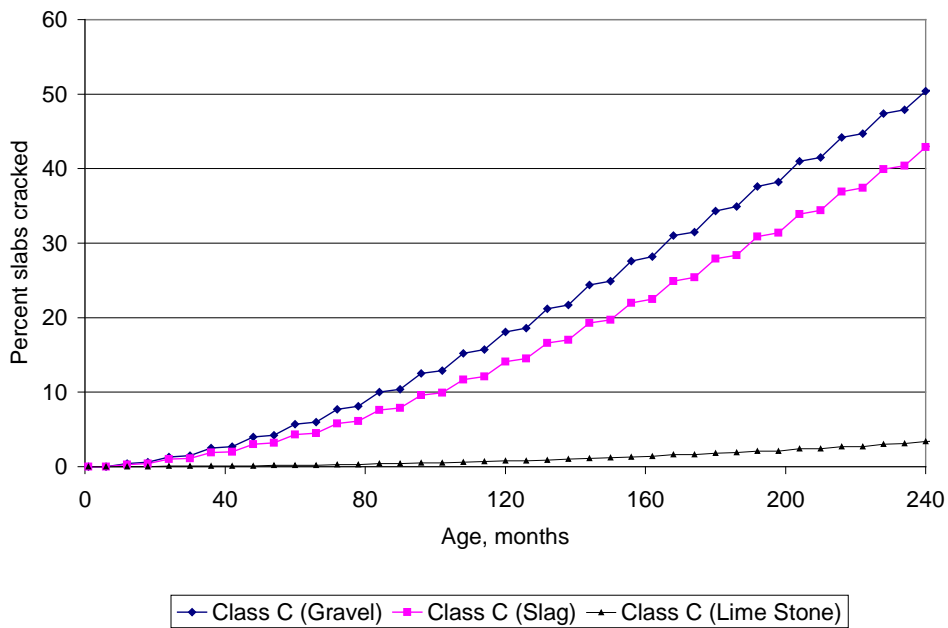


Figure 122. Plot of age versus percent slabs cracked showing the effect of changing aggregate type in baseline PCC.

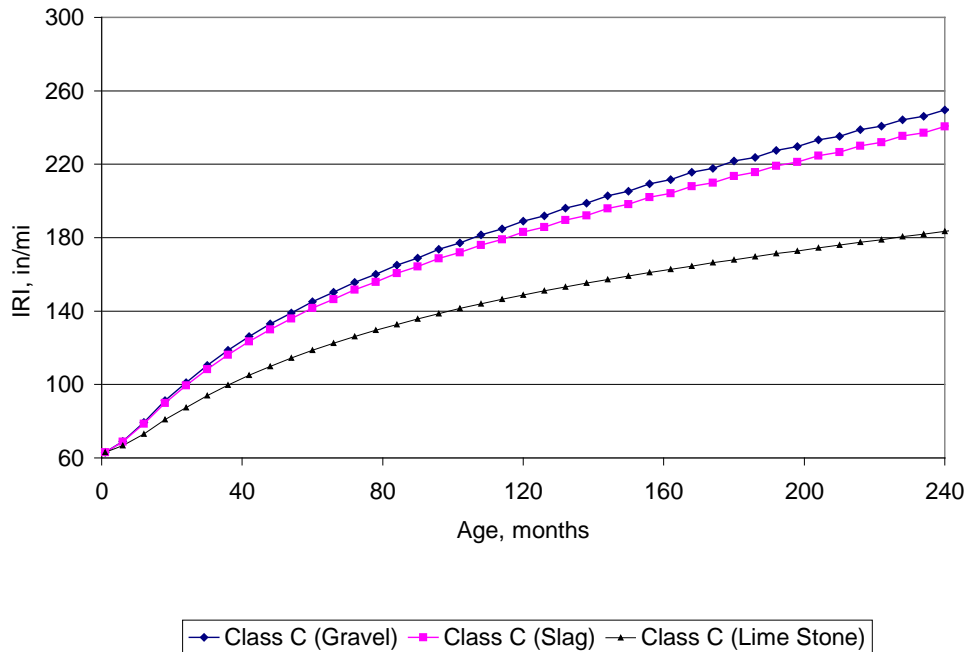


Figure 123. Plot of age versus IRI showing the effect of changing aggregate type in baseline PCC.

Table 36. Relative effect of coarse aggregate type on JPCP distress and IRI.

Distress/IRI	Effect of Coarse Aggregate Type on Distress/IRI
Joint faulting	High
Slab transverse cracking	High
IRI	High

Effect of PCC class and aggregate type

Ohio includes Type C and Type S concrete in their specifications although Type S is typically used for structures. The main difference is in the flexural strength where Type S is 800 psi and Type C is 650 psi (with corresponding changes in the modulus of elasticity). These mixes were run across the three coarse aggregate types. Results of the sensitivity analysis are shown in figures 124 to 126. The Type S concrete clearly shows less cracking and lower IRI due to the higher 28-day strength. The aggregate type shows results similar to the previous section. A summary is shown in table 37.

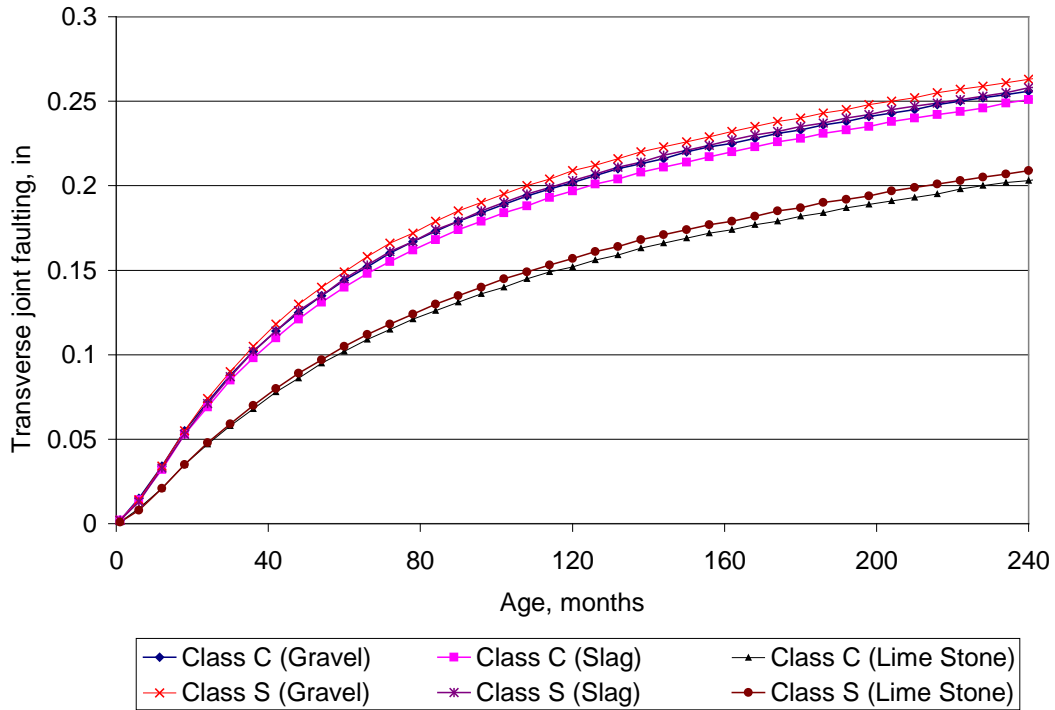


Figure 124. Plot of age versus transverse joint faulting showing the effect of type of PCC and aggregate.

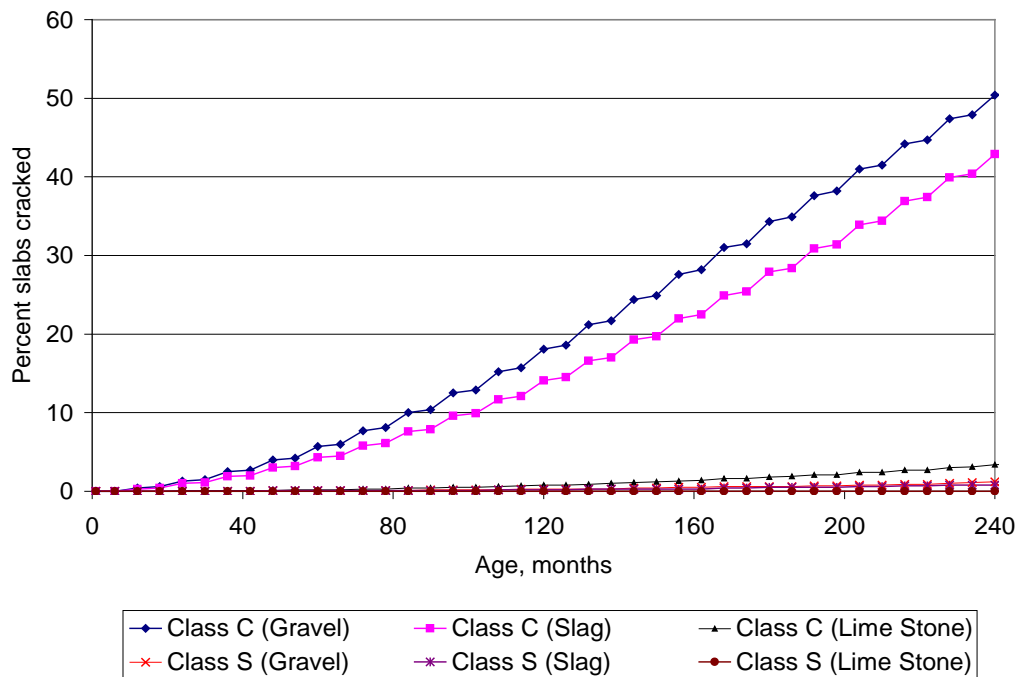


Figure 125. Plot of age versus percent slabs cracked showing the effect of type of PCC and aggregate.

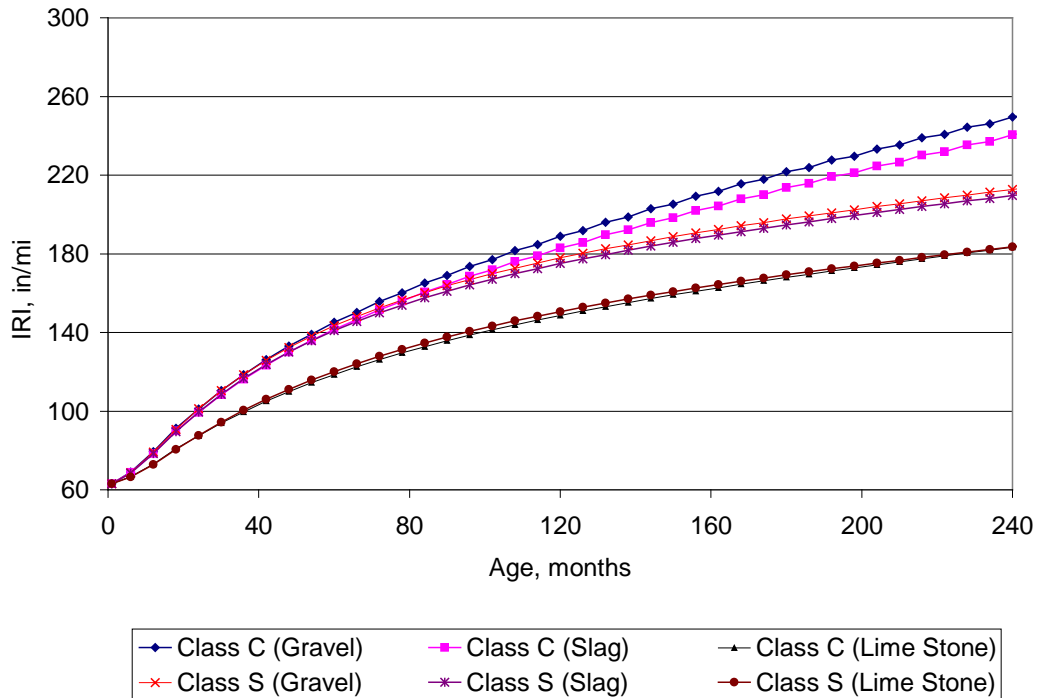


Figure 126. Plot of age versus IRI showing the effect of type of PCC and aggregate.

Table 37. Relative effect of concrete class and coarse aggregate type on JPCP distress and IRI.

Distress/IRI	Effect of Concrete Class and Aggregate Type on Distress/IRI
Joint faulting	Low
Slab transverse cracking	High
IRI	Low

Effect of pavement edge support (shoulder type)

The pavement edge support, either free edge (asphalt shoulder) or a tied PCC shoulder reduces the edge stress and the corner deflection. The long term load transfer efficiency (LTE) was assumed to be only 40 percent (which is fairly low). A higher value of say 60 percent would produce a more pronounced effect. This should result in lowering the amount of joint faulting and cracking. Results from the sensitivity analyses are shown in figure 127 to 129. The tied PCC shoulder does indeed lower joint faulting and slab cracking resulting in a lower IRI. A summary of results is shown in table 38.



Figure 127. Plot of age versus transverse joint faulting showing the effect of pavement edge support.

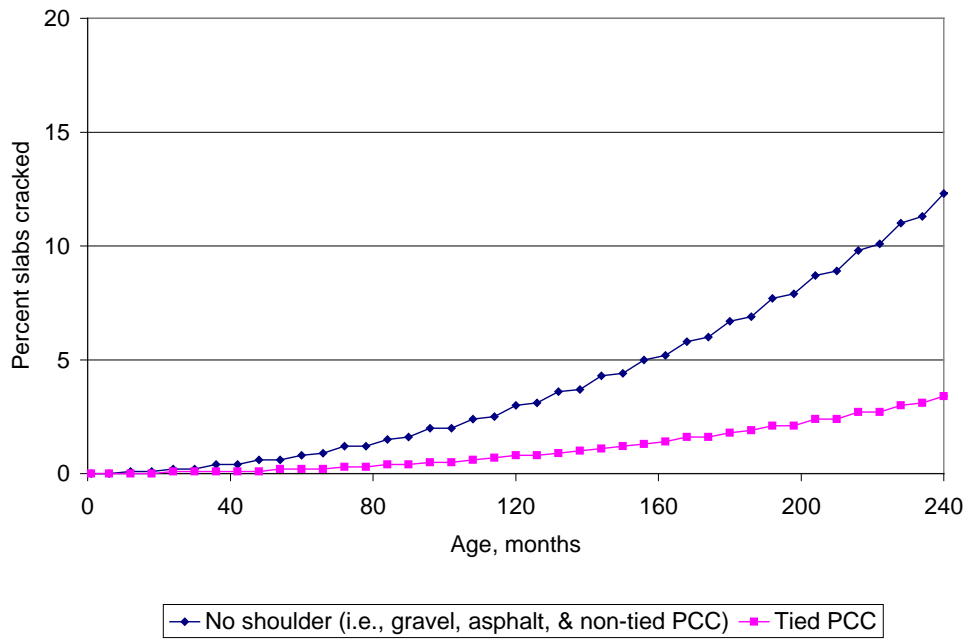


Figure 128. Plot of age versus percent slabs cracked showing the effect of pavement edge support.

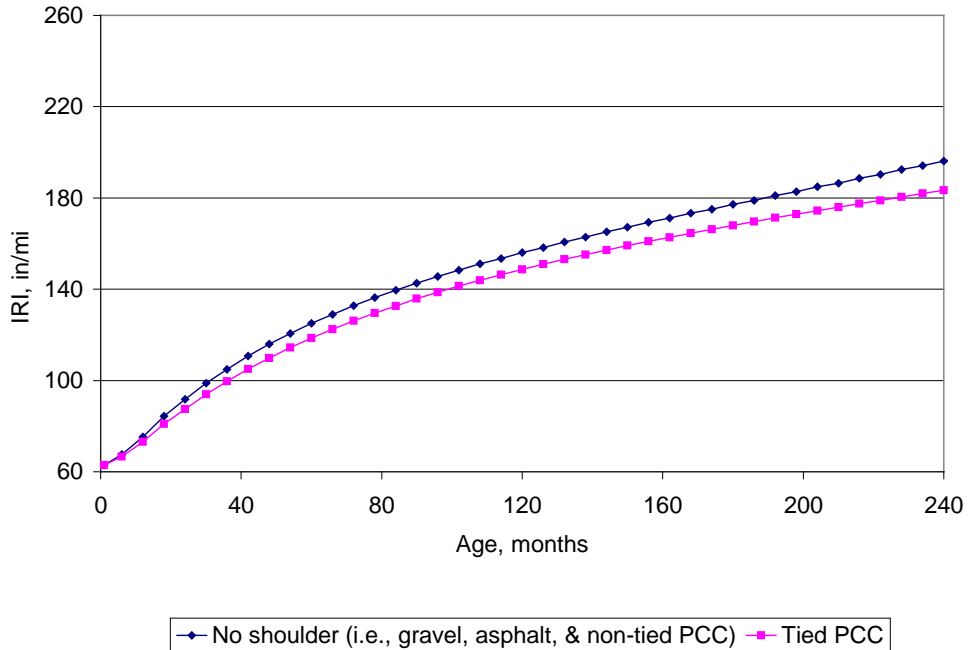


Figure 129. Plot of age versus IRI showing the effect of pavement edge support.

Table 38. Relative effect of edge support on JPCP distress and IRI.

Distress/IRI	Effect of Edge Support on Distress/IRI
Joint faulting	Low
Slab transverse cracking	High
IRI	Low

### Effect of traffic composition

The effect of traffic composition (vehicle class and axle load distribution) is shown in figures 130 to 132. The definition of the classes is the same as that for asphalt pavement. The results show that the different vehicle class distributions at these locations have a large effect on slab cracking and a small effect on joint faulting and IRI. The results are summarized in table 39.

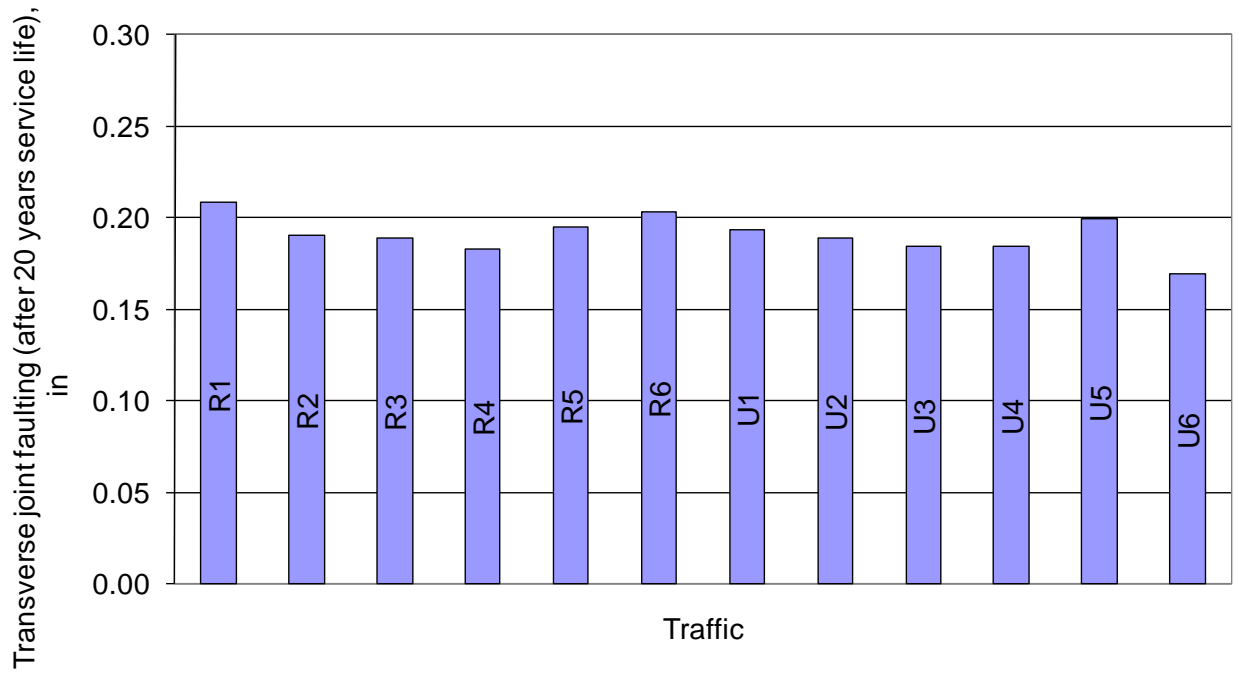


Figure 130. Plot of age versus transverse joint faulting showing the effect of traffic composition.

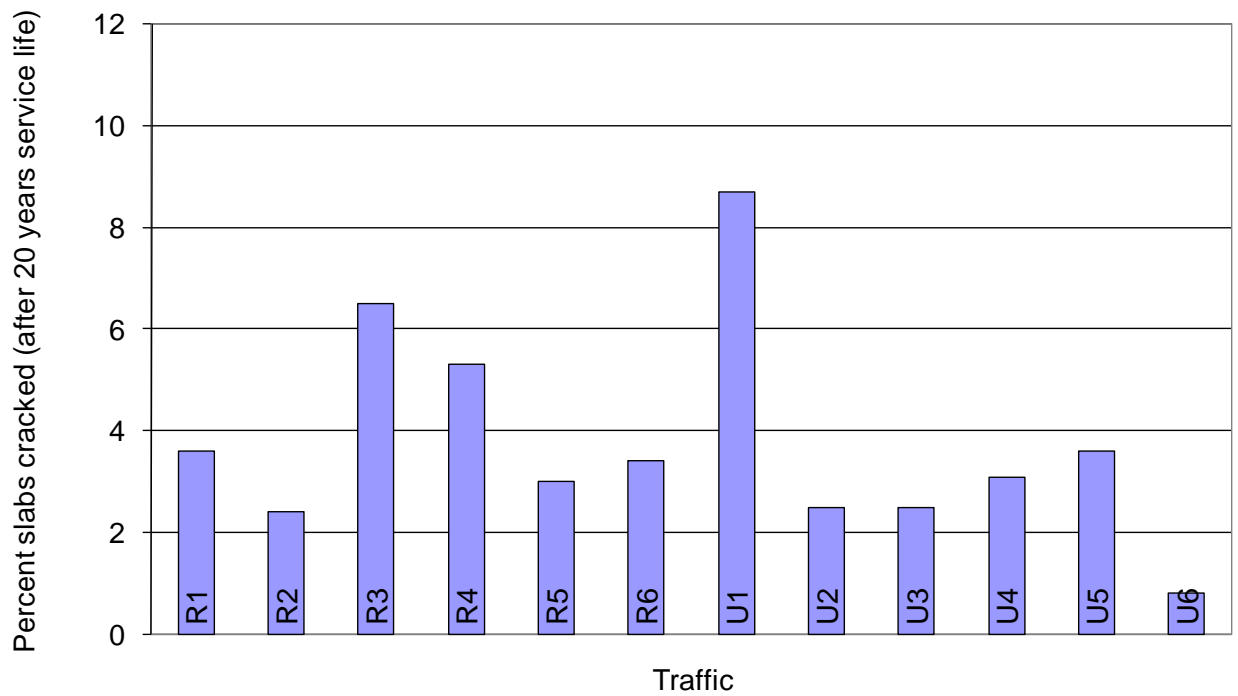


Figure 131. Plot of age versus percent slabs cracked showing the effect of traffic composition.

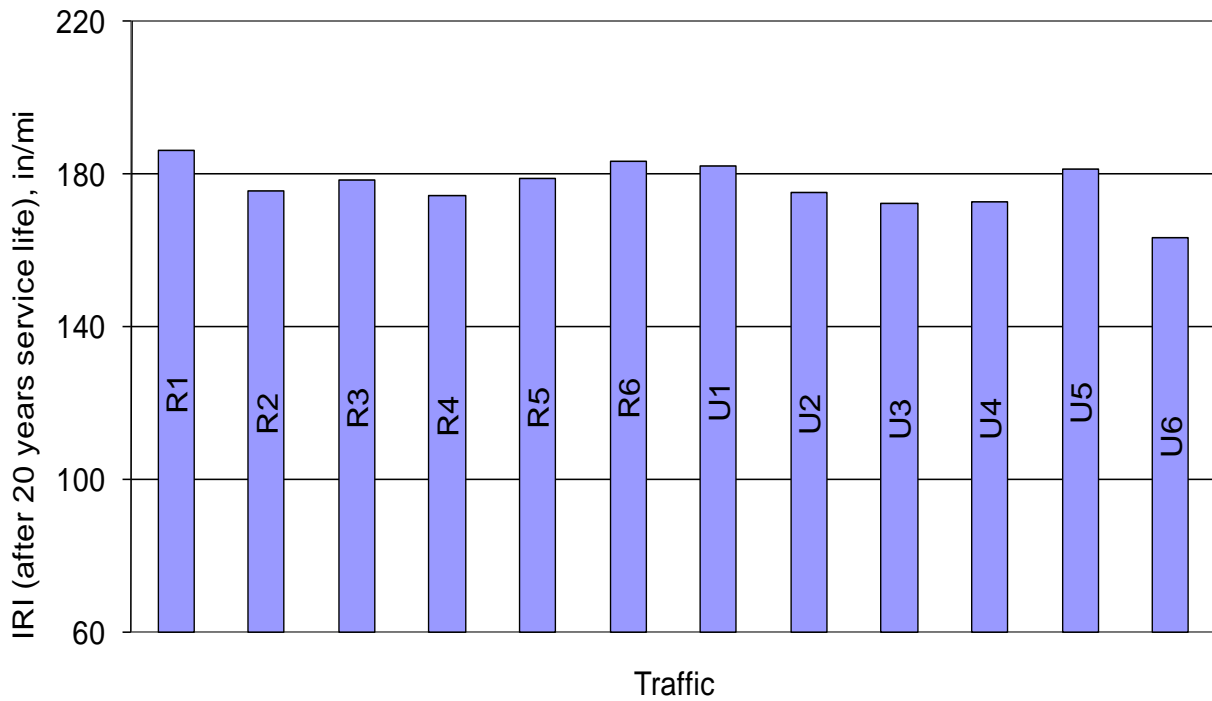


Figure 132. Plot of age versus IRI showing the effect of traffic composition.

Table 39. Relative effect of traffic composition on JPCP distress and IRI.

Distress/IRI	Effect of Traffic Composition on Distress/IRI
Joint faulting	Low
Slab transverse cracking	High
IRI	Low

# CHAPTER 4. SENSITIVITY ANALYSIS OF HMA OVERLAY DESIGN OF RUBBLIZED PCC PAVEMENTS

## Rehabilitation Design Types Considered

The structural design of the HMA overlay placed over a rubblized PCC slab was identified by ODOT as one of potential application areas of the MPEDG technology. ODOT usually considers performing this type of major rehabilitation on pavements if the ODOT pavement condition rating (PCR) falls below 55 which represent a pavement in poor condition by definition. This section describes the sensitivity of the MEPDG distress and IRI models to the various MEPDG inputs considered in this rehabilitation design type.

## Description of the Existing JRCF Pavement to be used in the Baseline Designs for the Rubblization Example

LTPP project 39\_4031, an existing JRCF pavement in Ohio, was selected as the PCC pavement to be rubblized for the purposes of this analysis. Key features and properties of the existing JRCF prior to rubblization are summarized as follows:

- Inventory
  - Construction date: June 1969.
- Design:
  - Shoulder type: asphalt.
  - Joint spacing: 60-ft.
  - Load transfer: Round dowel.
  - Percent longitudinal steel: 0.16
- Existing JRCF structure and layer thicknesses (see figure 133).
- Existing JRCF surface condition (assumed).
  - The ODOT PCR value was determined to be less than 55.
  - Visual survey results:

Distress	Severity	Extent
Patching	Less than 1-ft <sup>2</sup> deterioration	10 to 20 patches per mile
Average joint faulting	0.3-in	20 to 50 percent of all joints
Transverse cracking	Transverse cracks typically 2 per 60-ft slab, all cracks were spalled and faulted	30 to 50 percent all slabs
Corner breaks	Width of 0.25 to 1.0-in	4 to 10 per mile

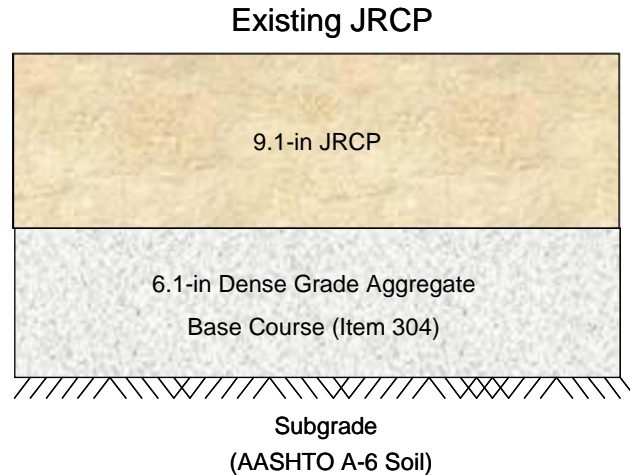


Figure 133. Existing JRCP structure prior to rehabilitation (i.e. rubblization and rolling, and placement of HMA overlay).

### **HMA Over Rubblized PCC Baseline Design**

The baseline ODOT HMA over rubblized PCC design inputs were developed using information gathered from various sources including (1) ODOT pavement design and construction specifications and manuals, (2) ODOT research reports, and (3) LTPP database. A description of the baseline design is presented in the following sections.

#### Baseline HMA over Rubblized PCC Pavement Design Construction Date and Analysis Period

It was assumed that the HMA overlay will be placed in October and opened to traffic in November. An analysis period of 20 years was selected which conforms to ODOT's major rehabilitation design guidance. Figure 134 show an MEPDG screen shot showing the dates of construction and opening to traffic for the baseline ODOT HMA over rubblized PCC design.

#### Analysis Parameters (Initial IRI) for the Baseline HMA over Rubblized PCC Design

The initial IRI at construction for the baseline pavement was assumed to be approximately 63 in/mile.

#### Location of Baseline HMA over Rubblized PCC Pavement

The baseline HMA over Rubblized PCC pavement section was assumed to be located in the city of Newark in central Ohio.

## 20-yr Traffic Projections for the Baseline HMA over Rubblized PCC Pavement

The traffic inputs used for developing HMA over rubblized PCC pavement baseline design were the same as those used for new HMA baseline design and described earlier (refer figure 6; the only difference here is that the traffic opening date for the HMA overlay was assumed to be in the month of November). Initial 2-way AADTT was assumed to be 12,893 with a 0.5 directional distribution factor, and a lane distribution factor of 0.825. This results in a total of 70 million trucks passing over the pavement in the outer lane over the 20 year design period.

The screenshot shows a software dialog box titled "General Information". It contains the following fields and options:

- Project Name:
- Description:
- Design Life (years):
- Existing pavement construction month:  Year:
- Pavement overlay construction month:  Year:
- Traffic open month:  Year:
- Type of Design:
  - New Pavement:
    - Flexible Pavement
    - Jointed Plain Concrete Pavement (JPCP)
    - Continuously Reinforced Concrete Pavement (CRCP)
  - Restoration:
    - Jointed Plain Concrete Pavement (JPCP)
  - Overlay:
    - Asphalt Concrete Overlay
      -
    - PCC Overlay
      -

Buttons:

Figure 134. General information for baseline HMA over rubblized PCC design.

## Climate Data Input for Baseline HMA over Rubblized PCC Pavement Section

The location of the weather stations and other climate related inputs needed by the MEPDG for the baseline HMA over rubblized PCC pavement section are the same as for the new HMA pavement described previously in this Volume. Climate inputs for the MEPDG are presented in figure 16.

## Pavement Surface Properties for Baseline HMA over Rubblized PCC Pavement Section

A surface shortwave absorptivity of 0.85 was assumed for the HMA overlay (used in all global calibration work during the development of the MEPDG).

## Structure and Materials of the HMA over Rubblized PCC Pavement Design

### *Structure*

The baseline HMA over Rubblized PCC pavement structure is shown in figures 135. Figure 136 shows the baseline pavement structure as entered into the MEPDG software. The HMA overlay was chosen to be made of similar materials as those used for the new HMA pavement design (figure 6).

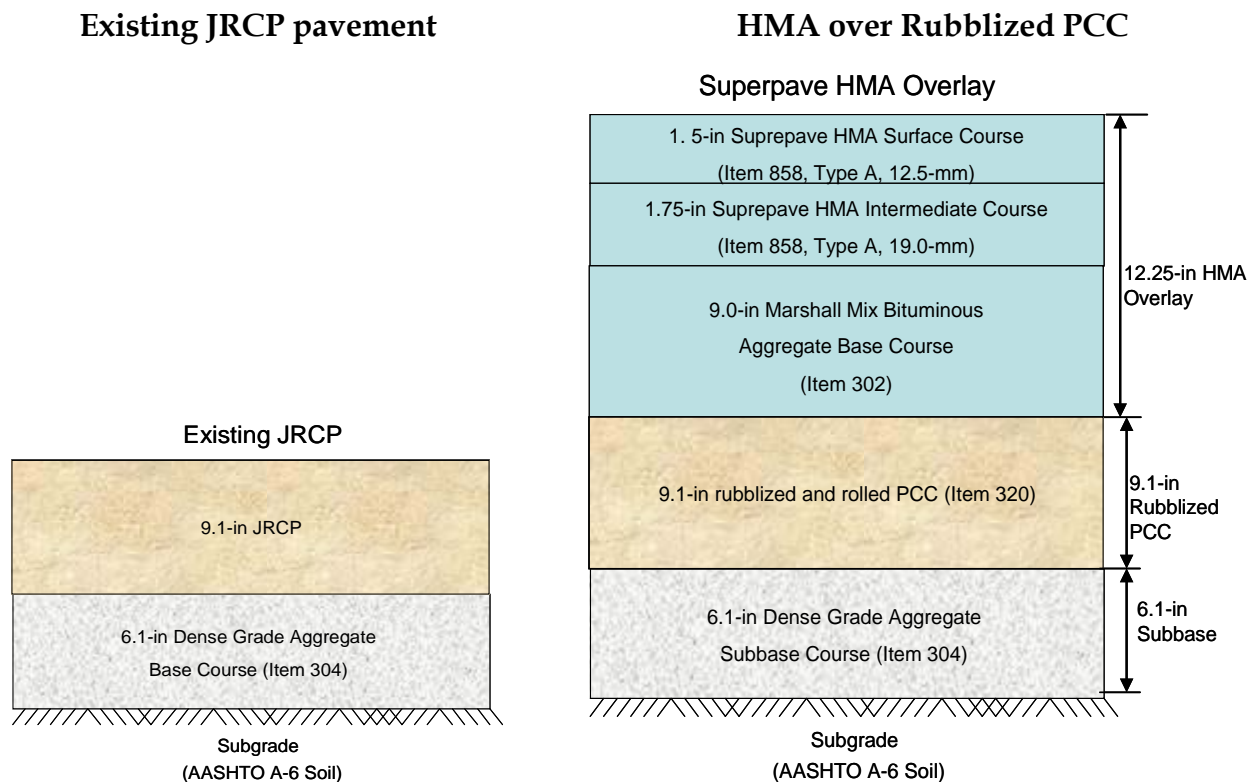


Figure 135. Baseline HMA over Rubblized PCC pavement design to be used in sensitivity analysis.

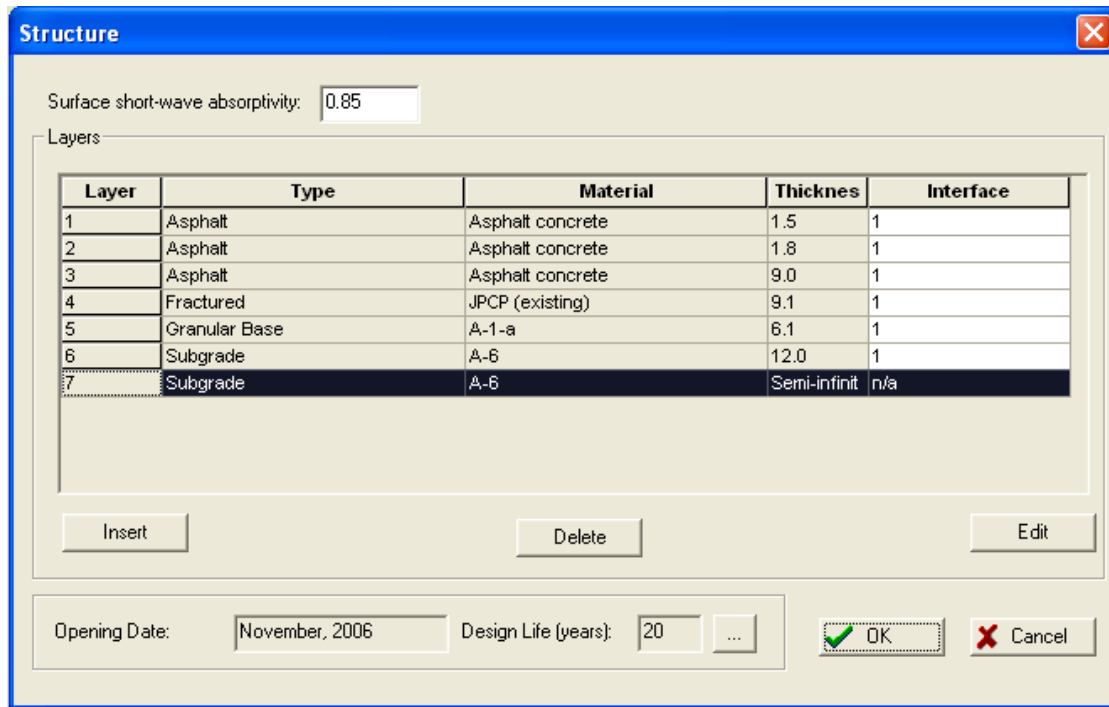


Figure 136. Layers used for baseline HMA over Rubblized PCC pavement section.

The baseline design assumes high levels of traffic and thus typical HMA overlay thickness will be approximately 12.25-in. The HMA overlay will be placed over the rubblized and rolled existing 9.1-in JRCP. Rubblization and rolling was assumed to be done as per ODOT specifications (see Item 320). The 12.25-in HMA overlay consists of the following:

- 1.5-in Superpave HMA mix surface course (as per ODOT Item 442, type A, 12.5 mm).
- 1.75-in Superpave HMA mix intermediate course (as per ODOT Item 442, type A, 19.0 mm).
- 9.0-in Marshall mix bituminous base course (as per ODOT Item 302).

*HMA Overlay Mix Properties (MEPDG Layers 1 through 3) for HMA over Rubblized PCC Design*

The properties of the HMA surface, intermediate, and base layers are the same as those of the new HMA baseline design.

*Rubblized PCC Layer Material Properties (MEPDG Layer 4)*

Inputs required by the MEPDG for fractured PCC (including rubblized PCC) are shown in figure 137. For the baseline design, the existing concrete slab thickness of 9.1-in was assumed along with default MEPDG values for rubblized PCC unit weight, Poisson's ratio, thermal conductivity, and heat capacity.

Currently, the ODOT rehabilitation design procedure recommends that the rubblized PCC layer be treated as a dense graded aggregate or crushed stone layer. The design procedure thus recommends a modulus of 30,000 psi. The ODOT recommended modulus of 30,000 psi will be used in the baseline analysis for this layer even though this value appears to be very conservative based on literature. The MEPDG recommends a range of modulus values from 50,000 to 150,000 psi for rubblized layers.

The image shows a software dialog box titled "JPCP (existing) Material". It is divided into three sections: General Properties, Strength Properties, and Thermal Properties. The General Properties section includes fields for Material type (JPCP (existing)), Layer thickness (in) (9.1), Unit weight (pcf) (130), and Poisson's ratio (0.35). The Strength Properties section includes fields for Elastic/resilient modulus (psi) (30000), Minimum elastic/resilient modulus (psi) (n/a), Modulus of rupture (psi) (n/a), and Type fracture (Rubblization). The Thermal Properties section includes fields for Thermal conductivity (BTU/hr-ft-F\*) (1.25) and Heat capacity (BTU/lb-F\*) (0.28). At the bottom are OK and Cancel buttons.

Section	Property	Value
General Properties	Material type	JPCP (existing)
	Layer thickness (in)	9.1
	Unit weight (pcf)	130
	Poisson's ratio	0.35
Strength Properties	Elastic/resilient modulus (psi)	30000
	Minimum elastic/resilient modulus (psi)	n/a
	Modulus of rupture (psi)	n/a
	Type fracture	Rubblization
Thermal Properties	Thermal conductivity (BTU/hr-ft-F*)	1.25
	Heat capacity (BTU/lb-F*)	0.28

Figure 137. Properties of rubblized PCC layer for baseline HMA over rubblized PCC pavement section.

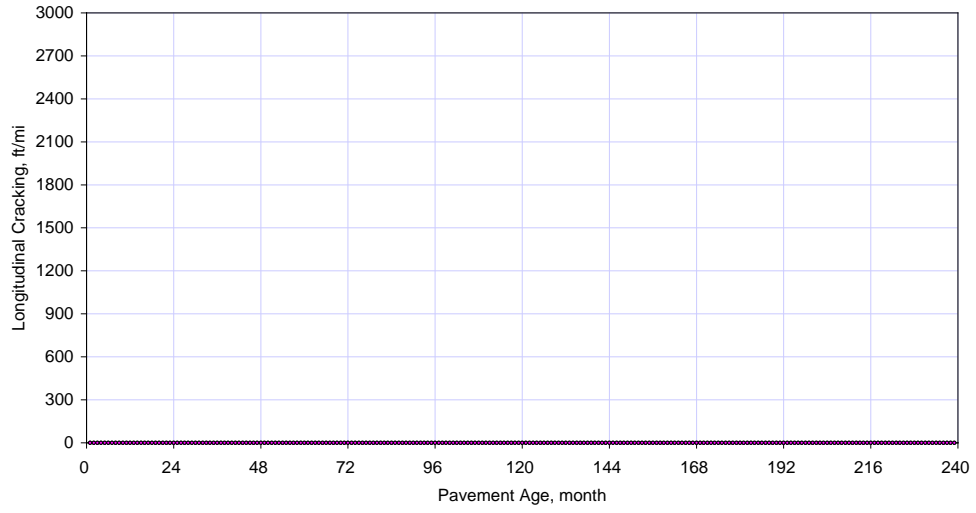


Figure 138. Plot of predicted longitudinal cracking versus pavement age.

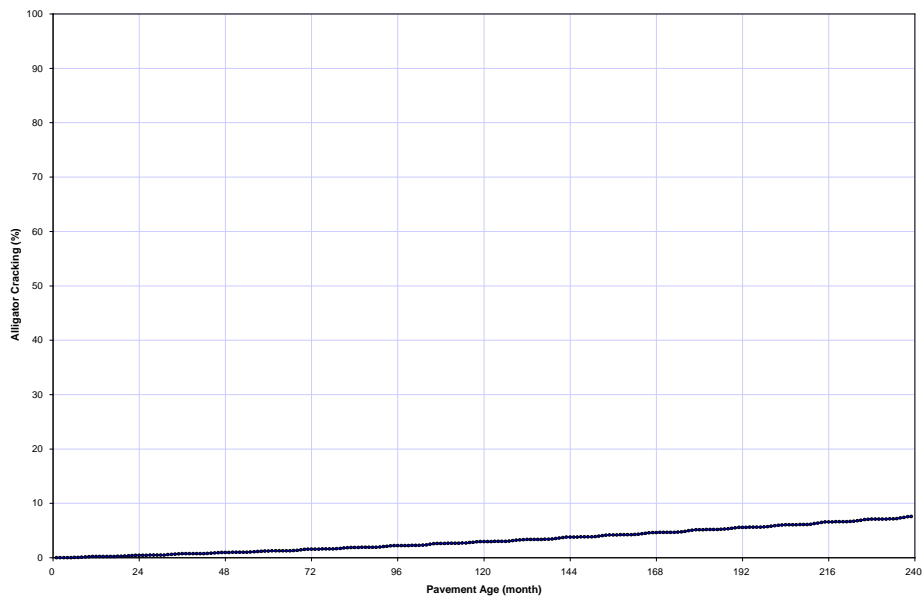


Figure 139. Plot of predicted alligator cracking versus pavement age.

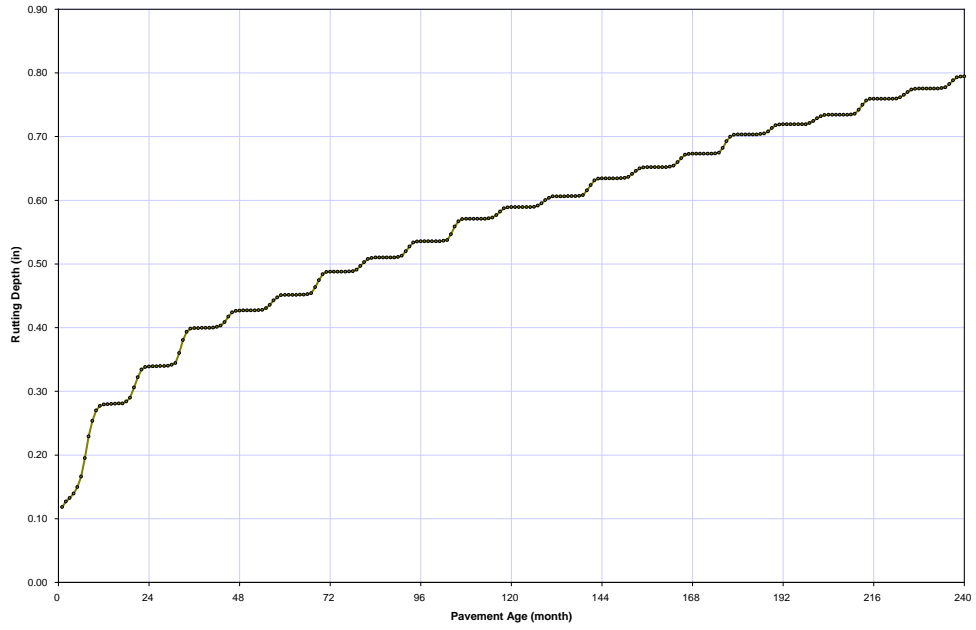


Figure 140. Plot of predicted total rutting versus pavement age.

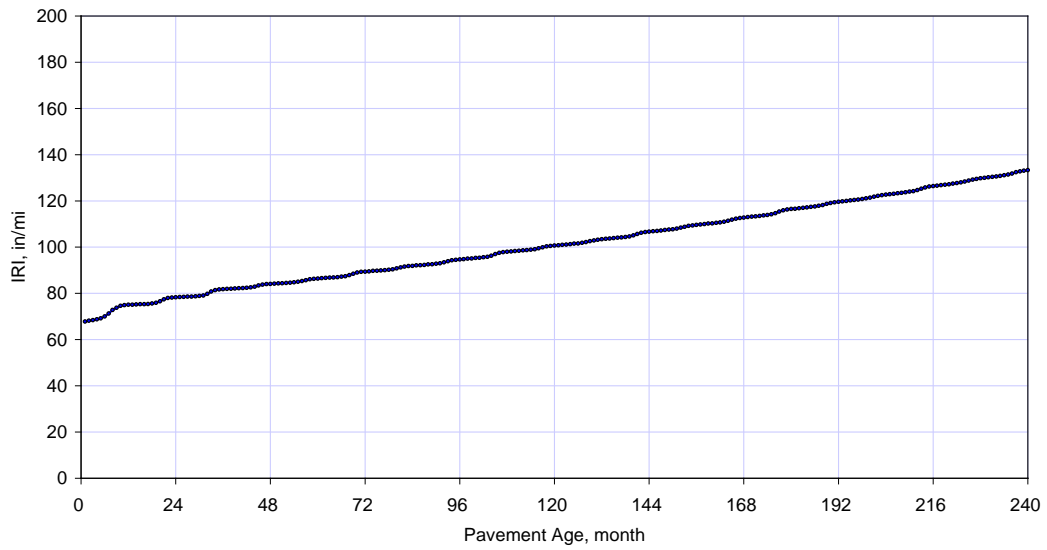


Figure 141. Plot of predicted IRI versus pavement age.

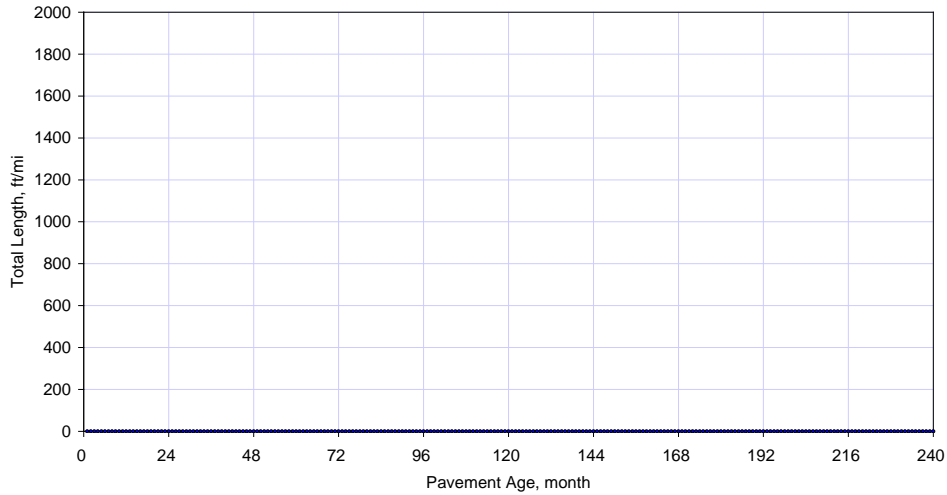


Figure 142. Plot of predicted transverse cracking versus pavement age.

Table 40. Summary of predicted distress and IRI obtained from the MEPDG for HMA overlay of rubblized JRCP.

Pavement Age, years	Longitudinal Cracking (ft/mi)	Alligator Cracking (Percent Area)	Transverse Cracking (ft/mi)	Total Rutting (in)	IRI (in/mi)	Heavy Trucks (cumulative)
0.08	0	0.0063	0	0.118	67.8	161,878
1	0	0.211	0	0.279	74.7	1,942,530
2	0	0.442	0	0.339	77.9	4,049,010
3	0	0.722	0	0.399	81.4	6,319,440
4	0	0.968	0	0.427	83.7	8,753,830
5	0	1.24	0	0.451	86	11,352,200
6	0	1.57	0	0.488	89	14,114,400
7	0	1.88	0	0.51	91.5	17,040,700
8	0	2.22	0	0.535	94.3	20,130,800
9	0	2.63	0	0.571	97.6	23,385,000
10	0	2.97	0	0.589	100.2	26,803,100
11	0	3.35	0	0.606	103	30,385,100
12	0	3.79	0	0.634	106.3	34,131,100
13	0	4.19	0	0.652	109.2	38,041,000
14	0	4.63	0	0.673	112.4	42,114,900
15	0	5.15	0	0.703	116.1	46,352,700
16	0	5.58	0	0.719	119.2	50,754,500
17	0	6.05	0	0.734	122.4	55,320,200
18	0	6.58	0	0.759	126.1	60,049,900
19	0	7.08	0	0.775	129.4	64,943,500
20	0	7.6	0	0.795	133	70,001,100

## MEPDG Predicted Performance for Baseline HMA over Rubblized PCC Design

Figures 138 through 142 and table 40 show predicted distress and IRI for the baseline design presented. A review of the predictions indicates that the baseline design provide reasonable levels of distress and IRI as expected making the design suitable as the basis for sensitivity analysis. A list of key input parameters known to influence HMA distress/IRI was developed and used as the basis for sensitivity analysis based on the familiarity of the project team with the MEPDG prediction models. The listed input parameters along with the levels of variations are presented in table 41.

Table 41. Input parameters of interest to be used for HMA over Rubblized PCC sensitivity analysis.

MEPDG Input Parameter	Levels of Input (*indicates the baseline representative design)
HMA overlay thickness	7-, 9-, 12.25*-, 14-, 16-in (varying the bituminous base thickness only)
HMA overlay air voids content	6.5-, 7.5-, 8.5*-, 9.5-, 10.5 percent
HMA overlay volumetric binder content	9-, 10-, 11.1*-, 12-, 13-percent
HMA overlay surface course type	<ul style="list-style-type: none"> <li>• Superpave HMA Mix Surface Course, ODOT Item 442, Type A, 12.5mm, (MEPDG Layer 1)*</li> <li>• SMA surface course (Item 443), refer table 7 for more details</li> </ul>
Rubblized PCC modulus	30,000*-, 75,000-, 150,000-psi
Rubblized PCC thickness	7-, 9*-, 11-in

\*HMA over Rubblized PCC baseline project.

\*\*Default MEPDG gradations will be used, where applicable.

\*\*\*For the sensitivity analysis, another HMA material type – stone matrix asphalt (SMA) (Item 443) was considered. For SMA, the 1.5-in surface course was replaced with the SMA surface course.

### Effect of HMA Overlay Thickness

The effect of HMA overlay thickness on distresses and IRI are shown in figures 143 to 146. Longitudinal fatigue (top down) cracking was affected only when HMA thickness was reduced to 7-in which caused it to increase greatly. HMA thickness had a large effect on both alligator cracking and rutting and thus IRI as one would expect. These effects are shown in figures 143 through 146 for a thickness range of 7- to 16-in.

Information presented in figures 143 through 146 summarizes all of these effects. The trends observed were reasonable with the highest distress/IRI observed for the thinner HMA. Alligator cracking, rutting, and IRI all decreased with increased HMA overlay thickness.

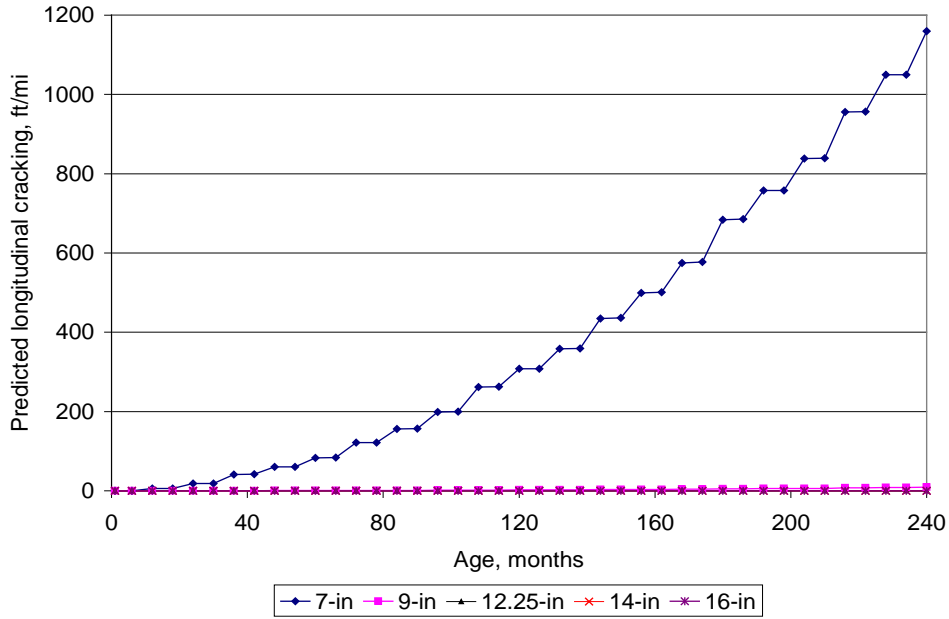


Figure 143. Plot of age versus top-down fatigue (longitudinal) cracking showing the effect of total HMA overlay thickness.

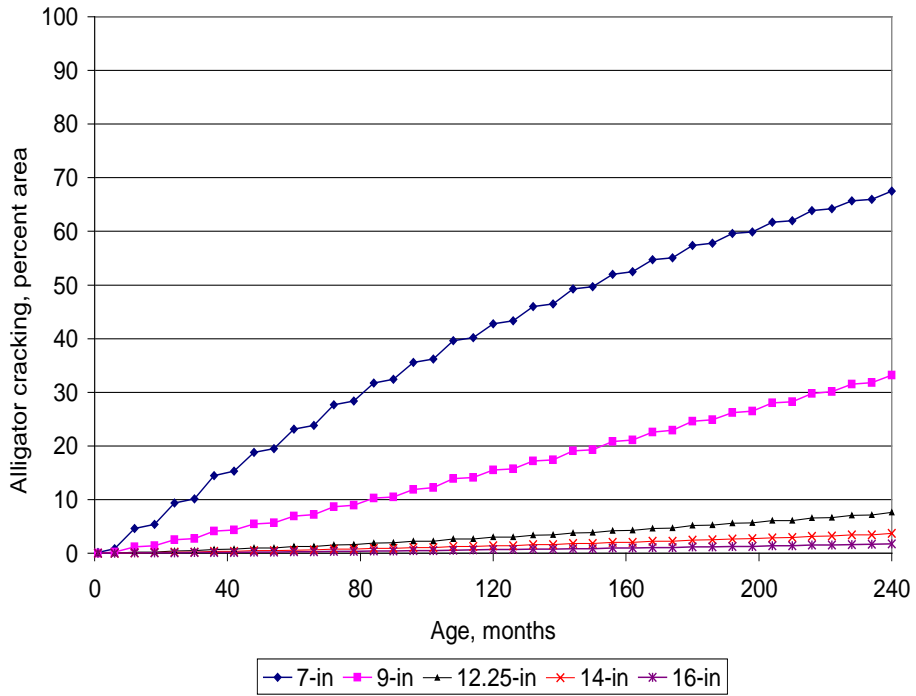


Figure 144. Plot of age versus bottom-up fatigue (alligator) cracking showing the effect of total HMA overlay thickness.

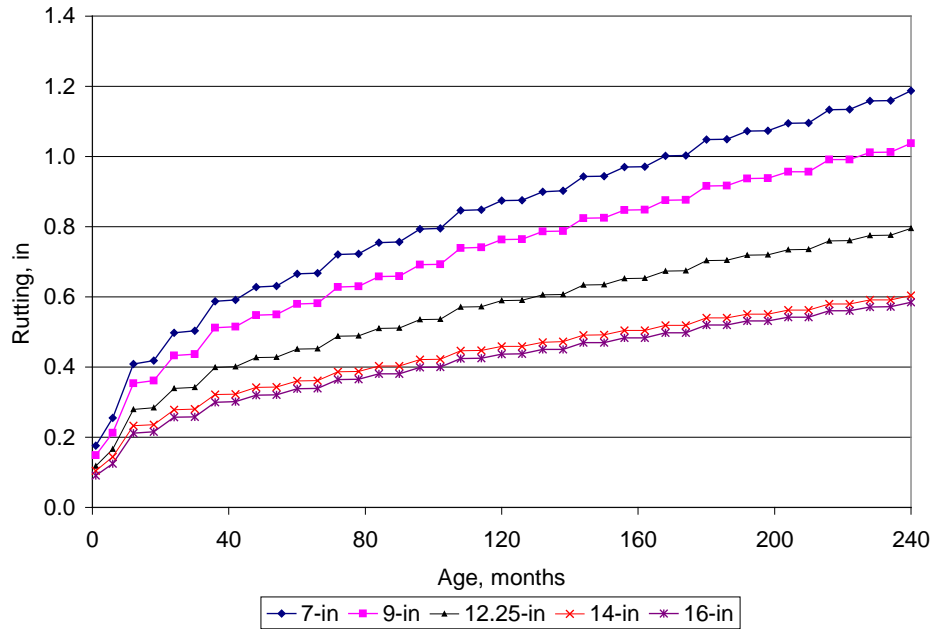


Figure 145. Plot of age versus rutting showing the effect of total HMA overlay thickness.

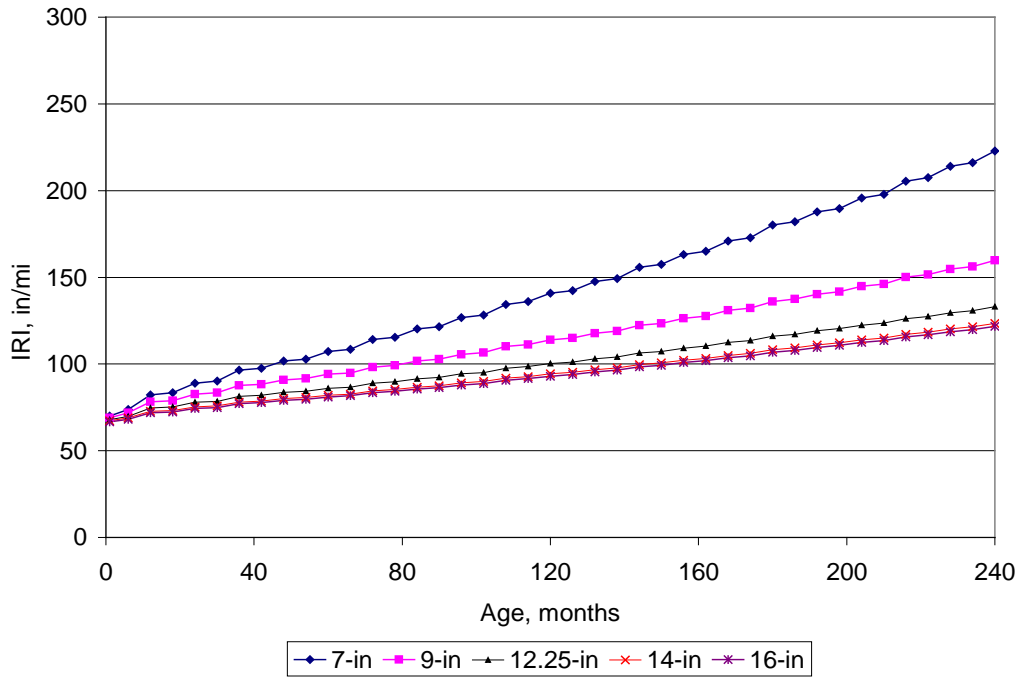


Figure 146. Plot of age versus IRI showing the effect of total HMA overlay thickness.

Table 42 summarizes the relative effect of HMA overlay thickness on all distress and IRI. Information presented in table 42 shows that alligator cracking, rutting, and IRI were all highly influenced by HMA thickness. As HMA increases in thickness the alligator cracking, rutting, and IRI all decrease as would be expected.

Table 42. Relative effect of HMA overlay thickness on HMA/rubblized PCC distress and IRI.

<b>Distress/IRI</b>	<b>Effect of HMA Overlay Thickness on Distress/IRI</b>
Low temperature transverse cracking	None
Longitudinal fatigue cracking	Large effect < 7-in HMA
Bottom-up fatigue (alligator) cracking	High
Rutting	High
IRI	High

#### Effect of HMA In-Situ Air Voids & Binder Content

The effect of in situ air voids and binder content on distress and IRI for HMA overlay of rubblized JRCP was the same as that for new HMA pavement. Refer to the new HMA section for these results.

#### Effect of ODOT Surface HMA Mix Type

The effect of ODOT surface HMA mix type on distress and IRI for HMA overlay of rubblized JRCP was the same as that for new HMA pavement. Refer to the new HMA section for these results.

#### Effect of Rubblized PCC Modulus

The modulus of the rubblized PCC pavement can vary greatly with construction process used to rubblize the JRCP. The effect of modulus of the rubblized PCC on distresses and IRI are shown in figures 147 through 149. Figure 147 shows a plot of the effect that varying the rubblized PCC pavement modulus has on alligator fatigue cracking. The effect is very high as would be expected since the modulus of the rubblized layer directly effects the bending strain at the bottom of the HMA layer which is directly related to bottom up alligator fatigue cracking. As this modulus varies from 30,000 to 150,000 psi the alligator cracking reduces greatly from about 8 to less than 2 percent. Thus, this result shows that it is extremely important what modulus is chosen for design of the HMA overlay of the rubblized section. The change in rubblized PCC modulus has little effect on rutting and IRI. Table 43 summarizes the relative effect of modulus of the rubblized PCC on all distress and IRI.

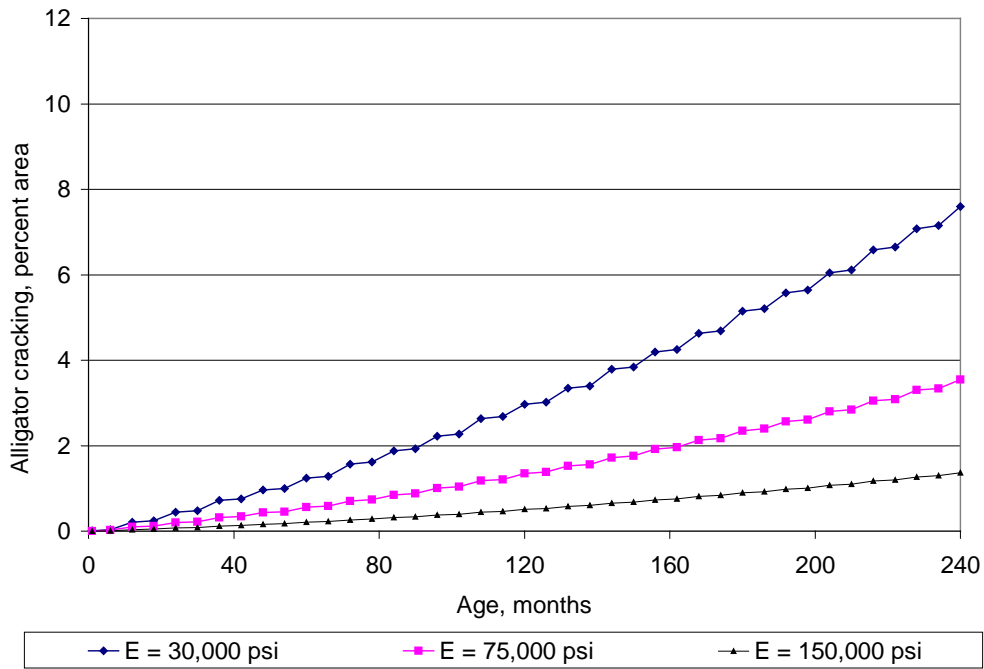


Figure 147. Plot of age versus bottom-up fatigue (alligator) cracking showing the effect of rubblized PCC modulus.

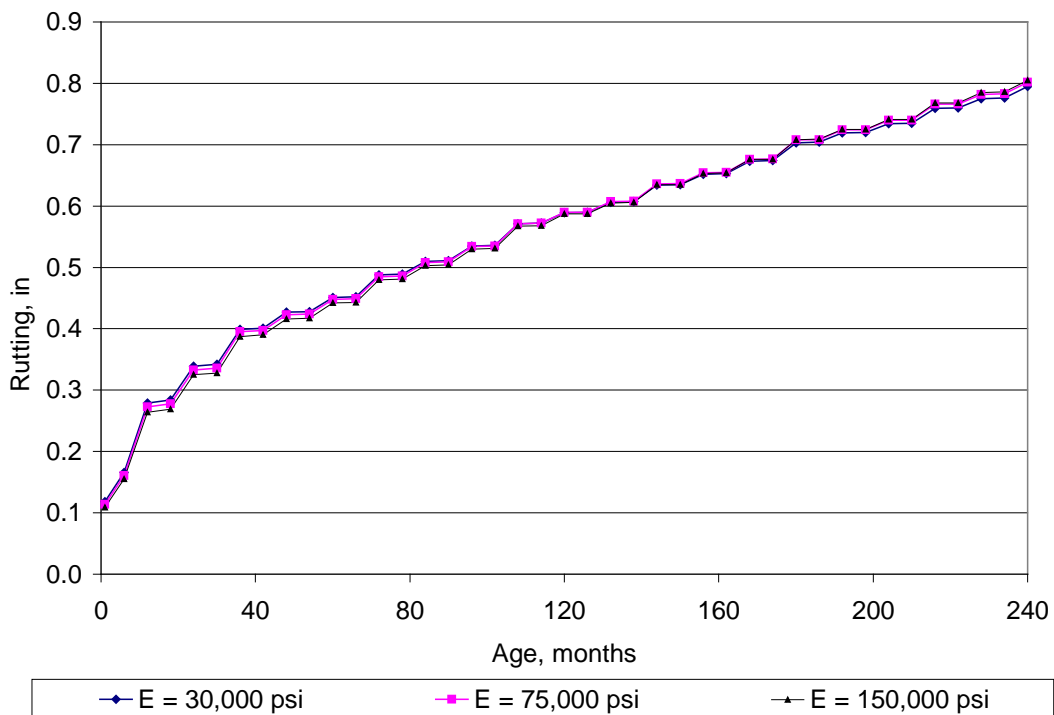


Figure 148. Plot of age versus rutting cracking showing the effect of rubblized PCC modulus

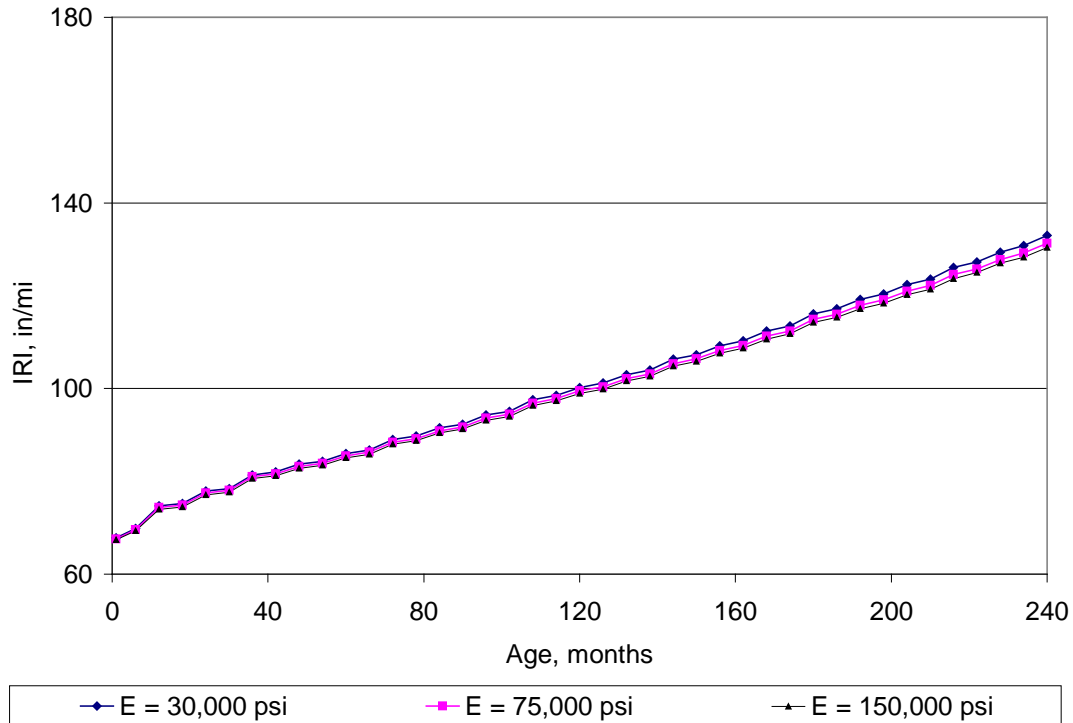


Figure 149. Plot of age versus IRI showing the effect of rubblized PCC modulus

Table 43. Relative effect of rubblized PCC modulus on HMA overlay distress and IRI.

Distress/IRI	Effect of rubblized PCC Modulus on HMA Overlay Distress/IRI
Longitudinal fatigue cracking	None
Low temperature transverse cracking	None
Bottom-up fatigue (alligator) cracking	High
Rutting	Low
IRI	Low

### Effect of Rubblized PCC Thickness

The thickness of the rubblized PCC pavement would of course vary with the original slab thickness. This was varied from 7 to 11 in to determine if it has a significant effect on distress and IRI. The effect of modulus of the rubblized PCC on distresses and IRI are shown in figures 150 through 152. Figure 150 shows a plot of the effect that varying the rubblized PCC pavement thickness has on alligator fatigue cracking. The effect is moderate only as would be expected over this range. The change in rubblized PCC modulus has little effect on rutting and IRI. Table 44 presents the relative effect of rubblized PCC thickness on HMA distress and IRI.

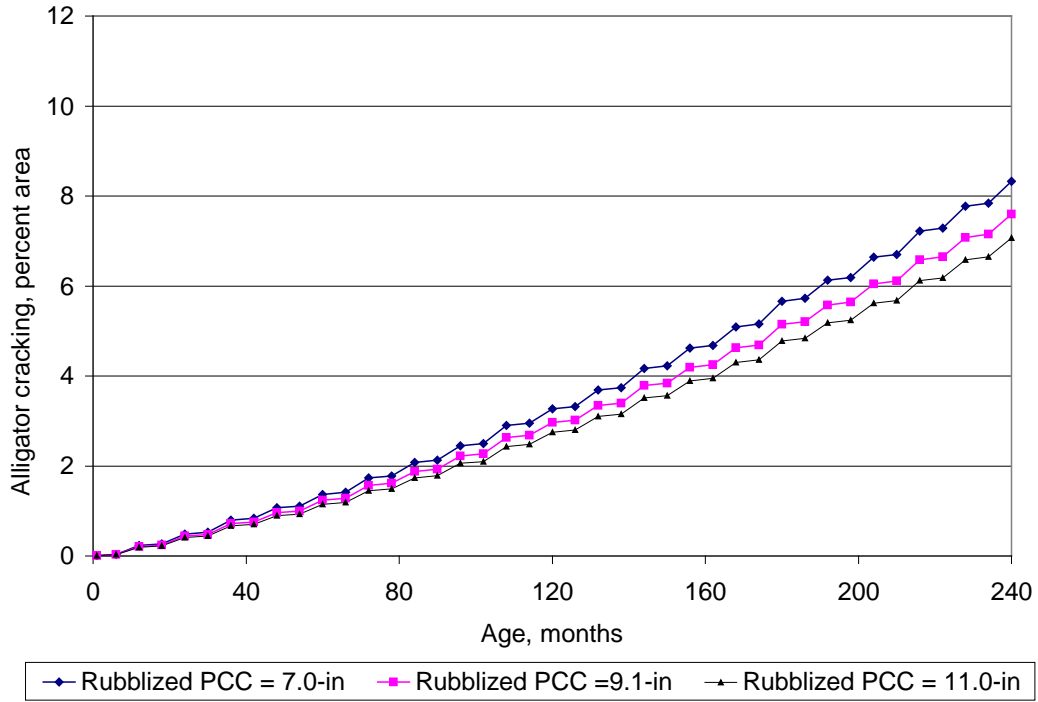


Figure 150. Plot of age versus bottom-up fatigue (alligator) cracking showing the effect of rubblized PCC thickness.

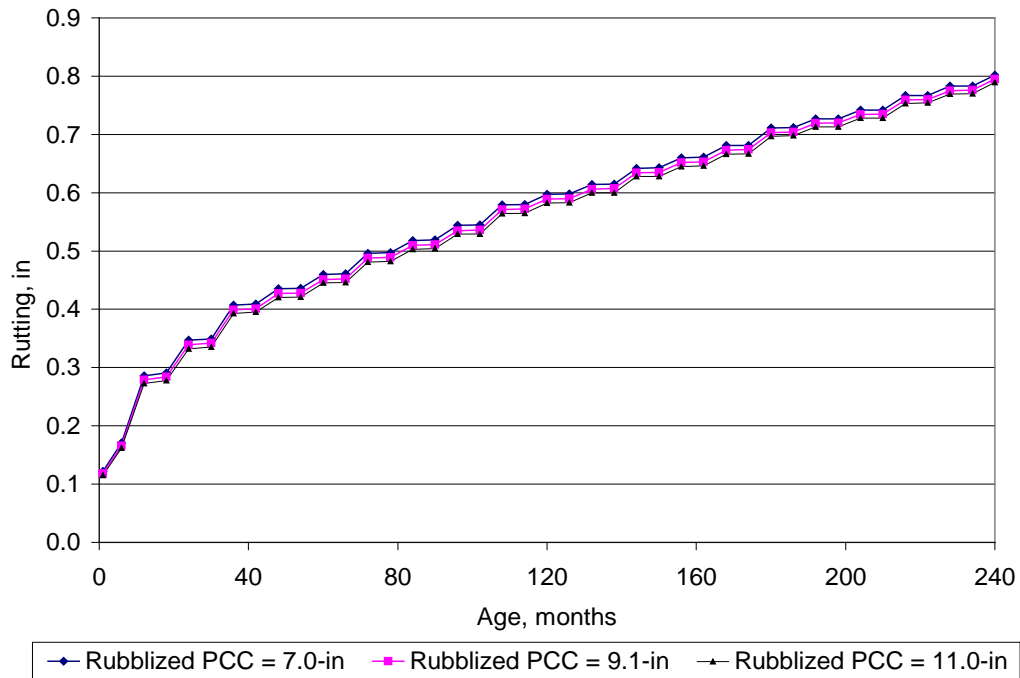


Figure 151. Plot of age versus rutting showing the effect of rubblized PCC thickness.

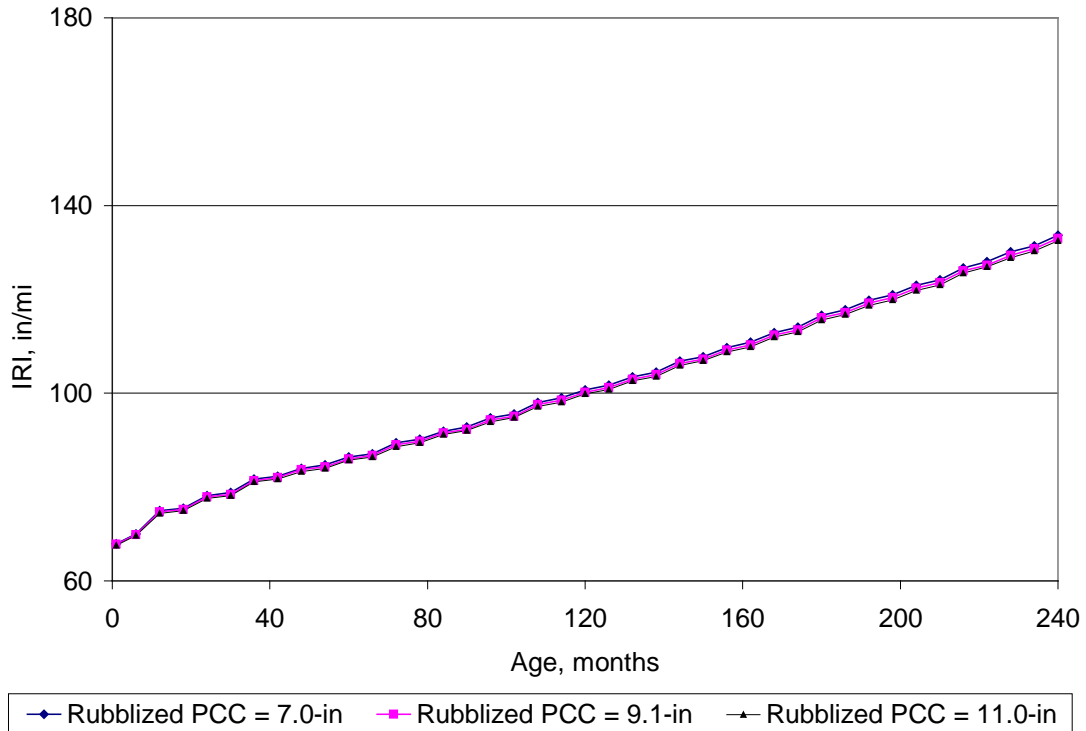


Figure 152. Plot of age versus IRI showing the effect of rubblized PCC thickness.

Table 44. Relative effect of rubblized PCC thickness on HMA distress and IRI.

Distress/IRI	Effect of Rubblized PCC Thickness on Distress/IRI
Longitudinal fatigue cracking	None
Low temperature transverse cracking	None
Bottom-up fatigue (alligator) cracking	Moderate
Rutting	Low
IRI	Low



## CHAPTER 5. UNBONDED JPCP OVERLAY SENSITIVITY ANALYSIS

The unbonded JPCP overlay of an existing rigid or composite pavement is essentially a new JPCP placed on top of an old, deteriorated rigid or composite pavement. A thin separation layer (usually an HMA layer) is placed between the new and existing surfaces to isolate the movements of the base PCC pavement slabs from those of the JPCP overlay. ODOT overlay design procedure recommends a minimum JPCP overlay thickness of 8.0-in. It also recommends considering the use of dowel bars to enhance load transfer across the transverse joints.

### Baseline Unbonded JPCP Overlay Design

The ODOT unbonded JPCP overlay over existing JRCP baseline design was developed using information gathered from various sources including (1) ODOT pavement design and construction manuals, (2) ODOT research reports, and (3) LTPP database. Using the baseline design, a sensitivity analysis was conducted to determine how MEPDG input parameters were sensitive to the following JPCP performance indicators:

- Slab “transverse” fatigue cracking.
- Transverse joint faulting.
- IRI.

A description of the unbonded JPCP overlay over existing JRCP baseline design is presented in the following sections.

### Baseline Unbonded JPCP Overlay over Existing JRCP Design Construction Date and Analysis Period

It was assumed that the unbonded overlay would be constructed in October and opened to traffic in November.

An analysis period of 20 years was selected which adequately covers the expected service life of the typical ODOT unbonded JPCP overlays. Figure 153 shows the dates of construction and opening to traffic for the baseline design along with the analysis period.

Figure 153. General information for the baseline unbonded JPCP overlay over existing JRC design.

Baseline Unbonded JPCP Overlay over Existing JRC Design Analysis Parameters (Initial IRI)

The initial IRI at construction was assumed to be approximately 63 in/mile.

Baseline Unbonded JPCP Overlay over Existing JRC Design Location

The baseline design is located in the city of Newark in central Ohio.

20-yr Traffic Projection for the Baseline Unbonded JPCP Overlay over Existing JRC Design

The traffic inputs used for developing a baseline for the unbonded JPCP overlay over existing JRC design were the same as those used for the new HMA baseline design described earlier in the memorandum. Initial 2-way AADTT was assumed to be 12,893 with a 0.5 directional distribution factor, and a lane distribution factor of 0.825.

## Climate Data for Baseline Unbonded JPCP Overlay over Existing JRCP Design

Climate related data required for the MEPDG is obtained from weather stations located across the State (including neighboring States). The required information is stored in the MEPDG software as defaults. For this design, the default climate information for the City of Newark was selected. Detailed description of the data has been described for new HMA baseline design. (See figure 16).

## Surface Shortwave Absorptivity for the Baseline Unbonded JPCP Overlay over Existing JRCP Design

A default surface shortwave absorptivity of 0.85 was assumed.

## Layering of the JPCP Pavement and Subgrade for Baseline Unbonded JPCP Overlay over Existing JRCP Design

The baseline design consisted of a 10-in JPCP overlay placed over a 9.1-in existing JRCP layer (modeled as a JPCP) overlying a 6.1-in granular base (A-1-a material) and a prepared (A-6 material) subgrade. A thin 1.0-in HMA bond breaker (ODOT Superpave Item 442 Intermediate course, Type A, 9.5-mm mix with binder type PG 64-28) was placed between the JPCP overlay and the existing JRCP layer as recommended by ODOT. The baseline pavement structure is shown in figures 154 and 155. Note that figure 141 shows the baseline pavement structure as coded in the MEPDG.

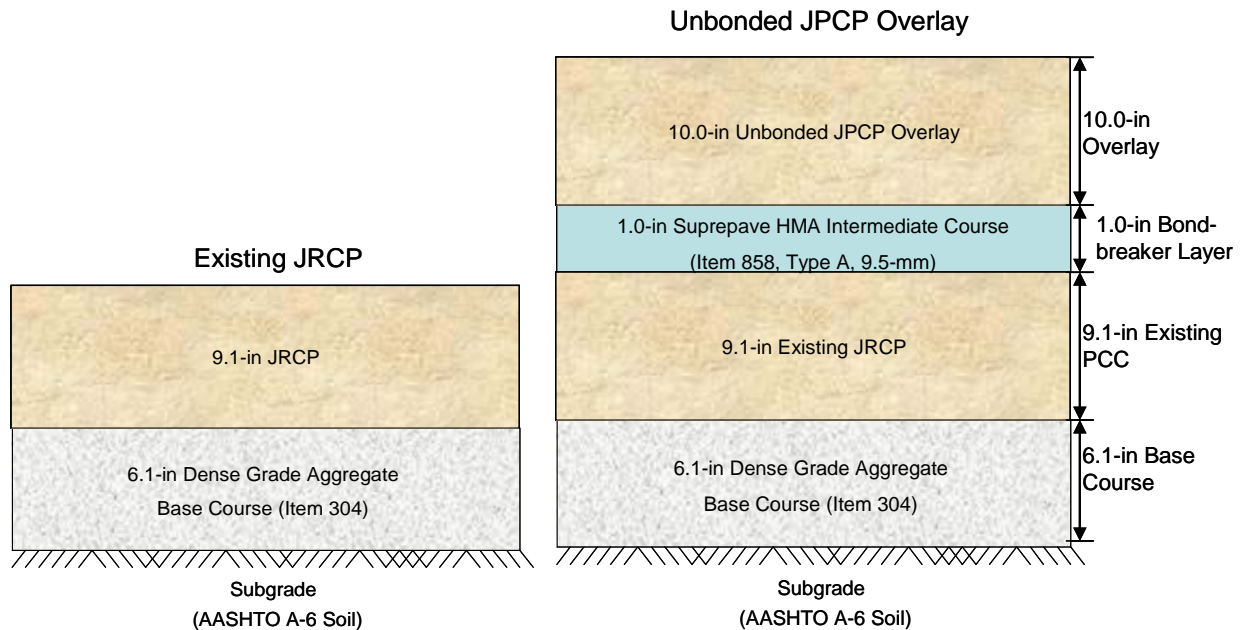


Figure 154. Baseline JPCP overlay over existing JRCP design (modeled as a JPCP).

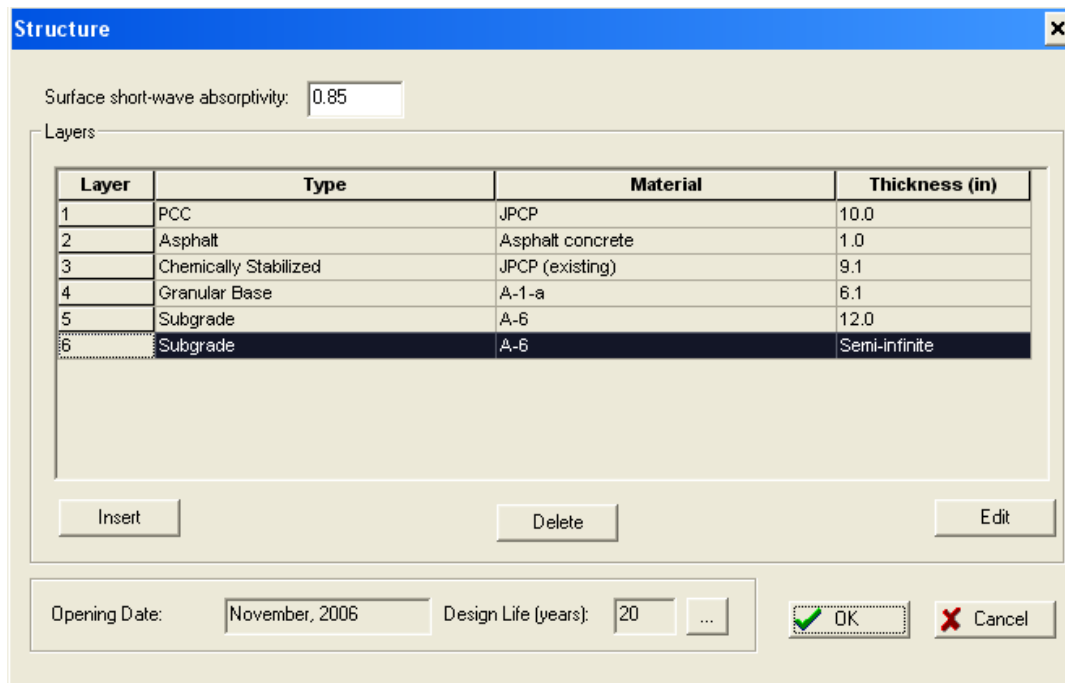


Figure 155. Structure of baseline JPCP overlay over existing JRC design.

### *JPCP Overlay Mix Properties*

The material properties for the unbonded JPCP overlay were assumed to be the same as that for a new JPCP PCC layer. Details description of new JPCP PCC material properties were described in the previous sections.

### *HMA Separation Layer Mix Properties*

The ODOT Superpave HMA intermediate course (Item 442, Type A, 9.5mm) was selected and used as separation layer between the existing PCC surface layer and PCC overlay. Inputs required by the MEPDG for the HMA separation layer are presented in table 45 and figure 156. Default MEPDG unit weight, thermal conductivity, heat capacity, Poisson's ratio were assumed for this layer.

Table 45. Summary of baseline design HMA separation layer properties.

MEPD G Layer number	Material Types	Performance PG Grade	Gradation (Percent Passing Sieve Size)*													Vol. Binder Content, percent* *	HMA Mix Air Voids**
			2-in	1.5- in	1.0- in	3/4-in	1/2-in	3/8- in	No. 4	No. 8	No. 16	No. 30	No. 50	No. 100	No. 200		
2	Superpave HMA Mix Intermediate Course (Item 442, Type A, 9mm)	PG 64-28	—	—	—	—	100.0	95.0	70.0	42.0	—	—	—	—	5.0	11.0	8.5

\* Typical mix design gradations obtained from ODOT. Note that the MEPDG requires only the percent retained on the following sieve sizes 3/4-in, 3/8-in, and No. 4 along with percent passing the No. 200 sieve size.

\*\*Estimated based on mix gradations, gravimetric binder content, and other volumetric properties such as air voids, VMA, VFA, etc.

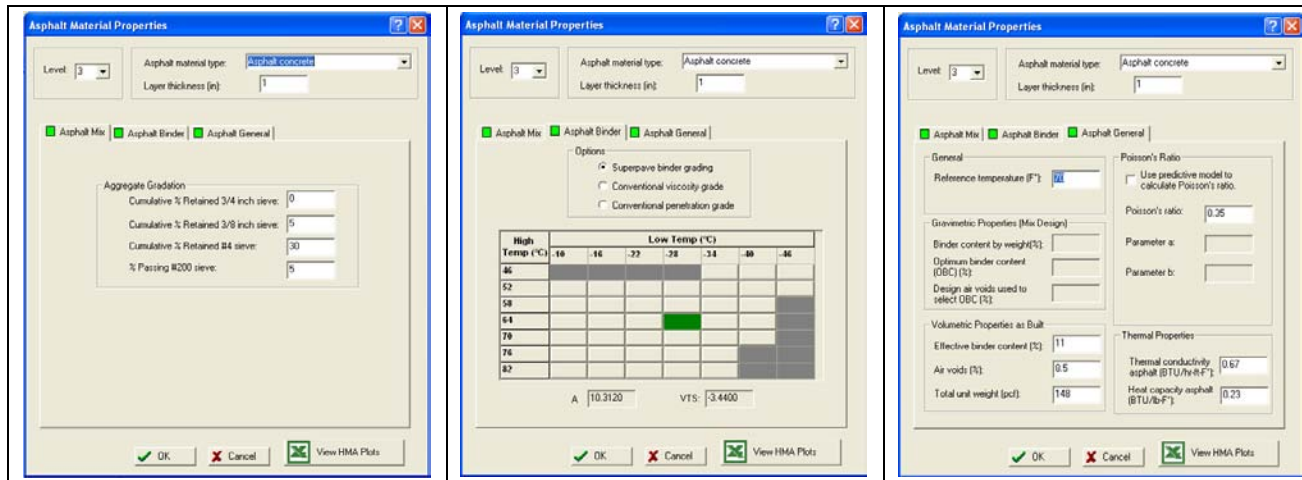


Figure 156. HMA separation layer properties for the baseline unbonded JPCP over existing JRCP design.

### Existing JRC PCC Properties

The existing JRC slab elastic modulus is the key input required by the MEPDG. The average long-term PCC elastic modulus for a typical ODOT pavement was assumed to be approximately 4,068,690 psi (obtained from LTPP project 39\_4031).

### Intact PCC

For unbonded PCC overlays, characterizing the condition of the existing pavement just prior to the overlay and its modulus is a requirement. For the purposes of the sensitivity analysis, after a thorough search of the LTPP database, Ohio LTPP project 39\_4031 was selected as a likely candidate for providing typical long-term strength and modulus values. The following data were downloaded from the LTPP database for this project:

- Inventory
  - Construction date: June 1969.
- Design:
  - Shoulder type: asphalt.
  - Joint spacing: 60-ft.
  - Load transfer: Round dowel.
  - Percent longitudinal steel: 0.16
- Existing JRC structure and layer thicknesses (see figure 133).
- Existing JRC surface condition (assumed).
  - Visual survey results:

Distress	Severity	Extent
Patching	Less than 1-ft <sup>2</sup> deterioration	10 to 20 patches per mile
Average joint faulting	0.3-in	20 to 50 percent of all joints
Transverse cracking	Transverse cracks typically 2 per 60-ft slab, all cracks were spalled and faulted	30 to 50 percent all slabs
Corner breaks	Width of 0.25 to 1.0-in	4 to 10 per mile

- Long-term PCC strength and elastic modulus:

Backcalculation Method**	Core No.	Compressive Strength, psi (after 21 years)	Elastic Modulus, psi (after 21 years)
—	1	—	4,200,000
—	2	—	3,700,000
—	1	8880	5,371,324*
—	2	7050	4,785,964*
Assumed dense-liquid foundation	—	—	3,683,882 ***
Assumed elastic-solid foundation	—	—	2,670,970 ***

\*Estimated using the ACI equation:  $E_c = 33\rho^{3/2} (f'_c)^{1/2}$

\*\* Data derive from LTPP tables. Backcalculation performed using FWD deflections and ERESBACK v2.2 program.

\*\*\*Backcalculated modulus multiplied by 0.8 to convert from dynamic to static modulus.

The information presented indicated that mean elastic modulus ranges from 3,700,000 to 5,371,324 psi, with a mean of 4,068,698. The mean elastic modulus value was assumed for design.

The long-term elastic modulus value reported by LTPP is for intact PCC in very good condition. In order to estimate a representative PCC elastic modulus value that accounts for the existing pavement deterioration, the intact PCC elastic modulus is multiplied by an adjusting factor in the MEPDG. The appropriate adjustment factor is selected based on existing pavement condition characterized using visual distress. The results of the “assumed” visual distress survey conducted as part of field evaluation of the existing pavement indicated a pavement in moderate condition.

Presented below are the estimates of design elastic modulus (i.e., intact PCC elastic modulus adjusted for overall pavement condition). For the baseline design, an elastic modulus of 1,301,981 psi, which represents an existing JRCP in moderate condition, was selected. Default MEPDG input values were assumed for unit weight, thermal conductivity, heat capacity, Poisson’s ratio, etc. Input values as coded into the MEPDG software are shown in figure 157.

<b>Pavement Condition Adjustment Factor</b>	<b>Existing Pavement Condition</b>	<b>Design Elastic Modulus (psi)</b>
0.59	Good	2,400,527
0.32	Moderate	1,301,981*
0.13	Severe	528,930

\*Baseline long-term existing JRCP elastic modulus.

#### Design Features for the Baseline Unbonded JPCP Overlay over Existing JRCP Design

Design features for the baseline design are the same as those selected for new JPCP baseline design. The baseline new JPCP design features were described in the previous sections of the report (see figure 158).

**JPCP (existing) Material**

**General Properties**

Material type: JPCP (existing)

Layer thickness (in): 9.1

Unit weight (pcf): 143

Poisson's ratio: 0.20

**Strength Properties**

Elastic/resilient modulus (psi): 1301981

Minimum elastic/resilient modulus (psi): n/a

Modulus of rupture (psi): n/a

Type fracture: User Defined

**Thermal Properties**

Thermal conductivity (BTU/hr-ft-F): 1.25

Heat capacity (BTU/lb-F): 0.28

OK Cancel

Figure 157. Existing JPCP slab mix and strength properties used in the baseline unbonded JPCP over existing JRCP design.

**JPCP Design Features**

Slab thickness (in): 10 Permanent curl/warp effective temperature difference (°F): -10

**Joint Design**

Joint spacing (ft): 15 Sealant type: Liquid

Random joint spacing (ft):

Doweled transverse joints Dowel diameter (in): 1.25 Dowel bar spacing (in): 12

**Edge Support**

Tied PCC shoulder Long-term LTE(%):

Widened slab Slab width(ft):

**Base Properties**

Base type: Asphalt treated

**PCC-Base Interface**

Full friction contact Erodibility index: Extremely Resistant (1)

Zero friction contact Loss of full friction (age in months):

OK Cancel

Figure 158. Unbonded JPCP overlay design parameters used in the baseline design.

## MEPDG Results for the Baseline Unbonded JPCP Overlay over Existing JRCF Design

Figures 159 through 161 and table 46 show predicted distress and IRI for the base line design presented. Information presented shows reasonable predictions of distress/IRI. A review of the MEPDG predictions indicates the following:

- The baseline unbonded JPCP overlay design is representative of current ODOT unbonded JPCP overlay over an existing JRCF pavement design and construction practices.
- Predicts reasonable levels of distress and IRI making the design suitable as the basis for sensitivity analysis with the exception of dowel diameter. Use of a 1.25 in dowel diameter for 10 in concrete slab for this level of traffic is too small. Faulting goes very high over the design life.

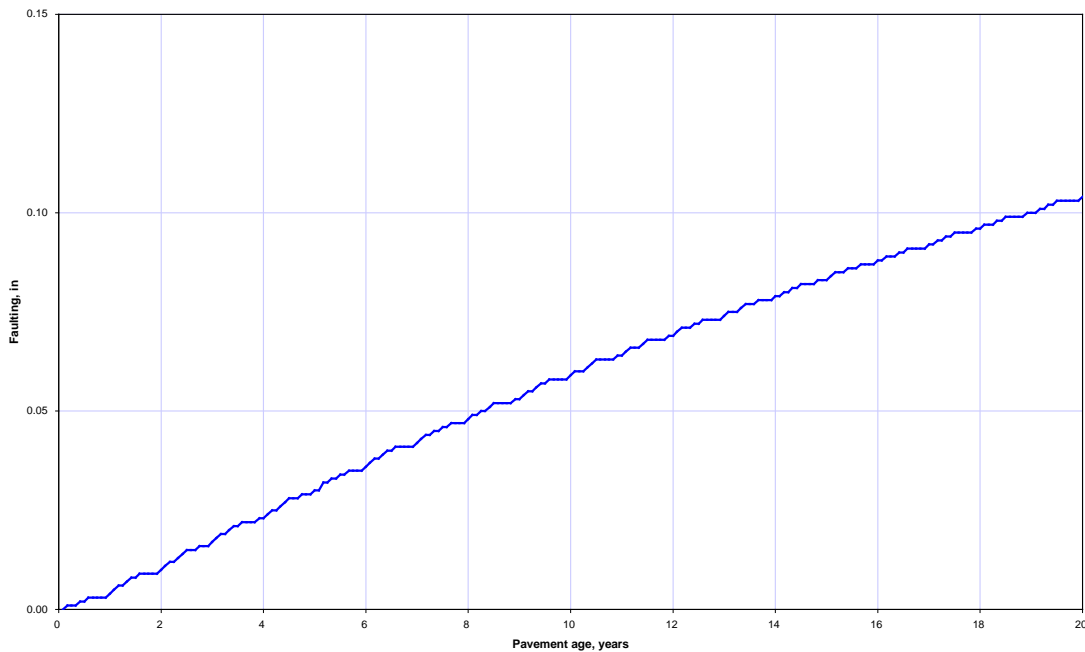


Figure 159. Plot showing predicted faulting versus age.

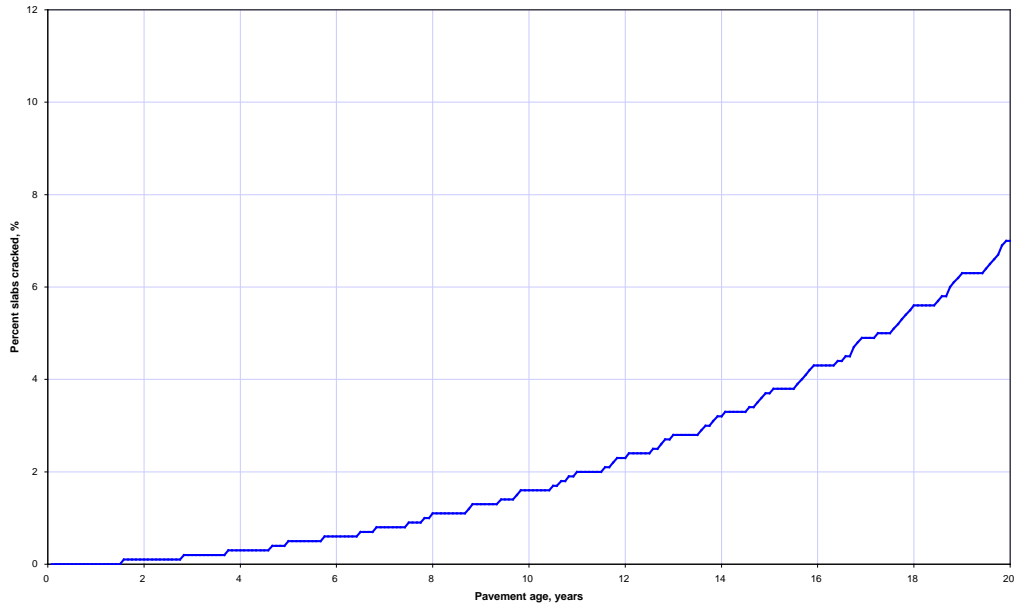


Figure 160. Plot showing predicted percent slabs cracked versus age.

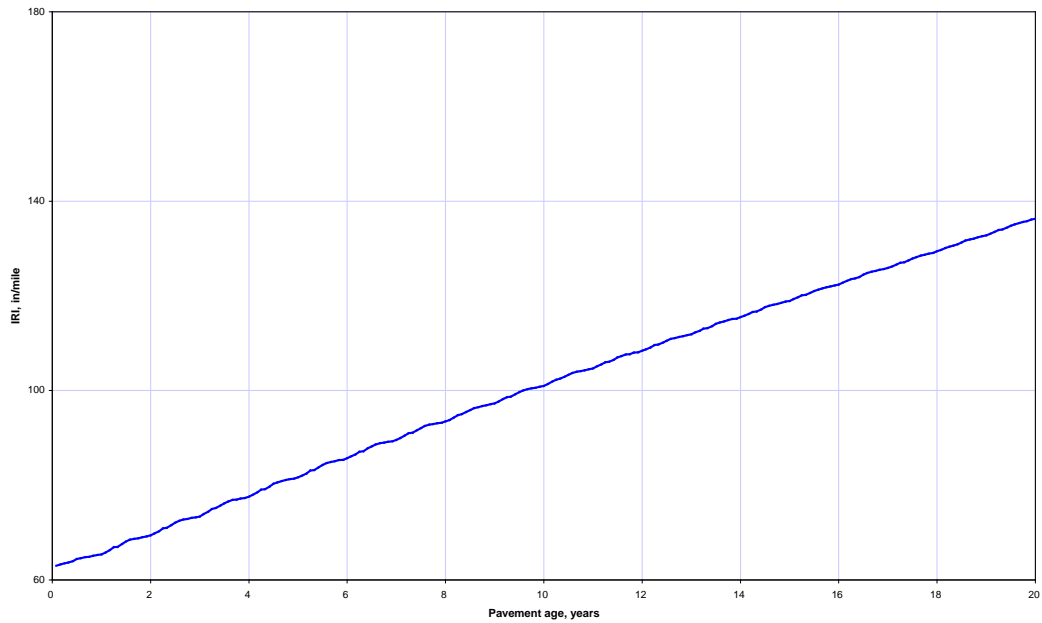


Figure 161. Plot showing predicted IRI versus age.

Table 46. Summary of distress/IRI predicts for baseline unbonded JPCP over existing JRCP design.

Pavement Age, Years	PCC Elastic Modulus, Mpsi	Base Modulus, ksi	Dyn. Modulus of Subgrade Reaction (k-value), psi/in	Mean Transverse Joint Faulting, In*	Mean Percent slabs cracked*	Mean IRI in/mile*	Cumulative Heavy Trucks
0.08	4.09	1308	176	0	0	63	161,878
1	4.48	1308	178	0.004	0	65.4	1,942,530
2	4.57	1308	178	0.01	0.1	69.4	4,049,010
3	4.62	1308	178	0.017	0.2	73.4	6,319,440
4	4.65	1308	178	0.023	0.3	77.6	8,753,830
5	4.68	1308	178	0.03	0.5	81.7	11,352,200
6	4.7	1308	178	0.036	0.6	85.7	14,114,400
7	4.71	1308	178	0.042	0.8	89.6	17,040,700
8	4.73	1308	178	0.048	1.1	93.5	20,130,800
9	4.74	1308	178	0.053	1.3	97.3	23,385,000
10	4.75	1308	178	0.059	1.6	101	26,803,100
11	4.75	1308	178	0.064	2	104.7	30,385,100
12	4.76	1308	178	0.069	2.3	108.4	34,131,100
13	4.76	1308	178	0.074	2.8	111.9	38,041,000
14	4.76	1308	178	0.079	3.2	115.5	42,114,900
15	4.77	1308	178	0.083	3.7	118.9	46,352,700
16	4.77	1308	178	0.088	4.3	122.4	50,754,500
17	4.78	1308	178	0.092	4.9	125.9	55,320,200
18	4.78	1308	178	0.096	5.6	129.4	60,049,900
19	4.79	1308	178	0.1	6.3	132.8	64,943,500
20	4.8	1308	178	0.104	7	136.3	70,001,100

\*Mean prediction at 50 percent reliability.

A sensitivity analysis was performed to determine the sensitivity of predicted distress/IRI based on changes to the MEPDG input parameters. A list of key input parameters known to influence JPCP distress/IRI was developed and used as the basis for sensitivity analysis based on the familiarity of the project team with the MEPDG prediction models. The input parameters along with the levels of variations are presented in table 47.

Table 47. Input parameters to be used in JPCP overlay over existing JRCF sensitivity analysis.

MEPDG Input Parameter	Levels of Input (*Indicates the Baseline ODOT Representative Design)
HMA bond-breaker layer thickness	1.0-*, 1.5-, and 2.0-in
Transverse joint load transfer efficiency (LTE) (for JPCP Overlay)	No dowel (0-in), 1.0-, 1.25-*, and 1.5-in
Limestone PCC CTE (for JPCP Overlay)	5.2-, 5.4-*, and $6.7 \times 10^{-6}/^{\circ}\text{F}$
PCC flexural strength and elastic modulus (for JPCP Overlay)	601-, 650-*, 736-, and 850-psi
PCC overlay thickness	8-, 9-, 10-*, 11-, 12-, 13-, and 14-in
PCC slab length (joint spacing) (for JPCP Overlay)	12.5-, 15.0-*, 17.5-, 20.0-, 22.5-ft
PCC slab width (for JPCP Overlay)	12-*, 13-, 14.0-ft
PCC concrete type (for JPCP Overlay)	<p>Class C*, and high early strength concrete                      For the sensitivity analysis, other commonly used ODOT PCC material types were used. Specifically the following were considered:</p> <ul style="list-style-type: none"> <li>• ODOT class C concrete with limestone (PCC CTE = <math>5.4 \times 10^{-6}/^{\circ}\text{F}</math>).</li> <li>• ODOT class C concrete with gravel (PCC CTE = <math>6.4 \times 10^{-6}/^{\circ}\text{F}</math>).</li> <li>• ODOT class C concrete with slag (PCC CTE = <math>6.3 \times 10^{-6}/^{\circ}\text{F}</math>).</li> <li>• ODOT class S concrete with limestone (PCC CTE = <math>5.4 \times 10^{-6}/^{\circ}\text{F}</math>).</li> <li>• ODOT class S concrete with gravel (PCC CTE = <math>6.4 \times 10^{-6}/^{\circ}\text{F}</math>).</li> <li>• ODOT class S concrete with slag (PCC CTE = <math>6.3 \times 10^{-6}/^{\circ}\text{F}</math>).</li> </ul> <p>Additional properties for the class S concretes are as follows:</p> <ul style="list-style-type: none"> <li>• Cement type: Type I.</li> <li>• Cementitious content: 715 lbs/yd<sup>3</sup>.</li> <li>• Aggregate type: Limestone, Gravel, or Slag (limestone selected for baseline design).</li> <li>• 28-day flexural strength: 800 psi (Masada et al. 2004).</li> <li>• Water-to-cementitious material ratio: 0.44.</li> </ul> <p>Default MEPDG input values were assumed for other PCC properties such as unit weight, Poisson's ratio, etc.</p>
PCC aggregate type (for JPCP Overlay)	Gravel, Limestone*, and Slag
Existing JRCF elastic modulus	528,930; 1,301,981*; 2,400,527
Shoulder type	None (i.e., gravel, asphalt, and non-tied PCC) and tied PCC

\*Unbonded JPCP over Existing JRCF baseline project.

\*\*Default MEPDG gradations will be used, where applicable.

## Effect of Bond-breaker Layer Thickness on MEPDG Predicted Unbonded Overlay Performance

The effect of the HMA separation layer thickness on unbonded overlay performance using the MEPDG Design Guide is shown in figures 162 to 164. Results show very little effect between 1 and 2 in on distress and IRI as summarized in table 48.

## Effect of Using Load Transfer Devices on transverse joint faulting

The effect of the transverse joint dowels size on unbonded overlay performance using the MEPDG Design Guide is shown in figures 165 to 167. Figures 165 and 167 shows the large impact that transverse joint dowels have on joint faulting and IRI, respectively. The larger the bar diameter the lower the bearing stress and the lower the joint faulting over time. There is no effect on transverse slab cracking but the faulting effect carries into smoothness (or IRI). Table 49 summarizes the overall relative effect of transverse joint dowels size on performance.

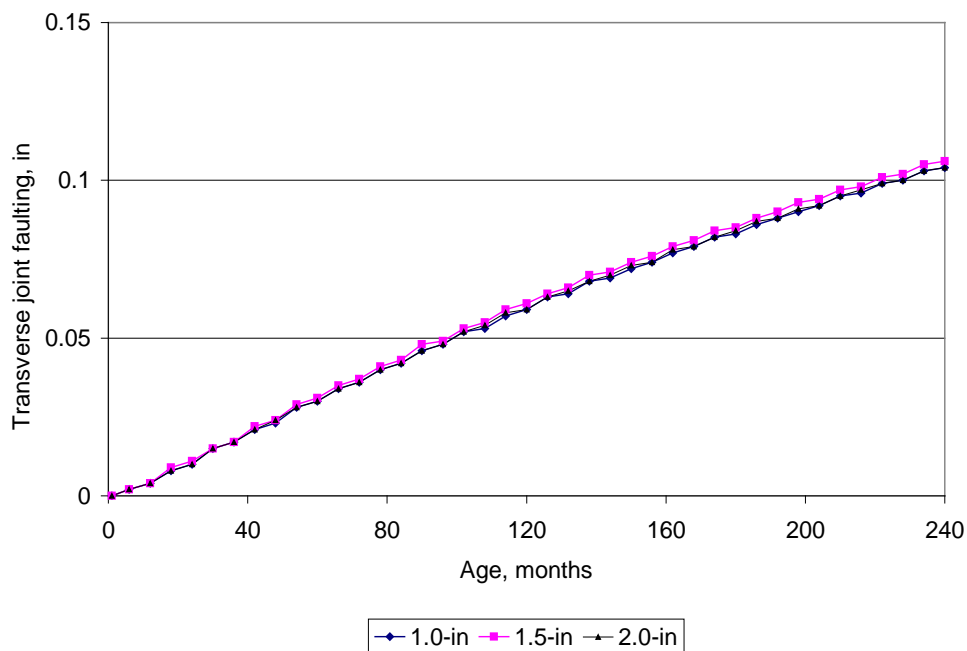


Figure 162. Plot of unbonded overlay age versus transverse joint faulting showing the effect of HMA separation layer thickness.

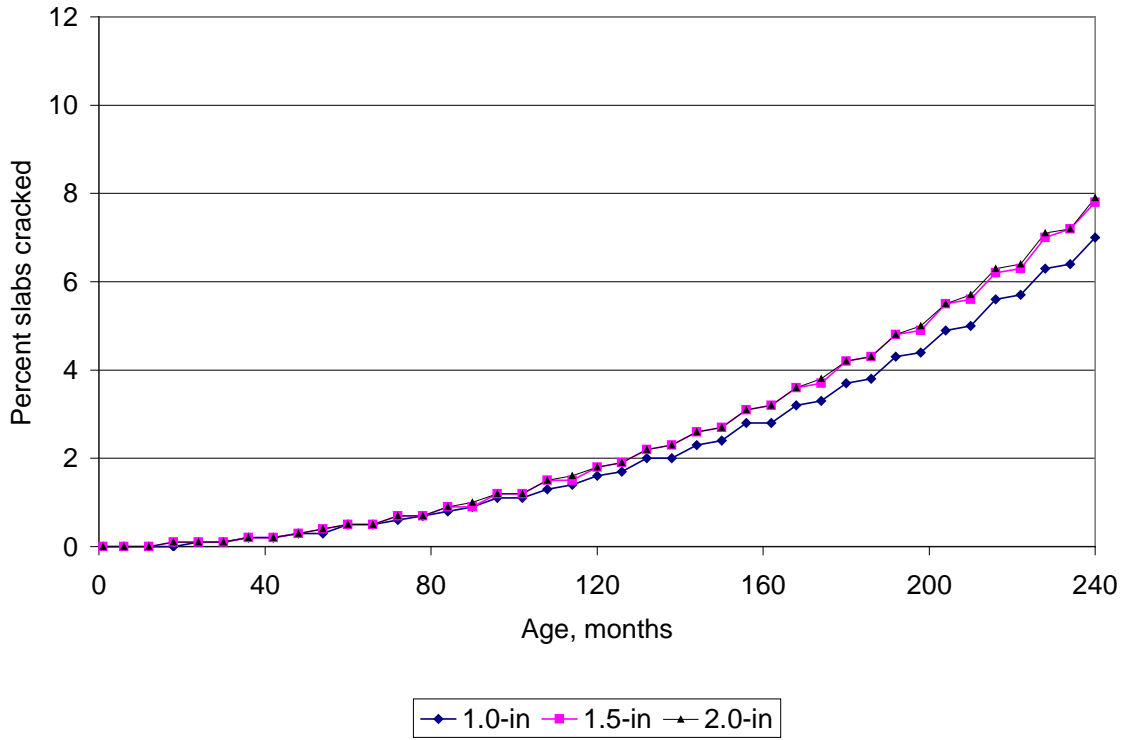


Figure 163. Plot of unbonded overlay age versus percent slabs cracked showing the effect of HMA separation layer thickness.

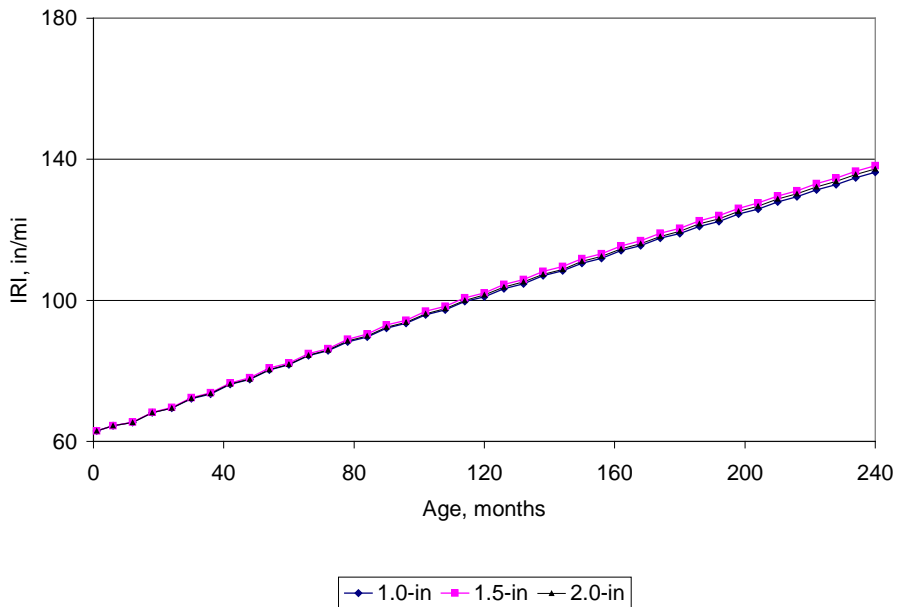


Figure 164. Plot of unbonded overlay age versus IRI showing the effect of HMA separation layer thickness.

Table 48. Relative effect of HMA separation layer thickness on overlay distress and IRI.

Distress/IRI	Effect of Bond-Breaker Thickness on Distress/IRI
Joint faulting	None
Transverse slab cracking	Low
IRI	None

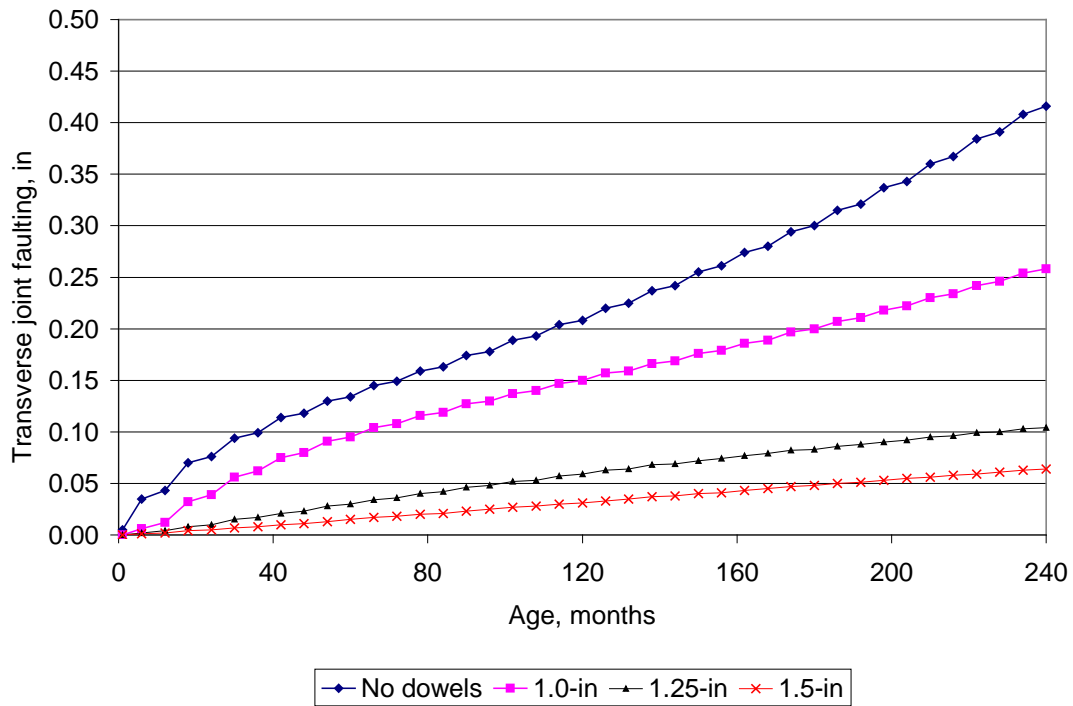


Figure 165. Plot of age versus transverse joint faulting showing the effect using load transfer devices.

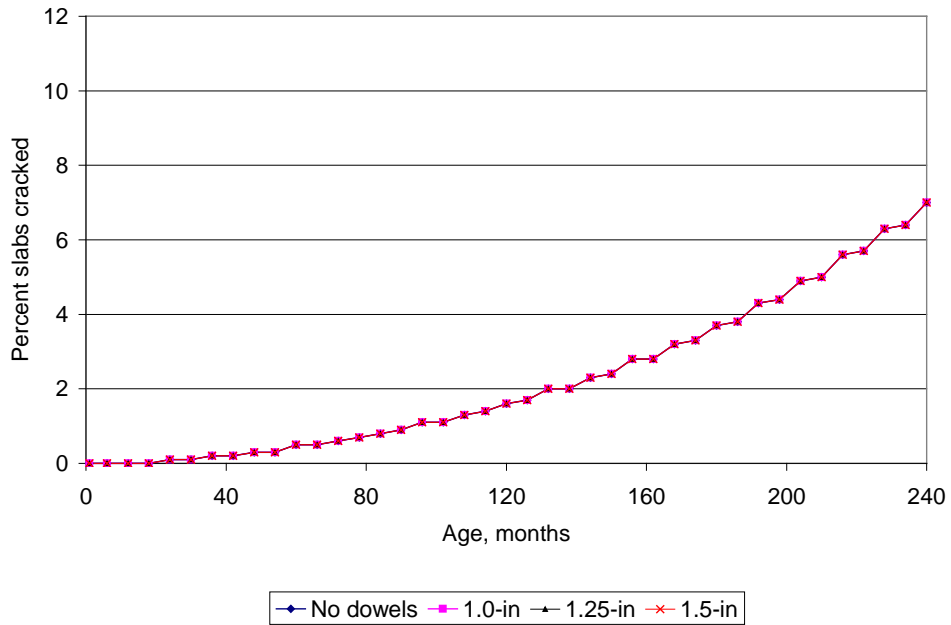


Figure 166. Plot of age versus percent slabs cracked showing the effect using load transfer devices.

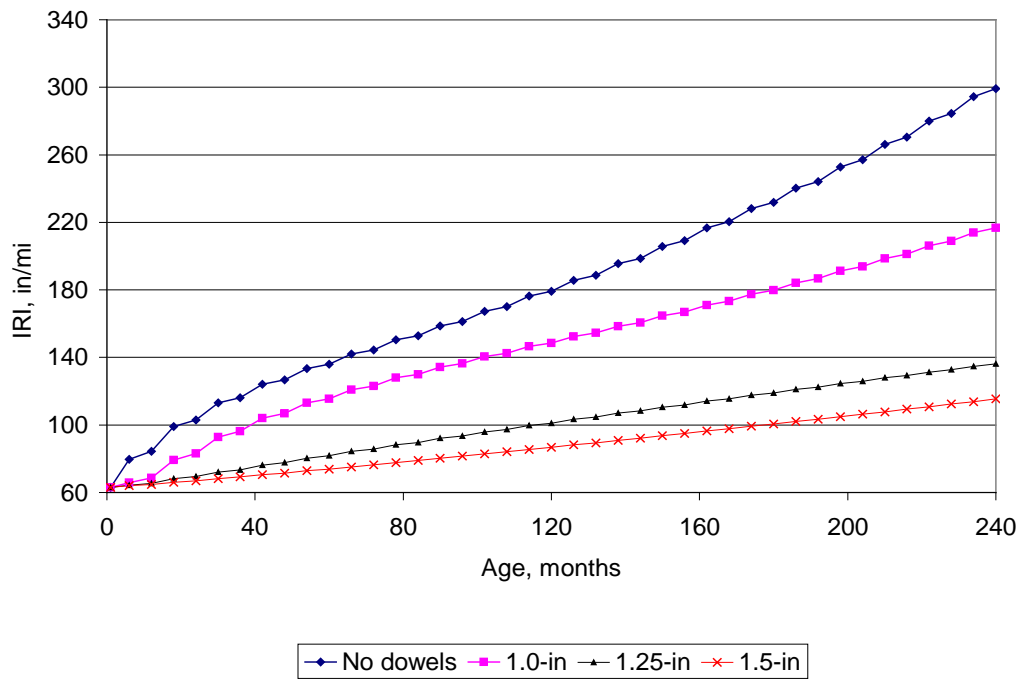


Figure 167. Plot of age versus IRI showing the effect using load transfer devices.

Table 49. Relative effect of transverse joint load transfer devices on overlay distress and IRI.

Distress/IRI	Effect of Transverse Joint Load Transfer Devices on Distress/IRI
Joint faulting	High
Transverse slab cracking	None
IRI	High

Effect of Concrete Coefficient of Thermal Expansion

The coefficient of thermal expansion (CTE) has a major effect on joint faulting, slab cracking, and on IRI (see figures 168 through 170). Higher CTE results in greater opening of joints in cool weather and higher CTE also leads to higher stresses from temperature gradient through the slab resulting in increased slab cracking. A summary of the effect of CTE on performance is given in table 50.

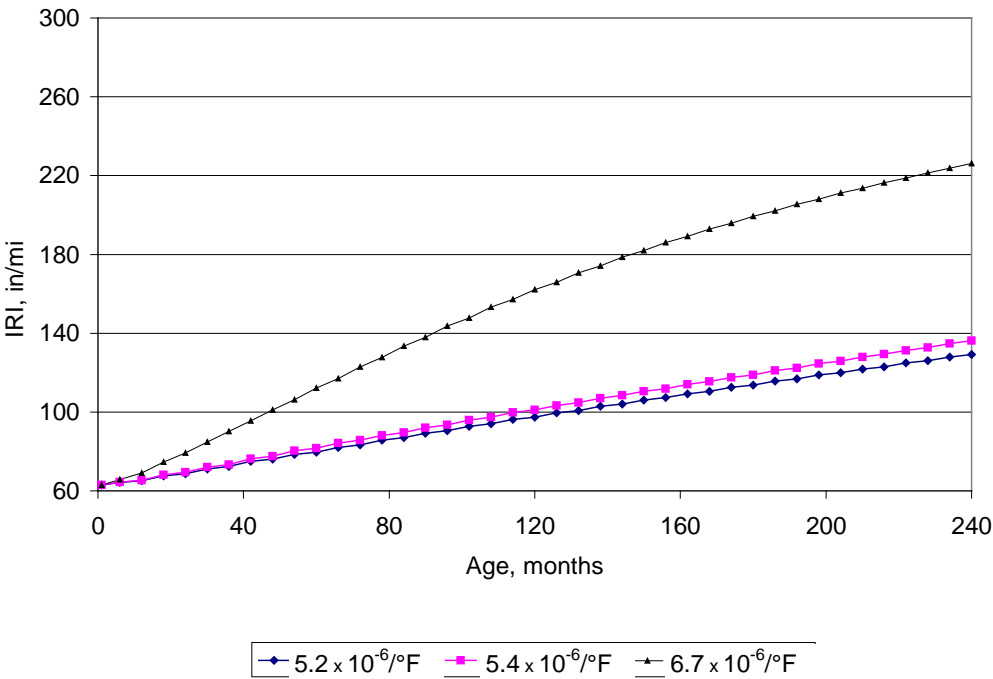


Figure 168. Plot of age versus transverse joint faulting showing the effect of CTE.

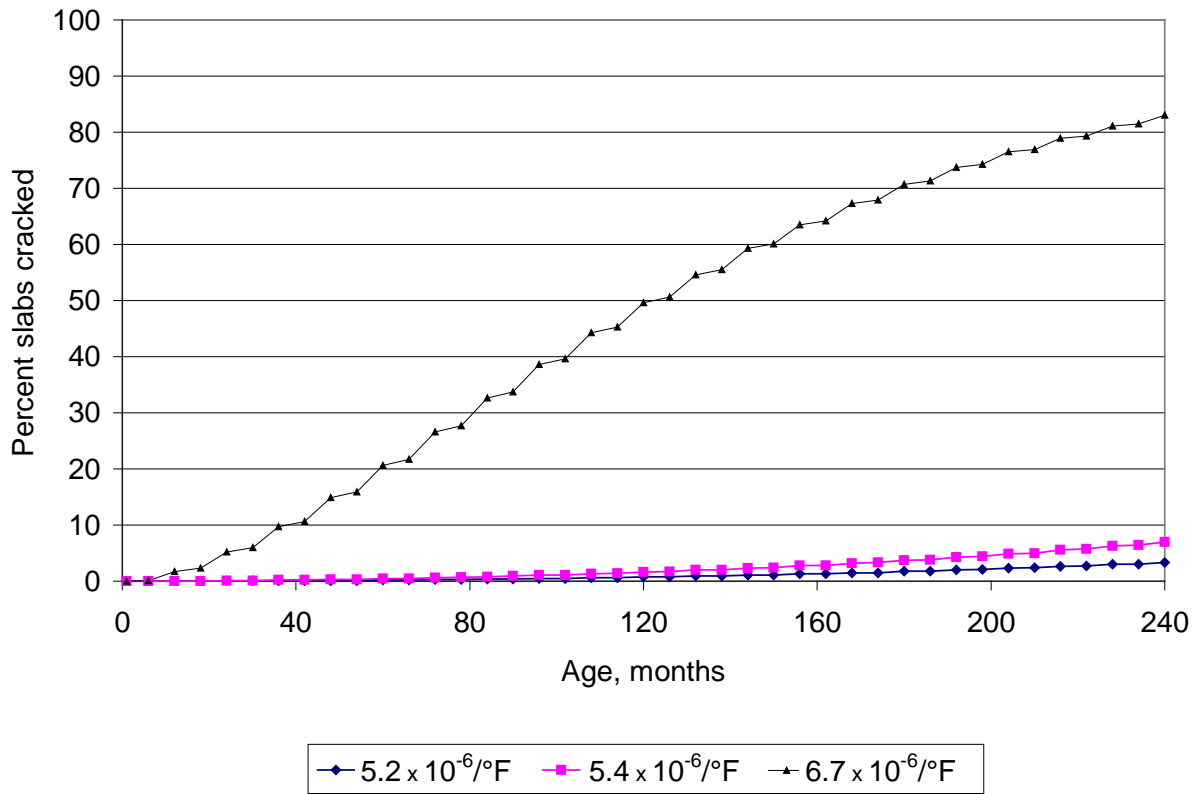


Figure 169. Plot of age versus percent slabs cracked showing the effect of CTE.

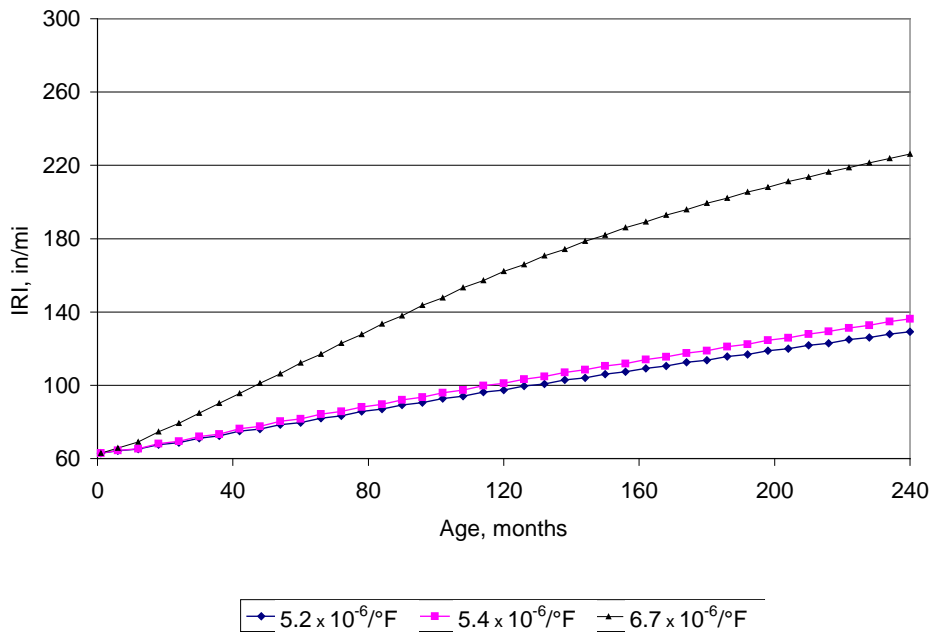


Figure 170. Plot of age versus IRI showing the effect of CTE.

Table 50. Relative effect of concrete coefficient of thermal expansion (CTE) on JPCP overlay distress and IRI.

Distress/IRI	Effect of Concrete Coefficient of Thermal Expansion on Distress/IRI
Joint faulting	High
Transverse slab cracking	High
IRI	High

Effect of Concrete Overlay Flexural strength

The impact of the flexural strength (and elastic modulus through correlation) of the JPCP overlay is shown in figure 171 through 173. Strength only effects slab cracking significantly with higher strength and modulus with higher strength having lower cracking due to reduced fatigue damage. A summary of the effect of concrete flexural strength on performance is given in table 51.

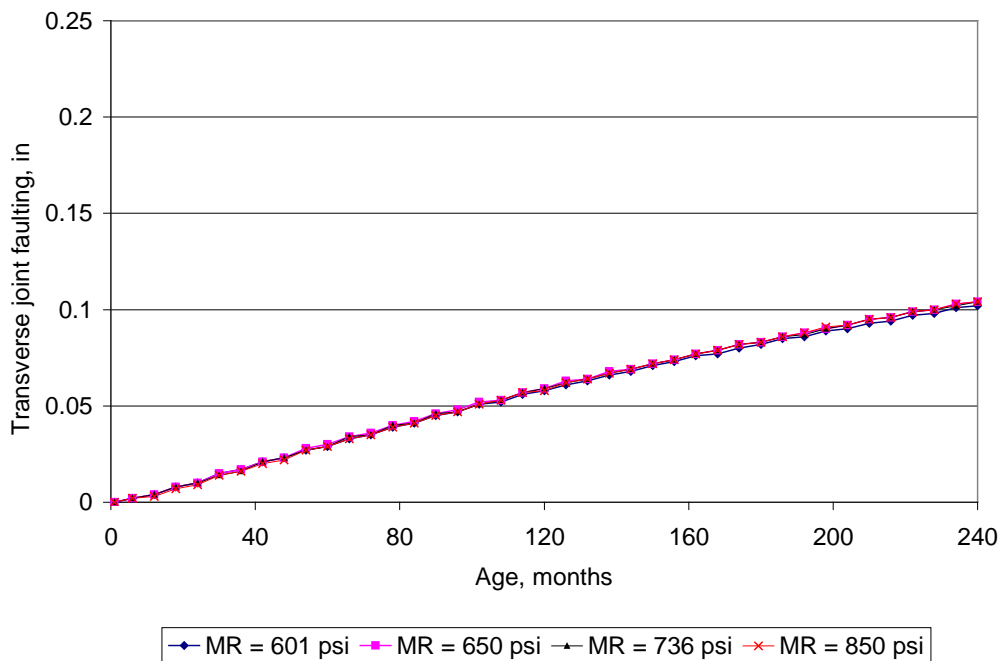


Figure 171. Plot of age versus transverse joint faulting showing the effect of overlay flexural strength.

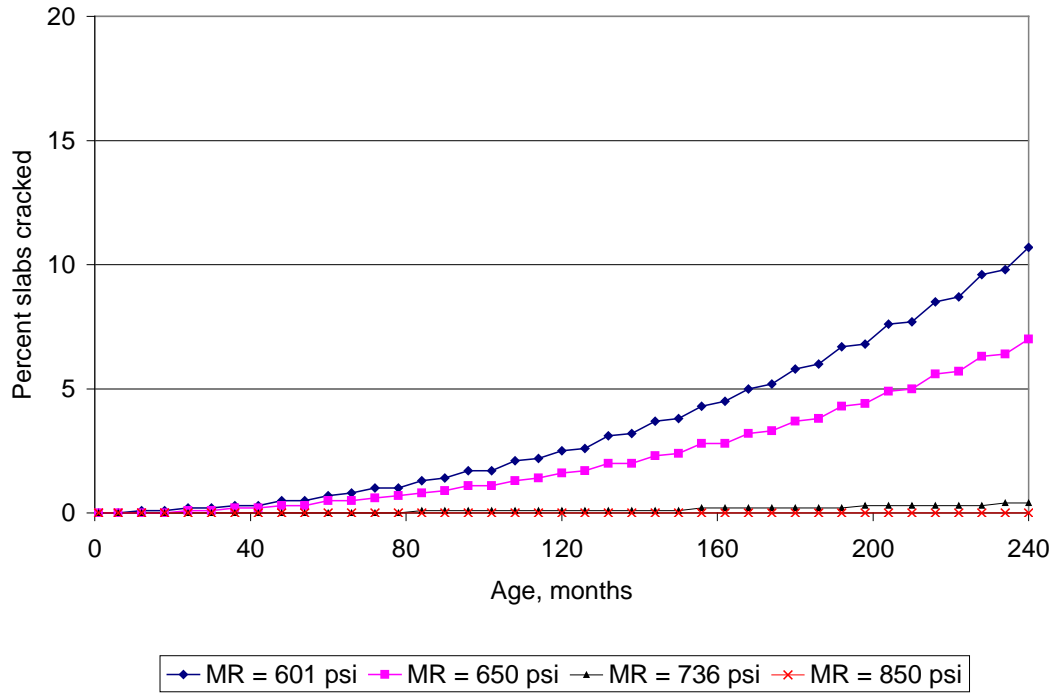


Figure 172. Plot of age versus percent slabs cracked showing the effect of overlay flexural strength.

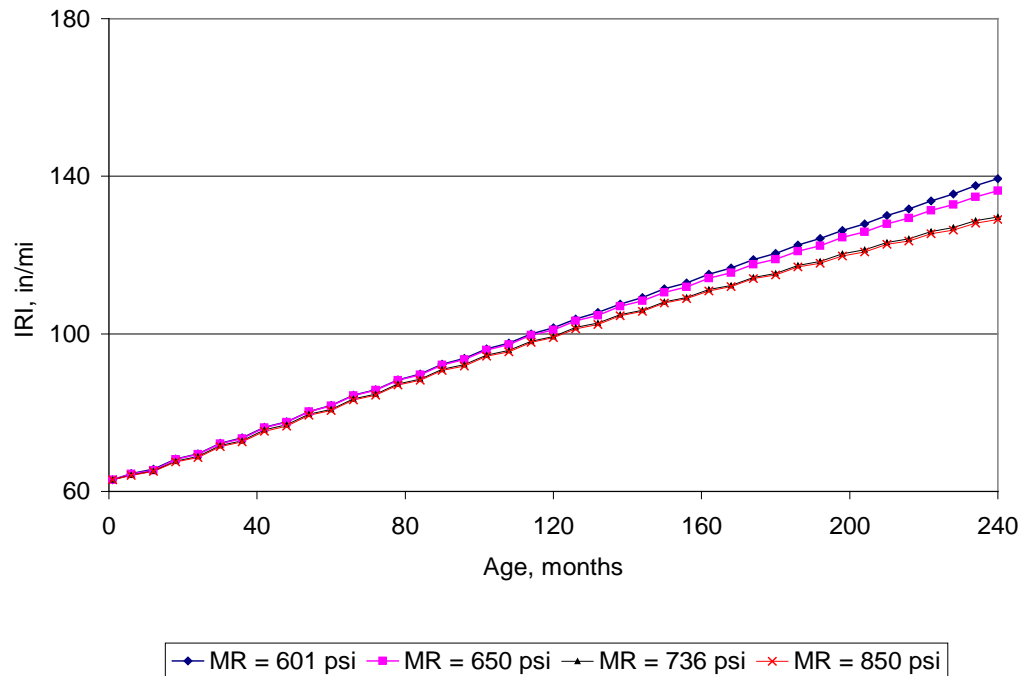


Figure 173. Plot of age versus IRI showing the effect of overlay flexural strength.

Table 51. Relative effect of concrete overlay flexural strength and modulus on overlay distress and IRI.

Distress/IRI	Effect of Concrete Overlay Flexural Strength/Modulus on Distress/IRI
Joint faulting	Low
Transverse slab cracking	High
IRI	Low

Effect of Concrete Overlay Thickness

The impact of the concrete overlay thickness of the JPCP overlay is shown in figures 174 through 176. Overlay thickness effects slab cracking and IRI significantly with a much lower effect on joint faulting. The greater slab thickness results in lower slab cracking and IRI due to reduced fatigue damage. A summary of the effect of slab thickness on performance is given in table 52.

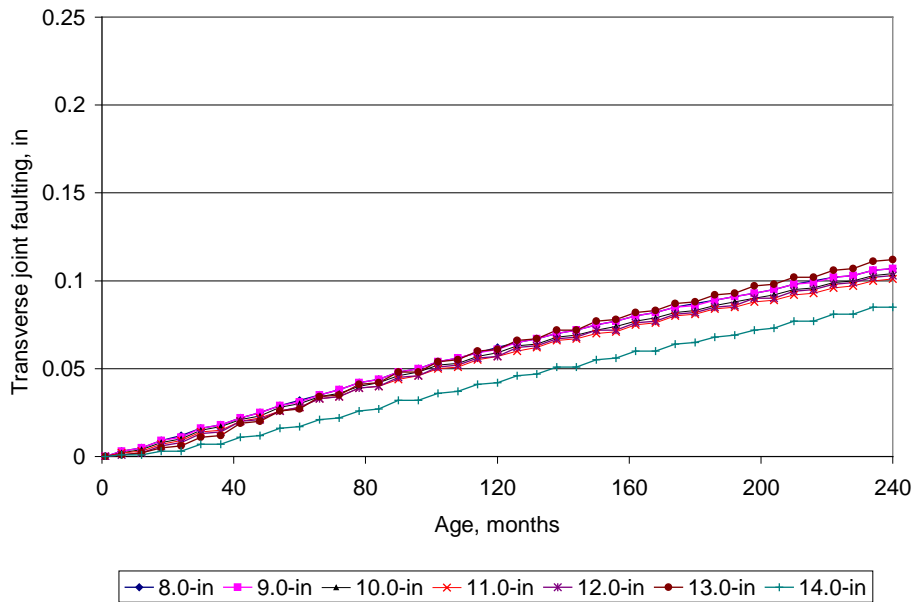


Figure 174. Plot of age versus transverse joint faulting showing the effect of overlay thickness.

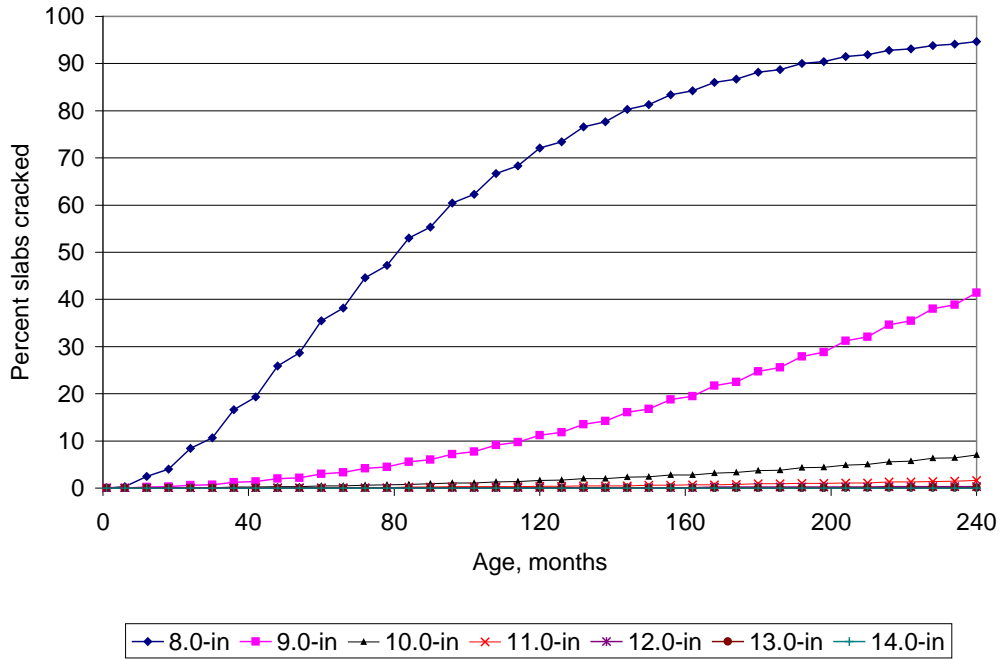


Figure 175. Plot of age versus percent slabs cracked showing the effect of overlay thickness.

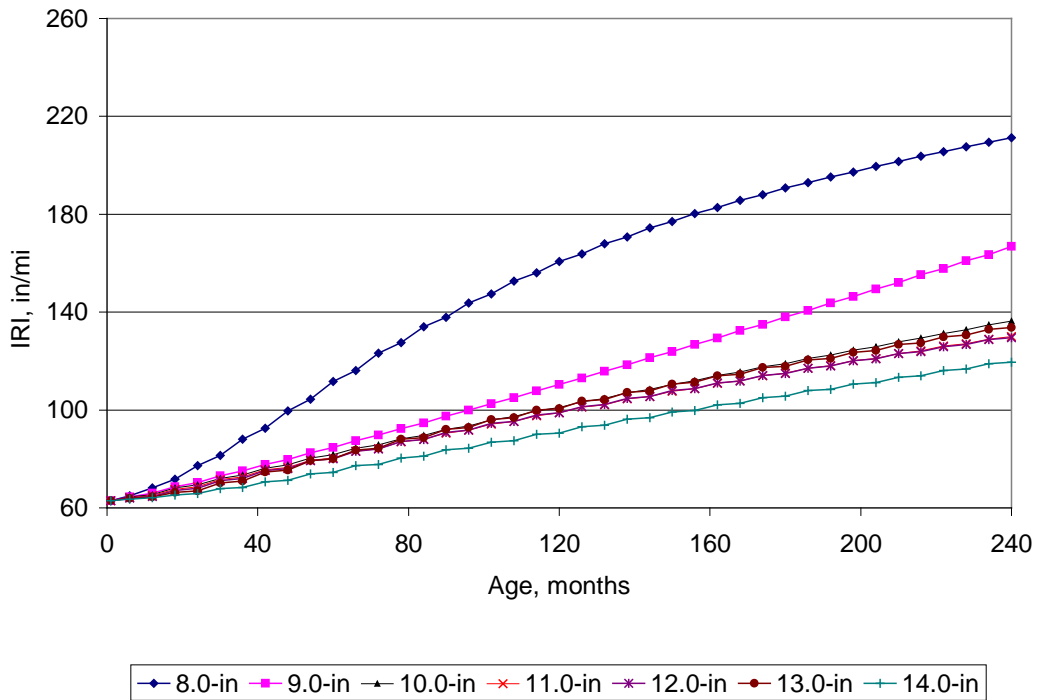


Figure 176. Plot of age versus IRI showing the effect of overlay thickness.

Table 52. Relative effect of concrete overlay thickness on overlay distress and IRI.

Distress/IRI	Effect of Concrete Overlay Thickness on Distress/IRI
Joint faulting	Low
Transverse slab cracking	High
IRI	High

### Effect of Concrete Overlay Joint Spacing

The impact of the concrete overlay joint spacing of the JPCP overlay is shown in figures 177 through 179. Overlay joint spacing effects joint faulting, slab cracking, and IRI very significantly. The longer joint spacing results in higher joint faulting, slab cracking and IRI due to increased joint openings and increased curling stresses in the slab causing increased fatigue damage. A summary of the effect of joint spacing on performance is given in table 53.

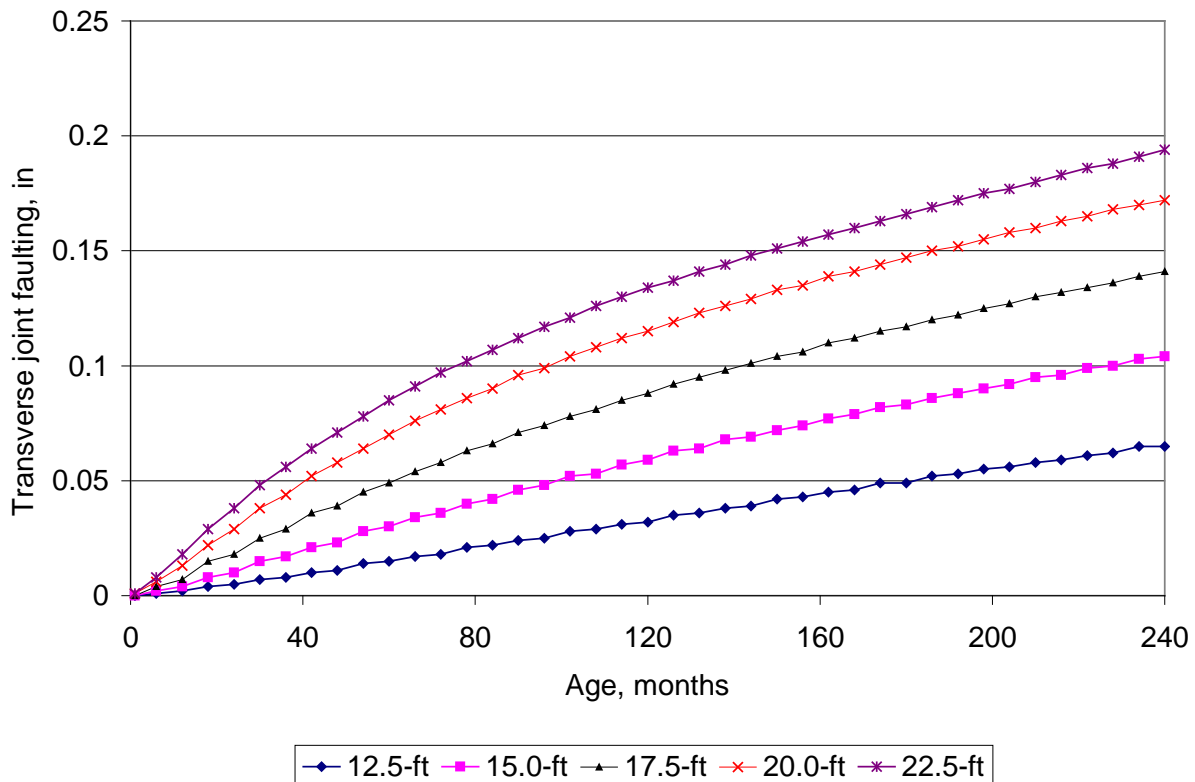


Figure 177. Plot of age versus transverse joint faulting showing the effect of overlay joint spacing.

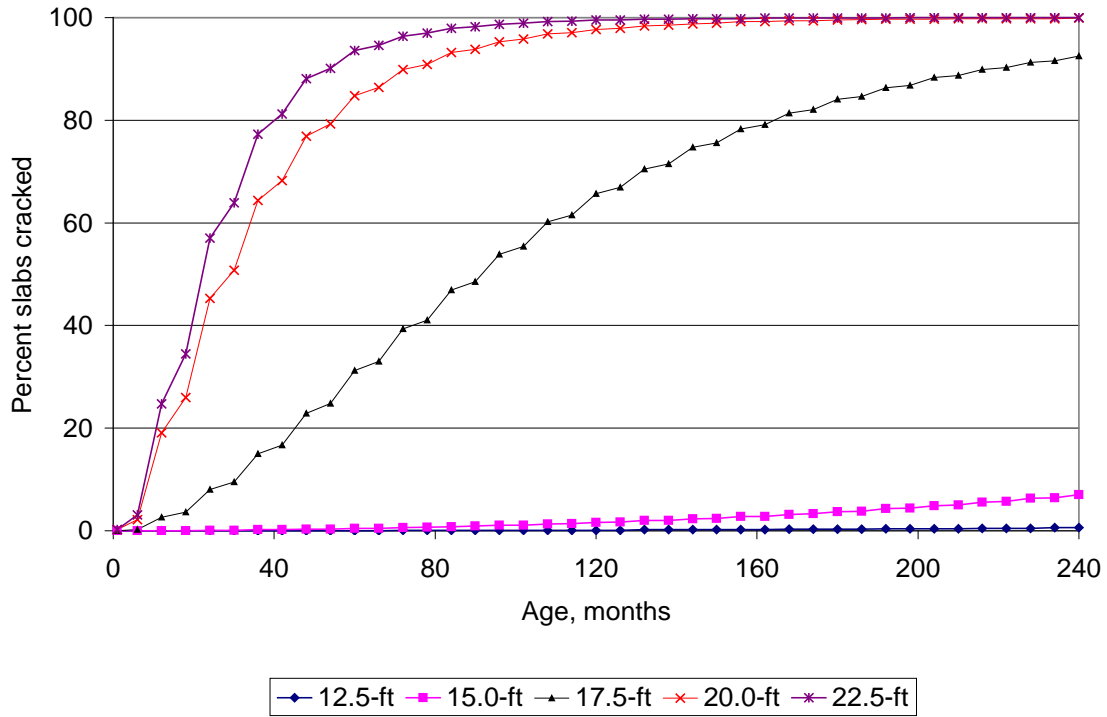


Figure 178. Plot of age versus percent slabs cracked showing the effect of overlay joint spacing.

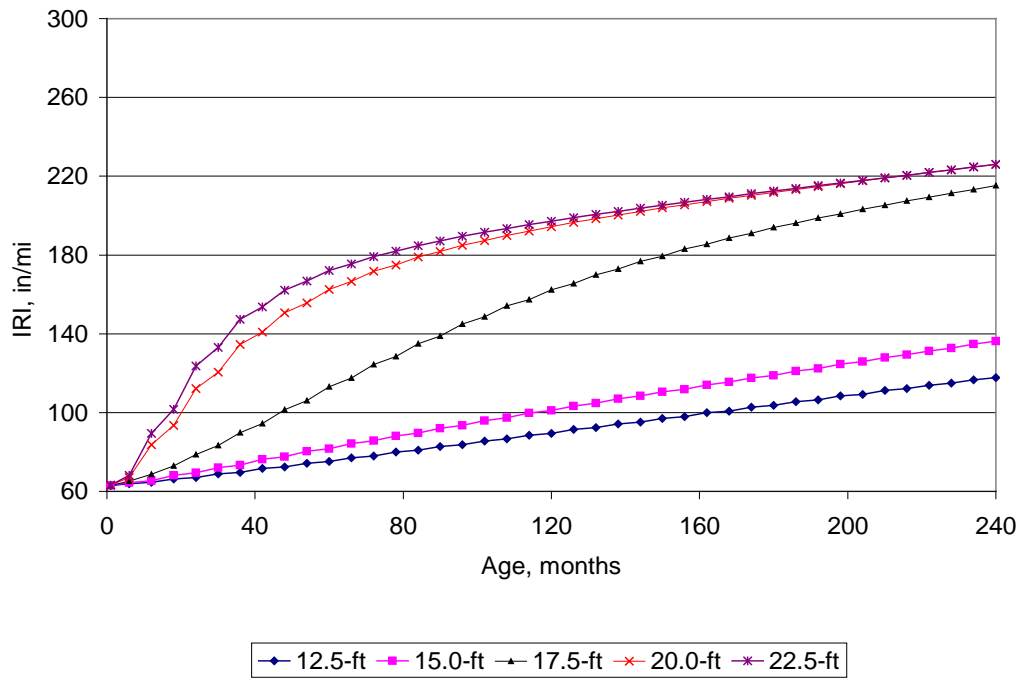


Figure 179. Plot of age versus IRI showing the effect of overlay joint spacing.

Table 53. Relative effect of concrete overlay joint spacing on overlay distress and IRI.

Distress/IRI	Effect of Concrete Overlay Joint Spacing on Distress/IRI
Joint faulting	High
Transverse slab cracking	High
IRI	High

Effect of Concrete Overlay Slab Width

The impact of the slab width of the JPCP overlay is shown in figures 180 through 182. Overlay slab width effects joint faulting, slab cracking, and IRI very significantly. The wider the slab the lower the joint faulting, slab cracking and IRI. This is due to the positive effects of keeping truck tires away from the free edge on reducing corner deflections and fatigue damage. A summary of the effect of slab width on performance is given in table 54.

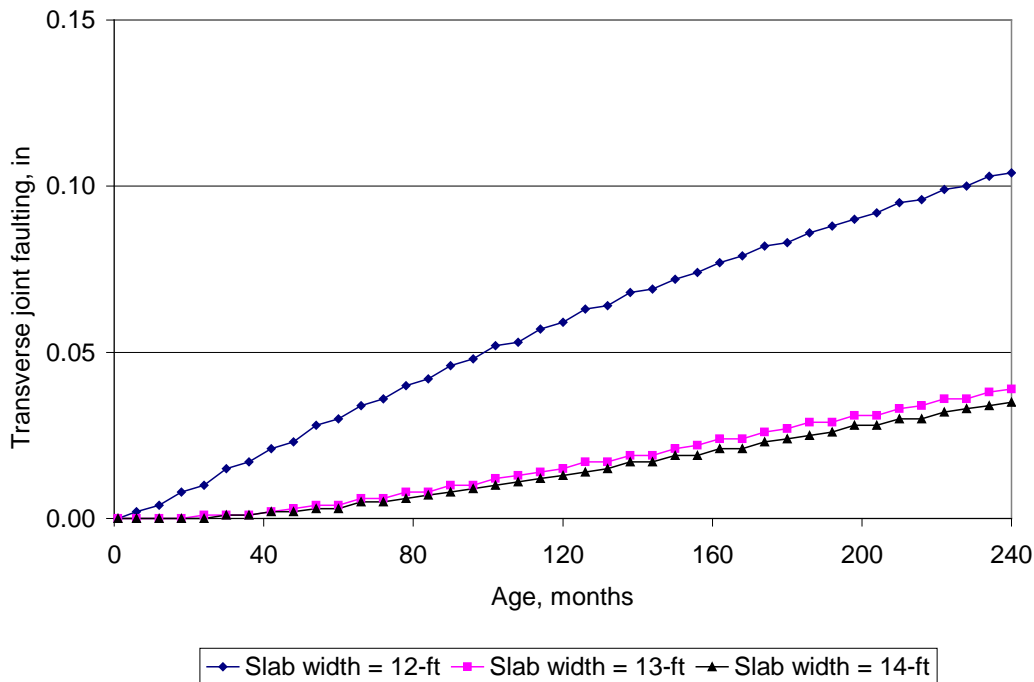


Figure 180. Plot of age versus transverse joint faulting showing the effect of overlay slab width.

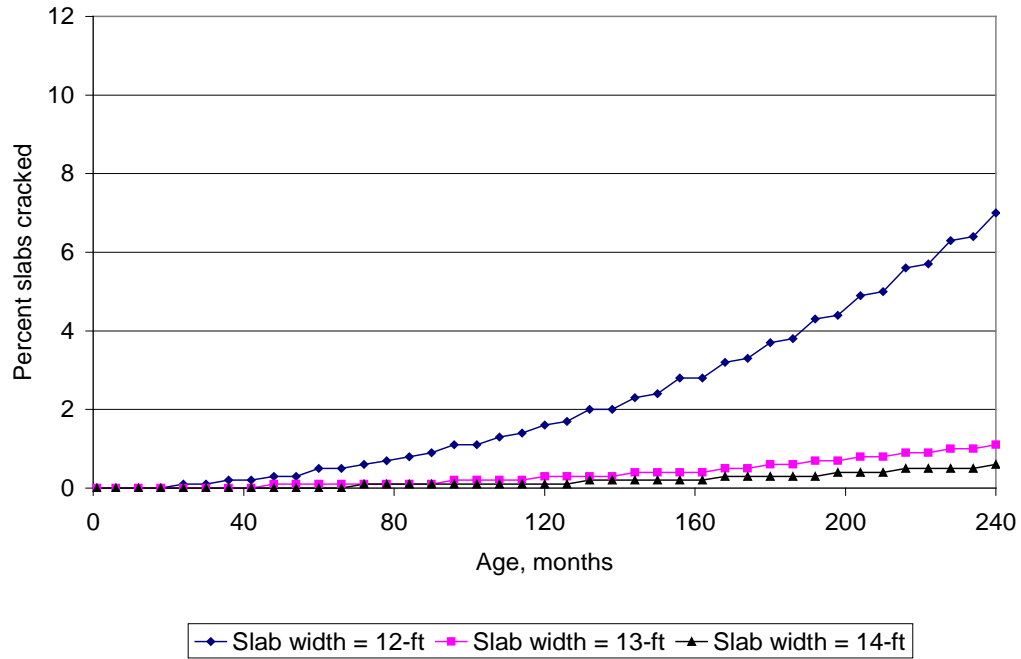


Figure 181. Plot of age versus percent slabs cracked showing the effect of overlay slab width.

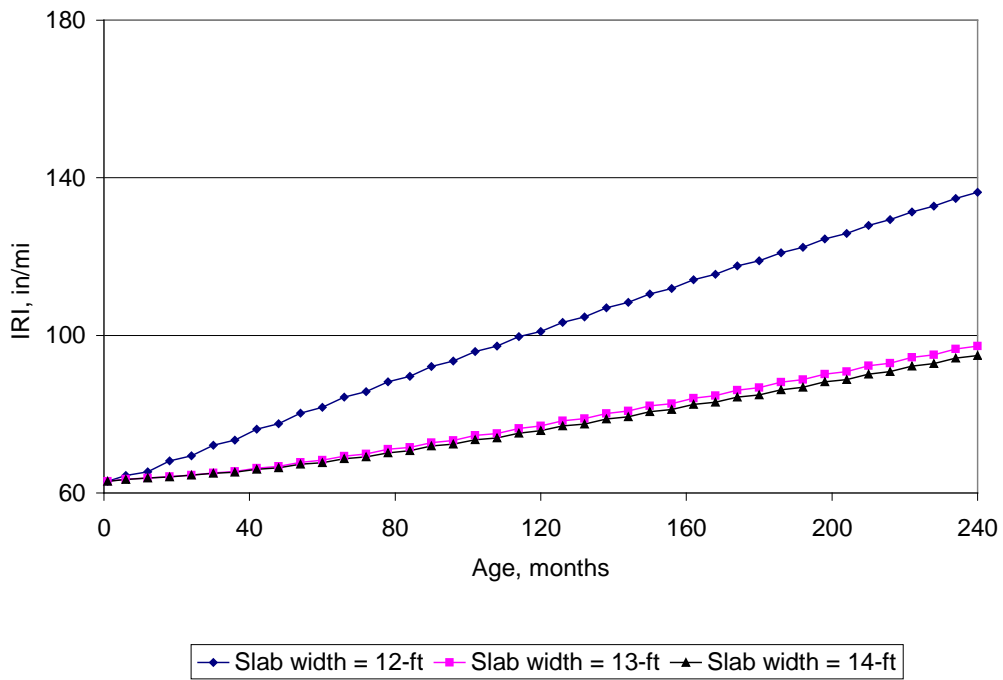


Figure 182. Plot of age versus IRI showing the effect of overlay slab width.

Table 54. Relative effect of concrete overlay slab width (12, 13 and 14-ft) on overlay distress and IRI.

Distress/IRI	Effect of Concrete Overlay Slab Width on Distress/IRI
Joint faulting	High
Transverse slab cracking	High
IRI	High

Effect of changing aggregate type on baseline PCC

Three different aggregate types were Class C gravel, slag, and limestone. These were each run with the baseline design and distress and IRI predicted as shown in figures 183 through 185. The main difference was the CTE of the coarse aggregate with values of  $6.4 \times 10^{-6}/^{\circ}\text{F}$  for gravel,  $6.2 \times 10^{-6}/^{\circ}\text{F}$  for slag, and  $5.4 \times 10^{-6}/^{\circ}\text{F}$  for limestone. The results show a large difference in faulting, cracking, and IRI between limestone (with the low CTE) and the other two aggregates. Table 55 shows the summary of the effect. This is obviously an input that must be carefully considered in design, possibly through specifications.

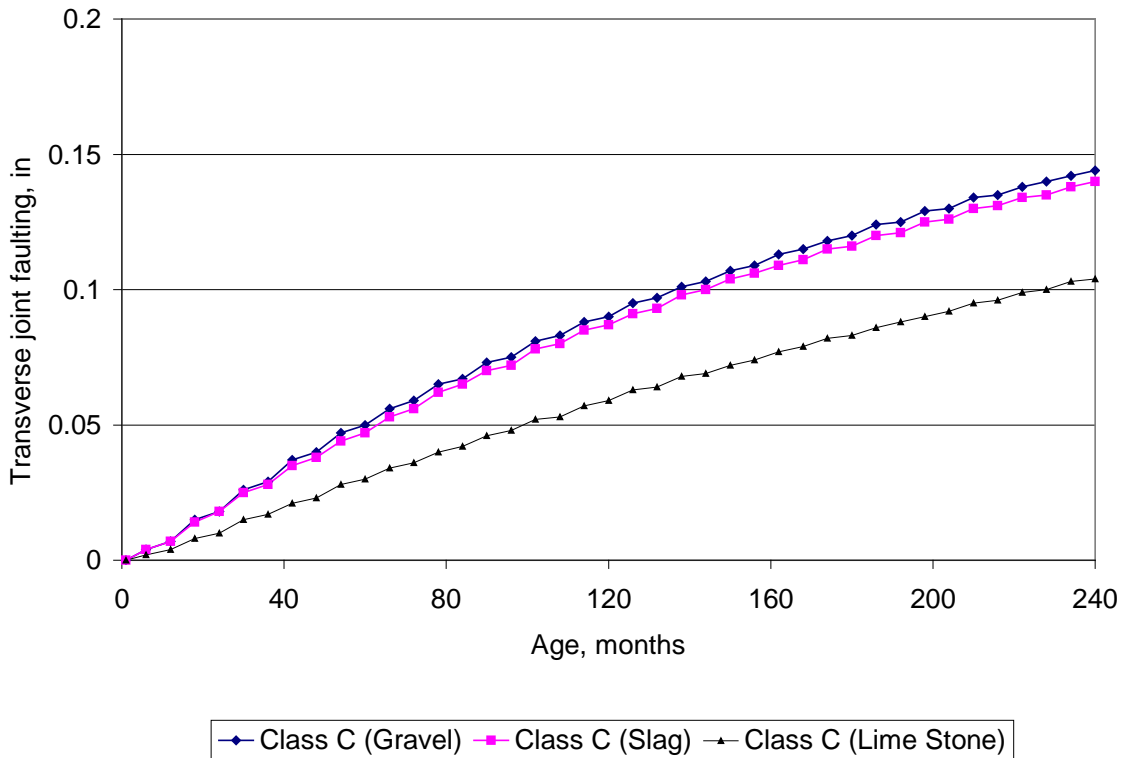


Figure 183. Plot of age versus transverse joint faulting showing the effect of changing aggregate type in baseline overlay concrete.

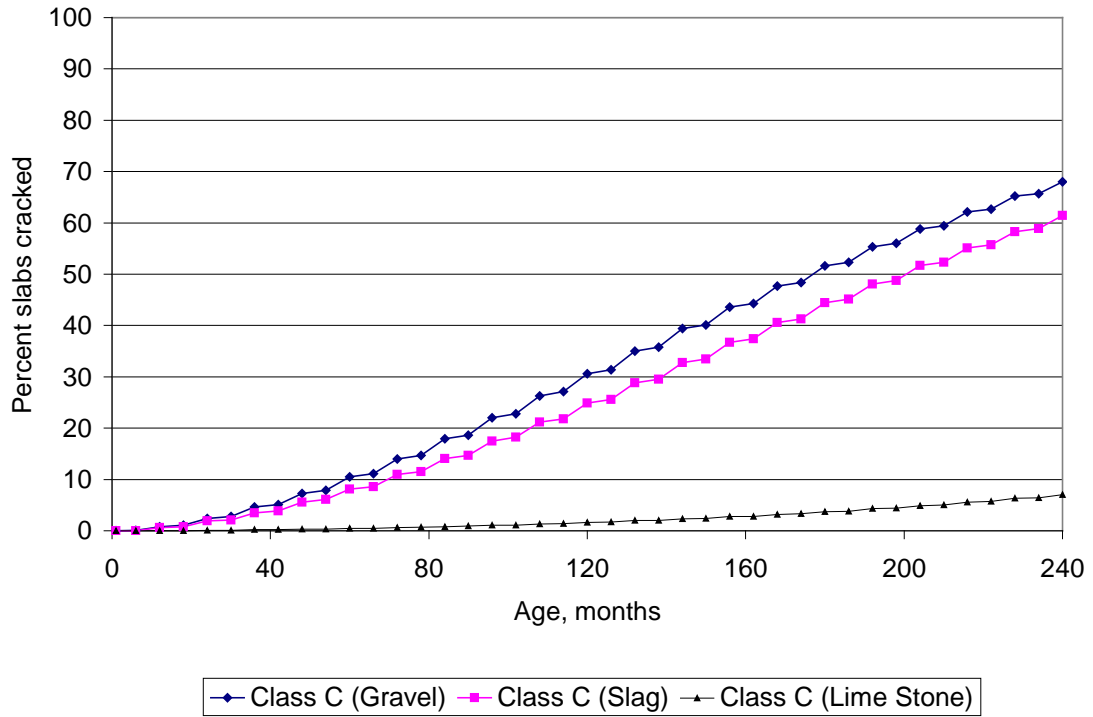


Figure 184. Plot of age versus percent slabs cracked showing the effect of changing aggregate type in baseline overlay concrete.

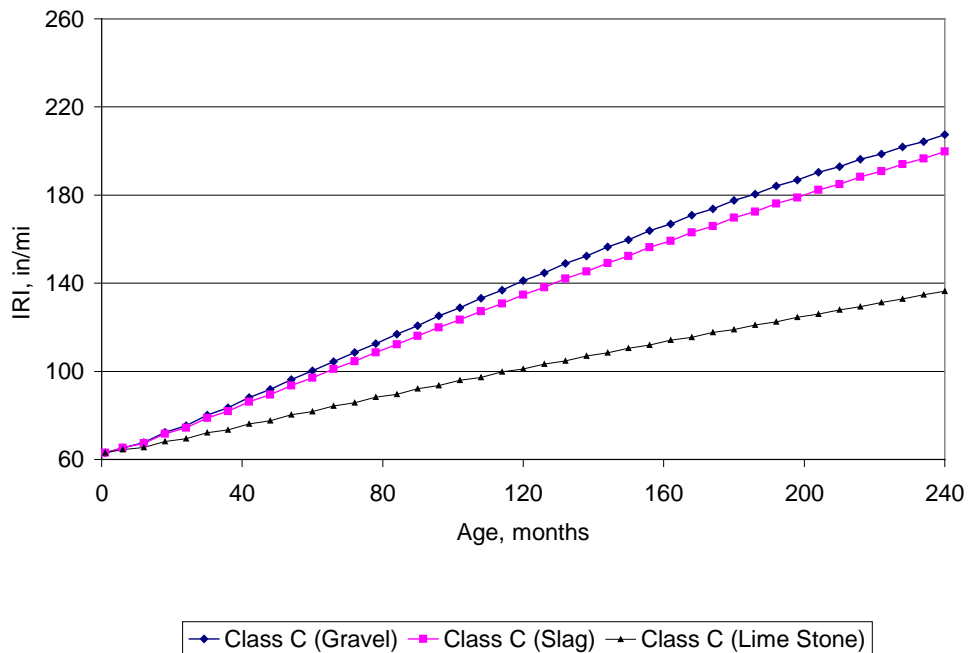


Figure 185. Plot of age versus IRI showing the effect of changing aggregate type in baseline overlay concrete.

Table 55. Relative effect of coarse concrete overlay aggregate type on overlay distress and IRI.

Distress/IRI	Effect of Concrete Overlay Coarse Aggregate Type on Distress/IRI
Joint faulting	High
Transverse slab cracking	High
IRI	High

Effect of Existing Old Slab Elastic Modulus

The impact of the existing slab elastic modulus is shown in figures 186 through 188. Different elastic moduli would occur due to the extent of cracking of the slab. The existing slab elastic modulus effects joint faulting, slab cracking, and IRI significantly. The lower the existing slab modulus the higher the joint faulting, slab cracking and IRI. This is due to the increased joint deflections and slab stresses and damage from having an increased amount of cracking in the existing slab. A summary of the effect of existing slab elastic modulus on performance of the JPCP overlay is given in table 56.

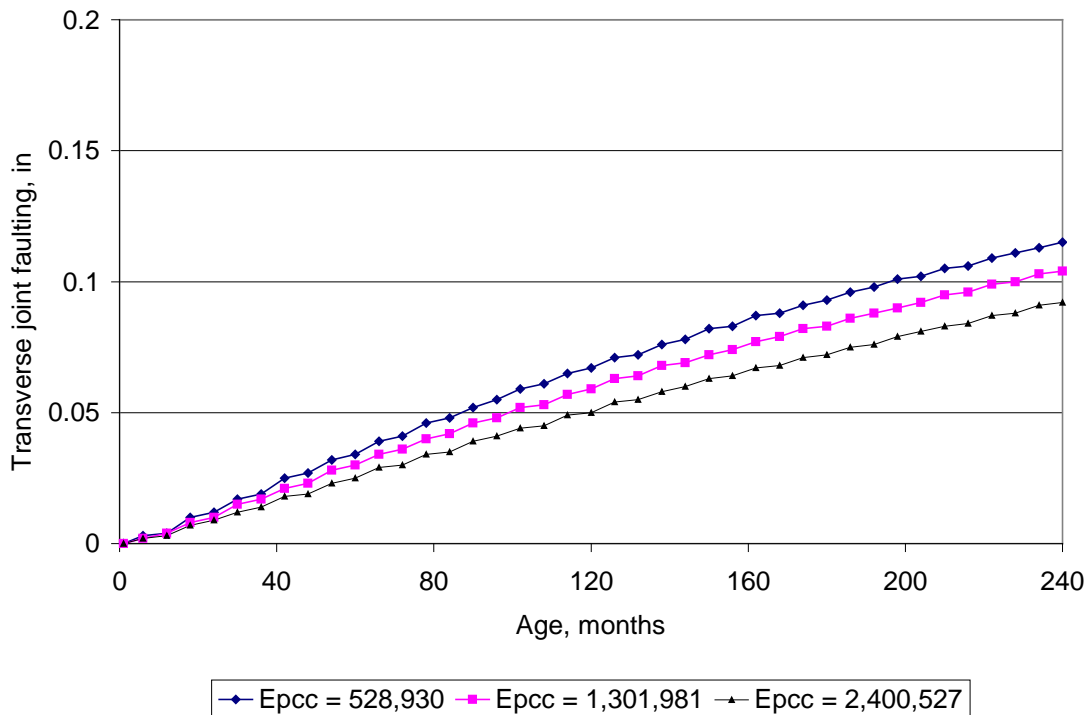


Figure 186. Plot of age versus transverse joint faulting showing the effect of existing JRPC elastic modulus.

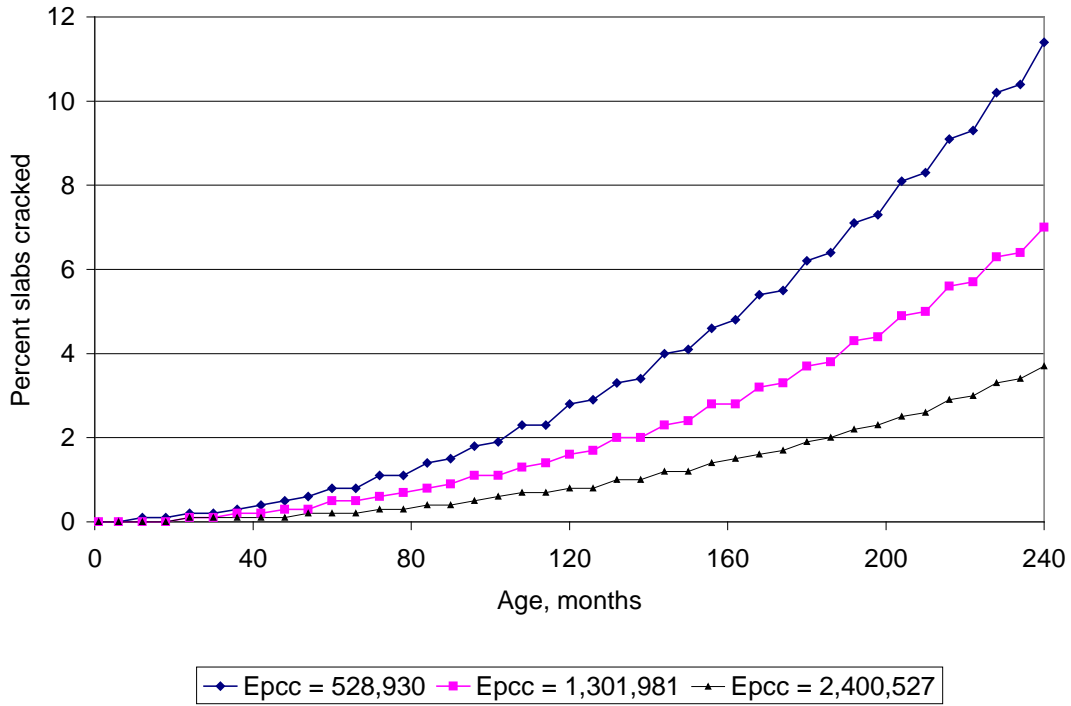


Figure 187. Plot of age versus percent slabs cracked showing the effect of existing slab elastic modulus.

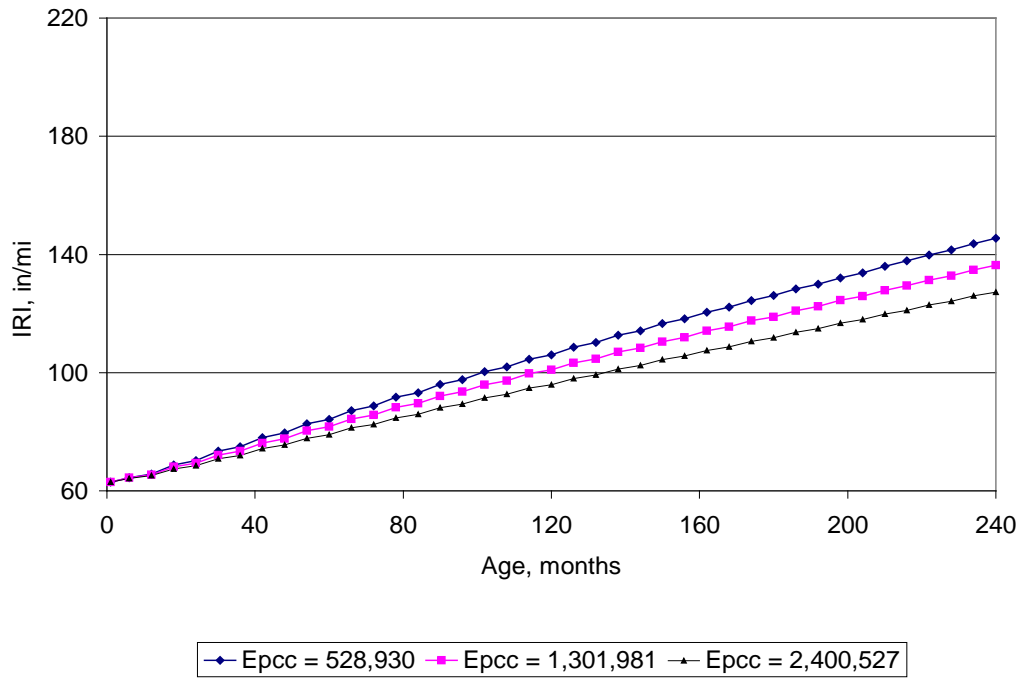


Figure 188. Plot of age versus IRI showing the effect of existing slab elastic modulus.

Table 56. Relative effect of existing slab elastic modulus on overlay distress and IRI.

Distress/IRI	Effect of Existing Slab Elastic Modulus on Distress/IRI
Joint faulting	Moderate
Transverse slab cracking	High
IRI	Moderate

Effect of Pavement Edge Support (Shoulder Type)

The impact of the slab edge support of the JPCP overlay (free edge such as an asphalt shoulder or a tied PCC shoulder) is shown in figures 189 through 191. Overlay edge support effects joint faulting moderately, slab cracking highly, and IRI moderately. The slab edge support effects are due to the positive effects of reducing corner deflections and fatigue damage with a tied PCC shoulder. A summary of the effect of slab edge support on performance is given in table 57.

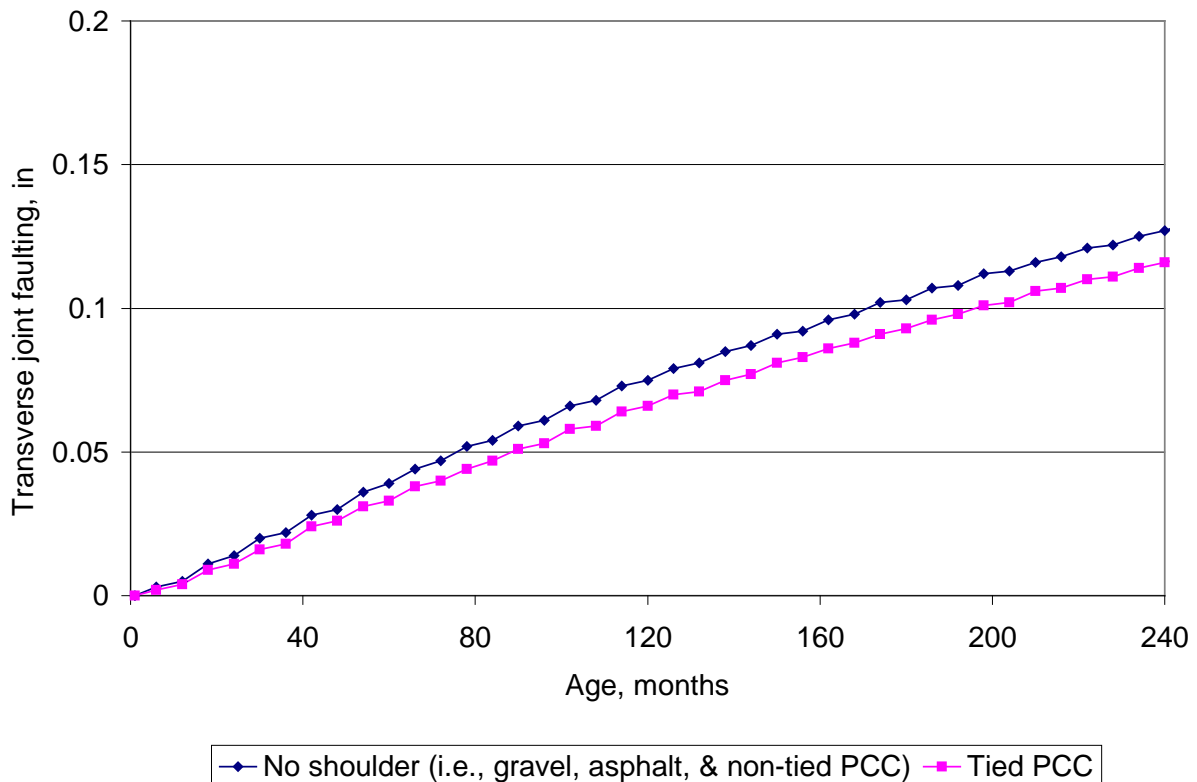


Figure 189. Plot of age versus transverse joint faulting showing the effect of pavement edge support.

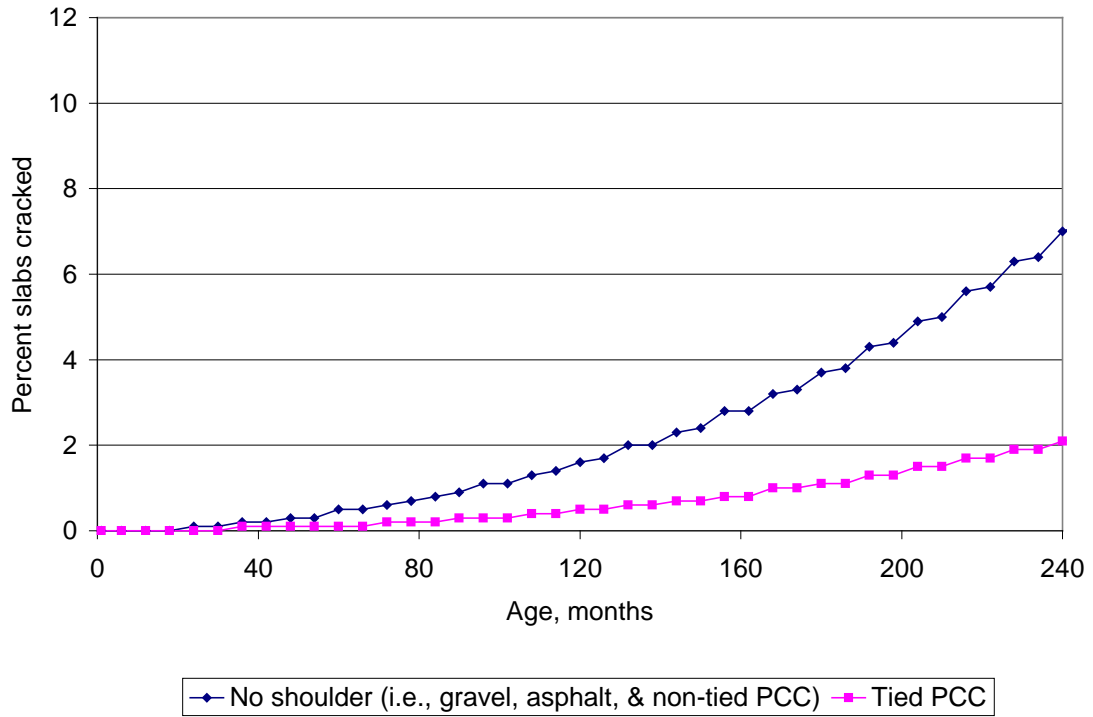


Figure 190. Plot of age versus percent slabs cracked showing the effect of pavement edge support.

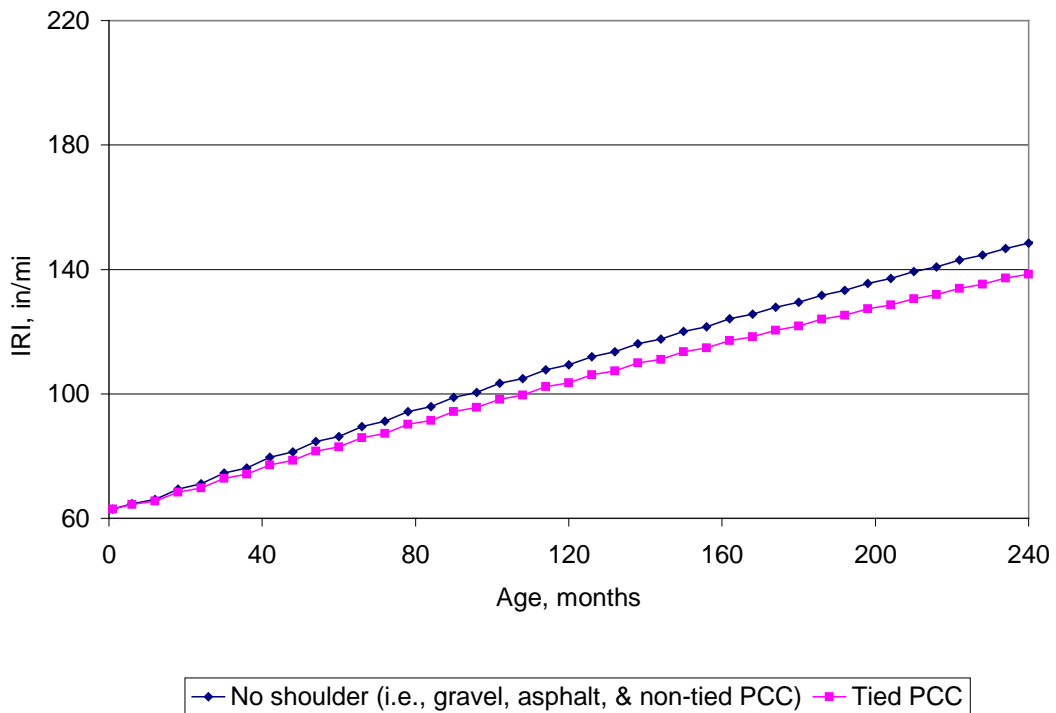


Figure 191. Plot of age versus IRI showing the effect of pavement edge support.

Table 57. Relative effect of edge support on overlay distress and IRI.

<b>Distress/IRI</b>	<b>Effect of Edge Support on Distress/IRI</b>
Joint faulting	Low
Transverse slab cracking	High
IRI	Low



## CHAPTER 6. CONCLUSIONS AND RECOMMENDATIONS

### Conclusions

Sensitivity analyses of four new and rehabilitated pavements are presented. The baseline designs are representative of current ODOT designs and include the following:

1. HMA new pavement.
2. JPCP new pavement.
3. HMA overlay of rubblized PCC.
4. Unbonded JPCP overlay of PCC pavement.

A summary of predicted MEPDG distress/IRI for all the baseline designs appears to be reasonable and as-expected for ODOT site conditions. A sensitivity analysis was conducted around each of these baseline designs to show how the performance varied with practical changes in the design inputs. The results showed that a number of inputs had very high effect on distress and IRI while some had moderate, low, or no effect. These results are used to develop recommendations for establishing guidelines for estimating the inputs for design.

### Recommendations

A summary of the effect that these variables had on performance for each type of pavement is provided for each type of pavement in tables 58 through 61. Included in these tables are recommendations for input selection. These recommendations will be considered during further implementation of the MEPDG in Ohio along with other considerations including costs and equipment needed for lab and field testing.

Table 58. New HMA pavement summary of sensitivity results and input recommendations.

<b>Input Variable</b>	<b>Distress/IRI</b>	<b>Level of Effect</b>	<b>Input Selection Implementation</b>
Base type: unbound aggregate, asphalt treated	Bottom-up fatigue (alligator) cracking	High	Selected in design. Asphalt treated base has less alligator cracking.
	Rutting	High	Selected in design. Asphalt treated base has less rutting.
	IRI		Selected in design. Asphalt treated base has lower IRI.
Climate across Ohio	Bottom-up fatigue (alligator) cracking	Moderate	Some locations showed more alligator cracking. Need to locate nearest weather station(s).
	Rutting	Moderate	Some locations showed more rutting.
	IRI	Low	Some locations showed slightly higher IRI.
HMA thickness	Bottom-up fatigue (alligator) cracking	High	Selected in design to limit distress. Thicker HMA has less alligator cracking.
	Rutting	High	Selected in design to limit distress. Thicker HMA has less rutting.
	IRI	High	Selected in design to limit distress. Thicker HMA has lower IRI.
	Top-down fatigue longitudinal cracking	High (for only HMA thickness <= 8 in) No effect for thicker HMA.	Selected in design. HMA thickness > 8 in had no longitudinal cracking.
Subgrade Type (soil classification and resilient modulus)	Bottom-up fatigue (alligator) cracking	High	Fine grained soils had greater alligator cracking. Need to determine subgrade parameters to establish classification and resilient modulus.
	Rutting	Moderate	Fine grained soils had greater rutting.
	IRI	Low	Fine grained soils had slightly higher IRI.

Table 58. New HMA pavement summary of sensitivity results and input recommendations. (Continued)

<b>Input Variable</b>	<b>Distress/IRI</b>	<b>Level of Effect</b>	<b>Input Selection Implementation</b>
Treatment of top of Subgrade (with lime or cement)	Bottom-up fatigue (alligator) cracking	High	Treatment reduced alligator cracking. Need to specify during design.
	Rutting	Moderate	Treatment reduced rutting. Need to specify during design.
	IRI	Moderate	Treatment resulted in lower IRI. Need to specify during design.
HMA In Situ Air Voids	Bottom-up fatigue (alligator) cracking	High	Higher air voids in lower most HMA layer increased alligator cracking. Need to specify maximum in construction.
	Rutting	Moderate	Higher air voids in upper most HMA layer increased rutting. Need to specify maximum in construction.
	IRI	Low	Higher air voids slightly increased IRI.
HMA In Situ Binder Content	Bottom-up fatigue (alligator) cracking	High	Higher binder content in lower most HMA layer decreased alligator cracking. Input is specified in mixture design.
	Rutting	Moderate	Higher binder content in upper most HMA layer increased rutting. Input is specified in mixture design.
	IRI	Low	Higher binder content slightly increased IRI.
Traffic vehicle classification and axle load distribution	Bottom-up fatigue (alligator) cracking	High	Different WIM sites resulted in different amounts of alligator cracking. Input data should consider best representative WIM site.
	Rutting	Moderate	Different WIM sites resulted in different amounts of rutting. Input data should consider best representative WIM site.
	IRI	Low	Different WIM sites resulted in only slightly different amounts of alligator cracking.
Surface HMA Mixture Type (SMA or SP)	Bottom-up fatigue (alligator) cracking	Low	Very little effect of Ohio surface HMA mixture type on alligator cracking.
	Rutting	Low	Very little effect of Ohio surface HMA mixture type on rutting.
	IRI	Low	Very little effect of Ohio surface HMA mixture type on IRI.

Table 59. New JPCP pavement summary of sensitivity results and input recommendations.

<b>Input Variable</b>	<b>Distress/IRI</b>	<b>Level of Effect</b>	<b>Input Selection Implementation</b>
Base Type: untreated base, asphalt treated base	Joint faulting	High	Selected in design. Asphalt treated base has less joint faulting.
	Transverse slab cracking	High	Selected in design. Asphalt treated base has less transverse cracking.
	IRI	High	Selected in design. Asphalt treated base has lower IRI.
Climate across Ohio	Joint faulting	Moderate	Some locations showed more faulting. Need to locate nearest weather station(s).
	Transverse slab cracking	High	Some locations showed more transverse cracking. Need to locate nearest weather station(s).
	IRI	Moderate	Some locations showed higher IRI. Need to locate nearest weather station(s).
Slab thickness (and dowel diameter which varied with thickness)	Joint faulting	High	Selected in design to control distress and IRI. Thicker slabs had lower faulting due to both thickness and larger dowel diameter.
	Transverse slab cracking	High	Selected in design to control distress and IRI. Thicker slabs had lower cracking.
	IRI	High	Selected in design to control distress and IRI. Thicker slabs had lower IRI.
Subgrade Type	Joint faulting	Low	Fine grained soils had slightly greater joint faulting.
	Transverse slab cracking	High	Fine grained soils had lower transverse cracking. Need to determine subgrade parameters to establish classification and resilient modulus.
	IRI	Moderate	Fine grained soils had lower transverse cracking. Need to determine subgrade parameters to establish classification and resilient modulus.
Treatment of top of Subgrade (with lime or cement)	Joint faulting	None	Need to specify during design.
	Transverse slab cracking	Moderate	Treatment reduced transverse cracking. Need to specify during design.
	IRI	None	Need to specify during design.

Table 59. New JPCP pavement summary of sensitivity results and input recommendations. (Continued)

Input Variable	Distress/IRI	Level of Effect	Input Selection Implementation
Joint Spacing	Joint faulting	High	Need to specify during design. Larger joint spacing results in higher joint faulting.
	Transverse slab cracking	High	Need to specify during design. Larger joint spacing results in higher transverse cracking.
	IRI	High	Need to specify during design. Larger joint spacing results in higher IRI.
Coefficient of thermal expansion of concrete	Joint faulting	High	Larger CTE results in higher joint faulting. Need to measure during design or specify upper limit in construction specification.
	Transverse slab cracking	High	Larger CTE results in higher cracking. Need to measure during design or specify upper limit in construction specification.
	IRI	High	Larger CTE results in higher IRI. Need to measure during design or specify upper limit in construction specification.
Joint Load Transfer (dowel diameter)	Joint faulting	High	Input selected during design to limit distress/IRI. Large dowel diameter the lower the joint faulting.
	Transverse slab cracking	None	
	IRI	High	Input selected during design to limit distress/IRI. Large dowel diameter the lower the IRI.
Concrete flexural strength and modulus of elasticity	Joint faulting	Low	Input selected during design to limit distress/IRI.
	Transverse slab cracking	High	Input selected during design to limit distress/IRI. The higher the strength and corresponding modulus the lower the transverse cracking. Input must be selected based on mean (not lower spec level) field results based on specification requirements.
	IRI	Low	Input selected during design to limit distress/IRI.

Table 59. New JPCP pavement summary of sensitivity results and input recommendations, continued.

<b>Input Variable</b>	<b>Distress/IRI</b>	<b>Level of Effect</b>	<b>Input Selection Implementation</b>
Slab width (adding two ft. on outer edge of slab)	Joint faulting	High	This input is selected during design. An additional slab width reduces joint faulting.
	Transverse slab cracking	High	This input is selected during design. An additional slab width reduces slab transverse cracking.
	IRI	High	This input is selected during design. An additional slab width reduces IRI.
Aggregate type in Concrete (gravel, slag, and limestone)	Joint faulting	High	Larger CTE in gravel and slag results in higher joint faulting. Need to measure CTE during design or specify upper limit in construction specification.
	Transverse slab cracking	High	Larger CTE in gravel and slag results in higher cracking. Need to measure during design or specify upper limit in construction specification.
	IRI	High	Larger CTE in gravel and slag results in higher IRI. Need to measure during design or specify upper limit in construction specification.
Concrete Class (S and C) and aggregate type	Joint faulting	High	Concrete type is specified in design. Aggregate type may need to have spec. on CTE. Slag/gravel aggregates cause higher joint faulting.
	Transverse slab cracking	High	Concrete type is specified in design. Aggregate type may need to have spec. to limit CTE. Concrete strength and slag/gravel aggregates cause higher slab cracking.
	IRI	High	Concrete type is specified in design. Aggregate type may need to have spec. on CTE. Type S (higher strength) and slag/gravel aggregates cause higher IRI.
Edge Support (asphalt shoulder versus tied concrete shoulder)	Joint faulting	Low	Edge support is specified in design. Tied concrete shoulder reduces faulting slightly.
	Transverse slab cracking	High	Edge support is specified in design. Tied concrete shoulder reduces slab cracking greatly.
	IRI	Low	Edge support is specified in design. Tied concrete shoulder reduces IRI slightly.
Traffic vehicle classification and axle load distribution	Joint faulting	Low	Different WIM sites resulted in only slightly different amounts of joint faulting.
	Transverse slab cracking	High	Different WIM sites resulted in different amounts of transverse slab cracking. Input data should consider best representative WIM site data.
	IRI	Moderate	Different WIM sites resulted in different levels of IRI. Input data should consider best representative WIM site data.

Table 60. HMA overlay over rubblized PCC pavement summary of sensitivity results and input recommendations. (Note: only differences between the HMA overlay of rubblized concrete and new HMA pavement are noted here. All other inputs have same effect as for new HMA pavement).

<b>Input Variable</b>	<b>Distress/IRI</b>	<b>Level of Effect</b>	<b>Input Selection Implementation</b>
HMA Overlay Thickness	Bottom-up fatigue (alligator) cracking	High	Selected in design. Increased HMA overlay thickness results in less alligator cracking.
	Rutting	High	Selected in design. Increased HMA overlay thickness results in less rutting.
	IRI	High	Selected in design. Increased HMA overlay thickness results in lower IRI.
Modulus of Rubblized Concrete	Bottom-up fatigue (alligator) cracking	High	Increased rubblized concrete modulus resulted in decreased alligator cracking. This input must be selected in design phase and should ideally be based on backcalculation results from other similar projects and guidelines provided.
	Rutting	Low	Increased rubblized concrete modulus resulted in slightly decreased rutting.
	IRI	Low	Increased rubblized concrete modulus resulted in slightly decreased IRI.
Thickness of rubblized concrete	Bottom-up fatigue (alligator) cracking	Moderate	Increased rubblized concrete thickness resulted in decreased alligator cracking. This input is measured in design phase.
	Rutting	Low	Increased rubblized concrete thickness resulted in slightly decreased rutting.
	IRI	None	

Table 61. Unbonded JPCP Overlay Summary of Sensitivity Results and Input Recommendations (Note: Only Differences between the Overlay and New JPCP are noted here. All Other Inputs have Same Effect as for New JPCP).

<b>Input Variable</b>	<b>Distress/IRI</b>	<b>Level of Effect</b>	<b>Input Selection Implementation</b>
HMA Separation Layer thickness	Joint faulting	None	This input is selected during design.
	Transverse slab cracking	Moderate	This input is selected during design. An increase in HMA separation layer thickness reduces slab transverse cracking.
	IRI	None	This input is selected during design.
Elastic modulus of existing old concrete slab	Joint faulting	Moderate	A lower elastic modulus from extensive cracking results in higher joint faulting.
	Transverse slab cracking	High	A lower elastic modulus from extensive cracking results in higher slab cracking. Need to estimate based on existing cracking during design phase.
	IRI	Moderate	A lower elastic modulus from extensive cracking results in higher IRI. Need to estimate based on existing cracking during design phase.

## REFERENCES

1. Harman T., D'Angelo J., Bukowski J., and Paugh C. *Superpave Asphalt Mixture Design Workshop, Workbook Version 8.0.*, Federal Highway Administration, McLean, 2002.
2. Masada T., and Sargand, S. M. *Laboratory Characterization of Materials & Data Management for Ohio-SHRP Projects*. State Job No. 14695(0), Report No. FHWA/OH-01/07, Submitted to Ohio Department of Transportation, Ohio University, 2002.
3. Masada, T., S. M. Sargand, B. Abdalla, and J. L. Figueroa. *Material Properties for Implementation of Mechanistic-Empirical (M-E) Pavement Design Procedures*, State Job No. 14767, Submitted to Ohio Department of Transportation, Ohio University, 2004.
4. NCHRP. 2004. *MEPDG Design Guide*, NCHRP Project 1-37A, Final Report. Washington, DC: Transportation Research Board, National Research Council.
5. *ODOT Pavement Design and Rehabilitation Manual*. Ohio Department of Transportation, Columbus, OH, 1999.
6. *ODOT Construction and Material Specifications*, Ohio Department of Transportation, Columbus, OH, 2005.
7. Sargand, S. M., and Hazen, G. A. *Evaluation on Resilient Modulus by Back-Calculation Technique*. State Job No. 14425(0), Report No. FHWA/OH-91/005, Submitted to Ohio Department of Transportation, Ohio University, 1991.
8. Sargand, S. M., and Hazen, G. A. *A Demonstration Project on Instrumentation of a Flexible Pavement System*. State Job No. 14561(0), Report No. FHWA/OH-96, Submitted to Ohio Department of Transportation, Ohio University, 1996.
9. Sargand, S. M., and Edwards, W. F. *Effectiveness of Base Type on the Performance of PCC Pavement on ERI/LOR 2*. State Job No. 14562(0), Report No. FHWA/OH-2000/005, Submitted to Ohio Department of Transportation, Ohio University, 2000.